INTERNATIONAL SERIES IN PURE AND APPLIED PHYSICS

G. P. HARNWELL, CONSULTING EDITOR

LOW TEMPERATURE PHYSICS

INTERNATIONAL SERIES IN PURE AND APPLIED PHYSICS

G. P. HARNWELL, CONSULTING EDITOR

ADVISORY EDITORIAL COMMITTEE: E. U. Condon, George R. Harrison
Elmer Hutchisson, K. K. Darrow

Allis and Herlin Thermodynamics and Statistical Mechanics
Cady Piezoelectricity
Clark Applied X-rays
Edwards Analytic and Vector Mechanics
Finkelnburg Atomic Physics
Gurney Introduction to Statistical Mechanics
Hall Introduction to Electron Microscopy
Hardy and Perrin The Principles of Optics
Harnwell Electricity and Electromagnetism
Harnwell and Livingood Experimental Atomic Physics
Houston Principles of Mathematical Physics
Houston Principles of Quantum Mechanics
Hughes and DuBridge Photoelectric Phenomena
Hund High-frequency Measurements
Kemble The Fundamental Principles of Quantum Mechanics
Kennard Kinetic Theory of Gases
Marshak Meson Physics
Morse Vibration and Sound
Morse and Feshbach Methods of Theoretical Physics
Muskat Physical Principles of Oil Production
Richtmyer and Kennard Introduction to Modern Physics
Ruark and Urey Atoms, Molecules, and Quanta
Schiff Quantum Mechanics
Seitz The Modern Theory of Solids
Slater Introduction to Chemical Physics
Slater Microwave Transmission
Slater Quantum Theory of Matter
Slater and Frank Electromagnetism
Slater and Frank Introduction to Theoretical Physics
Slater and Frank Mechanics
Smythe Static and Dynamic Electricity
Squire Low Temperature Physics
Stratton Electromagnetic Theory
Thorndike Mesons: A Summary of Experimental Facts
White Introduction to Atomic Spectra

The late F. K. Richtmyer was Consulting Editor of the series from its inception in 1929 to his death in 1939. Lee A. DuBridge was Consulting Editor of the series from 1939 to 1946.

LOW TEMPERATURE PHYSICS

CHARLES F. SQUIRE
Professor of Physics
The Rice Institute, Houston, Texas

New York Toronto London
McGRAW-HILL BOOK COMPANY, INC.
1953

LOW TEMPERATURE PHYSICS

Copyright, 1953, by the McGraw-Hill Book Company, Inc. Printed in the United States of America. All rights reserved. This book, or parts thereof, may not be reproduced in any form without permission of the publishers.

Library of Congress Catalog Card Number: 52-12365

THE MAPLE PRESS COMPANY, YORK, PA.

The author wishes to express his appreciation also for the careful attention and criticism provided by Dr. John R. Pellam of the National Bureau of Standards, and by Professor Kurt A. G. Mendelssohn, F.R.S., of Oxford University. During 1952–1953 the author lectured this material at The Sorbonne, and he acknowledges this privilege with the warmest thanks to the Faculty of Science, University of Paris, for their generous invitation. The considerable task of the actual preparation of manuscript was made pleasant through the use of "Tall Timbers," for which the author thanks Dr. and Mrs. J. Bryan Eby. The author is most grateful for the unfailing confidence and encouragement shown by Jane Hafner Squire.

Charles F. Squire

Paris, France
March, 1953

CONTENTS

Preface v

Chapter I Gas Liquefaction and the Equation of State 1

Equation of State for a Gas 1
Entropy and Enthalpy 4
Production of Low Temperatures with Gases 5
  Claude Expander 5
    Entropy Changes and Temperature Drop 6
  Joule-Thomson Cooling—Linde Process 8
Engineering Applications 9
Physical Constants of Various Gases 11

Chapter II Experimental Methods of Low-temperature Physics 12

Compressors 12
Gasholders 13
Helium Liquefiers 15
Storage Containers for Liquid Helium 20
Liquid Hydrogen by Condensation 21
Cryostats for Experiments 21
Temperature Measurements 25
  Vapor Pressure of Liquid Helium 25
  Vapor Pressure of Liquid Hydrogen 27
  Equipment for Vapor-pressure Measurements 27
  Constant-volume Gas Thermometer 28
  Resistance Thermometer 29
  Thermocouples 30
Heat Flow into Cryostats 30

Chapter III Theoretical Considerations of the Equation of State 32

Classical Quantum Statistics 32
Lennard-Jones Potential 34
Second Virial Coefficient in Classical Statistics 36
Third Virial Coefficient in Classical Statistics 39
De Boer Theory of the Equation of State 41
Calculations of the Molecular Constants σ and ϵ 46
Quantum-mechanical Partition Function 48
Transformation of the Slater Sum 49
  Slater Sums in Some Simple Examples 50
Second Virial Coefficient for an Ideal Quantum Gas 53
Kirkwood Expansion of the Slater Sum 55
Second Virial Coefficient at Low Temperatures 56
Equation of State of Compressed Gases and Liquids 58

Chapter IV Liquid Helium—Thermal Properties 60

Liquid Helium I and Liquid Helium II 61
  Diagram of State p vs. T 61
Specific Heat of Liquid Helium 61
Entropy of Liquid Helium 62
Zero-point Energy 64
Latent Heat of Vaporization 65
Density and Dielectric Constant of Liquid Helium 66
Viscosity of Liquid Helium 68
Thermal Properties of He^3 Isotope 70

Chapter V Liquid Helium—Dynamic Properties 74

Flow Phenomena in Capillaries 74
Film Flow in Liquid Helium II 75
Mechano-caloric Effect 77
Entropy of Helium II—Flow Studies by P. Kapitza 78
Hydrodynamic Studies—Fountain Effect 79
Heat Conductivity 82
Velocity and Attenuation of Sound in Liquid Helium 84
Second Sound or Thermal Waves in Liquid Helium II 86
  Second-sound Velocity at Very Low Temperatures 88
Thermal Rayleigh Disk in Helium II 89
Mixtures of He^3 and He^4 in Vapor and Liquid Phase 93

Chapter VI Theories of Liquid Helium 97

Quantum Theories of F. London 97
Thermodynamics of the Two-fluid Model for Liquid Helium II 103
Tisza's Phenomenological Theory of the Dynamic Properties of He II 104
  Second-sound-wave Equation 105
Transmission Line Analogy 107
The Theory of L. Landau 108

Chapter VII Superconductivity 110

Resistance Studies 111
Crystal Structure and Volume 112
Isotope Effect 113
Consequences of Infinite Conductivity 113
Magnetic Critical Field 114
Meissner Effect 115
Thermal Properties of Superconductors 117
  Specific Heat and Entropy 117
Magneto-caloric Effect in Superconductors 121
Electrodynamic Studies 121
  Gyro-magnetic Effect 121
  Torsion Pendulum Studies—Infinite Conductivity and Superconductivity 123
Skin Depth of Penetration of a Magnetic Field 125
Thermal Conductivity of Superconductors 126
Thermoelectric Effect in Superconductors 126
Effect of Strain on a Superconductor 127
High-frequency Measurements on Superconductors 127
The Theories of Superconductivity 131
  Theory of H. London and F. London 131
  Quantum Theories of Superconductivity 134
Two-electron Fluid Model 136

Chapter VIII Magnetism at Low Temperatures 138

- Some Fundamental Concepts of Magnetization 138
- Electronic Magnetic Moment—Orbital Motion 139
- Larmor Precession 139
- Diamagnetism 141
- Electron Spin Magnetic Moment 141
- Spin-orbit Coupling 142
- Statistical Mechanics of Paramagnetism 143
- Low Temperatures and High Magnetic Fields—Saturation 144
  - Brillouin Function 145
- Measurement of Magnetic Susceptibility and Moments 145
  - Balance Method 145
  - Induction Coils for Magnetic Susceptibility at Low Temperatures 147
  - Demagnetization Factor 148
- Some Typical Experimental Results 148
  - Ideal Salts—Curie Law 148
  - Antiferromagnetism 150
- Magnetic Cooling 151
  - Thermodynamics and Statistical Mechanics of the Method 151
  - Experimental Methods in Magnetic Cooling 154
    - Remarks on the Magnetization Process 155
    - Demagnetization 156
  - Determination of Temperature 156
- Experimental Results 157
  - Iron Ammonium Alum 157
  - Chromium Potassium Alum 161
- Theoretical Analysis 161
- Nuclear Alignment 163
- Magnetic Resonance 164
  - Nuclear Magnetic Induction 167
    - Theoretical Analysis of Magnetic Induction 167
    - Particular Solution 170
    - Some General Remarks about Magnetic Induction and Absorption 172
    - Experimental Results 173
    - Solid Hydrogen 173
    - Studies on Solids at Low Temperature 175
  - Paramagnetic Resonance Absorption by Electron Systems 176
  - Diamagnetism of Free Electrons 180
    - de Haas-van Alphen Effect 180
    - Theory of Diamagnetism of Free Electrons 181

Chapter IX Thermal Energy in the Solid State at Low Temperatures 186

- Lattice Vibrations 186
- The Difference $C_p - C_v$ for Solids 191
- Electronic Specific Heat at Low Temperatures in Metals 192
- Some Characteristic Experimental Results on Metals 194
  - Copper 194
  - Silver and Gold 196
  - Iron, Cobalt, and Nickel 196
  - Palladium and Platinum 197
- Specific Heat of Superconductors 197
  - Tin 197
  - Tantalum 198
- Experimental Results on Metals with Anomalous Specific Heats 199
  - Tungsten 199
  - Lithium 200
  - Beryllium 201
  - Rare-earth Elements: Lanthanum, Cerium, Neodymium, and Praseodymium 201
  - Chromium and Manganese 202
  - Germanium and Hafnium 202
- Specific Heat of Solids with Several Types of Atoms 202
- Rotation of Atoms and Molecules in the Solid State 205
  - Theory of Cooperative Phenomena 207
  - Specific Heats Showing λ Transitions 210
- Experimental Methods 211
- Heat Conductivity in Solids 214

Chapter X Dielectric Properties at Low Temperatures 220

Some Fundamental Concepts 220
Barium Titanate 222
Strontium Titanate 225
Ferro-electric Tartrates 226
Solid Hydrogen Bromide 227
Theory of Barium Titanate 228

Appendix 229

Agreed Vapor Pressure of Liquid Helium 229
Deviations with Kistemaker's Temperature Scale 234
Vapor Pressure of Liquid Hydrogen 234
Vapor Pressure of Liquid Oxygen 235
Vapor Pressure of Mixture of He^3 and He^4 236
Physical Constants 238

Index 239

CHAPTER 1

GAS LIQUEFACTION AND THE EQUATION OF STATE

It has been well over one hundred years since the first liquefaction of gases took place by means of simple compression and some seventy years since scientists began to understand that cooling with compression could liquefy a further group of gases. The early research by Cailletet, Andrews, and Claude opened up the field of the study of thermodynamic equilibrium between the gas, liquid, and solid states. By the year 1900 several low-temperature laboratories existed, notably at Krakow in Poland and at Leiden in Holland. By then the entire problem of liquefying gases was well understood so that the era of commercial gases was opened. The invention of the Dewar flask, of heat insulation by glass wool, and the development of suitable compressors are but a few of the engineering aspects which have led to the ease of attaining low temperature. There are now many laboratories in nearly every country in the world in which the production of many liters of liquid helium is regarded as rather commonplace and as simply one of many research tools used to study the properties of matter. The Claude process of cooling by an adiabatic expansion engine has had the most spectacular success. With the clever developments by Peter Kapitza and by Samuel Collins the expansion engine has become the most widely used device for producing liquid helium. These expansion engines are not the whole story of the production of liquid helium, and we shall see that the Linde process was used by Kamerlingh Onnes in Leiden and that an expansion bomb has been widely used by F. E. Simon at Oxford. In this first chapter we shall discuss the Claude process and the Linde process.

Equation of State for a Gas

We must review the thermal properties of ordinary gases. In Fig. 1.1 the well-known plot of pressure against volume for a series of isothermals is reproduced for a standard substance such as nitrogen and serves to illustrate the existence of an equation of state. The functional relation between volume, pressure, and temperature is simple for the gas at relatively high temperatures and becomes more complicated at temperatures approaching possible liquefaction. The curves for constant temperature in Fig. 1.1 show the following important experimental facts:

1. At temperatures above the T_c curve, isothermal compression does

not lead to formation of a coexistent liquid phase. In such high-temperature regions the simple kinetic theory of atoms moving rapidly about leads to the equation $PV = nRT$, where P is the pressure in atmospheres, V the volume in liters, n the number of moles of the gas, R the gas constant in units of energy per mole degree, and T the absolute temperature.

2. Compression along the critical isotherm leads to complete liquefaction at the critical point without change of volume. There is no latent heat of vaporization at the critical point.

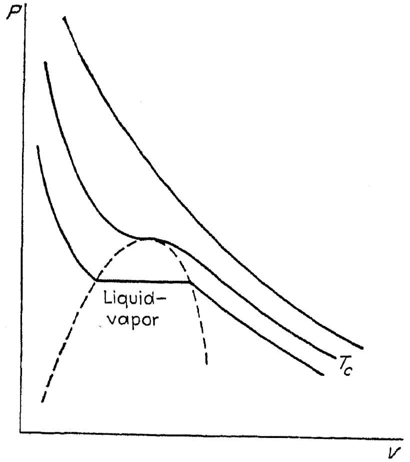

FIG. 1.1. Pressure plotted against volume for an arbitrary gas.

3. Temperatures below T_c are characterized by a region in which the gas may be liquefied by compression, during which the pressure remains constant. The further the temperature is lowered below the critical temperature, the smaller is the pressure needed for liquefaction. The region between all liquid and all gas is marked by dotted curves.

The equation of state is not simple for the gas phase whose temperature is near or below the critical temperature T_c. The best representation may be given by a power series expansion due to Kamerlingh Onnes:

$$PV = nRT\left(1 + \frac{nB}{V} + \frac{n^2C}{V^2} + \cdots\right) \tag{1.1}$$

In this equation of state the new quantities B and C are called the second and third *virial* coefficients, and their values may be taken from experimental isotherms. The derivation of the virial coefficients from atomic theory constitutes the material to be treated in Chap. 3. The word *virial* was used by Professor R. Clausius in discussing gas kinetic theory.[1] Clausius' virial theorem implied the existence of forces between molecules, and the word virial was carried over by Onnes to give the coefficients a descriptive meaning.

An earlier form of the equation of state was given by van der Waals:

$$\left[P + a\left(\frac{n}{V}\right)^2\right][V - nb] = nRT \tag{1.2}$$

---

[1] R. Clausius, *Ann. Phys. u. Chem.*, **141**, 3, 1870; *Compt. rend.*, **70**, 1314, 1870.

where the new constants introduced are a and b. The constant a has the effect of altering the pressure exerted on the volume walls due to attraction forces between the atoms. The constant b accounts for the volume occupied by the atoms themselves in the space. Table 1.1 gives some values of these van der Waals constants for a few gases. It will be noted that the fourth column of the table, giving the volume per mole of the liquid, shows a smaller value than the constant b for all gases except helium. Here is the first clue to an important low-temperature physics problem, *i.e.*, the large volume occupied by liquid helium.

TABLE 1.1. VALUES OF THE VAN DER WAALS CONSTANTS FOR SOME GASES

Gas	a, dyne cm^4/mole^2	b, cm^3/mole	V/n, liquid phase
A	1.27×10^{12}	36	
O_2	1.49×10^{12}	32.2	25.7
N_2	1.36	38.3	32.8
Ne	0.207	24.0	
H_2	0.25	26.5	26.4
He	0.035	23.6	27.4
CO_2	3.64	42.5	41.7
H_2O	5.53	30.4	18.0

The van der Waals equation is not accurately valid, but it is a useful equation to discuss because it brings out many fundamental characteristics which guide our thinking about the production of low temperatures. Suppose we consider the van der Waals equation for the critical temperature T_c and solve for the pressure

$$P = \frac{nRT_c}{V - nb} - \frac{n^2a}{V^2} \tag{1.3}$$

We may set the first two derivatives of P by V equal to zero at the critical point because the plot of P against V shows an inflection point.

$$\left(\frac{\partial P_c}{\partial V}\right)_T = 0; \qquad \left(\frac{\partial^2 P_c}{\partial V^2}\right)_T = 0$$

These equations allow us to solve for the critical values

$$P_c = \frac{a}{27b^2}; \qquad V_c = 3nb; \qquad RT_c = \frac{8a}{27b}$$

In Table 1.2 are given the critical temperature and pressure for a number of gases. A little study of the magnitude of the values shows at once that the constant a in the van der Waals equation plays the most important role with respect to the temperatures required to liquefy any gas. A small constant a means going to very low temperatures to produce the liquid. An interesting relationship called the *law of corresponding states* may be obtained if we simply express the pressure, volume, and temperature in the van der Waals equation in units of their critical values.

$$\left[\frac{P}{P_c} + \frac{3}{(V/V_c)^2}\right]\left[\frac{V}{V_c} - \frac{1}{3}\right] = \frac{8T}{3T_c} \tag{1.4}$$

Reducing all gases to one equation of state allows us to see at a glance for any given gas whether the temperature and pressure existing within the working volume are to be considered high or low for that substance. Thus, room temperature would be considered a very high temperature for nitrogen because the ratio 290:126 is much larger than 1. Yet room temperature is comparatively low for Xe and very low for water. We shall seek justification for the law of corresponding states in Chap. 3.

TABLE 1.2. EXPERIMENTAL CRITICAL TEMPERATURE AND PRESSURE VALUES

Gas	T_c, °K	P_c, atm
CO_2	304.2	73.00
Xe	289.8	58.22
Kr	209.4	54.24
A	150.7	48.00
O_2	154.0	49.7
N_2	126.0	33.49
Ne	44.8	26.88
H_2	33.2	12.8
He	5.25	2.26

Entropy and Enthalpy

It will be useful to remind the reader of the thermodynamic concepts of entropy and enthalpy of a system. The entropy S in units of energy per degree absolute temperature T is identified with the Clausius theorem concerning any reversible cycle. During the reversible process, the system may absorb an increment of heat $đQ$, and the entropy change is

$$dS = \frac{đQ}{T} \tag{1.5}$$

If the inexact differential $đQ$ can be expressed by the thermodynamic variables, we may divide by T and integrate the expression to obtain the entropy of the system. This formulation of the second law leads one to examine the entropy increase in all naturally occurring processes. One must deduce that the entropy of a system is a measure of the degree of disorder existing in the system because in all naturally occurring processes entropy and disorder increase together. As is well known, statistical mechanics then formulates the entropy of a system from this concept.[1]

A useful thermodynamic potential is the enthalpy H of a system such as a gas:

$$H = U + PV \tag{1.6}$$

The internal energy U of the system is defined through its differential:

$$dU = đQ - P\,dV \tag{1.7}$$

In the discussion which follows we shall use these broad definitions of entropy and of enthalpy. Later on we shall need the thermodynamic potentials $A = U - TS$ and $G = H - TS$; these are the Helmholtz potential and Gibbs potential, respectively.[2]

Production of Low Temperatures with Gases

Claude Expander. Now let us return to the problem of producing low temperatures by means of gas liquefaction with the combined arrangement of a Claude expansion engine and a Joule-Thomson expansion valve. Figure 1.2 gives the scheme of the process. Gas is compressed mechanically, and by water cooling the heat developed during the work is removed. The gas then enters the liquefier where it immediately begins to be cooled with the cold gas which has been through the liquefier ahead of it. How that gas became cold we shall presently describe.

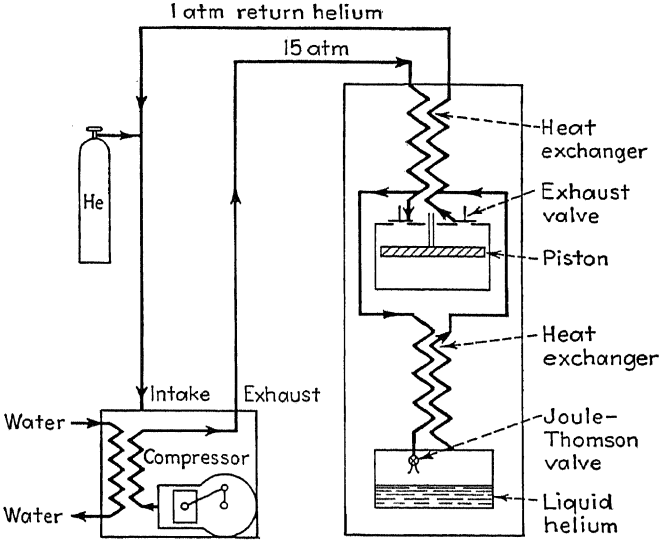

FIG. 1.2. Flow diagram of helium liquefier.

---

[1] J. C. Slater, "Introduction to Chemical Physics," New York, McGraw-Hill, 1939.

[2] M. Zemansky, "Heat and Thermodynamics," 2d ed., New York, McGraw-Hill, 1943.

From the heat exchanger, the gas enters the expansion chamber whenever the inlet valve is opened. The inlet valve closes quickly, and the gas continues to expand, doing work on the piston. This work is mechanically absorbed by means of a drive-rod and crankshaft arrangement. These operations are easily followed on a pressure-against-volume plot in Fig. 1.3. They are marked *a* for valve open, *b* for valve shut, and the point *c* is the bottom of the cylinder stroke. At this point the exhaust valve opens to allow the gas to be pushed out of the expansion chamber. Finally the exhaust valve is closed at point *d*, and the cycle is ready to repeat with the next charge of gas from the high-pressure line. All of this is very elementary, but now let us see how this has produced a drop in temperature. The expansion has taken place at nearly constant entropy, and neglecting frictional effects, we may simply state that the drop in temperature of the gas is required to offset the drop in pressure which took place in the expander.

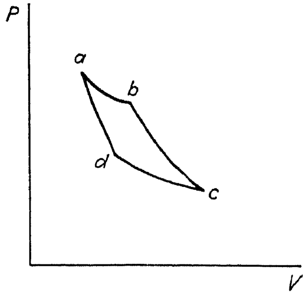

FIG. 1.3. Pressure-vs.-volume diagram showing expansion-engine cycle.

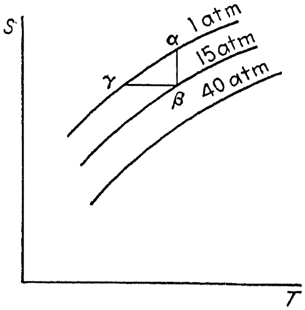

FIG. 1.4. Entropy-vs.-temperature diagram showing isothermal compression and constant-entropy expansion.

Entropy Changes and Temperature Drop. These concepts are basic to our understanding of the production of low temperatures. The physical meaning of entropy as a measure of the degree of disorder in the system helps us to visualize the process. The entropy-against-temperature plot in Fig. 1.4 shows a series of constant-pressure curves. At any given temperature the amount of disorder (entropy) may be reduced by squeezing the atoms into a smaller volume (raising the pressure) because surely then the random motion is more confined. In Fig. 1.4 we may go from point α to point β by use of a compressor and remove any heat generated by use of a heat interchanger. The Claude expansion engine is simply a device for allowing us to go from point β to point γ on the plot. This is done at constant entropy so that we may think of the pressure and temperature variables as having suitably shifted to preserve the degree of disorder. Energy has been removed from the gas in two steps: during the compression by the water cooling and during the expansion by means of the drive rod. The drive rod may be connected to a crankshaft so that energy may be absorbed.

With curves like that in Fig. 1.4 given for any gas, the constant-entropy condition for the expansion engine allows one to determine the temperature drop for any pressure change. We may determine the temperature drop from the gas laws and thermodynamic considerations. Since no heat is added to or taken out of the expander during the process, then by the first law $dU + P\,dV = 0$. Consider now an ideal gas for which $dU = C_v dT$ and $PV = RT$. The symbols have their usual meaning, with U the internal energy per mole of the system and C_v the specific heat at constant volume per mole of gas. We define C_p as the specific heat at constant pressure per mole of gas and γ the ratio C_p/C_v. We may differentiate the last equation above and substitute the relation $R = C_p - C_v$ and obtain $R\,dT = P\,dV + V\,dP$. Substitution gives

$$\frac{C_v P\,dV + C_v V\,dP}{C_p - C_v} + P\,dV = 0 \tag{1.8}$$

Using the ratio γ, we then have $\gamma\,dV/V + dP/P = 0$, and this equation integrates to the equation of curve bc of Fig. 1.3; $PV^\gamma =$ constant. We may also write this last equation in the form $TP^{(1-\gamma)/\gamma} =$ constant. Suppose we consider that the gas enters the Claude expander at a temperature T_1 and pressure P_1, and we wish to know the temperature T after the expansion to the pressure P. We may then write $TP^{(1-\gamma)/\gamma} = T_1 P_1^{(1-\gamma)/\gamma}$ and have then

$$T_1 - T = T_1\left[1 - \left(\frac{P_1}{P}\right)^{(1-\gamma)/\gamma}\right] \tag{1.9}$$

Putting in some values for helium gas, $\gamma = 1.67$, $P_1 = 15$ atm, $P = 1.1$ atm, and allowing the gas to enter the expander at $T_1 = 100°\text{K}$, we obtain $T = 40°\text{K}$. Allowing for a loss factor of 40 per cent, we still get an appreciable temperature drop. We may define the amount of refrigeration made available as $nC_p(T_1 - T)$, where n moles of gas per unit of time pass through the expander. The expanded gas passes counterflow to the incoming gas through the heat exchanger and then back to the compressor. Gradually the incoming high-pressure gas enters the expander at a lower and lower temperature. If this process continues and if the heat leaks from external sources are not too great, a liquid mist could form during the expansion stroke. The compressor would then have a maximum task of pushing a sufficient mass of gas to keep up the pressure. This limitation results in the use of the Claude expander down to such temperatures as efficiency permits, and then the last bit of cooling for liquefaction is done with the Joule-Thomson expansion valve.

Joule-Thomson Cooling—Linde Process. Figure 1.2 shows the block diagram of the compressor, heat exchanger, Claude expander, further heat exchanger, and finally the Joule-Thomson valve. The incoming high-pressure gas is thus allowed to have two expansion paths located as parallel circuits but with decidedly different temperatures at their respective expansion points. The course of the gas flow on a temperature entropy plot is shown in Fig. 1.5. Part of the high-pressure gas expands at nearly constant entropy, and the remainder expands at the valve to make some liquid. Expansion through a throttle valve is a constant-enthalpy, H, process, and a drop in temperature does not always occur. The complication which arises here lies with the nature of the constants in the van der Waals equation. For some gases, such as helium, even at liquid air temperatures the throttle process will raise the temperature. Since $dH = 0 = dU + P\,dV + V\,dP$, and considering the functional dependence of internal energy, we write

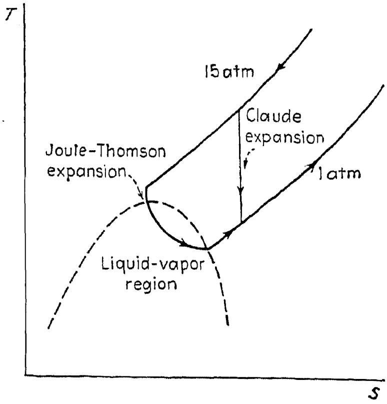

FIG. 1.5. Temperature-vs.-entropy diagram showing Claude expansion and in parallel Joule-Thomson expansion for liquefaction.

$$\left(\frac{\partial U}{\partial T}\right)_P dT + \left(\frac{\partial U}{\partial P}\right)_T dP + P\,dV + V\,dP = 0 \tag{1.10}$$

Using the equation of state, we may further expand to obtain

$$\left(\frac{\partial U}{\partial T}\right)_p dT + \left(\frac{\partial U}{\partial p}\right)_T dp + p\left(\frac{\partial V}{\partial T}\right)_p dT + p\left(\frac{\partial V}{\partial p}\right)_T dp + V\,dp = 0 \tag{1.11}$$

Using now the thermodynamic relation $dU = T\,dS - p\,dV$, we have

$$\left(\frac{\partial U}{\partial p}\right)_T = -p\left(\frac{\partial V}{\partial p}\right)_T + T\left(\frac{\partial S}{\partial p}\right)_T = -p\left(\frac{\partial V}{\partial p}\right)_T - T\left(\frac{\partial V}{\partial T}\right)_p \tag{1.12}$$

Combining these equations gives

$$\left[\left(\frac{\partial U}{\partial T}\right)_p + p\left(\frac{\partial V}{\partial T}\right)_p\right] dT = T\left(\frac{\partial V}{\partial T}\right)_p dp - V\,dp \tag{1.13}$$

This is equivalent to

$$C_p\,dT = \left[T\left(\frac{\partial V}{\partial T}\right)_p - V\right] dp \tag{1.14}$$

Thus the change in temperature with pressure at constant enthalpy is

$$\left(\frac{\partial T}{\partial p}\right)_H = \frac{T(\partial V/\partial T)_p - V}{nC_p} \tag{1.15}$$

For an ideal gas where $pV = nRT$, there is no cooling. For a van der Waals gas, one can easily show that

$$\left(\frac{\partial V}{\partial T}\right)_p = \frac{V - nb + 2na/RT}{T} \tag{1.16}$$

and the change in temperature with pressure at constant enthalpy is

$$\left(\frac{\partial T}{\partial p}\right)_H = \frac{n(-b + 2a/RT)}{nC_p} \tag{1.17}$$

If the value of a is small and if the temperature T is relatively high, we may get an increase in temperature with a drop in pressure. Thus in practice one must only open the Joule-Thomson valve on helium for cooling at temperatures below about 15°K so that the second term may be large enough compared to the constant b to produce a negative value of dT when a negative value of dp is used. In the case of hydrogen gas, the valve can be operated to produce cooling at temperatures obtainable with cooled nitrogen liquid, some 60°K. Kamerlingh Onnes at Leiden University used the Joule-Thomson effect to liquefy hydrogen and then helium in 1908. The inversion of the Joule-Thomson coefficient from plus to minus has been explained qualitatively by the use of the van der Waals equation, and it should be borne in mind that the more complete equation of state using the virial coefficients should be used.

Engineering Applications

We shall add at this point a few remarks concerning the work which the mechanical engineers and physical chemists have done in the field of refrigeration. The use of freon and other substances such as ammonia has been popular in the field of refrigeration and air conditioning. Figure 1.6 shows the scheme of a unit. It has a compressor which may be water-cooled so that the compression is made nearly isothermal. The throttle valve or Joule-Thomson valve is located in the region to be chilled. In air-conditioning equipment the freon expands into tubing provided with a large fin area. Air is blown across the fins and so cooled. If the air is moist, a great deal of water condenses out on the fins and is drained away. This adds to the comfort. Automatic thermal control of the expansion valve permits control of the desired room temperature. Pressure controls also automatically operate the compressor. The humidity may be adjusted by water-vapor injection. Where the air is blown across the cooling coils and then through ducts to the various rooms of a building, trouble may arise from two causes. The noise of the air being forced out of the ducts is sometimes troublesome and requires the use of acoustic filters. The ducts must be insulated to prevent sweating because such moisture can drip off and cause damage. Refrigerators for food storage and for ice-cream production have an obviously simpler problem.

The steel industry and the oil industry use oxygen-enriched air for certain processes, and hundreds of tons of liquid air per day are used in this way. The turbine expansion engine has replaced ordinary reciprocating pistons in such large-scale production. For this reason engineers have put a great deal of effort into the measurement of the enthalpy vs. temperature and at various pressures for air. Heat-transfer properties and viscosity of air over a wide range of temperature and pressure are important known quantities. Reversing exchangers have been developed which purify air by freezing out water and CO_2.

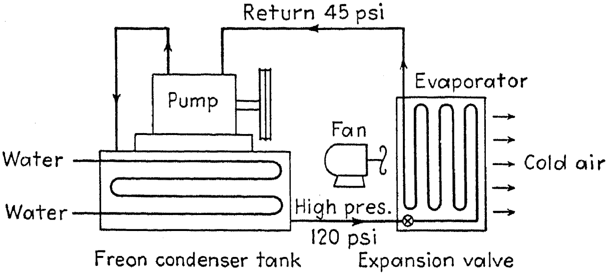

FIG. 1.6. Diagram of air-conditioning system.

When an airplane carries passengers at altitudes where the pressure is well below $\frac{1}{2}$ atm, the cabin is pressurized for passenger comfort. The compression and other sources of heat require air-cooling equipment. The use of turbine expanders in airplanes is popular because of the very light weight.

We conclude this chapter with Table 1.3, which gives some useful physical constants of various gases, and Table 1.4, which gives the fixed temperature points of several gases. In the next chapter we shall consider the details of the equipment used in low-temperature physics.

TABLE 1.3. PHYSICAL CONSTANTS OF VARIOUS GASES

Constant	A	CO_2	N_2	O_2	H_2	He^4
Normal boiling point at 1 atm, T_b, °K	87.40	Sublimes at 194.67	77.32	90.19	20.39[a]	4.21
Freezing point, T_f, °K	83.94	....	63.14	54.36	14.04	No solid[b]
Triple point, pressure, mm Hg	512.17	3.884	96.4	1.2	51.4	
Density of gas at 1 atm, and 0°C, g/cc	1.7832×10^{-3}	1.9760×10^{-3}	1.2568×10^{-3}	1.4290×10^{-3}	8.988×10^{-5}	1.785×10^{-4}
Density of liquid at T_b, g/cc	1.374 at 89.9°K	....	0.807	1.149	0.0709	0.1255
Density of solid, g/cc	1.65 at 40°K	1.566 at 193°K	1.026 at 20.7°K	1.425 at 20.7°K	0.0808 at 11.1°K	
Viscosity of gas at 20°C, centipoises	2.227×10^{-2}	1.4768×10^{-2}	1.755×10^{-2}	2.032×10^{-2}	8.881×10^{-3}	1.9525×10^{-2}
Viscosity of liquid at T_b, centipoises	0.252	....	0.158	0.190	0.0130	0.0047
Thermal conductivity at 0°C, $10^4 \times \frac{\text{cal}}{(\text{sec})(\text{cm}^2)(°\text{C per cm})}$	0.378	0.327	0.545	0.557	3.80	3.32
Latent heat of vaporization at T_b, cal/g	37.7	Sublimes 136.9 at 194.6°K	47.6	50.8	106.5	5.5

[a] Hydrogen gas whose high-temperature equilibrium is 0.25 para H_2 and 0.75 ortho H_2.

[b] Liquid helium becomes solid at pressures somewhat above 25 atm.

TABLE 1.4. FIXED TEMPERATURE POINTS OF SOME GASES

Gas	Standard boiling point, °K	Standard freezing point, °K
Ammonia	239.8	195
Freon-12 (CCl_2F_2)	243.1	115
Methyl chloride	249.4	175
Sulfur dioxide	263.1	200
Propane	230.8	
Acetylene	189.1	
Ethane	184.8	
Methane	111.7	
Neon	27.2	
Tritium	25.1	
Deuterium	23.6	
Helium isotope^3	3.2	

NOTE: See Table 1.2 for critical temperatures and pressures of gases.

CHAPTER 2

EXPERIMENTAL METHODS OF LOW-TEMPERATURE PHYSICS

Compressors

In this chapter we shall discuss the details of experimental methods and apparatus. We shall begin with a discussion of compressors and then go on to liquefiers and their use. Finally we shall discuss cryostats used for special problems and the measuring techniques used with them. We start with compressors because they are the heart of the laboratory and because the researcher must expect trouble from this source. Thus it is customary to place the compressor in a spot where it may be easily serviced and where early symptoms of trouble may be detected at once. Before each use of the compressor, a check list should be gone over with care. This should include such things as

1. Lubrication of motor and proper oil level in the crankcase. Drain all surge chambers and check force-feed lubricators. Stuffing boxes on the flywheel shaft of the crankcase should be lubricated and gastight.
2. Check that all gas lines and water-cooling lines are not leaking.
3. The compressor should be pulled through by hand before starting to make sure that it is quite free. Stand by and watch the compressor at the start with power so that bad vibration, stuck valves, or any other trouble may be detected at once. Check the crankcase temperature at reasonable intervals, and if it is too hot, stop operations. Burned-out bearings can lead to great destruction.

Installation of the compressor should be rigid to prevent vibration. Temperature control[1] on the water-cooling line will ensure that the compressor is turned off automatically and will prevent hot gas from reaching the liquefier. The compressor motor should have a solenoid magnetic-switch starter box. The temperature controller can operate the solenoid. Another must in the safety precautions is that a safety valve be placed between the high-pressure line and the low-pressure line so that in the event of stoppage at the liquefier, the safety valve will at once vent the high pressure. A simple type with a silver rupture disk is made commercially.[2]

Compressors which are not especially constructed for low-temperature work must be carefully made ready for the task. The stock grade of compressor should be completely taken apart and inspected. All bearings should be in perfect condition, and particular attention should be paid to this when needle bearings are used. If the housing is out of round, the needle bearing is not free to operate smoothly. After removing all foreign particles from the crankcase, valve chamber, etc., the assembly should be made such that the entire compressor is gastight. This calls for special care with gaskets and in building stuffing boxes that are reliable. On occasion, blowholes are found in the casting for the compressor, and these must be eliminated. It has been found best to break in a compressor by operating under no load condition for at least 10 hr. The oil to be used in the compressor should have a low vapor pressure, and the type used in standard vacuum pumps has been found adequate. Pressure gauges should be installed for each stage of compression and their standard operating pressure marked on the dial face so that performance can be checked at a glance. When installing the compressor and all component parts, it is important that ease of servicing and not economy of space be considered.

---

[1] Minneapolis-Honeywell type T415A.

[2] Black, Sivalls and Bryson Co., Kansas City, Mo.

Many modern low-temperature laboratories are now equipped with a Collins helium cryostat, and the compressor used for this does not require high pressure or very large volume flow. The compressor is driven by a 10-hp 220-volt a-c electric motor. The compressor delivers about 25 ft^3/min of helium at a pressure of about 200 psi at the fourth stage of compression. There are still many leading laboratories equipped with hydrogen liquefiers. These use very high pressure compressors. Such compressors should be installed by the manufacturer and elaborate safety precautions taken, not only against high-pressure ruptures but also against fire and explosion.

Gasholders

During liquefaction the helium gas is consumed at a rate of some 50 ft^3/hr. The fresh supply of helium gas comes from the commercially available cylinders[1] and is fed to a gasholder of capacity from 10 to 20 ft^3. It is desirable to pass the gas from the high-pressure cylinder supply through a charcoal trap immersed in liquid nitrogen so that all foreign particles and gases may be removed. The gasholder should be gastight, and it should not allow moisture from the atmosphere to diffuse into the pure helium being stored. Since it is desirable to pump the gasholder out at the beginning of each run, a type has been used in which the volume of the gasholder collapses as the gas is removed. An inexpensive and reliable type has been constructed from neoprene rubber. This is done by using two sheets cut as rectangles 12 by 4 ft. The edges are fastened together with rubber cement and then clamped with strips of wood 4 by 1 in. thick. The inlet tube resembles the construction of an automobile inner-tube connection. The gas envelope thus resembles two hands placed palm to palm. Actually each wall of the gas bag is a double layer of neoprene rubber, and between these layers are placed two overlapping aluminum sheets. With the swelling of the bag as gas enters, the thin aluminum sheets may slide over one another. It is also good to coat both sides of the aluminum sheet with a layer of petroleum jelly. Thus each wall of the gas bag is made up of an outer layer of neoprene rubber, an aluminum sheet coated with jelly, and an inner wall of neo-

---

[1] U.S. Bureau of Mines, Amarillo, Tex. (Grade A, oil-free).

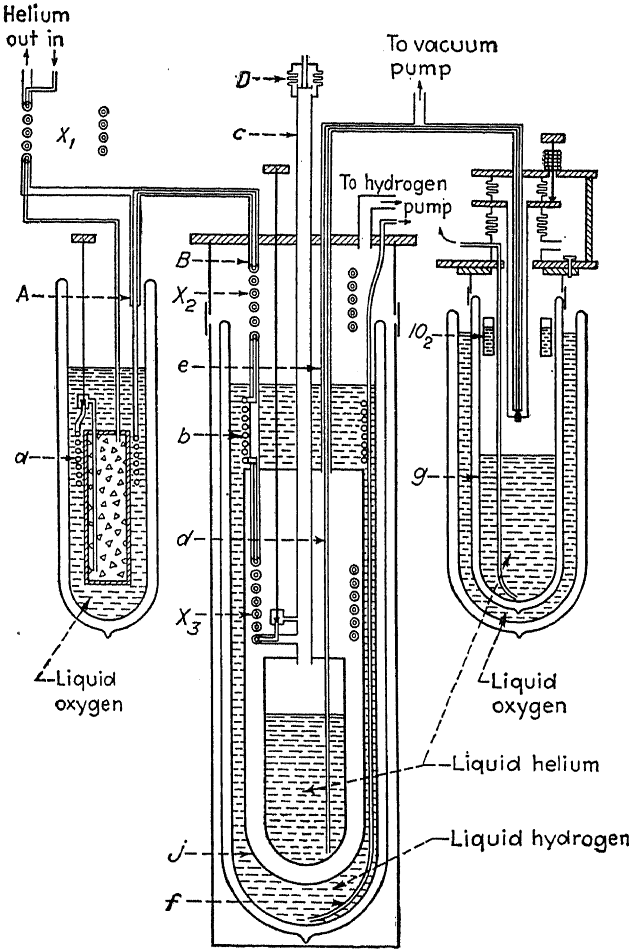

FIG. 2.1. Schematic diagram of helium liquefier together with precooling stage and a transfer vessel. (*Hercus and White, J. Sci. Instruments,* **28,** 4, 1951.)

prene. The bag may be hung from the ceiling in the vicinity of the compressor. Where helium gas is to be carefully conserved, it is necessary to have a small compressor capable of delivering high pressure such that the helium may be compressed back into storage cylinders or high-pressure tanks. It is always best to pass such gas through a liquid nitrogen trap to clean it up of oil. Safety valves on all storage bags and containers are important to prevent damage.

Helium Liquefiers

Helium was first liquefied by Kamerlingh Onnes at Leiden, Holland, by the use of liquid nitrogen and liquid hydrogen as precooling agents. Professor Onnes allowed the expansion of helium gas from high pressure to take place through a Joule-Thomson valve. Many other laboratories, such as the one at Berkeley, Calif., continue to use this proven technique. Figure 2.1 shows a simple helium liquefier which was based on this method and recently constructed at Oxford, England. At Oxford there are in use a number of cryostats where the Simon expansion bomb (Fig. 2.2) is used to produce small quantities of liquid helium. It will be noted that the method also uses liquid hydrogen as a precooling agent. The helium in the bomb is held at about 100 atm and cooled to about 12°K with the help of vigorously pumped hydrogen. The helium within the bomb is then allowed to expand, and the bomb is left with about 75 per cent of its volume filled with liquid helium at its normal boiling point.

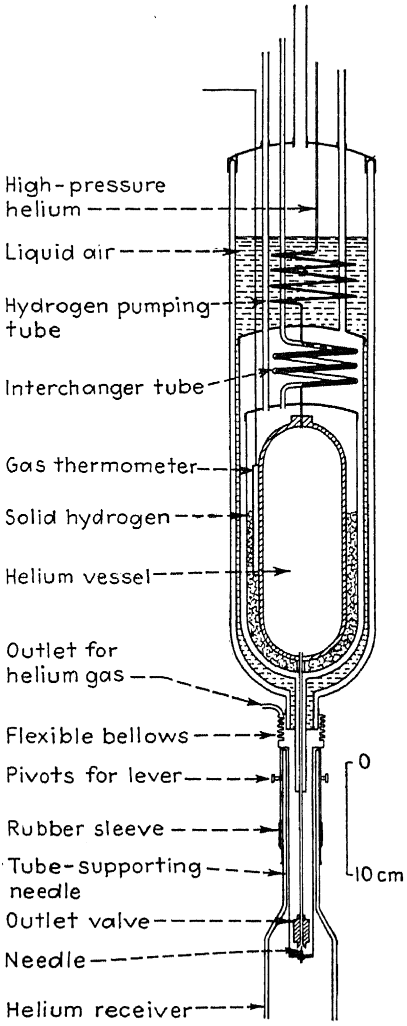

FIG. 2.2. Simon expansion bomb helium liquefier. (*Cooke, Rollin, and Simon, Rev. Sci. Instruments,* **10**, 251, 1939.)

At Cambridge, England, and in many laboratories in America and elsewhere the modified design of the helium liquefier first built by Peter Kapitza has been in use. Recently at M.I.T. a modification of the

Kapitza expansion engine was constructed by S. C. Collins.[1] We shall briefly describe this machine. Figure 2.3 shows the flow sheet for the Collins cryostat. The compressor unit delivers the gas to the top of the heat exchanger where it begins to be cooled by the mass of gas which has already run through the expander. In most cryostats there is provision to speed the cooling by heat interchange with liquid nitrogen supplied from an external source. The high-pressure gas then passes in parallel to three places where it may expand. Two of these are expansion pistons, as shown on the flow sheet (Fig. 2.3). The final expansion is where liquefaction takes place at the Joule-Thomson valve. Figure 2.4 shows the details of the expansion engine. The drive rod of the piston fits into a small well at the top and extends vertically out through the valve head to the top of the cryostat. The piston itself fits into the cylinder with a clearance of about 0.0005 in. on the diameter. The grooves in the piston serve to equalize gas pressure along the side and to keep the piston centered; also the grooves serve to prevent easy flow of the high-pressure gas along the walls to the exhaust side. The valve construction is difficult to make but simple as an idea. The intake gas enters the valve chamber and is denied entrance to the expansion chamber by the leather pad shown held down by the spring. The gas cannot escape out along the valve rod because it is housed by a tube which runs to the top of the cryostat where a stuffing box allows small motion of the valve rod without permitting the gas to escape. The valve rod lifts about $\frac{3}{32}$ in. so that high-pressure gas may enter the expansion chamber. At the bottom of the stroke of the piston, the exhaust port

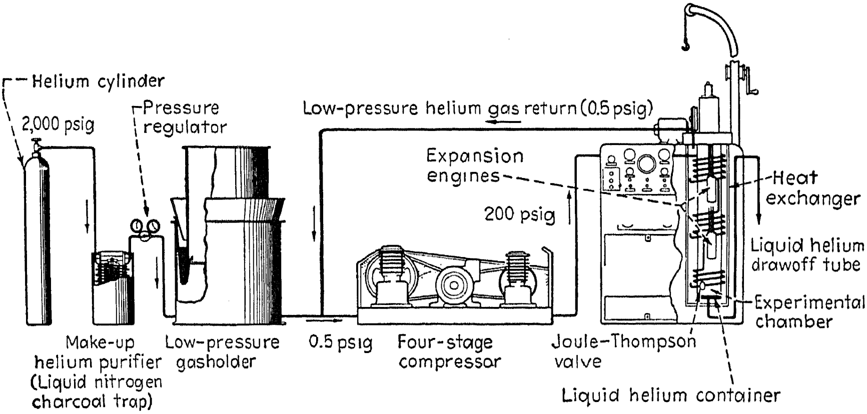

FIG. 2.3. Flow sheet for the Collins cryostat. There are over fifty such installations throughout the world.

---

[1] S. C. Collins, *Rev. Sci. Instruments*, **18**, 157, 1947; *Science*, **116**, 289, 1952.

opens, and the low-pressure gas passes on to the interchanger where it cools the incoming gas flow. The entire assembly of cylinder, piston, valve chamber, and valve rods is clamped together as shown in Fig. 2.4 and is held in alignment by a rigid stainless-steel tube extending to the top of the cryostat. The intake line and exhaust line are coupled to the interchanger with pressure couplings of standard refrigeration design, and the tubing is flexible copper bellows capable of withstanding the pressure used. Pipe wall thickness in inches, $t = PD/2S$, where P is maximum working pressure in psi, D is outside diameter in inches, and S = 4,000 psi for copper and brass tubing.

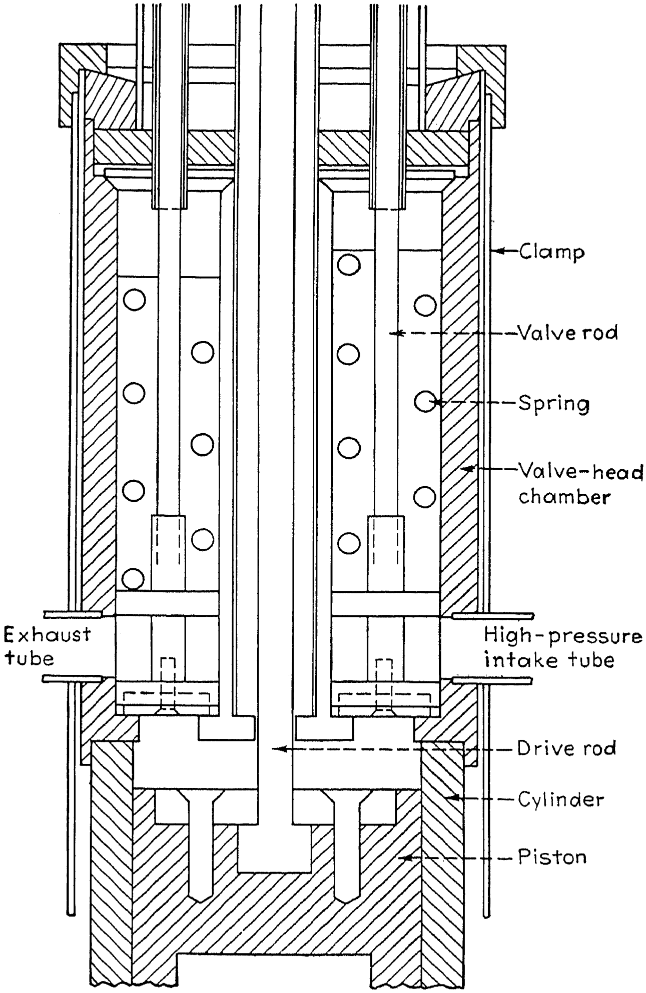

FIG. 2.4. Valve chamber for expansion engine.

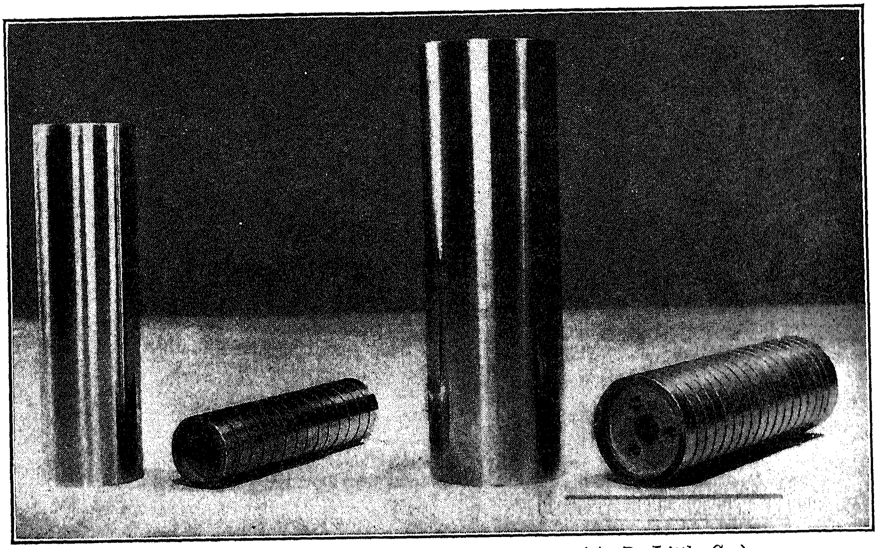

Piston and cylinder of expansion engines. (*A. D. Little Co.*)

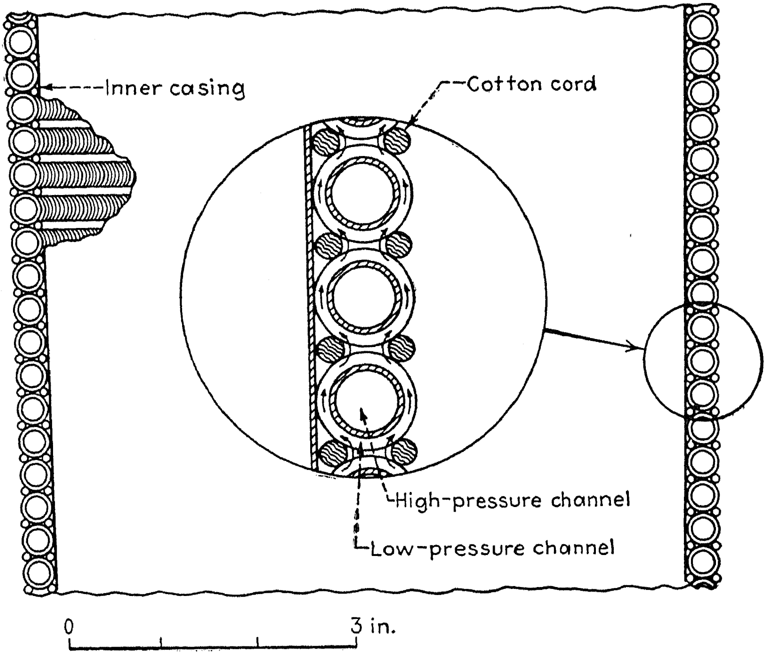

FIG. 2.5. Detail of heat exchanger for Collins cryostat.

The interchanger used in the Collins cryostat is shown in Fig. 2.5. It consists of thin-walled brass tubing wound as a helix on a large cone-shaped stainless-steel form. The entire interchanger is then fitted into the inner wall of the vacuum chamber of the cryostat. Thus the inner wall of the vacuum chamber forms the outer wall of the annular space allowed for the low-pressure gas. By soldering on thin copper strips made from flattening soft copper wire, the high-pressure tubing is given a fin. The fin runs helically along the tube length. The point about all this construction is that one has a very lightweight heat exchanger which is most efficient in operation. There has been a wide variation in the design of the mechanical arrangement at the top of the cryostat. This equipment permits the valve timing action and the removal of the mechanical energy imparted to the piston rods. A double-walled Monel metal tube with a vacuum between the walls is extended down into the

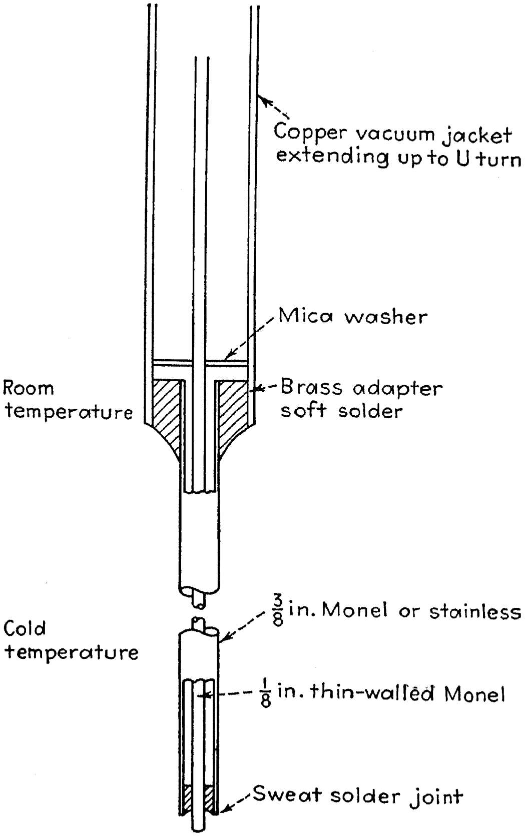
Copper vacuum jacket extending up to U turn
Mica washer
Room temperature
Brass adapter soft solder
Cold temperature
$\frac{3}{8}$ in. Monel or stainless
$\frac{1}{8}$ in. thin-walled Monel
Sweat solder joint

FIG. 2.6. Detail of vacuum-jacketed transfer tube.

liquid helium from the top of the cryostat. This allows the liquid helium to be drawn off into external flasks (Fig. 2.6).

This brief description of the Collins cryostat gives the idea of the machine but it is in no way detailed enough to permit construction. These machines are available as a commercial item.[1] Research men can literally push a button and some four hours later can tap off a considerable amount of liquid helium.

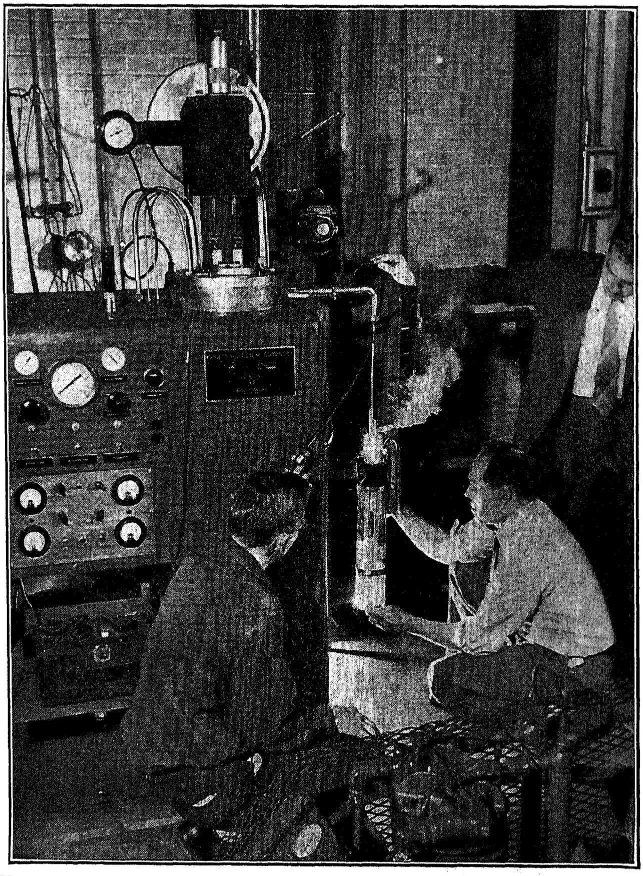

Transferring liquid helium to external Dewar. (*A. D. Little Co.*)

Storage Containers for Liquid Helium

It is sometimes useful to store the liquid helium in a container for many hours so that it may then be transported to the experimental cryostat. Giauque[2] has described such a vessel, and more recently

---

[1] A. D. Little Co., Cambridge, Mass.

[2] W. F. Giauque, *Rev. Sci. Instruments,* **18,** 852, 1947.

Wexler and Jacket[1] have described a new design. These vessels must be surrounded by liquid nitrogen and protected from radiation.

Liquid Hydrogen by Condensation

The production of liquid hydrogen without danger from high pressure and without elaborate equipment is now possible with the Collins cryostat. It goes without saying that liquid hydrogen can be made by the Linde process, and for large-scale production such a method is more efficient. In the Collins cryostat the helium gas is the refrigerant, and the hydrogen is condensed in a closed system of tubing, liquefaction chamber, and transfer tube. At 20°K the helium equipment simply receives the heat load of the condensed hydrogen, and the refrigeration produced goes into making liquid hydrogen. The hydrogen must be clean to avoid explosion. This means a charcoal trap at liquid nitrogen temperatures must be used to eliminate traces of oxygen from the high-pressure hydrogen supply cylinder. All safety precautions must be taken that air does not condense into the liquid hydrogen container. Fire and electric sparks must be kept at great distance.

Cryostats for Experiments

The cryostats used in many laboratories for measuring the properties of matter at low temperatures vary widely, and each has some unique feature and reason for its speciality. Occasionally experiments are done directly in the liquefier. Such methods are relatively crude, and one usually employs a cryostat in which the liquid temperature may be more accurately regulated.

In the liquid helium range the use of an inner Dewar flask to hold helium and an outer Dewar to hold the liquid nitrogen is common. Figure 2.7 shows the two-flask assembly for studies in the liquid helium range. The inner Dewar is of special construction because helium can diffuse through the Pyrex glass, and provision must be made to pump out the double-wall region before each use. Actually this arrangement has the advantage of allowing air to be in the double-wall portion during the cooling down to liquid nitrogen temperatures. After this cooling, one pumps to establish high vacuum insulation.[2] The inner Dewar in Fig. 2.7 becomes a single-wall tube at a ring seal which is just below the liquid nitrogen level. The top of the single-wall section terminates in the commercially available glass taper joint. In this case the glass is joined to a metal cap with the rubber gasket and is vacuumtight. Many laboratories have used a glass-to-metal seal for the upper part of the cryostat. They are not so rugged, and they are more expensive than the Pyrex glass pipe joint used in some cryostats (see Fig. 2.7). The Dewar flasks, both inner and outer, have clear windows or slits where the silver has not been allowed to deposit. In this way the helium level may be observed and equipment may be aligned.[1] It is not always convenient to insert a level indicator. Level indicators have been developed which are compact and certainly most useful. At Leiden the change of buoyance of a small bulb hung from a fiber and balanced by a spring is used as a level indicator. Even a ping-pong ball will float in liquid helium. At Rutgers University the liquid level is sometimes indicated by a wire of tantalum metal; that part dipped in the liquid is superconducting. In general the initial level is needed, and then the rate of evaporation can be taken by allowing the evolved gas to pass through

---

[1] A. Wexler and H. S. Jacket, *Rev. Sci. Instruments*, **22**, 282, 1951.

[2] These flasks are filled with liquid helium by using a vacuum-walled transfer tube extending to the bottom.

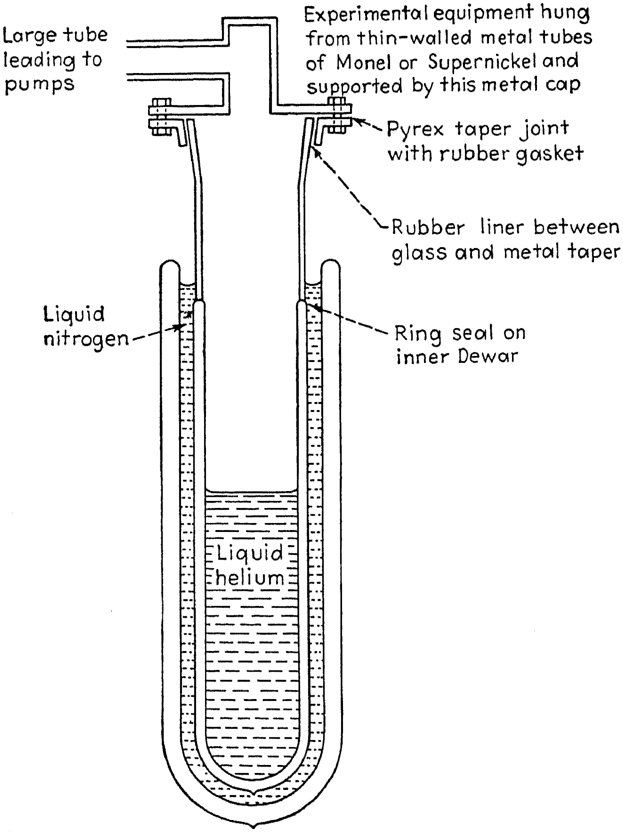
Large tube leading to pumps
Experimental equipment hung from thin-walled metal tubes of Monel or Supernickel and supported by this metal cap
Pyrex taper joint with rubber gasket
Rubber liner between glass and metal taper
Liquid nitrogen
Ring seal on inner Dewar
Liquid helium

FIG. 2.7. Cryostat for experiments at liquid helium temperatures.

---

[1] The use of reliable plastic apparatus at low temperatures has been described by W. F. Giauque *et al.*, *Rev. Sci. Instruments*, **23**, 169, 1952.

the gasometer. One liter of gas at standard conditions equals 1.3 cc of liquid helium. Another useful conversion is that 28 ft^3 of gas equals 1 liter of liquid helium. In cryostats such as that shown in Fig. 2.7 the rate of evaporation is from 20 to 100 cc/hr of liquid depending on heat leaks. Heat evolved from electrical or mechanical sources can require considerable liquid helium.

Cryostats for magnetic work at very low temperatures call for special construction of the Dewar, such that pole pieces of the electromagnet may be sufficiently close to permit maintenance of high magnetic fields.

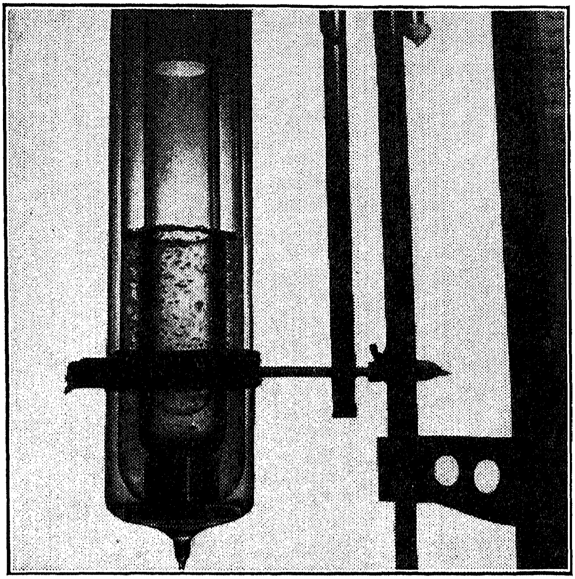

Liquid helium II surrounded by liquid nitrogen. (*R. Cavileer, M.I.T.*)

At Leiden ingeniously constructed multiwalled flasks are used. In Russia there have been some flasks with cleverly designed optically flat windows.[1] Those laboratories which produce liquid helium with the aid of liquid hydrogen usually surround the helium Dewar flask with a liquid hydrogen bath. Under these conditions the rate of evaporation of liquid helium is small indeed. There is no real question of which is the better method; a wide variation is possible, and one uses what one has and gets the research done.

It has often been observed with low-temperature liquids that spontaneous vibrations may occur in open tubes leading down to the liquid. The temperature of the tube containing the gas column varies markedly along its length. This results in a large amount of energy as pressure waves being pumped down into the liquid helium or hydrogen and boils away the liquid at a very rapid rate. When the phenomenon appears for any open-end tube, one may simply close off the end. The theory of these oscillations has not been given, although the work of H. A. Kramers and K. W. Taconis indicates that nonlinear differential equations may be required.[1] The quantum nature of these light gases plays a considerable role at low temperatures. The amplitude of the pressure oscillations is quite large, and atoms of helium can easily oscillate between a temperature region of 40 to 30°K. As we shall see in Chap. 3, the second virial coefficient changes sign in this region of temperature. At the high

---

[1] A cryostat for optical studies has been described by W. Duerig and I. Mador, *Rev. Sci. Instruments*, **23**, 421, 1952.

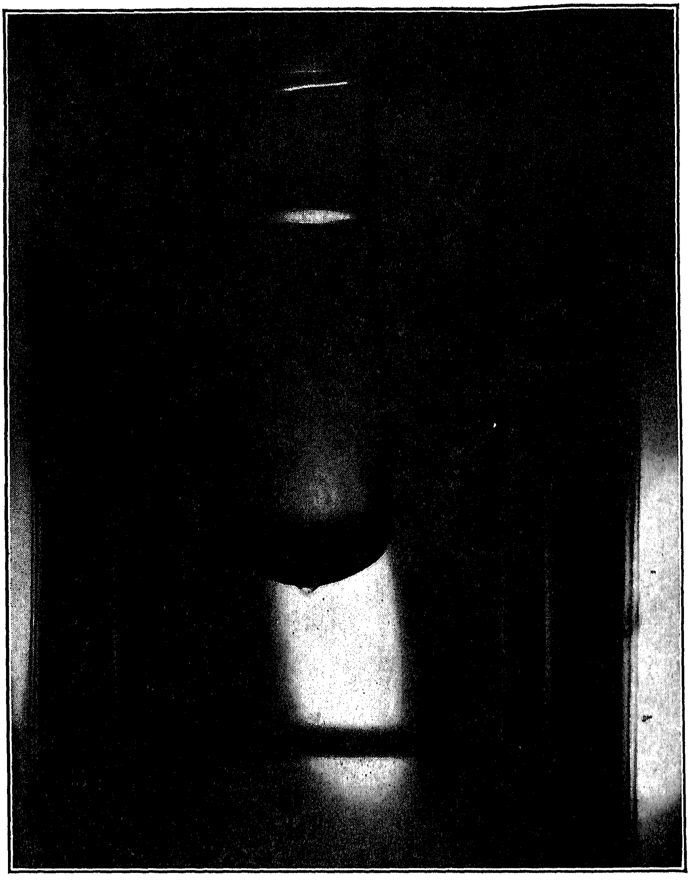

Superfluid helium II creeping over the sides of a small test tube and dripping off the bottom into the larger volume of helium II. (*A. D. Little Co.*)

---

[1] H. A. Kramers and K. W. Taconis, *Physica*, **15**, 733, 971, 1949.

temperature the atoms attract one another with a virial coefficient of positive sign. The situation presents an interesting problem.

Pumping on the liquid helium to produce temperatures in the region of 1°K requires a comprehension of the unusual properties of liquid helium (Chaps. 4 and 5). The peculiar creep property of liquid helium which exists at temperatures below 2.19°K permits it to flow against the gravitational potential to regions which are warmer. Such superfluid helium is called liquid helium II. The creep property makes it difficult to pump the bath down to very low temperatures. It is not so much a question of reducing the pressure by fast pumping as it is of reducing the available area across which the superfluid can flow. This is often done by placing a constriction whose diameter is such as to allow very little of the superfluid to flow through the orifice per unit of time. Owing to the zero viscosity of liquid helium II, one gets a considerable flow through a small orifice, and the pumps have trouble enough removing the evaporated quantities. In Fig. 2.7 we have shown a liquid helium cryostat without the constriction, but at the top there is a very large pumping line. Diffusion pumps of 2,000 liters/min capacity at a pressure of 0.1 mm may be placed in the line. The oil used is dibutyl phthalate, and the fore pump used must be of large capacity. Vapor pressures may be held constant over a bath of liquid by use of a sensitive hand-regulated valve which the operator adjusts according to indications from an oil differential manometer.

Temperature Measurements

Vapor Pressure of Liquid Helium. Tables of the vapor pressure of liquid helium are given in the Appendix. These tables were compiled under the direction of Professor D. Shoenberg, Cambridge University, England. We shall quote from his preface to the tables.[1]

> The usual method of measuring absolute temperature T in the liquid helium range is to measure the vapor pressure p and convert it by means of an empirically determined p-T relation. In the past, confusion has sometimes arisen owing to the existence of several determinations of the p-T relation which differ appreciably from each other. At an informal meeting between Great Britain and European laboratories held in Amsterdam in July 1948, it was decided to use an agreed[2] relation in the future and to present this relation in the form of tables for practical use. The most reliable existing data are not wholly satisfactory, but since they are unlikely to be superseded for some years it was thought best to make them the basis of the agreed relation until more accurate results are available.
>
> Between 0°K and 1.6°K it was agreed to base the relation on the formula of Bleaney and Simon.[3]

---

[1] D. Shoenberg, mimeographed tables, Cambridge University, England.

[2] H. van Dijk and D. Shoenberg, *Nature*, **164**, 151, 1949.

[3] B. Bleaney and F. Simon, *Trans. Faraday Soc.*, **35**, 1205, 1939.

$$\log_{10} p_{\mathrm{mm}} = -\frac{3.117}{T} + 2.5 \log_{10} T + 2.196 - 2.27 \times 10^{-3} T^3 + \Delta$$

where Δ is a small correction term whose dependence on T is given graphically and p is in mm. of Hg at 0°C. Above 1.6°K, it was agreed to base the relation on the scale of Schmidt and Keesom[1] (1937), given in the form of a graph of corrections to an earlier (Keesom, 1932) scale; Kistemaker[2] (1946) has suggested modifications between 1.6 and 2.19°K, but it was considered that they should not be used until confirmed by an independent method over a larger range of temperatures. Between 4.3°K and the critical point, 5.2°K, the only data are five pairs of values of p and T due to Kamerlingh Onnes and Weber[3] (1915); these can be represented by the interpolation formula

$$T = 2.967 + 1.905 \times 10^{-3} p_{\mathrm{mm}} - 3.52 \times 10^{-7} p_{\mathrm{mm}}^2$$

This formula departs at most by 0.03°K from the experimental points and joins smoothly on to the relation at 4.3°K.

The Kamerlingh Onnes Laboratory at Leiden computed a table (unpublished) of p (in mm of Hg at 20°C) as a function of T at intervals of T of 0.01°K based on the Bleaney and Simon formula from 1.0°K to 1.6°K and on the 1937 results from 1.6°K to 4.3°K, with smoothing in the region of the lambda point. Since this table is already used at Leiden, it was agreed to regard it as representing the most reliable information between 1.0°K and 4.3°K. This table is reproduced together with extensions below 1.0°K by the Bleaney and Simon formula, and above 4.3°K by the above-mentioned interpolation formula. Below 0.9°K and above 4.3°K it is unlikely that accurate values of p as a function of T will often be required, so values of p are given only at intervals of 0.1°K of T.

The computing accuracy between 1.0°K and 1.6°K is such that departures of as much as 1 in 300 from the Bleaney and Simon formula are not excluded but the departures of T for given p from the formula do not exceed 0.001°K. Between 1.6°K and 4.3°K the departures from the explicit formula of Keesom and Lignac[4] (also designed to represent the 1937 results), nowhere exceed a few thousandths of a degree, which is not greater than the inaccuracies of the original measurements.

For practical purposes, the most useful form of table is one which presents T as a function of p, since precision is more often required in translating an observed vapour pressure into absolute temperature than vice-versa. With the help of the Cambridge Mathematical Laboratory, the tables presented in these pages have been computed in this form from the information described above; p throughout is expressed in mm. of Hg at 20°C. The accuracy of the tables cannot, of course, be better than that of the data on which they are based, and it is unlikely that this is better than a few thousandths of a degree. Since, however, relative accuracy is sometimes important, care has been taken that the computing errors in deriving T as a function of P should nowhere exceed one unit in the last significant figure.

---

[1] G. Schmidt and W. Keesom, *Commun. Kamerlingh Onnes Lab. Univ. Leiden,* **250c**; *Physica,* **4**, 1937.

[2] J. Kistemaker, *Commun. Kamerlingh Onnes Lab. Univ. Leiden,* **269c**; *Physica,* **12**, 272, 1946.

[3] H. Kamerlingh Onnes and S. Weber, *Commun. Kamerlingh Onnes Lab. Univ. Leiden,* **147b**, 1915.

[4] W. Keesom, *Commun. Kamerlingh Omnes Lab. Univ. Leiden,* **71d**, 1932; W. Keesom and W. P. Lignac, *ibid.*, **90c**, 1939.

Figure A.1 shows the deviation between T_K according to Kistemaker[1] and the table of agreed temperature T_A.

Vapor Pressure of Liquid Hydrogen. There is a difficulty about the use of hydrogen as a thermometer, and that is the fact that the molecule of hydrogen is influenced by the relative orientations of the spins of the atomic nuclei. Two separate sets of available energy levels[2] are associated with the two possible molecular types which are known as para hydrogen and ortho hydrogen. Taking mixtures from a commercial cylinder (0.25 para hydrogen and 0.75 ortho hydrogen) and condensing this mixture to a liquid, there will result the vapor-pressure-against-temperature relation given by Table A.2. The values are from Wolley, Scott, and Brickwedde.[3] The mixture changes with time rather slowly, but this means that great accuracy cannot be claimed. Hoge and Arnold[4] have measured the vapor pressure for the equilibrium mixture at 20.4°K, and this is for 0.979 para hydrogen and 0.021 ortho hydrogen. The vapor pressure for this mixture at 20.4069°K is 789.6 mm Hg. The vapor pressure of liquid deuterium is of course entirely different by virtue of its mass, and here again the mixture is a problem. E. R. Grilly[5] has measured the vapor pressure of tritium, and numerical values can be found for it, together with values for hydrogen and deuterium, in his publications. Table 1.3 gives the normal boiling points of these liquids. The vapor pressure of liquid oxygen has been determined by Hoge,[6] and the values are given in Table A.3.

Equipment for Vapor-pressure Measurements. The vapor pressure of liquid gases can be measured by use of a manometer filled with clean mercury, as shown in Fig. 2.8. One side of the manometer is pumped out thoroughly, and the other side is connected by a gastight tube which enters the cryostat. The manometer is read with a cathetometer with its traveling telescope and vernier scale. Small McLeod gauges may be used below 1 mm Hg with care to ensure that absolute values are valid. Thermo-molecular pressure effects are small for wide tubes. The hydrostatic pressure of the helium bath must be accounted for in the determination of the temperature at a point in the bath. Where accuracy in temperature measurements is required in the liquid helium temperature range at 1°K and below, the magnetic susceptibility of a dilute paramagnetic salt is used (see Chap. 8).

---

[1] J. Kistemaker, *Commun. Kamerlingh Onnes Lab. Univ. Leiden*, **269c**; *Physica*, **12**, 272, 1946.

[2] D. M. Dennison, *Proc. Roy. Soc. (London)*, **115**, 483, 1927.

[3] R. Wolley, R. Scott, and F. Brickwedde, *J. Research Nat. Bur. Standards*, **41**, 379, 1948.

[4] H. Hoge and R. Arnold, *J. Research Nat. Bur. Standards*, **47**, 63, 1951.

[5] E. R. Grilly, *J. Research Nat. Bur. Standards*, **47**, 63, 1951; *J. Am. Chem. Soc.*, **73**, 843, 1951.

[6] H. Hoge, *J. Research Nat. Bur. Standards*, **44**, 321, 1950.

Constant-volume Gas Thermometer. The concept of temperature was given its thermodynamic foundation by Lord Kelvin, and this is stated for a reversible process:

$$T = \frac{\delta Q}{\delta S}$$

Under sufficiently low pressures and high temperatures the constant-volume gas thermometer approaches a nearly ideal primary standard for the direct measurement of the thermodynamic temperature. Different gases have different expansion coefficients so that at low temperatures and high pressures the deviation is considerable. On the other hand, the constant-volume gas thermometer is of no value at temperatures so high that the container melts or lets the gas diffuse through the walls. The ratio of the pressure read by the constant-volume thermometer at the steam point to the pressure read at the ice point becomes a constant for all gases approaching the ideal condition of smaller and smaller density. The numerical value of the constant is 1.36609 ± 0.00004. This constant ratio is also equal to the ratio of the temperature of the steam point to the temperature of the ice point. If the interval between these temperatures is called 100, then the steam-point temperature is 373.16 ± 0.03 and the ice-point temperature is 273.16 ± 0.03. By the steam point we mean equilibrium between the vapor and the liquid such that the vapor pressure is 760 mm Hg. The ice point is not so well defined because it is not the triple point; it is the temperature at which ice, and water, and air are in equilibrium such that the air has a barometric pressure of 760 mm. This is almost impossible for the normal laboratory to reproduce. A number of standard points may be taken from Table 1.3.

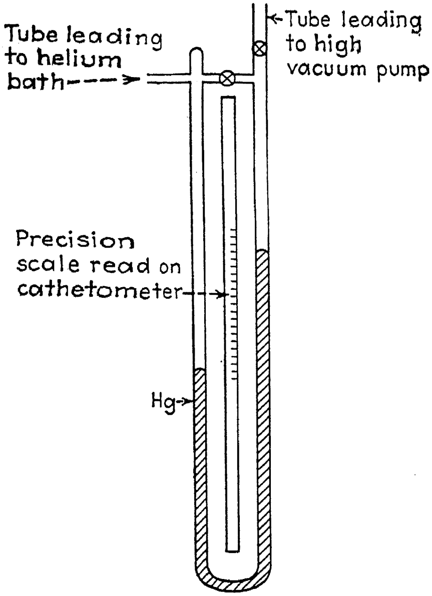
Tube leading to helium bath
Tube leading to high vacuum pump
Precision scale read on cathetometer
Hg

FIG. 2.8. Scheme of vapor-pressure-measuring equipment.

The constant-volume thermometer is shown in Fig. 2.9, and there are several features about its construction and operation which should be pointed out. In the first place, a cathetometer is used for reading the mercury levels corresponding to the different pressures required to keep the volume constant when the temperature in the bulb B changes. The tube leading from the bulb is a capillary whose volume is so small that the correction, though always made, is not a large correction. On the other hand, this tube must not be too small because thermo-pressure effects then become important. The capillary tube enters the dead space D at the top of the mercury column, and this space should be kept small. The adjustment of the height of the mercury is apparent from the figure. Helium gas is used in the primary thermometer, and the equation of state is taken from the series expansion. The virial coefficients for helium as a function of temperature are given in Chap. 3. The theory behind these virial coefficients and the equation of state is a most important problem in low-temperature physics as well as in thermometry.

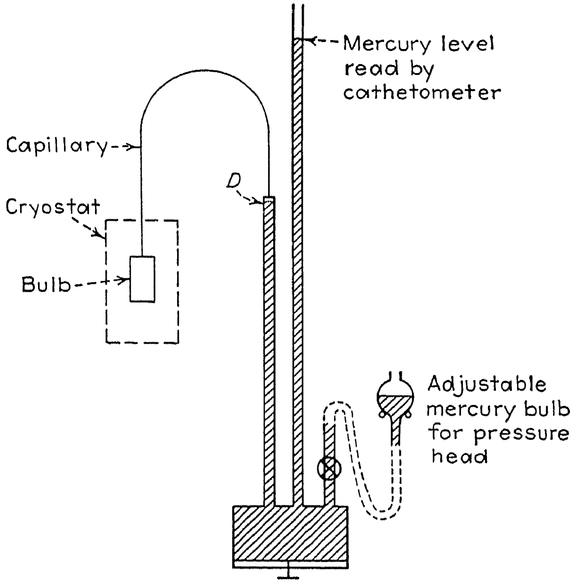

FIG. 2.9. Scheme of constant-volume gas thermometer.

Resistance Thermometer. A potential drop across an electrical resistance can be measured with great accuracy, and this permits a temperature determination which is very satisfactory where dR/dT is of sufficient size. Where rough values are adequate, a simple bridge or ohmmeter can be used.

Platinum wire as a resistance thermometer has come into use as an International Temperature Scale from -183 to $+660°C$. Once properly annealed and mounted, the thermometer is very reliable. Platinum wires of 0.05 mm diameter and slightly larger may be used at liquid helium temperatures by starting with 150 ohms at room temperature. Gold wire has been used for calorimetric work at liquid helium temperatures. Alloys of such type as phosphor bronze and constantan have become more popular (Fig. 2.10).

Carbon thermometers have been used with considerable ease, but they must be calibrated each time the cryostat is put in use. Boorse, Zemansky, and Brown[1] have reported using carbon thermometers for specific heat determinations between 2 and 20°K. Silicon and germanium have also been used but with some caution because they are very sensitive to impurities and are not ohmic resistors. Electric leads may be put on such resistors by applying a silver paste and baking in an oven. These sensitive semiconductor thermometers can rarely be relied upon to reproduce their extreme low-temperature resistance values once they have been brought back up to room temperature. This means that calibration against the vapor pressure of helium or hydrogen must be carried out on every experiment.

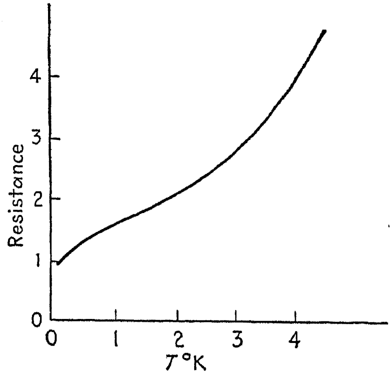

FIG. 2.10. Resistance of phosphor-bronze wire in zero magnetic field (*van Dijk and Keesom, Physica,* **7**, 970, 1940.)

Thermocouples. Copper-constantan thermocouples are used by most laboratories for rough measurements of temperature down to 50°K. They are easy to handle and take up almost no space in the experimental equipment. The intake and exhaust temperatures of the Collins machine show thermocouple differences of emf even below 20°K and thus give useful information.

Heat Flow into Cryostats

The design problem for every new experimental cryostat is that of the heat flow into the low-temperature bath. Most equipment is constructed with german silver or stainless steel as the structural link between the high temperature and the bath. Berman[2] has published a convenient table which gives the rate of heat flow along specimens of german silver and stainless steel, 10 cm by 1 mm^2 cross-sectional area, and along a constantan wire of 36 gauge (2.9×10^{-2} mm^2) and also 10 cm long, when the temperatures at the ends vary from 80 to 0°K. Table 2.1 gives the rate of heat flow along the specimen in watts. Berman has pointed out that 1 watt evaporates about 100 cc/hr of liquid hydrogen and about 1 litre/hr of liquid helium.

---

[1] H. Boorse, M. Zemansky, and N. Brown, *Phys. Rev.*, **84**, 1050, 1951; J. R. Clement and E. H. Quinnell, *Rev. Sci. Instruments*, **23**, 213, 1952.

[2] R. Berman, *Phil. Mag.*, **43**, 642, 1951.

TABLE 2.1. RATE OF HEAT FLOW ALONG SPECIMEN, WATTS

Temperatures at ends of specimen, °K		German silver, 10 cm long, 1 mm^2 cross section	Stainless steel, 10 cm long, 1 mm^2 cross section	Constantan, 36 gauge, (2.9×10^{-2} mm^2) 10 cm long
T_2	T_1			
80	20	8.0×10^{-3}	3.0×10^{-3}	2.7×10^{-4}
60	20	4.8×10^{-3}	1.7×10^{-3}	1.6×10^{-4}
20	4	5.8×10^{-4}	1.7×10^{-4}	2.1×10^{-5}
10	4	9.3×10^{-5}	3.1×10^{-5}	3.5×10^{-6}
4	1	1.0×10^{-5}	4.2×10^{-6}	3.5×10^{-7}
1	0	4.0×10^{-7}	1.8×10^{-7}	1.0×10^{-8}

CHAPTER 3

THEORETICAL CONSIDERATIONS OF THE EQUATION OF STATE

Classical Quantum Statistics

The expression $PV = nRT(1 + nB/V + n^2C/V + \cdots)$, where the virial coefficients B, C, etc., are functions of the intermolecular fields and of the temperature, is the equation of state we shall seek to justify. We shall now examine the statistical mechanics theory leading to this expression and, in doing so, establish the general background needed for an understanding of the recent research showing the large quantum effects in helium and hydrogen gases at low temperatures. It is nearly as easy to start with fundamental concepts and construct the statistical theory as to begin the discussion with well-known statistical partition functions and discuss their meaning and limitations. We shall use these statistical concepts in the theory of magnetism and elsewhere in this book, so it is useful to state the principles here.

The classical statistics allow one to compute the Helmholtz potential $A = U - TS$ rather easily, and from this we may compute the pressure from the relation $P = -(\partial A/\partial V)_T$. In using the classical statistics, we shall require that the quantum energy states available be so closely spaced as to permit integration where summation is more rigorously required. The classical statistics introduce the $6N$-dimensional phase space to describe the state of a system of N particles: $3N$ space coordinates and $3N$ momentum coordinates. The state of the system is specified by a point in phase space.

Next the concept of a large number of copies of this system is introduced, and this is called an assembly. The assembly is called a canonical assembly if no energy is fed in or out. However, there is exchange of energy within the degrees of freedom such that the point in $6N$-dimensional phase space may move with time to some other point consistent with the concept of constant energy. Indeed, a system spends an equal amount of time at every available point in phase space if one averages over a sufficiently large time interval. The canonical assembly is then determined by a cloud of representative points $(p_1,p_2, \ldots ,p_{3N},q_1,q_2, \ldots ,q_{3N} = p,q)$ in phase space. The probability Ω of finding the system chosen at random, in the volume element $dp\, dq$, is

$$\Omega(pq)\, dp\, dq = \frac{1}{N!h^{3N}} e^{[A-H(pq)]/kT}\, dp\, dq \tag{3.1}$$

where k is the Boltzmann constant, T is the absolute temperature, N is the number of particles in the system, h is Planck's constant, A is the Helmholtz potential, and H is the Hamiltonian expression for the total energy. The probability of finding the system somewhere in phase space is unity if we integrate over all of phase space:

$$\int \Omega(pq)\, dp\, dq = 1 \tag{3.2}$$

Thus we obtain by integration

$$e^{-A/kT} = \frac{1}{N!h^{3N}} \int e^{-H(pq)/kT}\, dp\, dq \tag{3.3}$$

The factor $N!$ arises from the indistinguishability of the particles in the system, and the term h^{3N} arises from the uncertainty principle for fundamental molecular particles. Using the well-known Sterling approximation $1/N! = (e/N)^N$, we may solve the above equation for the Helmholtz potential:

$$A = -kT \ln Z \tag{3.4}$$

The partition function Z is given by

$$Z = \left(\frac{e}{Nh^3}\right)^N \int \cdots \int e^{-H(pq)/kT}\, dp\, dq \tag{3.5}$$

To obtain the equation of state it is clear that one must first evaluate the partition function Z and from this use the above equation to compute the Helmholtz potential and finally to compute the gas pressure from $P = -(\partial A/\partial V)_T$.

Let us examine the partition function by writing out the Hamiltonian H for the total energy of all the particles within the system:

$$H = \sum_{i}^{3N} \tfrac{1}{2} m v_i^2 + \sum \text{(vibration, rotation) energy} + \sum_{i \neq j}^{N} \varphi(r_{ij}) \tag{3.6}$$

The last term, $\varphi(r_{ij})$, represents the potential energy of interaction of the particles. Denoting the part of the partition function involving the vibration and rotation of the molecules by Z^0, we may describe the total partition function by

$$Z = [Z^0]^N \left[\frac{e(2\pi mkT)^{\frac{3}{2}}}{Nh^3}\right]^N \int \cdots \int e^{-\Sigma\varphi(r_{ij})/kT}\, dq_1 \cdots dq_N \tag{3.7}$$

We have used the fact that the kinetic energy term $p^2/2m$ allows us to integrate over the momentum coordinates. The last term in the above equation is called the configuration integral, and it is the evaluation of this part of the total partition function which constitutes the major problem. We shall repeatedly return to the configuration integral.

It is perhaps useful to inject at this point a remark about the partition function formed from the quantum statistics:

$$Z = Z^0 \sum_n e^{-E_n/kT} \tag{3.8}$$

In this expression the characteristic energy values E_n are to be obtained from the quantum equation of Schrödinger:

$$(H - E_n)\psi_n = 0 \tag{3.9}$$

The potential function $\varphi(r_{ij})$ will appear in the Hamiltonian operator. We shall see that we must use the quantum expression for gases such as hydrogen and helium at temperatures below 50°K.

Returning now to the classical partition function, we see that, if we define a perfect gas as one having no interaction forces and if therefore we write $\varphi(r_{ij}) = 0$, we have

$$Z = [Z^0]^N \left[\frac{e(2\pi mkT)^{\frac{3}{2}}}{Nh^3}\right]^N V^N \tag{3.10}$$

The Helmholtz potential becomes from this partition function

$$A = -\tfrac{3}{2}NkT \ln T - NkT \ln V - NkT \ln Z^0 - \cdots - [NkT][\ln e(2\pi mk)^{\frac{3}{2}} - \ln Nh^3] \tag{3.11}$$

And from this we have $P = -(\partial A/\partial V)_T = NkT/V$, the equation of state for an ideal gas. Note that many of the terms in the Helmholtz potential play no role in the determination of the equation of state. We shall see that with the quantum statistics, even without the potential function, the equation of state for an ideal gas has a second virial coefficient which becomes important at low temperatures.

Lennard-Jones Potential

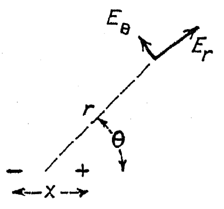

FIG. 3.1. Electric field of a dipole.

Since the potential energy term $\varphi(r_{ij})$ may not be neglected in all real gases, we must now investigate its dependence on interatomic distances. Let us think for the moment of the noble gases such as He, Ne, etc., and suppose that there is an instantaneous electric dipole $p = qx$, due to the electron cloud's being momentarily out of round. Figure 3.1 shows the dipole of charge q and separation x with the electric field at some distant point located at r from the center of the dipole. The electric field E in units of volts per meter has the components

$$E_r = -\frac{\partial V}{\partial r} = 2p\cos\frac{\theta}{\epsilon_0 r^3} \tag{3.12}$$

$$E_\theta = -\frac{\partial V}{\partial r}\frac{1}{r} = p\sin\frac{\theta}{\epsilon_0 r^3} \tag{3.13}$$

In these last two equations the symbol V is the electric potential. Now the force exerted on a molecule placed in the electric dipole field arises from the fact that the electric field can induce an electric dipole, and this will always pull the induced dipole toward the original dipole. The magnitude of the attractive force depends on the ease with which the electric field may induce a dipole, *i.e.*, the polarizability α of the molecule, and on the distance of separation. These matters are taken up again in Chap. 10, and we shall here make use of the well-known relation for the force on a dielectric placed in a field E:

$$F = \frac{1}{2} n\alpha \frac{d}{dr} (E^2) \cdot \text{volume} \tag{3.14}$$

where there are n dipoles per unit volume. From the electric field components of the original dipole we see that the force is proportional to the inverse seventh power of the distance of separation:

$$F \approx \frac{d}{dr}\left(\frac{1}{r^3}\right)^2 \approx \frac{1}{r^7} \tag{3.15}$$

The potential energy averaged over all directions is $\varphi(r) = a/r^6$, where the constant a is characteristic for each type of gas and is proportional to the volume of the molecule and to its polarizability.[1]

As the molecules approach more closely, a repulsive term arises from the electric charges of one atom on the other. This is extremely strong at close distances and gives the molecules the character of hard spheres. We may therefore write the potential term as the sum of a repulsive and an attractive term which together are known as the Lennard-Jones potential:

$$\varphi(r) = 4\epsilon\left[\left(\frac{\sigma}{r}\right)^{12} - \left(\frac{\sigma}{r}\right)^{6}\right] \tag{3.16}$$

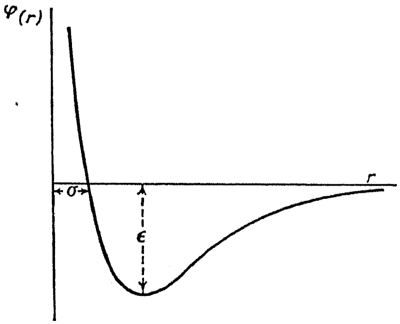

FIG. 3.2. Lennard-Jones potential for spherical nonpolar gases. [*Proc. Roy. Soc.* (*London*), **A163**, 63, 1937; *Physica*, **4**, 941, 1937.]

The potential function is represented in Fig. 3.2, and holds for gases, such as helium, neon, and argon, for which the potential field is spherical. Even so we shall use it for hydrogen, nitrogen, and other gases. The repulsive term is taken as proportional to $1/r^{12}$ for simplicity of calculation, and so far as our knowledge of the law is concerned it could be $1/r^{10}$ or $1/r^{14}$. Some authors have used an exponential term for repulsion of the form e^{-ar}. Each gas has two characteristic constants, σ and ϵ, if the above equation is valid. These values for a few gases are given in Table 3.1. Physically, ϵ is the depth of the potential energy well, and σ is the distance at which the potential energy is zero. It will be the task of much of the rest of this chapter to show how these constants are determined from experiments on the equation of state. In Table 3.1 the values of σ and ϵ are taken from (*a*) the work of J. De Boer and (*b*) that of J. Hirschfelder *et al.*

---

[1] R. Fowler, "Statistical Mechanics," Chap. 10, London, Cambridge, 1936.

In Table 3.1 the column marked $P^*_{\text{crit.}}$ and the column marked $T^*_{\text{crit.}}$ are given for these gases in order to show the law of corresponding states and to indicate how well-known the value of σ and ϵ must be. These dimensionless quantities are obtained by using the characteristic parameters σ and ϵ for each particular gas in the following way:

$$\begin{aligned} P^*_{\text{crit.}} &= \frac{\sigma^3}{\epsilon} P_{\text{crit.}} \\ T^*_{\text{crit.}} &= \frac{k}{\epsilon} T_{\text{crit.}} \end{aligned} \tag{3.17}$$

These columns show that for the heavy gases the reduced critical pressure and reduced critical temperature are nearly constant. On the other hand, the gases H_2 and He show the striking influence of quantum effects.

TABLE 3.1. CHARACTERISTIC CONSTANTS IN THE LENNARD-JONES POTENTIAL (ALSO THE REDUCED CRITICAL PRESSURE AND TEMPERATURE)

Gas	$\epsilon \times 10^{16}$ ergs		$\sigma \times 10^8$ cm		$P^*_{\text{crit.}}$		$T^*_{\text{crit.}}$	
	(*a*)	(*b*)	(*a*)	(*b*)	(*a*)	(*b*)	(*a*)	(*b*)
Xe	318	......	3.92	.....	0.122	.....	1.26	
Kr	230	......	3.65	.....	0.177	.....	1.26	
A	165	171.1	3.41	3.418	0.116	0.113	1.25	1.22
N_2	132.4	126.2	3.72	3.680	0.132	0.134	1.30	1.38
Ne	48.82	49.3	2.74	2.80	0.114	0.117	1.26	1.24
H_2	50.75	46.0	2.92	2.968	0.063	0.074	0.90	1.00
He^4	14.03	8.33	2.56	2.70	0.027	0.054	0.51	0.87
He^3	14.03	......	2.56	.....	0.013	.....	0.32	

$$P^*_{\text{crit.}} = P_{\text{crit.}} \frac{\sigma^3}{\epsilon} \quad \text{and} \quad T^*_{\text{crit.}} = T_{\text{crit.}} \frac{k}{\epsilon}$$

[a] J. De Boer, *Physica,* **14,** 139, 1948.

[b] J. Hirschfelder *et al., J. Chem. Phys.,* **18,** 1484, 1950.

For these very light gases $P^*_{\text{crit.}}$ and $T^*_{\text{crit.}}$ do not stay constant. It will be noticed that the large values of ϵ for a given gas correspond to the large value of the constant a for that gas in the van der Waals equation of state.

Second Virial Coefficient in Classical Statistics

We are now ready to put the Lennard-Jones potential into the configuration integral of the partition function (omitting vibration and rotation of the molecule). The partition function is

$$Z = \left[\frac{e(2\pi mkT)^{\frac{3}{2}}}{Nh^3}\right]^N \int \cdots \int e^{-\sum\limits^{i \neq j} \varphi(r_{ij})/kT} dq_1 \cdots dq_N \quad (3.18)$$

The configurational integral can be handled in the manner described by J. C. Slater.[1] In the following expression the Nth particle is separated out, and interaction is considered with all the other particles, $N - 1$ in number:

$$\int \cdots \int e^{-\Sigma\varphi(r_{ij})/kT} dq_1 \cdots dq_N = \int \cdots \int e^{-\Sigma'\varphi(r)/kT} dq_1 \cdots dq_{N-1} \cdot \int e^{-\sum\limits^{i \neq N} \varphi(r_{iN})/kT} dq_N \quad (3.19)$$

The last term on the right in the above equation is a single integral over the coordinates of the Nth particle, and this may be expressed as a quantity defining the integral W:

$$\begin{aligned} \int e^{-\sum\limits^{i \neq N} \varphi(r_{iN})/kT} dx_N\, dy_N\, dz_N &= \int dx_N\, dy_N\, dz_N \\ &\quad - \int (1 - e^{-\Sigma\varphi(r_{iN})/kT})\, dx_N\, dy_N\, dz_N \\ &= V - W \end{aligned} \quad (3.20)$$

Now those atoms which are far away from the Nth atom contribute nothing, while each atom that is close by contributes the quantity (small w)

$$w = \int (1 - e^{-\varphi(r_{iN})/kT})\, dx\, dy\, dz \cong \int_0^\infty 4\pi r^2 (1 - e^{-\varphi(r)/kT})\, dr \quad (3.21)$$

The limits of integration are taken as infinity because of the rapid falling off of the attraction force with distance. In this way the integral expression W may be written

$$W = (N - 1)w \quad (3.22)$$

Separating out the $(N - 1)$th particle, the total configuration integral may be written

$$\int \cdots \int e^{-\sum\limits^{i \neq j} \varphi(r_{ij})/kT} dq_1 \cdots dq_N = \int \cdots \int e^{-\Sigma''\varphi(r)/kT} dq_1 \cdots dq_{N-2} \cdot [V - (N - 2)w][V - (N - 1)w] \quad (3.23)$$

Continuing this process, we obtain a series expression which may be put into the complete partition function. Under the condition that Nw/V is small, the logarithm of the partition function becomes

$$\ln Z = N \ln \frac{e(2\pi mkT)^{\frac{3}{2}}}{Nh^3} + N \ln V - \frac{N^2 w}{2V} \quad (3.24)$$

[1] J. C. Slater, "Introduction to Chemical Physics," p. 192, New York, McGraw-Hill, 1939.

The pressure of the gas is then

$$P = -\left(\frac{\partial A}{\partial V}\right)_T = \frac{nRT}{V} + RT\left(\frac{n^2 N_0 w}{2V^2}\right) \tag{3.25}$$

The equation of state with number of moles n may be written

$$\frac{PV}{nRT} = \left(1 + \frac{nN_0 w}{2V}\right) = 1 + \frac{nB}{V} \tag{3.26}$$

where N_0 is the Avogadro number and B is the second virial coefficient

$$B = \frac{N_0 w}{2} = N_0 2\pi \int_0^\infty (1 - e^{-\varphi(r)/kT}) r^2\, dr \tag{3.27}$$

This last equation is the classical expression for the second virial coefficient. In the equation the term $\exp[-\varphi(r)/kT]$ has a quantum-mechanical meaning: it is the probability of finding two molecules a distance r apart from each other. In quantum statistics this probability would be

$$\sum_n e^{-E_n/kT} \psi_n^* \psi_n \tag{3.28}$$

where E_n and ψ_n are the characteristic energies and functions of the relative motion of the two molecules with respect to each other. The quantities are normalized so that for large r the sum is unity. In this connection we shall presently refer to the work of Uhlenbeck and Beth.[1] For the moment we shall be general about the probability function and write for the second virial coefficient

$$B = -\left[\frac{N}{2}\right] \int [W(q_1 q_2) - 1]\, dq_1\, dq_2 \tag{3.29}$$

Lennard-Jones[2] used his well-known potential function in the classical expression for the second virial coefficient in order to obtain the coefficient for a number of gases. Lennard-Jones gives the expression

$$B = \frac{2\pi N\sigma^3}{3} \sum_{s=0}^{\infty} a_s \left(\frac{4\epsilon}{kT}\right)^{\frac{1}{4}+s/2} \tag{3.30}$$

where the quantity

$$a_s = -3\, \frac{\Gamma[s(6-3)/12]}{12 \cdot s!} \tag{3.31}$$

and where Γ is the gamma function. If one already knows the potential function parameters σ and ϵ, then the virial coefficient may be computed; otherwise one determines the values σ and ϵ from a fit of the theory with the experimentally determined values of the second coefficient.

---

[1] G. Uhlenbeck and E. Beth, *Physica*, **3**, 729, 1936; *ibid.*, **4**, 915, 1937.

[2] J. Lennard-Jones, *Physica*, **4**, 941, 1937.

Recently Hirschfelder and coworkers[1] determined the values of σ and ϵ from viscosity data determined by Johnston and McCloskey.[2] These are listed in Table 3.1, and are in fair agreement with the values of De Boer except for the light gases. We shall presently consider the values for σ and ϵ determined by De Boer.

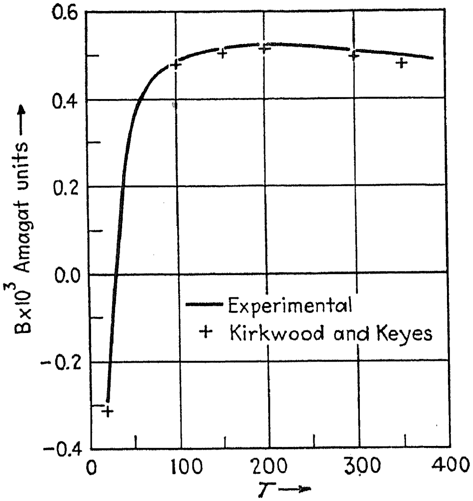

FIG. 3.3. Second virial coefficient for helium as a function of temperature.

Slater and Kirkwood[3] and Kirkwood and Keyes[4] have used the potential function (for helium gas)

$$\varphi(r) = \left[7.7e^{-2.43r/a_0} - \frac{0.68}{(r/a_0)^6}\right] \times 10^{-10} \qquad \text{ergs} \tag{3.32}$$

In the last equation a_0 is the radius of the Bohr orbit, $.529 \times 10^{-8}$ cm. These authors then computed the second virial coefficient. The results of their calculation are shown in Fig. 3.3, and the agreement in the high-temperature range is very good.

Third Virial Coefficient in Classical Statistics

The third virial coefficient arises from the interaction of three molecules in collision distance from one another so that they form a cluster (see

---

[1] J. Hirschfelder *et al.*, *J. Chem. Phys.*, **16**, 968, 1948.

[2] H. Johnston and K. McCloskey, *J. Phys. & Colloid Chem.*, **44**, 1038, 1939.

[3] J. Slater and J. Kirkwood, *Phys. Rev.*, **37**, 682, 1931.

[4] J. Kirkwood and F. Keyes, *Phys. Rev.*, **37**, 832, 1931.

Uhlenbeck and Beth[1]). The coefficient is

$$C(T) = -\frac{1}{3V}\int \cdots \int f_{12}f_{23}f_{31}\,dq_1\,dq_2\,dq_3 \tag{3.33}$$

where

$$f_{ij} = e^{-\varphi(r_{ij})/kT} - 1 \tag{3.34}$$

and where the Lennard-Jones potential $\varphi(r_{ij})$ is used as before with the distance r_{ij} between two of the three molecules. The coordinates of the ith molecule are denoted by dq_i. The force between any two molecules is assumed to be independent of the location of the third molecule in the cluster. Such a first approximation, while undoubtedly crude, is necessary for a computation. Kihara[2] reduced the integral to a complicated expansion somewhat analogous to the method used by Lennard-Jones. The calculations by Kihara are in good agreement with experiment. Recently Bird, Spotz, and Hirschfelder[3] published punched-card calculations of the third virial coefficients. In terms of the reduced temperature $T^* = kT/\epsilon$, the third virial coefficient is given by

$$C(T) = \left(\frac{2\pi N\sigma^3}{3}\right)^2 C_0(T^*) \tag{3.35}$$

The values of C_0 as a function of T^* are given in Table 3.2, and it is to be understood that Hirschfelder *et al.* computed these reduced third virial coefficients so that the third virial coefficient could be deduced for any gas at any temperature by means of the proper parameters of σ and ϵ for that gas. Of course not too low temperatures may be used, and in particular there is not good agreement with hydrogen, deuterium, and helium. Table 3.3 gives the adopted values from all experimental work on the second and third virial coefficient for helium gas.

TABLE 3.2. THIRD VIRIAL COEFFICIENT IN REDUCED COORDINATES[a]

T^*	$C_0(T^*)$	T^*	$C_0(T^*)$	T^*	$C_0(T^*)$
0.70	−3.37664	1.25	0.59326	3.20	0.34491
0.75	−1.79197	1.50	0.54339	3.60	0.33407
0.80	−0.84953	1.75	0.48320	4.00	0.32662
0.85	−0.27657	2.00	0.43710	4.50	0.32000
0.90	+0.07650	2.30	0.39900	5.0	0.31508
0.95	0.29509	2.60	0.37378	6.0	0.30771
1.00	0.42966	2.90	0.35675	9.0	0.29103

[a] R. Bird, E. Spotz, and J. Hirschfelder, *J. Chem. Phys.*, **18**, 1395, 1950.

---

[1] G. Uhlenbeck and E. Beth, *Physica*, **3**, 729, 1936.

[2] T. Kihara, *J. Phys. Soc. Japan*, **3**, 265, 1948.

[3] R. Bird, E. Spotz, and J. Hirschfelder, *J. Chem. Phys.*, **18**, 1395, 1950.

TABLE 3.3. SECOND AND THIRD VIRIAL COEFFICIENTS FOR HELIUM GAS[a]

T, °K	B, cm^3	C, cm^6	T, °K	B, cm^3	C, cm^6
2.6	−119		22	−2.26	455
3.0	−109		30	2.42	420
3.1	−106	-5.55×10^3	40	5.63	384
3.5	− 94	-1.21×10^3	50	7.59	354
4.0	− 81	-0.303×10^3	60	8.86	328
4.5	− 70.5	151	70	9.76	308
5.0	− 62.1	323	80	10.35	293
6	− 49.1	460	90	10.76	278
8	− 33.0	515	123	11.4	243
10	− 23.3	520	173	11.70	202
12	− 16.95	510	273	11.48	157
14	− 12.3	500	373	11.06	126
16	− 8.86	490	473	10.59	100
18	− 6.19	480	573	10.10	100
20	− 4.04	470			

[a] W. H. Keesom, "Helium," p. 49, Amsterdam, Elsevier, 1942.

De Boer Theory of the Equation of State

J. De Boer and R. Lunbeck[1] computed the vapor pressure of the helium isotope He^3 and published the work in 1948. Well after this prediction was made, the isotope He^3 was obtained in quantity, and the vapor pressure was measured by Sydoriak, Grilly, and Hammel[2] in 1949.

TABLE 3.4. VAPOR PRESSURE OF HELIUM ISOTOPE HE^3

T,°K	Theory,[a] cm Hg	Experiment,[b] cm Hg
2.0	14	15
2.4	27	30
2.8	48	50
3.0	59	63
3.2	75	76.4
3.4	88	

[a] Critical pressure, 0.9 to 1.2 atm; critical temperature, 3.2 to 3.5 °K; J. De Boer, *Physica*, **14**, 510, 1948.

[b] Critical pressure, 875 mm Hg; critical temperature, 3.34 °K; S. Sydoriak, E. Grilly, and E. Hammel, *Phys. Rev.*, **75**, 303, 1949.

The excellent agreement is brought out in Table 3.4, which gives the vapor pressure from the De Boer theory and from the experiments of the Los Alamos laboratories. Such a successful theory, which De Boer calls a new law of corresponding states, deserves our careful attention because it gives valuable information about the second virial coefficient of helium, hydrogen, and deuterium at extremely low temperatures. The importance of quantum statistics is measured by a parameter $\Lambda^* = h/\sigma\sqrt{m\epsilon}$, where h is Planck's constant, σ and ϵ are the potential constants, and m is the mass of the molecule. Table 3.5 gives this parameter Λ^* for several gases. It was first introduced by Uhlenbeck and Beth.[1]

---

[1] J. De Boer and R. Lunbeck, *Physica*, **14**, 510, 1948.

[2] S. Sydoriak, E. Grilly, and E. Hammel, *Phys. Rev.*, **75**, 303, 1949.

TABLE 3.5. QUANTUM PARAMETER FOR SOME GASES

Gas	Λ^*
Xe	0.064
Kr	0.102
A	0.187
N_2	0.225
Ne	0.591
D_2	1.22
H_2	1.73
He^4	2.64
He^3	3.05

In functional form, the new equation of state is defined

$$P^* = f(V^*,T^*,\Lambda^*) \tag{3.36}$$

The reduced parameters are defined as

$$P^* = \frac{P\sigma^3}{\epsilon}, \qquad V^* = \frac{V}{N\sigma^3}, \qquad T^* = \frac{kT}{\epsilon}, \qquad \Lambda^* = \frac{h}{\sigma\sqrt{m\epsilon}} \tag{3.37}$$

The values of P^* and of T^* at the critical point were given in Table 3.1 for a number of gases. We see from Table 3.5 that the value of Λ^* becomes quite large for hydrogen, deuterium, and helium; this large value is indicative of quantum effects at low temperatures. The parameter Λ^* may be identified with a sort of de Broglie wave length of relative motion of two molecules with energy ϵ. Only at low temperatures does $kT = \epsilon$. The true de Broglie wave length $\lambda = h/\sqrt{mkT}$ becomes large compared to the dimensions of the potential field for a gas like helium at 5°K. We shall presently see how the parameter Λ^* enters naturally into the statistics. But first let us simply use it, as De Boer did, to compute the critical points and the vapor pressure of the isotope He^3.

In Fig. 3.4 the values of $P^*_{\text{crit.}}$ taken from Table 3.1 are plotted against Λ^* for the gases Xe, Ne, D_2, H_2, He^4, and He^3. The value of Λ^* for He^3 is obtained by multiplying the value for He^4 by the factor $(\frac{4}{3})^{\frac{1}{2}}$. This is justified because the mass difference is the only quantity to be considered since the outer electron configuration remains unchanged and the potential field $\varphi(r)$ has the same parameters σ and ϵ for both isotopes of helium. In Fig. 3.4 the straight-line plot of $P^*_{\text{crit.}}$ vs. Λ^* allows one to read off the $P^*_{\text{crit.}}$ value for the isotope He^3, and this predicted value,

---

[1] G. Uhlenbeck and E. Beth, *Physica*, **3**, 729, 1936; *ibid.*, **4**, 915, 1937.

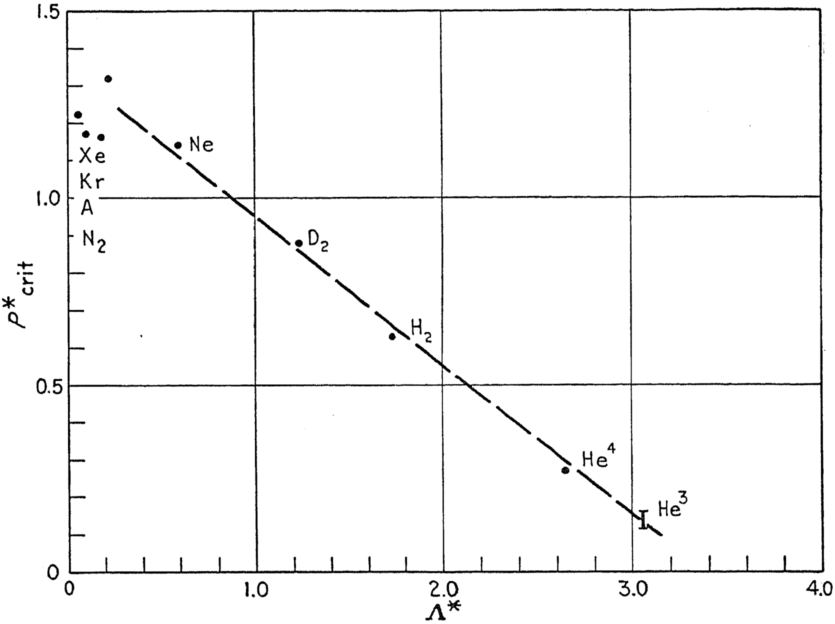

FIG. 3.4. Plot of reduced critical pressure $P^*_{crit.}$ vs. parameter Λ^*.

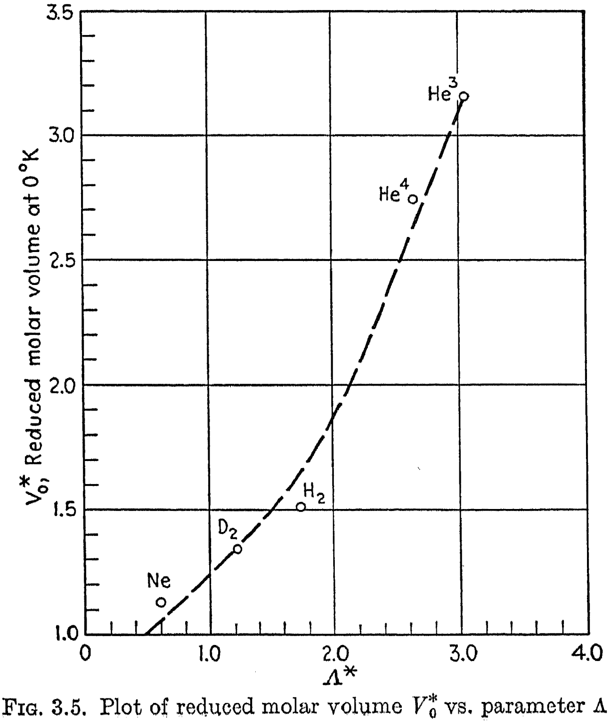

FIG. 3.5. Plot of reduced molar volume V_0^* vs. parameter Λ^*,

transformed to $P_{\text{crit.}}$, was observed experimentally. Similarly, the plot of $T^*_{\text{crit.}}$ vs. Λ^* gives the observed value for the new isotope of helium. In Fig. 3.5 the volume per mole at the absolute zero of temperature is transformed to the reduced volume $V_0^* = V_0/N\sigma^3$ and the new quantity plotted against Λ^* for several gases. This illustrates the "blowing up" or large volume of the condensed phase by large quantum effects for the light gases.

Finally in Fig. 3.6 we include De Boer's plot of the reduced vapor pressures from which the vapor pressure of He³ was deduced and in which again the departure of the very light element gases from the classical value is attributed to quantum effects, *i.e.*, a large Λ^*. An interesting feature about the vapor-pressure curve is that the usual integration of the Clapeyron equation gives the expression

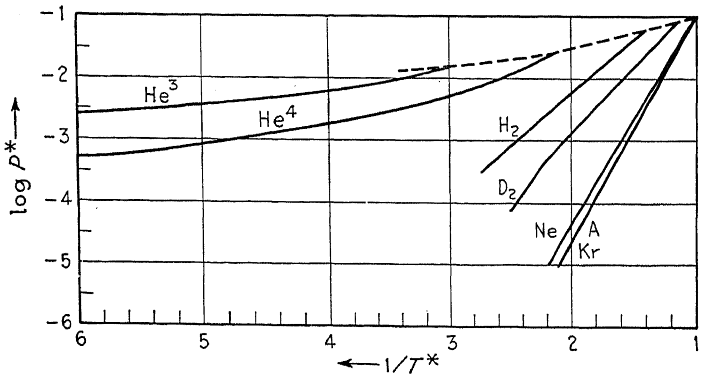

FIG. 3.6. Reduced vapor pressure P^* as a function of $1/T^*$.

$$\ln P = \frac{U_0}{RT} + \frac{5}{2} \ln T + C + \text{terms due to internal energy} \tag{3.38}$$

where U_0 is the latent heat of vaporization at the absolute zero and C the chemical constant. For He⁴ the latent heat at 0°K is extrapolated as 14.2 cal/mole, the chemical constant is

$$C = \ln \frac{(2\pi m)^{\frac{3}{2}} k^{\frac{5}{2}}}{h^3} \tag{3.39}$$

and the vapor-pressure equation becomes with the base 10 (in centimeters of Hg)

$$\log P_{\text{cm}} = -\frac{3.117}{T} + \frac{5}{2} \log T + 1.196 \tag{3.40}$$

The latent heat of vaporization for He³ may be obtained from a plot of U_0^* vs. Λ^* in a way similar to that shown in Figs. 3.4 and 3.5. The result is 5.1 cal/mole. This new value and the new chemical constant (changed by the mass) give the vapor pressure for He^3:

$$\log P_{\text{cm}} = -\frac{1.12}{T} + \frac{5}{2}\log T + 1.01 \tag{3.41}$$

and this equation is in good agreement with the values taken from the plot of Fig. 3.6.

It is worthy of note that the isotope He^3 nearly failed to liquefy at any temperature, so small is the latent heat. All of this is brought about by the very large zero-point energy of He^3. We shall return to a discussion of this point in examining the properties of liquid helium. What has been done in the last few paragraphs is to lay out the properties of gases in terms of the new theory of De Boer. If one knows that a new theory fits experiment, then one approaches an understanding of the theory with more vigor. Let us examine the meaning of Λ^*.

In the classical equation for the partition function we may now substitute into the configuration integral the dimensionless parameters $T^* = kT/\epsilon$ and $r^* = r/\sigma$ so that

$$Z = \left[\frac{e(2\pi mkT)^{\frac{3}{2}}}{Nh^3}\right]^N \sigma^{3N} \int_{V^*} \cdots \int e^{-\Sigma\varphi(r_{ij}^*)/T^*}\, dr_1^* \cdots dr_N^* \tag{3.42}$$

The partition function appears now as

$$Z = (\Lambda^*)^{-3N} Q(T^*V^*) \tag{3.43}$$

where $\Lambda^* = h/\sigma\sqrt{m\epsilon}$ and the function Q contains all other terms of the partition function. Thus we see that formally the quantity Λ^* appears in the classical quantum statistics. The reduced Helmholtz potential $A^* = A/N\epsilon$ gives

$$A^* = -\frac{T^*}{N}\ln Q(T^*V^*) - 3T^*\ln\Lambda^* \tag{3.44}$$

The reduced pressure $P^* = P\sigma^3/\epsilon$ is the expression

$$P^* = -\left(\frac{\partial A^*}{\partial V^*}\right)_{T^*} = \frac{T^*}{N}\frac{\partial \ln Q(T^*V^*)}{\partial V^*} \tag{3.45}$$

The equation of state therefore does not contain Λ^*, and yet it still contains the essential features involved in the expansion with virial coefficients.

But the quantum parameter Λ^* does appear in the equation of state if one considers the quantum statistics. We shall briefly indicate how this occurs and complete the discussion of De Boer's calculations of the quantities σ and ϵ from the measured virial coefficients. Let us consider the N atoms making up a system which obeys the Schrödinger equation:

$$[H_{(op)} - E_n]\psi_n = \left[-\frac{\hbar^2}{2m_i} \sum_i \nabla_i^2 + \sum_{i \neq j} \varphi(r_{ij}) - E_n \right] \psi_n(r_1 \cdot \cdot \cdot r_N) = 0 \tag{3.46}$$

and transform the equation into the dimensionless parameters by substitution for $E_n = NE_n^*$ and for $r = r^*\sigma$ so that

$$\left[-\frac{h^2}{m\epsilon\sigma^2} \sum_i \frac{\nabla_i^2}{8\pi^2} + \sum_{i \neq j} \varphi(r_{ij}^*) - NE_n^* \right] \psi_n(r_1^* \cdot \cdot \cdot r_N^*) = 0 \tag{3.47}$$

The coefficient of the kinetic energy is $\Lambda^{*2} = h^2/m\epsilon\sigma^2$. This means that in the quantum-statistical partition function

$$\sum_n e^{-E_n/kT} \tag{3.48}$$

the reduced characteristic energy E_n^* depends on V^* and on Λ^* so that the partition function is given by

$$Z^* = Q(V^*,T^*,\Lambda^*) \tag{3.49}$$

The dimensionless pressure P^* which determines the equation of state is now

$$P^* = \frac{T^*}{N} \frac{\partial \ln Q(V^*,T^*,\Lambda^*)}{\partial V^*} \tag{3.50}$$

Thus the equation of state from quantum statistics contains the parameter Λ^*. These qualitative remarks will presently be reviewed, but we may consider them as justification for the new law of corresponding states developed by De Boer.

Calculation of the Molecular Constants σ and ϵ

Returning now to the second virial coefficient B for a gas such as helium, we may plot the experimental values of $\log B$ against $\log T$. Now in De Boer's dimensionless parameters these quantities are

$$\log B = \log \frac{2\pi N\sigma^3}{3} + \log B^* \tag{3.51}$$

$$\log T = \log \frac{\epsilon}{k} + \log T^* \tag{3.52}$$

showing that each quantity differs by a constant. Let us take the Lennard-Jones expression for the virial coefficient expressed in the dimensionless parameters:

$$B^* = \sum_{s=0}^{\infty} a_s \left(\frac{4}{T^*}\right)^{\frac{1}{4}+s/2} \tag{3.53}$$

This is the theoretical value of B^* as a function of T^*. Thus with $\log B^*$ plotted against $\log T^*$, the comparison between theory and experiment is made by laying the experimental plot of $\log B$ vs. $\log T$ (on transparent paper) over the theoretical plot of $\log B^*$ vs. $\log T^*$. If the experimental points fit the theoretical curve at all temperatures, the difference in ordinates and abscissas directly leads to the values of σ and ϵ. For the classical gases where Λ^* is small, the values of σ and ϵ may be determined with considerable certainty.

The quantum term Λ^*, which has been introduced and which is important for the light gases, must now be introduced into B^*. We shall show that

$$B^* = \sum_{s=0}^{\infty} a_s \left(\frac{4}{T^*}\right)^{\frac{1}{4}+s/2} + \Lambda^{*2} \sum_{s=0}^{\infty} a_s^{(1)} \left(\frac{4}{T^*}\right)^{\frac{13}{12}+s/2} + \Lambda^{*4} \sum_{s=0}^{\infty} a_s^{(2)} \left(\frac{4}{T^*}\right)^{\frac{23}{12}+s/2} + \cdots \tag{3.54}$$

where the coefficients a_s, $a_s^{(1)}$, and $a_s^{(2)}$ are given by

$$a_s = \frac{-1}{4s!}\,\Gamma\left(-\frac{1}{4}+\frac{s}{2}\right) \tag{3.55}$$

$$a_s^{(1)} = \frac{36s-11}{768\pi^2 s!}\,\Gamma\left(-\frac{1}{12}+\frac{s}{2}\right) \tag{3.56}$$

$$a_s^{(2)} = \frac{-3024s^2+4728s+767}{491520\pi^4 s!}\,\Gamma\left(\frac{1}{12}+\frac{s}{2}\right) \tag{3.57}$$

Here again $\Gamma(x)$ is the Γ function for the argument x. The values of the coefficients are given in the following array:

s	a_s	$a_s^{(1)}$	$a_s^{(2)}$
0	1.226	18.48×10^{-3}	-184.5×10^{-6}
1	-0.9064	6.8×10^{-3}	-317.0×10^{-6}
2	-0.1532	4.26×10^{-3}	-447.0×10^{-6}
3	-0.0378	1.89×10^{-3}	-131.0×10^{-6}
4	-9.574×10^{-3}	0.709×10^{-3}	-61.6×10^{-6}

If we accept the above expression as the first quantum-mechanical approximation to the second virial coefficient, we may look for values of the molecular constants σ and ϵ for the gases helium, hydrogen, and deuterium, as follows:

First, values of ϵ and σ are determined, using the classical expression for B^*. These values of ϵ and σ are used to calculate a preliminary value of the parameter Λ^*, and then the full quantum expression for $\log B^*$ is plotted against $\log T^*$. By using the experimental values of B at not too low temperatures, the overlay plot of $\log B$ against $\log T$ compares well enough with the plot of $\log B^*$ against $\log T^*$ so that new values of ϵ and σ are determined. By repeated operation a final consistent set of values of ϵ, σ, and Λ^* is obtained. These are the values recorded in Tables 3.1 and 3.5. These values for ϵ, σ, and Λ^* for the light gases He, H_2, and D_2 are valid at all temperatures, but their use in the theory thus far discussed is limited to temperatures above 40°K. For these gases and below 40°K we must use the quantum-mechanical partition function.

Quantum-mechanical Partition Function

It is clear from the evaluation of the virial coefficients of the gases He, H_2, and D_2 that the quantum theory plays an important role at temperatures considerably above the critical temperature of these gases. Since we shall be interested in the physical properties of liquid helium and since this liquid is termed a quantum liquid, it is important to examine the theory of gases with the quantum-statistical mechanics. We may approach an understanding of the liquid state from the gas side.

In the quantum theory we describe the state of a system by the wave function $\psi(q)$, and the probability for finding the system in the configuration space volume dq is given by $\psi^*(q)\psi(q)\,dq$. The stationary states of the system, characterized by definite values E_n of the energy, are described by the characteristic functions $\psi_n(q)$ which are the solutions of the wave equation $H\left(\frac{\hbar}{i}\frac{\partial}{\partial q}, q\right)\psi_n(q) = E_n\psi_n(q)$. The partition function is

$$Z = \sum_n e^{-E_n/kT} \tag{3.58}$$

In quantum statistics this expression must not be replaced by an integral over phase space. Slater[1] has shown that the sum over states may be replaced by an integral over configuration space. For this purpose each term in Z is multiplied with the corresponding term:

$$\int |\psi_n(q_1 \cdots q_N)|^2 \, dq_1 \cdots dq_N = 1 \tag{3.59}$$

This gives a partition function:

$$Z = \int \Big[\sum_n |\psi_n(q_1 \cdots q_N)|^2 e^{-E_n/kT}\Big] \, dq_1 \cdots dq_N \tag{3.60}$$

---

[1] J. Slater, *Phys. Rev.*, **38**, 237, 1931.

We may multiply and divide by the quantity

$$N!\left(\frac{h^2}{2\pi mkT}\right)^{3N/2} \tag{3.61}$$

and bring the partition function into closer identity to the classical expression for Z. Thus

$$Z = \frac{1}{N!}\left(\frac{2\pi mkT}{h^2}\right)^{3N/2} Q_N \tag{3.62}$$

where

$$Q_N = \int W(q_1 \cdot \cdot \cdot q_N)\, dq_1 \cdot \cdot \cdot dq_N \tag{3.63}$$

and the so-called "Slater sum" is

$$W(q_1 \cdot \cdot \cdot q_N) = N!\left(\frac{h^2}{2\pi mkT}\right)^{3N/2} \sum_n |\psi_n(q_1 \cdot \cdot \cdot q_N)|^2 e^{-E_n/kT} \tag{3.64}$$

Obviously now, $W(q_1 \cdot \cdot \cdot q_N)$ has replaced the classical expression for the relative probability of a configuration specified by the coordinates $q_1 \cdot \cdot \cdot q_N$, which was $\exp\,[-\Sigma\varphi(r)/kT]$. This is not surprising because $|\psi_n(q_1 \cdot \cdot \cdot q_N)|^2$ gives the probability for a special configuration, when the system is in the stationary state E_n, and $\exp\,(-E_n/kT)$ gives the relative probability for the occurrence of the state E_n. Thus the total relative probability is formed by the sum of the product:

$$|\psi_n(q_1 \cdot \cdot \cdot q_N)|^2 e^{-E_n/kT}$$

over all possible states. At high temperatures the so-called Slater sum $W(q_1 \cdot \cdot \cdot q_N)$ must approach the corresponding classical expression. Deviations from classical statistics first occur as a result of the quantum mechanics without paying attention to the symmetrization of the wave functions. For a system of identical particles, the impossibility of discriminating between them requires the wave function to be either symmetrical or antisymmetrical in the coordinates of the molecules. This leads to symmetry effects. The general quantum expression for the second virial coefficient is

$$B = -\frac{N}{2}\int [W(q_1,q_2) - 1]\, dq_1\, dq_2 \tag{3.65}$$

for two particles interacting.

Transformation of the Slater Sum

The characteristic energy values and characteristic functions are determined by the Hamiltonian operator, and so the Slater sum is also determined by the Hamiltonian operator. This may be shown by repeated application of the operator H to the Schrödinger equation:

$$H\psi_n = E_n\psi_n \tag{3.66}$$

$$H^s\psi_n = E_n^s\psi_n \tag{3.67}$$

Therefore

$$e^{-E_n/kT}\psi_n = \left[\sum_{s=0}^{\infty}\left(-\frac{1}{kT}\right)^s \frac{E_n^s}{s!}\right]\psi_n = \left[\sum_{s=0}^{\infty}\left(-\frac{1}{kT}\right)^s \frac{H^s}{s!}\right]\psi_n \tag{3.68}$$

which is the power series development of the exponential function. The series in H may be defined as

$$e^{(-H/kT)} = \sum_{s=0}^{\infty}\left(-\frac{1}{kT}\right)^s \frac{H^s}{s!} \tag{3.69}$$

and so the Slater sum may be written as

$$W(q_1 \cdot \cdot \cdot q_N) = N!\left(\frac{h^2}{2\pi mkT}\right)^{3N/2} \sum_n \psi_n^*(q_1 \cdot \cdot \cdot q_N)e^{-H/kT}\psi_n(q_1 \cdot \cdot \cdot q_n) \tag{3.70}$$

We shall now wish to introduce a new complete orthogonal set of normalized functions $U_m(q_1 \cdot \cdot \cdot q_N)$ with which we may express the function ψ_n:

$$\psi_n = \sum_m c_{nm}U_m \tag{3.71}$$

The Slater sum may then be written as

$$W(q_1 \cdot \cdot \cdot q_N) = N!\left(\frac{h^2}{2\pi mkT}\right)^{3N/2} \sum_m U_m^* e^{-H/kT} U_m \tag{3.72}$$

We shall presently want to use for U_m the momentum characteristic functions of running waves. With these the Slater sum may be computed and the second virial coefficient obtained. But for the sake of a clear understanding we shall first consider some simple examples using ψ_n directly.

Slater Sums in Some Simple Examples. Consider a single mass point which may move on a line segment of length L. The classical partition function becomes

$$Z = \frac{1}{h}\int_{-\infty}^{\infty} e^{(-p^2/2mkT)}\,dp = \left(\frac{2\pi mkT}{h^2}\right)^{\frac{1}{2}} \tag{3.73}$$

where the particles have momentum p located in the segment $0 < x < L$. The quantum expression requires the normalized characteristic functions to be shaped like a string clamped at both boundaries and having a space dependent term

$$\psi_n = \left(\frac{2}{L}\right)^{\frac{1}{2}} \sin \frac{n\pi x}{L} \qquad n = 1, 2, \ldots \tag{3.74}$$

The Schrödinger wave equation is

$$\frac{d^2\psi}{dx^2} + \frac{2mE}{\hbar^2} = 0 \tag{3.75}$$

and so the characteristic energies are $E_n = n^2h^2/8mL^2$. The Slater sum is accordingly

$$W = \left(\frac{h^2}{2\pi mkT}\right)^{\frac{1}{2}} \cdot \frac{2}{L} \cdot \sum_{n=1}^{\infty} e^{-n^2h^2/8mL^2kT} \sin^2 \frac{n\pi x}{L} \tag{3.76}$$

or the partition function simply

$$Z = \frac{2}{L} \sum_{n=1}^{\infty} e^{-n^2h^2/8mL^2kT} \sin^2 \frac{nx}{L} \tag{3.77}$$

which must be integrated over the length L. For large L the exponential factor changes slowly with n, while for x not in the neighborhood of the boundaries the factor $\sin^2 (n\pi x/L)$ changes rapidly. We therefore may replace the latter factor by its mean value $\frac{1}{2}$ and replace the sum by an integral over n. This gives

$$W = \left(\frac{h^2}{2\pi mkT}\right)^{\frac{1}{2}} \left(\frac{2}{L}\right) \left(\frac{1}{2}\right) \int_0^{\infty} e^{-n^2h^2/8mkTL^2}\, dn \tag{3.78}$$

or that the partition function is

$$Z = \int_0^L \left(\frac{2\pi mkT}{h^2}\right)^{\frac{1}{2}} dx \tag{3.79}$$

Under these conditions the classical partition function is identical to the quantum partition function. Near the boundary this is not true because all waves reduce to zero on the boundary and hence are in phase.[1]

Within a wave length of the edges the partition function shows quantum effects. We may see this more clearly from the approximation

$$\int_0^{\infty} e^{-n^2h^2/8mL^2kT} \frac{2}{L} \sin^2 \frac{n\pi x}{L}\, dn = \frac{(2\pi mkT)^{\frac{1}{2}}}{h} \left(1 - e^{-8\pi^2\{[x(mkT)]^{\frac{1}{2}}/h\}^2}\right) \tag{3.80}$$

This is an expression which is valid for x in the neighborhood of the boundaries. For this case, if x is large compared to $h/(mkT)^{\frac{1}{2}}$, the exponential reduces to zero, and we have again the classical constant value. On the other hand, for x small, the distribution decreases to zero at the boundary. For hydrogen at 100°K the distance $h/(mkT)^{\frac{1}{2}}$ is $3.69A$.

---

[1] J. Slater, *ibid.*

These same quantum effects occur in the region where two molecules are in collision because here again the potential changes greatly in a single wave length.[1] We shall return to these effects in the theory of liquid helium, and so it is useful to consider two mass points which move freely on a line segment of length L. Let x_1 and x_2 be the coordinates of the two particles. Then the characteristic energy values are

$$E_{n_1n_2} = \frac{(n_1^2 + n_2^2)h^2}{8mL^2} \tag{3.81}$$

and the characteristic functions are

$$\psi^{(1)}_{n_1n_2} = \frac{2}{L} \sin \frac{n_1\pi x_1}{L} \sin \frac{n_2\pi x_2}{L} \tag{3.82}$$

$$\psi^{(2)}_{n_1n_2} = \frac{2}{L} \sin \frac{n_2\pi x_1}{L} \sin \frac{n_1\pi x_2}{L} \tag{3.83}$$

These functions represent all the ways the waves could be formed. Now the exclusion principle allows only one definite linear combination of $\psi^{(1)}_{n_1n_2}$ and $\psi^{(2)}_{n_1n_2}$. In the Einstein-Bose statistics this is the symmetrical combination

$$(\psi^{(1)}_{n_1n_2} + \psi^{(2)}_{n_1n_2}) \frac{1}{\sqrt{2}}$$

In the Fermi-Dirac statistics it is the antisymmetrical combination

$$(\psi^{(1)}_{n_1n_2} - \psi^{(2)}_{n_1n_2}) \frac{1}{\sqrt{2}}$$

Let the quantity $h^2/2\pi mkT$ equal λ^2 and now write the Slater sum in the Einstein-Bose statistics as

$$W_{\text{e.b.}}(x_1x_2) = \frac{2\lambda^2}{L^2} \sum_{n_1 \neq n_2} e^{-(n_1{}^2+n_2{}^2)h^2/8mL^2kT} \left(\sin \frac{n_1\pi x_1}{L} \sin \frac{n_2\pi x_2}{L} + \sin \frac{n_2\pi x_1}{L} \sin \frac{n_1\pi x_2}{L}\right)^2 + \frac{4\lambda^2}{L^2} \sum_{n=1}^{\infty} e^{-n^2h^2/4mL^2kT} \sin^2 \frac{n\pi x_1}{L} \sin^2 \frac{n\pi x_2}{L} \tag{3.84}$$

The last term in the above equation is where $n_1 = n_2$. The expression for the Fermi-Dirac statistics gives a Slater sum:

---

[1] L. Gropper and G. Uhlenbeck, *Phys. Rev.*, **41**, 79, 1932; B. Kahn, Dissertation, University of Utrecht, 1938.

$$W_{f.d.}(x_1x_2) = \frac{2\lambda^2}{L^2} \sum_{n_1 \neq n_2} e^{-(n_1^2+n_2^2)h^2/8mL^2kT} \left(\sin \frac{n_1\pi x_1}{L} \sin \frac{n_2\pi x_2}{L} - \sin \frac{n_2\pi x_1}{L} \sin \frac{n_1\pi x_2}{L} \right) \qquad (3.85)$$

These Slater sums may be conveniently written:

$$\begin{matrix} W_{e.b.} \\ W_{f.d.} \end{matrix} = \frac{2\lambda^2}{L^2} \left\{ \left[\sum_{n=1}^{\infty} e^{-n^2h^2/8mL^2kT} \sin^2 \frac{n\pi x_1}{L} \right] \left[\sum_{n=1}^{\infty} e^{-n^2h^2/8mL^2kT} \sin^2 \frac{n\pi x_2}{L} \right] \right\}$$
$$\pm \frac{\lambda^2}{2L^2} \left\{ \sum_{n=1}^{\infty} e^{-n^2h^2/8mL^2kT} \left[\cos \frac{n\pi(x_1 - x_2)}{L} - \cos \frac{n\pi(x_1 + x_2)}{L} \right] \right\}^2 \qquad (3.86)$$

Replacing sums by integration, we get

$$\begin{matrix} W_{e.b.} \\ W_{f.d.} \end{matrix} = W_B \pm \frac{1}{2\lambda^2} \left(e^{(-\pi/\lambda^2)(x_1-x_2)^2} - e^{(-\pi/\lambda^2)(x_1+x_2)^2} \right)^2 \qquad (3.87)$$

where $\lambda^2 = h^2/2\pi mkT$ and where W_B is the classical-valued first term. If $(\lambda \rightarrow 0)$, we have the usual classical value. The term in the last expression

$$e^{-(\pi/\lambda^2)(x_1+x_2)^2}$$

is important only when both particles are at the boundary. The term with the difference in the coordinates

$$e^{-(\pi/\lambda^2)(x_1-x_2)^2}$$

causes a maximum in the Einstein-Bose partition function and a minimum in the Fermi-Dirac function for $x_1 = x_2$. We have then an apparent attraction between E.B. particles and an apparent repulsion between F.D. particles. This is the truly important term when two particles are close together. We must bear in mind that no potential of interaction between the particles has been introduced into this example. A repulsive term in such a potential does not permit $x_1 = x_2$.

Second Virial Coefficient for an Ideal Quantum Gas

Let us enlarge on this last example by considering the two molecules without interaction and in a volume V, and take the wave functions as

$$\psi^0(q_1,q_2) = \frac{1}{V} e^{(2\pi i/h)(p_1q_1+p_2q_2)} \qquad (3.88)$$

where the running waves are characterized by the vectors p_k,q_k. The symmetrical combinations are

$$\psi^0_{\text{e.b.}}(q_1q_2) = \frac{1}{V\sqrt{2}}\left(e^{(2\pi i/h)(p_1q_1+p_2q_2)} + e^{(2\pi i/h)(p_1q_2+p_2q_1)}\right) \tag{3.89}$$

$$\psi^0_{\text{f.d.}}(q_1q_2) = \frac{1}{V\sqrt{2}}\left(e^{(2\pi i/h)(p_1q_1+p_2q_2)} - e^{(2\pi i/h)(p_1q_2+p_2q_1)}\right) \tag{3.90}$$

Transforming these functions with the coordinates $R = \frac{1}{2}(q_1 + q_2)$ and $r = (q_1 - q_2)$, we get a center of mass running wave which is modulated by the relative distance function

$$\psi^0_{\text{e.b.}}(q_1q_2) = \frac{1}{V\sqrt{2}}\, 2\cos\left[\frac{(p_1 - p_2)}{2\hbar}\, r\right] e^{(2\pi i/h)(p_1+p_2)R} \tag{3.91}$$

$$\psi^0_{\text{f.d.}}(q_1q_2) = \frac{1}{V\sqrt{2}}\, 2\sin\left[\frac{(p_1 - p_2)}{2\hbar}\, r\right] e^{(2\pi i/h)(p_1+p_2)R} \tag{3.92}$$

so that the square of the absolute magnitude is

$$|\psi^0_{\text{e.b.}}(q_1q_2)|^2 = \frac{2}{V^2}\cos^2\left[\frac{(p_1 - p_2)}{2\hbar}\, r\right] \tag{3.93}$$

$$|\psi^0_{\text{f.d.}}(q_1q_2)|^2 = \frac{2}{V^2}\sin^2\left[\frac{(p_1 - p_2)}{2\hbar}\, r\right] \tag{3.94}$$

The Slater sum for the two particles without potential field is

$$W(q_1q_2) = \left(\frac{h^2}{2\pi mkT}\right)^3 2! \sum_n |\psi_n(q_1q_2)|^2 e^{-E_n/kT} \tag{3.95}$$

and this now becomes evaluated with the values of $|\psi|^2$. At large distances r the average value of the cosine² and sine² functions will be $\frac{1}{2}$ so that $W(q_1q_2)$ approaches the value 1. At short distances r the cosine and sine functions are in phase so that $W(q_1q_2)$ approaches the value 2 or 0, respectively, for the Einstein-Bose and Fermi-Dirac statistics. We have then

$$\begin{matrix} W^0_{\text{e.b.}}(r) \\ W^0_{\text{f.d.}}(r) \end{matrix} = 1 \pm e^{(-2mkT/h^2)r^2} \tag{3.96}$$

The last expression leads to a second virial coefficient for an ideal gas:

$$B_{\left(\substack{\text{e.b.} \\ \text{f.d.}}\right)} = \mp \frac{N}{16}\left(\frac{h^2}{\pi mkT}\right)^{\frac{3}{2}} \tag{3.97}$$

We must alter this expression for an ideal gas if the gas molecules possess an intrinsic angular momentum or spin. He⁴ atoms have no spin so the problem does not arise; however, the isotope He³ does possess nuclear spin and alters the weights and symmetry properties of the different states. J. De Boer, J. Van Kranendonk, and K. Compaan[1] have

---

[1] J. De Boer, J. Van Kranendonk, and K. Compaan, *Physica*, **16**, 545, 1950.

shown that for He^3 whose nuclear spin value is $\frac{1}{2}$, the second virial coefficient is a 3-to-1 mixture of the coefficient computed from antisymmetrical states and of the coefficient computed from symmetrical states:

$$B(T) = \tfrac{3}{4}B^{(\text{a.s.})} + \tfrac{1}{4}B^{(s)} \tag{3.98}$$

where

$$B^{(\text{a.s.})} = B_{\text{n.id}}\ (l = \text{odd}) + \frac{N}{16}\left(\frac{h^2}{\pi mkT}\right)^{\frac{3}{2}} \tag{3.99}$$

$$B^{(s)} = B_{\text{n.id.}}\ (l = \text{even}) - \frac{N}{16}\left(\frac{h^2}{\pi mkT}\right)^{\frac{3}{2}} \tag{3.100}$$

The term $B_{\text{n.id.}}$ represents the virial coefficient for nonideal gas, *i.e.*, where the potential of interaction between molecules is not neglected. This term at high temperatures must be identical to the classical expression already discussed. At such high temperatures the second terms on the right in the above expression become extremely small. Let us see how $B_{\text{n.id.}}$ is evaluated at low temperatures. We shall begin with not too low temperatures.

Kirkwood Expansion of the Slater Sum

The expression for the Slater sum for N particles has been shown to be

$$W(q_1 \cdots q_N) = N!\left(\frac{h^2}{2\pi mkT}\right)^{3N/2} \sum \psi_n^*(q_1 \cdots q_N)e^{-H_{(op)}/kT}\psi_n(q_1 \cdots q_N) \tag{3.101}$$

For the characteristic functions ψ_n Kirkwood[1] introduced a set of functions of running waves:

$$W(q_1 \cdots q_N) = \left(\frac{1}{2\pi mkT}\right)^{3N/2} \int e^{-2\pi i/h \sum_{k=1}^{N} p_k q_k} e^{-H_{(op)}/kT} e^{2\pi i/h \sum_{k=1}^{N} p_k q_k}\, dp \tag{3.102}$$

where p_k and q_k are vector quantities which are the momentum vector and radius vector in the phase space of the particle k. The operator is

$$H_{(op)} = -\frac{\hbar^2}{m}\nabla^2 + \varphi(x,y,z) \tag{3.103}$$

Kirkwood[2] has shown the following expansion for not too low a temperature and in which the operator $H_{(op)}$ has become the Hamiltonian for the total energy of relative motion of two particles $(p^2/m + \varphi)$:

$$e^{-H_{(op)}/kT} e^{2\pi i/h \sum_{1}^{N} p_k q_k} = e^{-H_{(pq)}/kT} e^{2\pi i/h \sum_{1}^{N} p_k q_k} (1 + \hbar w_1 + \hbar^2 w_2 \cdots) \tag{3.104}$$

[1] J. Kirkwood, *Phys. Rev.*, **44**, 31, 1933.

[2] *Ibid.*

where in the series w_1 is the pure imaginary quantity

$$w_1 = -\frac{i\beta^2}{2m}\sum_1^N p_k\Delta_k\varphi \tag{3.105}$$

and where

$$w_2 = -\frac{\beta^2}{4m}\sum_1^N \Delta_k\varphi + \frac{\beta^3}{6m}\left[\sum_1^N (\nabla_k\varphi)^2 + \frac{1}{m}\left(\sum_1^N p_k\nabla_k\varphi\right)^2\right] - \frac{\beta^4}{8m^2}\left(\sum_1^N p_k\nabla_k\varphi\right)^2 \tag{3.106}$$

In these last expressions the quantity $\beta = 1/kT$, and φ is the potential energy term between pairs of molecules. The expansion is then put into the Slater sum and integrated over p. We have omitted the permutation operator in this discussion. The Slater sum becomes

$$W(q_1 \cdots q_N) = e^{-\beta\varphi(q_1 \cdots q_N)}\left\{1 - \frac{\hbar^2\beta^2}{12m}\sum_1^N\left[\Delta_k\varphi - \frac{\beta}{2}(\Delta_k\varphi)^2\right] + \cdots\right\} \tag{3.107}$$

Uhlenbeck and Beth[1] have repeated Kirkwood's work and extended the calculations. De Boer has taken this expression for the Slater sum and computed the second virial coefficient in terms of the reduced coordinates of his theory. He obtains a power series in Λ^*, which we have already given on page 47. For He gas, De Boer considered the expansion valid above 40°K, whereas for H_2 and D_2 the limits were 75 and 45°K, respectively.

Second Virial Coefficient at Low Temperatures

Let us now consider the quantum expression for the virial coefficient at low temperatures, taking into account the potential of interaction. These calculations were made first by Beth and Uhlenbeck,[2] B. Kahn,[3] and J. De Boer.[4] The expression for the virial coefficient of the ideal gas using Einstein-Bose or Fermi-Dirac statistics as required now has a term added to it representing the effect of the collisions between the molecules. For this we need consider the relative motion of two particles and see how the wave functions are altered if we permit a potential function of interaction. With such a potential the purely relative motion can be described by the wave equation

---

[1] G. Uhlenbeck and E. Beth, *Physica*, **3**, 729, 1936.

[2] G. Uhlenbeck and E. Beth, *Physica*, **4**, 915, 1937.

[3] B. Kahn, Dissertation, University of Utrecht, 1938.

[4] J. De Boer, Dissertation, University of Amsterdam, 1940.

$$-\frac{\hbar^2}{m}\frac{d^2r\psi_{nL}}{dr^2} + \left[V(r) + \frac{\hbar^2 L(L+1)}{mr^2}\right] r\psi_{nL} = E_{nL} r\psi_{nL} \qquad (3.108)$$

where n and L determine the energy and angular momentum quantum numbers and E_{nL} are the characteristic energies for the radial motion. These energy states are $(2L + 1)$-fold degenerate. There are no negative discrete characteristic values for He because the potential is too small to permit them (see De Boer[1] and Kilpatrick[2]). Now without the potential the radial motion of two molecules is

TABLE 3.6. SECOND VIRIAL COEFFICIENT OF HELIUM AT LOW TEMPERATURES

T, °K	$B_{\text{n.id.}}$, cm³	$B_{\text{b.e.}}$, cm³	B_{total}, cm³	$B_{\text{exptl.}}$, cm³
			(a)	(b)
2.050	−142	−25	−167	−180
2.647	−104	−16	−120	−128
3.105	−86	−12	−98.9	−107
4.240	−60.8	−8.0	− 68.8	−75.5
6.13	....	......	−42.4	−44.8

[a] Theoretical calculation, De Boer.
[b] Experiment, Keesom and Walstra.

$$-\frac{\hbar^2}{m}\frac{d^2r\psi^0_{nL}}{dr^2} + \frac{\hbar^2 L(L+1)}{mr^2} r\psi^0_{nL} = E^0_{nL} r\psi^0_{nL} \qquad (3.109)$$

Kahn[3] has shown that the solution of this wave equation at large values of r is

$$r\psi^0_{nL} = A \sin\left(k^0 r - \frac{L\pi}{2}\right) \qquad (3.110)$$

where

$$k^0 = \frac{(mE_{nL})^{\frac{1}{2}}}{\hbar} \qquad (3.111)$$

The asymptotic solution of the wave equation with potential is

$$r\psi_{nL}(r) = (A^2 + B^2)^{\frac{1}{2}} \sin\left(kr - \frac{L\pi}{2} + \eta_L k\right) \qquad (3.112)$$

which differs by the existence of a phase shift $\eta_L(k)$. The contribution

---

[1] *Ibid.*

[2] J. Kilpatrick, *J. Chem. Phys.*, **19**, 930, 1951.

[3] B. Kahn, Dissertation, University of Utrecht, 1938.

$B_{\text{n.id.}}$ can be expressed entirely in these phase shifts. We shall not pursue the argument further. The results of numerical integration for $B_{\text{n.id.}}$ are given in Table 3.6 for helium. In Table 3.6, column two is from the general quantum-mechanical expression for the second virial coefficient. It is obtained by numerical integration. Column three is the term for an ideal Einstein-Bose gas and gives a negative second virial coefficient. Column four gives the total from theory, and column five the experimental values.

Equation of State of Compressed Gases and Liquids

We shall add a few remarks concerning the equation of state for dense gases and liquids of the so-called "free-volume" type. We shall refer to the work of Lennard-Jones and Devonshire,[1] Henry Eyring *et al.*,[2] J. Kirkwood,[3] and J. Hirschfelder.[4] The characteristics of liquids are sometimes gaslike and sometimes can be identified with the solid state. Approaching the liquid state through the melting phenomenon of the solid, one has an entropy increase of R entropy units and more, according to the experimental results shown in Table 3.7. Now such an entropy increase can be accounted for by considering a partition function for N molecules in a volume V. If one divides up the volume with N equal compartments of little volume Δ and puts one molecule into each compartment, then one has a configuration integral different from that of the gas. We now have in general a sum of integrals over the individual cells, which according to Kirkwood is

Configuration integral

$$= \sum_{L_1=1}^{N} \cdots \sum_{L_N=1}^{N} \int^{\Delta L_1} \cdots \int^{\Delta L_N} e^{-\Sigma\varphi(r)/kT}\, dq_1 \cdots dq_N \qquad (3.113)$$

And this expression reduces to

$$\text{Configuration integral (dense gas)} = \int^{\Delta_1} \cdots \int^{\Delta_N} e^{-\Sigma\varphi(r)/kT}\, dq_1 \cdots dq_N \qquad (3.114)$$

for such high densities as to allow single occupancy of the cells. On the other hand, for densities approaching zero the configuration integral becomes

Configuration integral (density $\to$ 0)

$$= e^N \int^{\Delta_1} \cdots \int^{\Delta_N} e^{-\Sigma\varphi(r)/kT}\, dq_1 \cdots dq_N \qquad (3.115)$$

---

[1] J. Lennard-Jones and A. Devonshire, *Proc. Roy. Soc.* (*London*), **163**, 53, 1937; *ibid.*, **165**, 1, 1938.

[2] H. Eyring *et al.*, *J. Chem. Phys.*, **5**, 896, 1937; *ibid.*, **6**, 620, 1938.

[3] J. Kirkwood, *J. Chem. Phys.*, **18**, 350, 1950.

[4] J. Hirschfelder, *J. Chem. Phys.*, **18**, 1484, 1950.

From the complete partition function for these two extreme cases we may compute the Helmholtz potential for each and the entropy for each. The difference in entropy between the two cases is just $\Delta S = R \ln e = R$. This is called the *communal* entropy by Eyring, and for all real liquids must be some value $R \ln \sigma$ where the parameter σ is not yet determined by theory.

As a first approximation for a dense gas we may take the configuration integral to be

$$e^N V_f^N e^{-\Sigma\varphi(r)/kT} \tag{3.116}$$

where the potential energy is smeared to obtain radial symmetry within the cell and the free volume is the space within the cell where the molecule behaves like a gas. Hirschfelder[1] used the free-volume model with a cell equal to the specific volume divided by N. Using the Lennard-Jones potential with parameters ϵ and σ evaluated from viscosity data as listed in Table 3.1, Hirschfelder computed the equation of state for dense gases. The calculations are in good agreement with experiment for high density on most gases. Agreement is not good for hydrogen and helium. As we have seen, quantum considerations are important.

TABLE 3.7. ENTROPY OF MELTING FOR SOME ELEMENTS

Gas	Volume solid, cc/mole	Volume liquid, cc/mole	$T_{\text{melt.}}$, °K	$Q_{\text{melt.}}$, kcal/mole	$S_{\text{melt.}}$, cal/°K
A	24.2	28.1	83	0.28	3.38
H_2	26.5	28.7	14	0.028	2.0
N_2	27.2	32.8	63	0.218	3.46

---

[1] *Ibid.*

CHAPTER 4

LIQUID HELIUM—THERMAL PROPERTIES

One of the most interesting problems of low-temperature physics concerns the theory and experiments on liquid helium. The unusual physical properties once again point to the quantum laws which govern gross matter at low temperatures. A useful starting point is with the diagram of state giving pressure against temperature (Fig. 4.1). We see the normal vapor-pressure curve for the separation of the gas and liquid phase with a critical point at 5.25°K and 2.26 atm. The vapor-pressure curve has been discussed in Chap. 2, and tables are given in the Appendix.

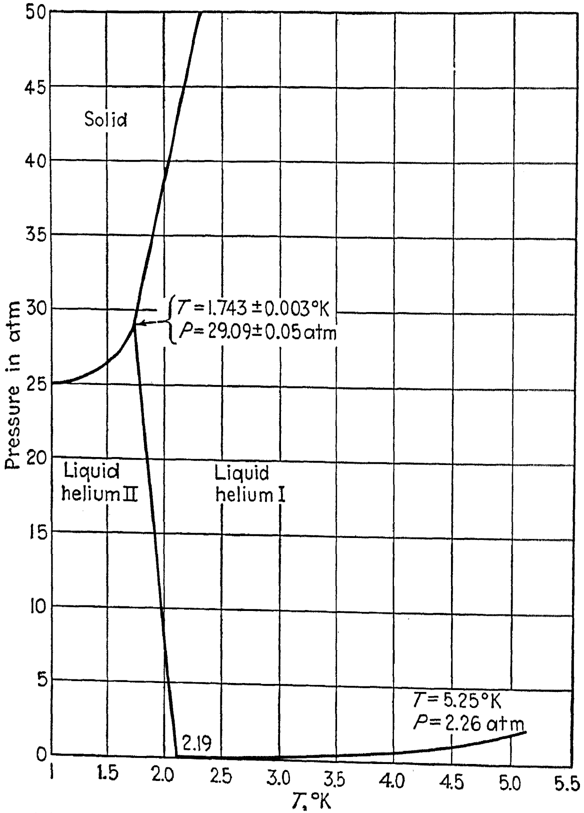

FIG. 4.1. Diagram of state for helium, pressure vs. temperature.

Figure 4.1 is drawn schematically for ease of presentation of the physical information. Following the vapor-pressure curve down to lower temperatures and pressures, *i.e.*, following the bottom curve in Fig. 4.1, we see that the gas and liquid continue an equilibrium curve on down to the absolute zero of temperature without interruption. At these low pressures helium remains a liquid all the way to the absolute zero of temperature. This is an extraordinary thing and sets helium aside as a unique liquid.

Liquid Helium I and Liquid Helium II

Diagram of State p vs. T. In Fig. 4.1 we show an equilibrium line between the two forms of liquid, helium I and helium II. Evidence for the existence of these two forms of liquid helium will be presented, but for the moment let us examine the equilibrium line with its negative temperature slope. Such a temperature dependence means that an isothermal compression of the substance as liquid helium II can force the substance into liquid helium I with a corresponding increase of entropy. It seems extraordinary that an isothermal compression can create disorder. Finally, the solid phase makes its reluctant appearance at relatively high pressures. The solid state may be obtained by an isothermal compression to well over 25 atm even at extremely low temperatures. Crossing the liquid to solid phase separation line requires work which is done against repulsion forces. A minute's reflection as to the possible meaning of this, and in addition the implication of the Nernst theorem applied to the solid and liquid phases at the absolute zero of temperature, convince us that the experimental values of the other thermodynamic variables must be interesting.

Specific Heat of Liquid Helium

In Fig. 4.2 the specific heat of liquid helium under its saturated vapor pressure is taken from the work of Keesom and Keesom.[1] The results have been recomputed by Miss Keesom to the 1937 temperature scale. Figure 4.2 shows the specific heat of liquid helium at constant volume made by Keesom.[2] We must conclude from these curves that the transition from liquid II to liquid I at the triple point is unlike the first-order phase transition generally supposed by the Gibbs phase rule. Figure 4.2 resembles the Greek letter lambda, and the temperature of 2.19°K has been called the λ point. If we are to identify the shape of the specific heat curve with similar curves found for the specific heat of alloys of metals showing order-disorder phenomena or with substances showing rotation of atoms in the solid state, we must call the transition a second-order phase transition. Strictly speaking there is no latent heat of transition, but we may think of a "smearing out" of the latent heat of transition over a temperature interval, and this gives a continuous drop in entropy with temperature.

---

[1] W. H. Keesom and A. Keesom, *Physica*, **2**, 557, 1933.

[2] W. H. Keesom, "Helium," Amsterdam, Elserier, 1943.

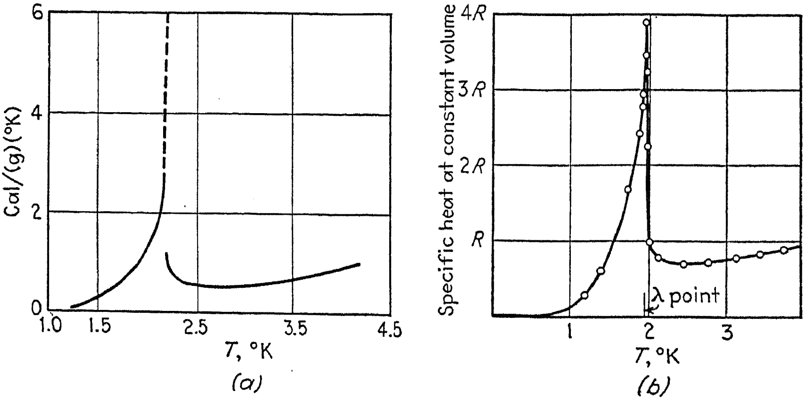

FIG. 4.2. (a) Specific heat of liquid helium under saturated vapor pressure. (b) Specific heat of liquid helium at constant volume (density = 0.1683 g/cm³). (*Keesom and Keesom.*)

Entropy of Liquid Helium

The entropy-against-temperature diagram is given in Fig. 4.3 for two pressure situations: (1) the liquid exposed to its saturate vapor pressure, which, of course, varies with temperature, (2) the liquid held at some constant high pressure such that the solid phase is reached on lowering the temperature. At extremely low temperatures both curves approach the same value. The drop in entropy at the λ point for the liquid phase implies an ordering process which surely cannot take place in ordinary volume space and so must occur in phase space. We shall therefore not be surprised at a theory which expresses the phase change as a condensation of the particles in momentum space. The entropy curve in Fig. 4.3 showing the solidification indicates the entropy drop to be expected on forcing the atoms into a regular crystal array. Even this transition seems to be slightly spread over a temperature interval. We may think of the solidification as involving a heat of fusion L. Using the thermodynamic relationship

$$L = T\,\Delta S = \Delta U + p\,\Delta V$$

and examining the entropy curves in Fig. 4.3, we must conclude that the latent heat of fusion must tend toward zero with falling temperature, since the entropy curves approach one another at extremely low temperatures. At the absolute zero of temperature the work $p\,\Delta V$ corresponds

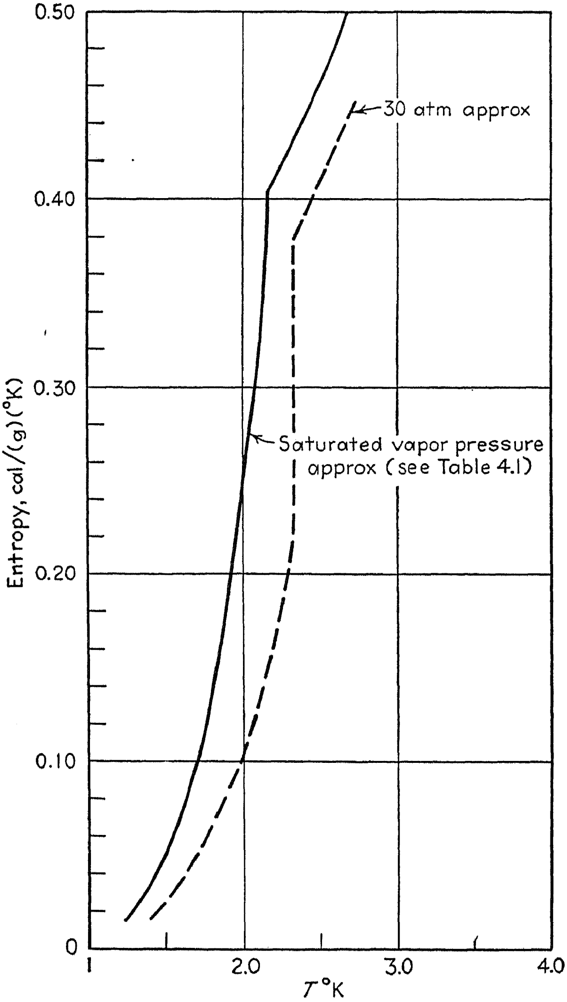

FIG. 4.3. Entropy vs. temperature for liquid helium under saturated vapor pressure and for a high constant pressure.

to a pressure change of from 0 to 25 atm, and the density change from liquid to solid is from 0.172 to 0.145. This gives about 1.3 cal/mole. If then L is to become zero at the absolute zero of temperature, then ΔU and $p\,\Delta V$ must become equal but of opposite sign. These conclusions were pointed out by Professor F. E. Simon,[1] and they imply that the energy of the liquid at 4°K is greater than that of the solid and that the energy difference vanished at about 2°K. At still lower temperatures the energy difference becomes negative. At extremely low temperatures we may therefore expect the specific heat of the solid phase to be greater than that of the liquid under its saturated vapor pressure. Simon[1] finds the solid phase obeys the Debye T^3 law with $\theta = 32.5°K$. The specific heat of the liquid at temperatures between 0.6 and 1.0°K obeys[2] the formula $10.0 \times 10^{-2}T^{6.2}$ and at temperatures below 0.6°K obeys[3] the formula $2.35 \times 10^{-2}T^3$. Table 4.1 gives the smoothed values of entropy for helium II.

---

[1] F. E. Simon, *Nature*, **133**, 529, 1934; *ibid.*, **133**, 460, 1934; F. Simon and C. A. Swenson, *Nature*, **165**, 829, 1950; C. A. Swenson, *Phys. Rev.*, **79**, 626, 1950; *ibid.*, **86**, 870, 1952.

TABLE 4.1. SMOOTHED VALUES OF THE SPECIFIC HEAT AND ENTROPY OF HELIUM II[a]

T, °K	$C_{\text{sat.}}$, joules/(g)(°K)	S, joules/(g)(°K)
0.60	0.0051	0.00169
0.65	0.0068	0.00215
0.70	0.0098	0.00276
0.75	0.0146	0.00358
0.80	0.0222	0.00475
0.85	0.0343	0.00644
0.90	0.0510	0.00885
0.95	0.0743	0.0122
1.00	0.1042	0.0168
1.05	0.142	0.0227
1.10	0.191	0.0304
1.15	0.250	0.0402
1.20	0.322	0.0523
1.30	0.516	0.0853
1.40	0.780	0.132
1.50	1.127	0.197
1.70	2.11	0.395
1.90	3.63	0.709
2.00	4.95	0.929
2.05	5.82	1.061
2.10	6.92	1.215
2.15	8.61	1.40
2.186	14.3	1.57

[a] H. C. Kramers, J. Wasscher, and C. J. Gorter, *Physica*, **18**, 329, 1952.

Zero-point Energy

F. Simon pointed out the existence of zero-point energy from the Debye theory (see Chap. 9). The quantum theory for such oscillators bound as if they were in a solid gives for the total energy of all oscillators

---

[1] F. E. Simon, *Nature*, **133**, 529, 1934.

[2] R. A. Hull, K. R. Wilkinson, and J. Wilks, *Proc. Phys. Soc. (London)*, **64**, 379, 1951.

[3] H. C. Kramers, J. Wasscher, and C. J. Gorter, *Physica*, **18**, 329, 1952.

$$E = \frac{9N}{\nu_D^3} \int_0^{\nu_{\max} = \nu_D} \left(\frac{1}{2} h\nu + \frac{h\nu}{e^{h\nu/kT} - 1} \right) \nu^2 \, d\nu$$

Integration gives the familiar expression for the zero-point energy plus the energy expressed with the Debye function

$$E = \frac{9}{8} Nh\nu_{\max} + 3NkTD\left(\frac{h\nu}{kT}\right)$$

Setting $k\theta = h\nu_{\max}$, we get for the zero-point energy $E_0 = 9Nk\theta/8$, and this gives with $\theta = 32.5°\text{K}$ a value of $E_0 = 73$ cal/g-atom. Simon suggested that this great zero-point energy prevents the liquid from ever becoming a solid at moderate pressures. An interesting thermodynamic relationship known as Trouton's rule gives

$$\frac{\text{Latent heat of vaporization}}{T} = 21 \text{ cal/(°K)(mole)}$$

This rule simply says that the change of entropy, *i.e.*, the amount of disorder, is the same for all liquid to gas phase transitions at their respective normal boiling points. Now if the zero-point energy is added to the latent heat of vaporization, then for liquid helium we do indeed obtain

$$\frac{\text{Latent heat of vaporization} + \text{zero-point energy}}{T} = 21$$

Latent Heat of Vaporization

Figure 4.4 gives the latent heat of vaporization in calories per gram as a function of the temperature. There is a slight cusp at the λ point, and from the continuity of the function at that point we may conclude that there is no marked difference in the binding force for an atom at the surface of the liquid. The anomaly shown by the vaporization heat curve was first shown by Dana and H. Kamerlingh Onnes.[1] This was the first indication of the peculiar discontinuity in the properties of liquid helium. There are some puzzling things about the dependence of the heat of vaporization on temperature. In order to discuss them, we inject the physical measurements on the density and on the dielectric constant.

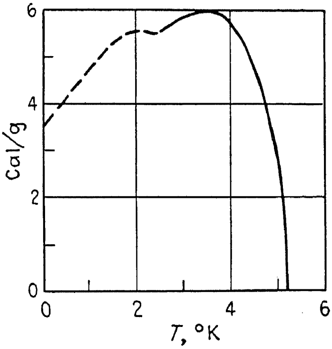

FIG. 4.4. Heat of vaporization of liquid helium.

---

[1] M. Dana and H. Kamerlingh Onnes, *Proc. Roy. Acad. Amsterdam*, **29**, 1051, 1926.

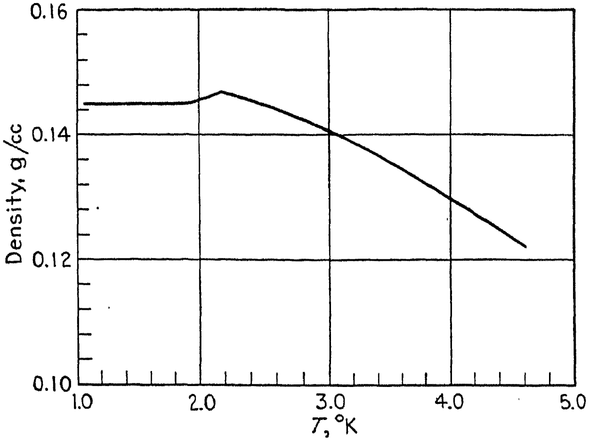

FIG. 4.5. Density of liquid helium vs. temperature.

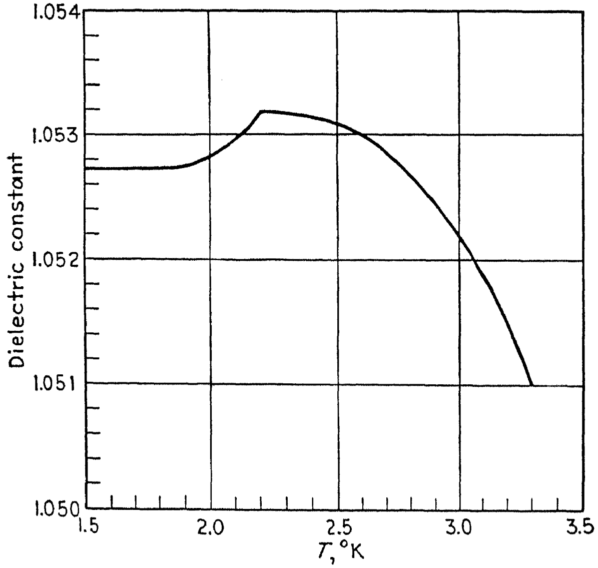

FIG. 4.6. Dielectric constant of liquid helium vs. temperature.

Density and Dielectric Constant of Liquid Helium

Figure 4.5 gives the density of liquid helium as a function of temperature. At the λ transition point, and quite sharply, the liquid seems to need more room and expands. Now the dielectric constant is given as a function of temperature in Fig. 4.6. It appears that the dielectric constant simply follows the density curve and indicates a constant polarizability of the atoms in the liquid phases. This is important because it means there is no change in the electronic state of the helium atom.

Indeed there are no optical effects which cannot be identified with a simple density change.

The latent heat curve then is unusual because it begins to fall off at temperatures above the break in the density curve. The falling off cannot be due to a weakening of the van der Waals binding forces because the polarizability does not change. With a van der Waals model we would expect the latent heat of vaporization to rise steadily from the temperature at the critical point and taper off to a steady value with lower temperatures. At these very low temperatures we must take into account the kinetic energy in the liquid and also the work of expansion in the gas phase to meet the kinetic energy requirement for that temperature. The resultant latent heat is shown in Fig. 4.7 as the algebraic sum of three quantities. The kinetic energy in the liquid is subtracted from the other two quantities in forming the resultant latent heat of vaporization. The more exact theory given by J. Kistemaker corrects the energy in the gas by use of the virial coefficients discussed in Chap. 3, and the energy in the liquid is taken from the measured data. This latter energy is more complicated than depicted in the simple sketch of Fig. 4.7. Kistemaker obtains the thermodynamic expression for latent heat Ω_T:

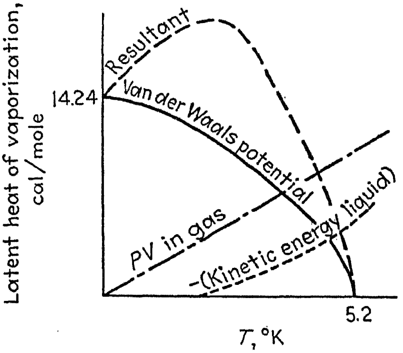

FIG. 4.7. Simple theory of latent heat of vaporization vs. temperature.

$$\Omega_T = T(S_g - S_l)$$

TABLE 4.2. VAPORIZATION HEAT OF LIQUID HELIUM FROM 0 TO 4.2°K, ergs/mole[a]

T, °K	TS_l	$pT(dB^*/dT)$	$\frac{1}{2}p^2T(dC^*/dT)$	$\Omega_{T\text{calc.}}$	Ω_T, measured by Keesom
4.2	59.1 × 10⁷	9.2 × 10⁷	2.7 × 10⁷	87.1 × 10⁷	79.7 × 10⁷
4.0	52.8	7.8	2.5	90.2	86.7
3.5	40.1	5.2	2.2	93.1	92.6
3.0	29.3	3.1	1.8	93.5	93.9
2.5	20.2	1.56	0.8	92.2	92.4
2.3	16.6	1.11	0.6	91.6	91.2
2.19	14.3	0.98	0.5	90.3	90.7
2.0	7.59	0.61	0.4	93.0	93.1
1.8	4.54	0.36	0.2	92.2	92.6
1.5	1.08	0.13	....	89.8	89.7
1.0	0.07	....	....	80.5	
0.0	....	....	....	59.65	

[a] J. Kistemaker, *Physica*, **12**, 281, 1946.

which gives

$$\Omega_T = -T\left\{R\ln\left[\frac{p}{T^{\frac{5}{2}}}\,\frac{h^3}{(2\pi m)\;k}\right] - \frac{5R}{2} + p\,\frac{dB^*}{dT} + \frac{1}{2}\,p^2\,\frac{dC^*}{dT} + S_l\right\}$$

where p is the vapor pressure, and B^* and C^* the virial coefficients in an equation of state

$$PV = RT + B^*p + C^*p^2 + \cdots$$

Kistemaker's results are given in Table 4.2.

Viscosity of Liquid Helium

For all other liquids the rise of the latent heat with lowering temperature from the critical temperature is even greater because of the onset of short-range order in the liquids. These other liquids continue to have an increase of order with lowering of temperature until solidification sets in. The viscosity of other liquids always increases with lowering of temperature, showing that it is more and more difficult for one atom to slip past another.

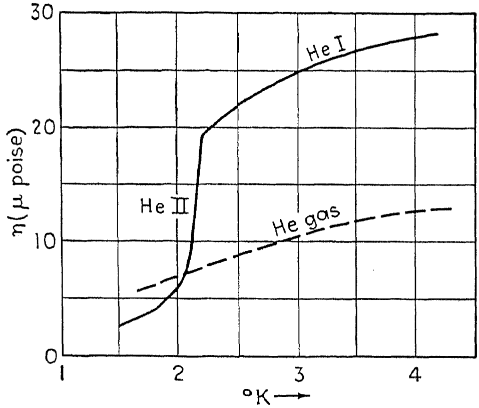

FIG. 4.8. Viscosity vs. temperature of liquid helium. (*Keesom and MacWood.*)

That liquid helium I is itself unique among all liquids is shown in Fig. 4.8 for the viscosity against temperature. These results were obtained first by Keesom and MacWood.[1] More recent results[2] from the Leiden laboratories are also shown in Fig. 4.8. Liquid helium I behaves more like a gas in that it gives a slightly lower viscosity with lower temperature. Liquid helium II shows a really fantastic property in that the viscosity rapidly vanishes as the temperature is lowered slightly below the transition point. These results were obtained by observing the damping action on a disk mounted as a torsion pendulum. Studies by

---

[1] W. Keesom and R. MacWood, *Physica*, **5**, 737; *ibid.*, **5**, 763, 1938.

[2] De Troyer, A. van Itterbeek, and G. J. van den Berg, *Physica*, **17**, 50, 1951.

Mendelssohn and Bowers[1] show the viscosity beginning to decrease rapidly with temperature even above the λ point (see Fig. 4.9). These authors used a flow method.

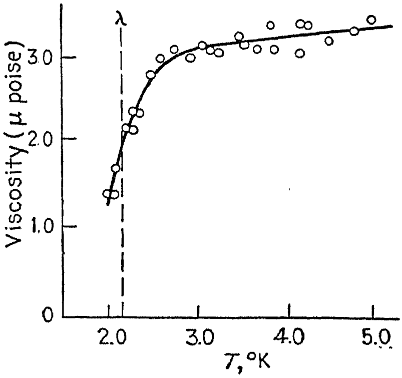

FIG. 4.9. Viscosity of liquid helium. (*Mendelssohn and Bowers.*)

The experiments on the viscosity of liquid helium II by E. Andronikashvili[2] lend support to the hypothesis that liquid helium II is composed of two fluids of density ρ_n and ρ_s, which is to say a normal fluid and a superfluid density. Andronikashvili was able to measure the temperature dependence of ρ_n. The equipment consisted of a torsion pendulum. The body of rotation consisted of a set of parallel and equidistant aluminum disks (Fig. 4.10) fixed on a common axis. From a fine torsion fiber the apparatus could undergo rotational oscillations about the axis passing perpendicularly through the plane of the disks. The normal fluid is dragged along by the disks because of viscous forces, while the superfluid remains stationary; thus the normal fluid contributes to the moment of

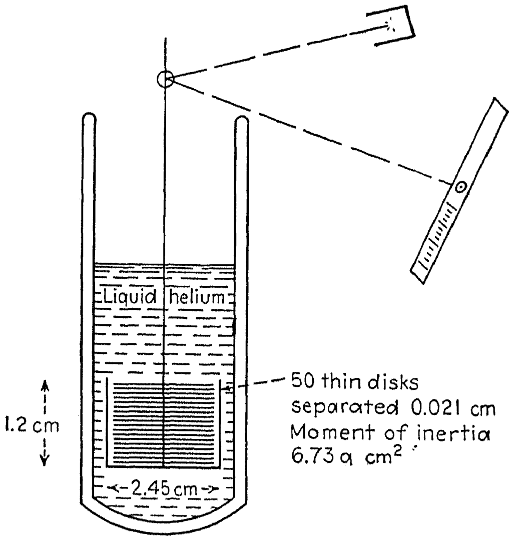
Liquid helium
50 thin disks separated 0.021 cm
Moment of inertia 6.73 g cm^2
1.2 cm
2.45 cm

FIG. 4.10. Andronikashvili's torsion pendulum equipment.

---

[1] K. Mendelssohn and R. Bowers, *Proc. Phys. Soc. (London)*, **62**, 394, 1949.

[2] E. Andronikashvili, *J. Exptl. Theoret. Phys. USSR*, **16**, 780, 1946; *ibid.*, **18**, 424, 429, 1948.

inertia, and the moment of inertia is determined by the period of oscillation. This means that ρ_n was determined, and the results are given in Table 4.3. The logarithmic decrement of the oscillation was measured, and from this Andronikashvili was able to deduce the product $\eta_n \rho_n$. Therefore the viscosity η_n of the normal component in liquid helium II was measured (see Fig. 4.11).

The experimental results of Andronikashvili have been repeated by Hollis-Hallett,[1] and in this paper the theory of the damping couple due to viscous drag is worked out completely. At 1.255°K, Hollis-Hallett finds the normal component viscosity $\eta_n = 35.4$ μpoise. These results are in accord with a theory by Landau and Khalatinov.[2]

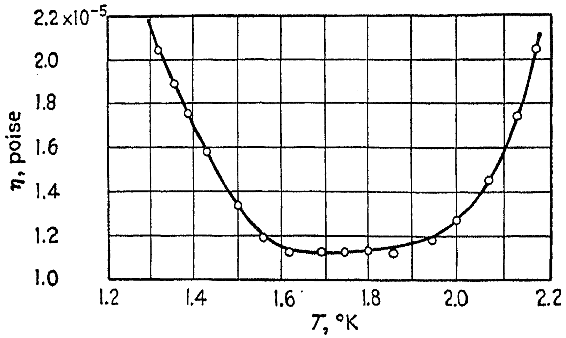

FIG. 4.11. Viscosity of normal component in liquid helium II.

TABLE 4.3. PERCENTAGE OF NORMAL COMPONENT IN LIQUID HELIUM II AT VARIOUS TEMPERATURES

T, °K	2.22	2.148	2.113	2.078	2.030	1.995	1.943	1.830	1.731	1.640
%, ρ_n	100	85.6	78.2	70.4	62.5	57.6	49.5	36.1	28.0	19.20

Thermal Properties of He³ Isotope

The vapor pressure of He³ isotope has been discussed in Chap. 3, where the quantum nature of the equation of state was brought out. The physical properties of He³ are of great importance because of the theoretical difference with the isotope He⁴. The isotope He³ probably remains a liquid to the absolute zero of temperature. But above 1°K it shows no superfluid properties. The solidification may be obtained by pressure.[3] Between the temperatures 1.02 and 1.51°K the following equation holds:

$$P = 27.0 + 13.0T^2 \qquad \text{atm}$$

---

[1] A. C. Hollis-Hallett, *Proc. Roy. Soc. (London)*, **210**, 404, 1952.

[2] L. Landau and I. Khalatinov, *J. Exptl. Theoret. Phys. USSR*, **19**, 637, 709, 1949.

[3] D. Osborne, B. Abraham, and B. Weinstock, *Phys. Rev.*, **82**, 263, 1951.

Thus the pressure-temperature curve separating solid and liquid bears a strong resemblance to He^4, and the same arguments concerning the internal energy of the liquid and solid hold for He^3 as for He^4. The internal energy of the liquid is less than that of the solid below about 1.44°K.

TABLE 4.4. SMOOTHED DENSITIES OF LIQUID AND VAPOR He^3

T, °K..........	1.0	1.5	2.0	2.5	2.8	3.1	3.34
Liquid, g/cc.....	0.0792	0.0792	0.0784	0.0744	0.0700	0.0618	0.0420
Vapor, g/cc.....	0.0055	0.0016	0.0036	0.0084	0.0132	0.0220	0.0420

The density of the liquid He^3 between 1.27 and 2.79°K was measured by Grilly, Hammel, and Sydoriak.[1] Table 4.4 gives the smoothed density of liquid and vapor He^3. These authors used the density data and their vapor-pressure data to give the computed heat of vaporization from the equation

$$\Delta H_{\text{vap.}} = T\,\Delta V\,\frac{dP}{dT}$$

In this equation, T is the absolute temperature, ΔV the change of volume between the liquid and gas, and dP/dT the slope of the vapor-pressure curve at that temperature. Figure 4.12 gives the results.

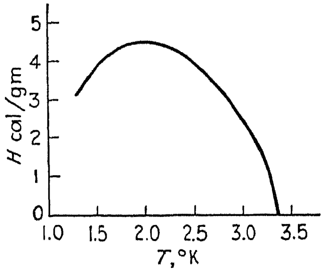

FIG. 4.12. Heat of vaporization vs. temperature for He^3 isotope. (*Grilly, Hammel, and Sydoriak, Phys. Rev.*, **75**, 1103, 1949.)

The vapor pressure, critical point, heat of vaporization, and entropy of liquid He^3 have been reported by Abraham, Osborne, and Weinstock.[2] Table 4.5 gives the vapor pressure of He^3 according to these authors. The data for pressure in millimeters of Hg are represented accurately by the equation

$$\log P_{\text{mm}} = -\frac{0.97796}{T} + 2.5\log T + 0.000302T^3 + 1.91594$$

The theoretical value of the constant term should be 2.0085 where the pressure is in millimeters of Hg. The critical temperature is 3.35 ± 0.02°K, and the critical pressure is 890 ± 20 mm Hg.

The heat of vaporization was computed from the new vapor-pressure data and from a slightly more accurate volume difference ΔV. Table 4.6 gives the data with extrapolation to 0°K. The calculated entropy of liquid He³, excluding the nuclear spin entropy, is 0.75 ± 0.1 cal/(°K)(mole) at 1°K. The extrapolated entropy at 0°K is 0.42 ± 0.1 cal/(°K)(mole). The zero temperature entropy arises from the constant term in the vapor pressure. If this term were equal to the theoretical value, then there would be zero entropy at the absolute zero of temperature. We must look for new studies on He³ liquid at temperatures

---

[1] E. Grilly, E. Hammel, and S. Sydoriak, *Phys. Rev.*, **75**, 1103, 1949.

[2] B. Abraham, D. Osborne, and B. Weinstock, *Phys. Rev.*, **80**, 366, 1950.

TABLE 4.5. VAPOR PRESSURE OF LIQUID HE³ AT EVEN TEMPERATURE INTERVALS

T_K, °K	T_A, °K	P, int. mm Hg	dP/dT, mm/°K
1.0	1.000	8.68	41.3
1.1	1.100	13.51	55.9
1.2	1.200	19.93	72.7
1.3	1.300	28.13	91.7
1.4	1.400	38.33	112.6
1.5	1.500	50.72	135.5
1.6	1.603	65.50	160.3
1.7	1.705	82.85	186.9
1.8	1.807	102.94	215.2
1.9	1.909	125.94	245.2
2.0	2.011	152.04	276.9
2.1	2.112	181.38	310.2
2.2	2.213	214.13	345.1
2.3	2.312	250.46	381.6
2.4	2.411	290.50	419.6
2.5	2.510	334.44	459.3
2.6	2.609	382.41	500.5
2.7	2.708	434.59	543.2
2.8	2.807	491.13	587.6
2.9	2.906	552.18	633.6
3.0	3.005	617.89	681.1
3.1	3.104	688.45	730.3
3.2	3.203	764.02	781.2
3.3	3.302	844.74	833.8
3.195	3.198	760	

TABLE 4.6. HEAT OF VAPORIZATION AND ENTROPY OF LIQUID HE³

T_K, °K	$\Delta H_{\text{vap.}}$, cal/mole	$\Delta H_{\text{vap.}}/T$, e.u.[a]	$S_{\text{ideal gas}}$, e.u.	$S_{\text{real}} - S_{\text{ideal}}$, e.u.	S_l, e.u.
0	(4.47)	∞	∞	0.00	(0.42 ± 0.11)
0.5	(6.95)	(13.89)	(14.34)	0.00	(0.45 ± 0.12)
1.0	9.12 ± 0.12	9.12	9.87	0.00	0.75 ± 0.14
1.5	10.65 ± 0.24	7.10	8.37	−0.02	1.25 ± 0.17
2.0	11.34 ± 0.41	5.67	7.62	−0.06	1.89 ± 0.22
2.5	10.81 ± 0.69	4.32	7.16	−0.11	2.73 ± 0.29

[a] e.u. = cal/(°K)(mole).

well below 1°K to see if a hump in the specific heat exists which can account for the entropy.*

The problem of the residual entropy for liquid helium isotope III has been considered by Lifshitz,[1] and he concludes that actually the residual entropy is even larger, *i.e.*, 1.8 cal/(mole)(°K). Lifshitz asserts that the entropy due to nuclear spin exists in the vapor phase but must vanish in the liquid because in the liquid the strong exchange interaction of the nuclear magnetic moment must lead to their ordered orientation.[2] Lifshitz computes the chemical potential of the liquid He^3 and finds this in accord with a Fermi-type gas. The specific heat according to his calculations is linear with temperature and is

$$C = 0.76RT \qquad \text{cal/(mole)(°K)}$$

Lifshitz compares this value of the specific heat with that of a degenerate Fermi gas (composed of particles with the same mass and having the same volume density, a specific volume of 38 cm^3/mole), and this would be

$$C = 1.0RT \qquad \text{cal/(mole)(°K)}$$

An investigation of the magnetic properties of liquid He^3 has not indicated an alignment of the nuclear moments according to Hammel, Laquer, Sydoriak, and McGee.[3]

---

* Note added in page proof: B. Weinstock, B. Abraham, and D. Osborne (*Phys. Rev.*, **89**, 787, 1953), have recalculated the entropy of liquid He^3 and find at 1.0°K the value 2.09 ± 0.14 e.u. Thus, the last three columns of Table 4.6 must be changed. These uncertainties emphasize the need for direct specific heat measurements. T. Chen and F. London (*Phys. Rev.*, **89**, 1038, 1953) find $S \rightarrow 0$ as $T \rightarrow 0$°K when they evaluate the vapor pressure data.

[1] E. M. Lifshitz, *J. Exptl. Theoret. Phys. USSR*, **21**, 659, 1951.

[2] I. Pomeranchuk, *J. Exptl. Theoret. Phys. USSR*, **20**, 919, 1950.

[3] E. Hammel *et al.*, *Phys. Rev.*, **86**, 432, 1952.

CHAPTER 5

LIQUID HELIUM—DYNAMIC PROPERTIES

In the last chapter we discussed the results of experiments on the thermodynamic properties of liquid helium. In the present chapter we shall discuss dynamic properties, *i.e.*, capillary flow of the superfluid, heat conduction, pressure waves or sound, and thermal waves or second sound. We have set these physical properties apart this way in two chapters in an effort to emphasize the need for a theoretical foundation for the basic thermal properties. And yet the experiments described in this present chapter are vital to the model we may choose for a statistical theory of liquid helium.

Flow Phenomena in Capillaries

The flow of a liquid in a narrow channel affords another method of determining the viscosity of the liquids. Since liquid helium II has such a small viscosity, flow methods were used at the same time by Kapitza and by Allen and Misener. Both groups found the viscosity of liquid helium II to be below 10^{-3} μpoise. Since this is many orders of magnitude smaller than any gas, let alone liquid, the experiments called for drastic measures. Kapitza allowed the liquid to flow out between two optically flat disks whose separation was measured by interference fringes, and the distance used was about half a micron. Allen and Misener had a reservoir of liquid helium with a capillary of cross section 1 mm and length 130 cm and then another one with cross section about 0.015 mm and length 93.5 cm. The rate of fall of the liquid level in the reservoir was observed as the liquid passed out of the capillary. Besides the very low viscosity, Allen and Misener found that the velocity of flow was almost independent of the pressure head and changed very little with change of cross section of the capillary. Since these experiments seem to indicate that the liquid helium II flows over the surface of the tube rather than as a bulk flow down the cross section, some attention is given to the nature of the walls of the tube. The importance of small differences of temperature was not realized in much of the early work.

Giauque, Stout, and Barieau measured the flow of liquid helium II through a channel of separation 10^{-4} cm. The viscosity determined by their improved techniques is given in Table 5.1 and is taken from a smoothed curve. These values obtained by the capillary-flow method do not agree very well at 2°K and on up to the λ point with the values obtained by Keesom and MacWood with the oscillating disk. They are in better accord with more recent Leiden results. Tisza[1] pointed out an essential difference in the two types of experiments. The oscillating disk is damped in liquid helium II by those kinds of atoms, called *normal* types, which are able to exchange momentum with the disk. But in the flow studies, and in particular in capillaries, it is the superfluid type of atom which contributes to the volume flow. The superfluid type of atom has zero viscosity and obeys a new quantum hydrodynamics. Just what the dissipation effects, if any, may be for the superfluid is not clear, but they should not be confused with a pure viscosity. Landau and Khalatinov[2] seem to agree with this interpretation.

TABLE 5.1. VISCOSITY OF LIQUID HELIUM II FROM CAPILLARY FLOW[a]

T, °K	1.4	1.5	1.6	1.7	1.8	1.9	2.0	2.1	2.2
η, μpoise	.07	.12	.18	.25	.35	.50	.80	1.5	15.0

[a] W. Giauque, J. Stout, and R. Barieau, *Phys. Rev.*, **54**, 147, 1938; *J. Am. Chem. Soc.*, **61**, 654, 1939.

Film Flow in Liquid Helium II

We shall return presently to the experiments on capillary flow. What has been said thus far has been meant as an introduction to the general nature of the problem. It seems better to inject some other experimental evidence about transfer effects which will help in understanding the capillary-flow experiments. Kamerlingh Onnes observed in 1922 that the surfaces of two volumes of liquid helium II contained in two concentric vessels adjusted themselves automatically to the same level. Rollin found that the loss from vessels containing liquid helium II is exceptionally high and attributed this to what is now called the *Rollin film*. That film is a thin layer of helium II on the walls connecting one bath to another or up the side walls of a vessel to warm temperatures where liquid helium I could exist. This brilliant idea has led to many experiments. Daunt and Mendelssohn[3] performed an experiment in which a small glass beaker was suspended on a thin glass fiber and could be lowered into a bath of liquid helium II or raised out of it. Quoting from their work,

> *A.* When the empty beaker was lowered into the liquid, it filled up to the level of the bath although the rim of the beaker was everywhere above the level of the liquid. (Kamerlingh Onnes effect, see Fig. 5.1*a*.)

---

[1] L. Tisza, *J. phys. radium*, **8**, 165, 350, 1940; *Phys. Rev.*, **72**, 838, 1947.

[2] L. Landau and I. Khalatinov, *J. Exptl. Theoret. Phys. USSR*, **19**, 637, 709, 1949.

[3] J. Daunt and K. Mendelssohn, *Nature*, **141**, 911, 1938; *ibid.*, **142**, 475, 1938; *Proc. Roy. Soc. (London)*, **170**, 423, 1939.

B. When the beaker was partly lifted out of the bath, the level of the liquid in the beaker fell at the same rate as it rose in 5.1*a*, and the level of the bath rose until both had reached the same height. (Fig. 5.1*b*.)

C. In order to establish whether the transfer took place by distillation through the gas phase or by transfer over the surface, the effect was examined by introducing "wicks" of twisted copper wire which increased the surface leading from one level to the other. It was found that this increased the rate of transfer to several times the previous rate so long as, but only so long as, the wick reached into the liquid at the higher level.

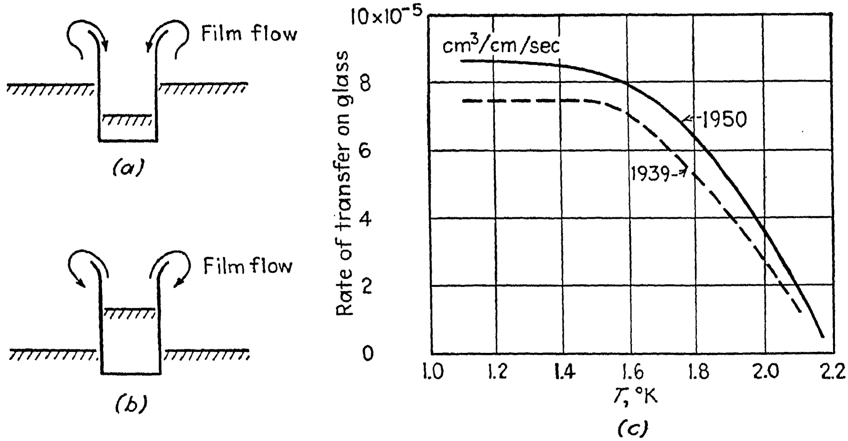

FIG. 5.1. (*a*) Film flow entering the vessel. (*b*) Film flow leaving the vessel. (*c*) Film-flow rate of transfer on glass vs. temperature.

D. When the beaker (without a wick) was lifted completely out of the bath, it was found that the liquid vanished at the same rate as when it was still partly dipping into it. This was accounted for when it was observed that the liquid collected in drops at the bottom of the beaker and dripped into the bath. (See photograph in Chap. 2.)

E. The rate of transfer did not appear to differ very much whether the beaker was almost full or nearly empty, the rate decreasing only by 20 per cent when the level had dropped from within 0.5 mm of the rim to some 20 mm from the rim.

F. As shown in the accompanying Fig. 5.1*c*, the rate of transfer increased rapidly with decreasing temperature. The rate is given in cubic centimeters of liquid per second per centimeter of glass surface cutting the surface of the liquid.

G. If any of these phenomena occur above the λ-point, the rate is so slow that they could not be observed in our experiments.

Recently Mendelssohn and White[1] have again measured the rate of transfer through the film on clean glass surfaces, and their results are shown in Fig. 5.1*c* (1950). Rates of film transfer are somewhat higher on metal surfaces. From these experiments the existence of the Rollin film is established and further that the rate of the transfer is not affected by the difference of heights between the two levels. Daunt and Mendelssohn estimated the film to be about 3.5×10^{-6} cm thick. Burge

[1] K. Mendelssohn and G. White, *Proc. Phys. Soc. (London)*, **63**, 1328, 1950.

and Jackson[1] have measured the helium film thickness by an optical method. Linearly polarized light was reflected from a stainless-steel mirror, the upper part of which was coated with a layer of barium stearate one molecule thick and the lower part with a similar layer three molecules thick. The reflected light passed through a mica compensating plate and a Nicol prism. Adjustment of the mica plate and Nicol gives equality of illumination on the 1 and 3 areas. If now a film of helium II covers the mirror, the Nicol must be rotated to restore equality of illumination. The rotation is a measure of the thickness of the helium film. The observed thickness at any given height above the liquid helium was found to be nearly independent of the temperature between 1.1 and 2.18°K but then decreased rapidly to zero at the λ point. The thickness at 1 cm height and 1.5°K is provisionally given as 1.9×10^{-6} cm.

Mechano-caloric Effect

Continuing the work on the surface transport in liquid helium II, Daunt and Mendelssohn[2] showed that, if a small heater coil raised the temperature of the liquid in the inner bath, the height of the inner bath no longer remained equal to the outer bath but was raised above it. This clearly showed that there exists a transfer of helium from a colder to a hotter place when a temperature gradient is imposed. This effect is analogous to the "fountain effect" which we shall discuss later.

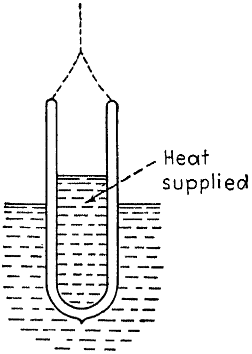

FIG. 5.2. Thermo-mechanical effect in liquid helium via surface film.

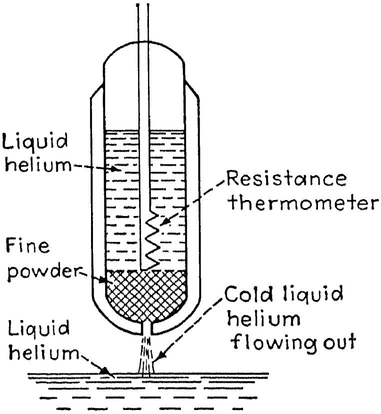

FIG. 5.3. Mechano-caloric effect. (*Predicted by Tisza, Nature,* **141,** 913, 1938.)

The effect discovered by Daunt and Mendelssohn is shown in Fig. 5.2.

---

[1] E. J. Burge and L. C. Jackson, *Proc. Roy. Soc. (London)*, **205,** 270, 1951.

[2] J. Daunt and K. Mendelssohn, *Nature,* **143,** 719, 1939; *Proc. Phys. Soc. (London),* **63,** 1305, 1950.

They then worked the reverse of the effect: a Dewar vessel (Fig. 5.3) was closed at the top and had a hole at the lower end which was constricted by a plug of fine emery powder. It contained a phosphor-bronze thermometer and was suspended in a bath of liquid helium II. When the Dewar vessel was lifted out of the bath, the liquid ran rapidly out of the vessel and fell into the outer bath. The temperature inside of the Dewar rose about 0.01°K during the flow process. When the Dewar was lowered so that the liquid ran from the bath into the vessel, the liquid inside was cooled by a similar amount. This is called the mechano-caloric effect. It was predicted by L. Tisza.[1] The interpretation comes as something of a surprise; those atoms which flow through the plug have nearly zero entropy.

Entropy of Helium II—Flow Studies by P. Kapitza

P. Kapitza published[2] some very difficult experiments on the heat transfer in helium II. The high heat conductivity in capillaries was explained by Kapitza as a circulation of the helium along the capillary (convection currents) so that with an increase of the heat load the circulation increases and eventually becomes so intense that it becomes turbulent. Kapitza postulated that the liquid flowing toward the heat source had almost zero energy. This led to his important entropy work.

Kapitza[3] has measured the heat content of liquid helium flowing through a narrow slit. The slit was made by the separation of two optically polished flat quartz disks to a distance of several microns and smaller (10^{-5} cm). The slit separated an inner vessel from the outer bath of liquid helium. Heat supplied to the liquid helium contained by the inner vessel caused liquid helium from the bath to rush through the slit such as to keep the temperature of the interior equal to the outer bath temperature. Too rapid heating of the interior vessel caused a temperature difference to appear. The energy per unit of time supplied to the interior vessel was measured, as well as the volume of the liquid helium per unit of time which entered the vessel. The difference between the specific heat content of helium flowing through the slit and the free helium bath accounts for the zero change of temperature in the interior vessel during the heating. The flow of helium through the slit was determined to be thermodynamically reversible (no dissipation effects). It was concluded that the entropy of the helium flowing through the narrow channel is equal to zero. Thus the entropy acquired by the liquid helium which had passed through the slit is $S = Q/T$, where the heat Q is supplied by the heater. The slit had thus served as a filter, permitting the part of the helium bath having zero entropy to enter. The entropy values taken from the specific heat of helium II by Keesom and Keesom[1] agree with the values P. Kapitza determined by his studies of flow through a narrow slit. Figure 5.4 gives Kapitza's values of Q against T.

---

[1] L. Tisza, *Nature*, **141**, 913, 1938.

[2] P. Kapitza, *J. Phys. USSR*, **4**, 181, 1941.

[3] P. Kapitza, *J. Phys. USSR*, **5**, 59, 1941.

It is interesting to note that H. London[2] had predicted the heating and cooling effect to be (per unit of volume transported)

$$Q = \rho S T$$

In this last equation the density of the liquid flowing is ρ. The entropy per unit mass S depends on the amount of normal fluid present in the liquid helium II by the equation

$$S = \frac{\rho_n}{\rho} S_\lambda$$

where S_λ is the entropy value at the λ point, ρ the total density, and ρ_n the density of the normal fluid component. Likewise, the entropy may be described by

$$S = S_\lambda \left(\frac{T}{T_\lambda}\right)^r$$

where $S_\lambda = 0.403$ cal/(g)(°K) and where $r = 5.6$. The temperature range over which this last empirical equation is valid is from 1.0 to 2.19°K which is the λ point.

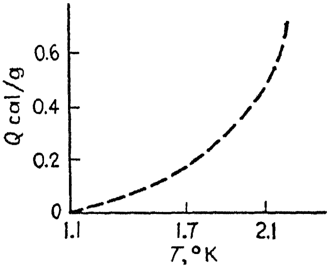

FIG. 5.4. Kapitza's values of heat content Q vs. temperature.

Hydrodynamic Studies—Fountain Effect

We are now perhaps better prepared to grasp the meaning of the experiments by Allen and his coworkers which actually preceded many of the experiments already discussed and which stimulated much of the experimental and theoretical work of the late thirties. Allen and Misener summarized their first experiments on the flow of liquid helium II through capillaries of various diameter and length as follows:[3]

> *A*. The dependence of the velocity of flow on pressure head becomes less; (*a*) as the radius of the capillary is reduced, (*b*) as the capillary is lengthened, (*c*) as the temperature is lowered.
>
> *B*. In the largest capillaries at a temperature close to the λ-point an approximation to laminar flow is observed.
>
> *C*. In all capillaries at low pressure heads, the velocity increases with decreasing temperature, but the reverse holds at higher pressure heads in large capillaries.

---

[1] W. H. Keesom and A. P. Keesom, *Physica*, **2**, 557, 1935.

[2] H. London, *Nature*, **142**, 612, 1938; *Proc. Roy. Soc. (London)*, **171**, 484, 1939.

[3] J. F. Allen and A. D. Misener, *Proc. Roy. Soc. (London)*, **172**, 467, 1939.

D. At all temperatures there is a minimum in the relation between the radius of the channel and the velocity at constant pressure head. For channels smaller than 5×10^{-4} cm in width, the velocity increases rapidly with decreasing channel size.

E. At pressure heads above 50 dynes/cm^2 in the narrowest channels the velocity is completely independent of pressure head at all temperatures. The curve between the velocity independent of pressure head and the temperature bears a strong resemblance both in magnitude and shape to that for mobile surface films of helium II above the hydrostatic surface of the liquid. See Fig. 5.5 where the ordinate does not have numbers because it represents a family of such curves.

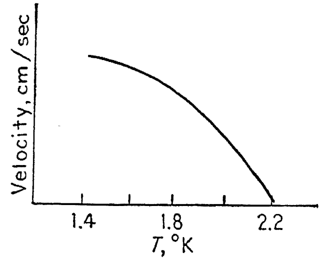

FIG. 5.5. Typical curve of capillary-flow velocity vs. temperature.

F. In channels less than 10^{-3} cm in width, at temperatures close to the λ-point, and at low pressure heads, the flow becomes laminar with evidence of an exceedingly small viscosity.

G. For flow through tightly packed fine powder the observed viscosity appears equal in magnitude and temperature variation to that observed in the narrowest smooth channels.

We must recall the classical expression given by Poiseuille for the velocity v for the flow of liquid with laminar motion in a narrow tube of radius

FIG. 5.6. Photograph of fountain effect. (*Cryogenic laboratory, National Bureau of Standards.*)

r, length L, viscosity η, and pressure difference $(p_1 - p_2)$ between the ends:

$$v = \frac{\pi r^4}{8\eta L}(p_1 - p_2)$$

For turbulent motion the velocity is proportional to the square root of the pressure. The results of Allen and Misener indicate (1) the onset of quantum hydrodynamics below the λ point and (2) the need for a distinction between laminar and turbulent flow in the quantum hydrodynamics. Their experiments showing the flow rate to be independent of the length of the flow channel and of the pressure difference at its ends have been repeated with variations by Bowers, Chandrasekhar, and Mendelssohn.[1] They find agreement, as did White in still more recent work.[2] Bowers and White[3] have studied the flow of liquid helium II through porous metallic membranes. Using two membranes of only slightly different flow resistance in series, it was found that almost all the pressure drop associated with the flow occurs across the membrane of higher resistance, the flow through the membrane of lower resistance taking place under almost zero pressure gradient.

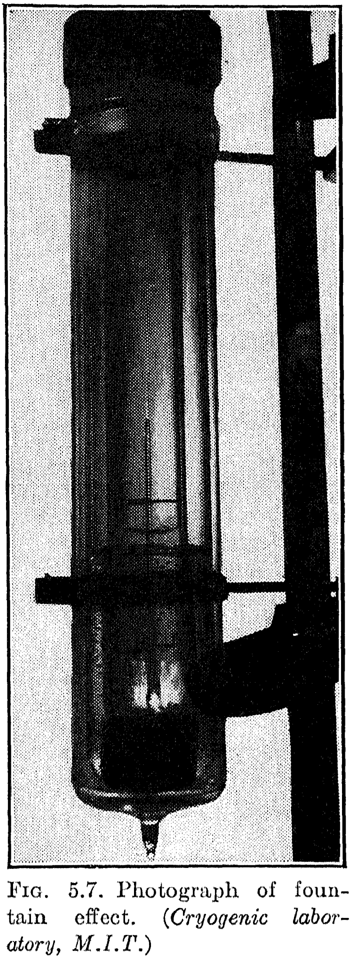

FIG. 5.7. Photograph of fountain effect. (*Cryogenic laboratory, M.I.T.*)

The fountain effect was observed by Allen and Jones[4] in 1938 and was further studied by Allen and Reekie.[5] Figures 5.6 and 5.7 show the tube whose upper end projected above the bath of liquid helium II and whose lower end was packed with fine emery powder. There is an open orifice at the bottom through which the helium can flow. When heat radiation was allowed to fall on the portion containing the powder, a stream of liquid helium was observed to flow out of the top of the tube. Jets become of the order of 30 cm in height at very low temperatures and with quite fine powder size. This amazing liquid pump works on a temperature gradient which then produces an effective pressure gradient. Recent work by Mellink[1] gives the dependence on heat current.

---

[1] R. Bowers, B. Chandrasekhar, and K. Mendelssohn, *Phys. Rev.*, **80**, 856, 1950.

[2] G. White, *Proc. Phys. Soc. (London)*, **64**, 554, 1951.

[3] R. Bowers and G. White, *Proc. Phys. Soc. (London)*, **64**, 558, 1951.

[4] J. F. Allen and H. Jones, *Nature*, **141**, 243, 1938.

[5] J. F. Allen and J. Reekie, *Proc. Cambridge Phil. Soc.*, **35**, 114, 1939.

Heat Conductivity

The heat conductivity of liquid helium I shows again its strong resemblance to a gas in that the order of magnitude and temperature dependence characterize it as such. The value of the heat conductivity defined by the ratio of the heat current density φ to the temperature gradient, $K = (\varphi)/(dT/dx)$, was measured by Keesom at 3.3°K to be

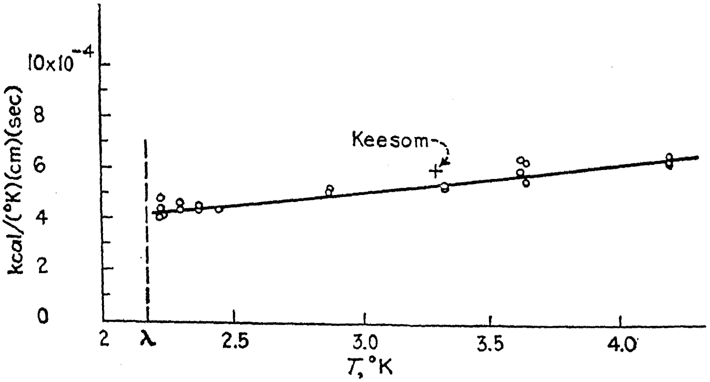

FIG. 5.8. Heat conductivity of liquid helium I. *(Grenier, The Rice Institute.)*

$$K = 6 \times 10^{-5} \text{ cal/(°K)(cm)(sec)}$$

Measurements as a function of temperature have been made by Grenier[2] and are shown in Fig. 5.8. Mendelssohn and Bowers[3] have obtained similar results for the heat conductivity of liquid helium I.

At temperatures below the λ point, Keesom[4] found the heat conductivity in capillary tubes to be about 190 cal/(°K)(cm)(sec), thereby making liquid helium II the best heat conductor known. At still lower temperatures the heat conductivity passes through a maximum at 1.92°K where it has a value of about 810 cal/(°K)(cm)(sec) and then rapidly diminishes until at extremely low temperatures, *i.e.*, below 0.1°K, the heat conduction is very small. We shall have cause to reexamine these very low-temperature results when we discuss the propagation of thermal waves (second sound) at these same temperatures in open baths. One should not hastily draw an analogy between the infinite conductivity of a superconducting metal and the high heat conductivity of liquid helium

---

[1] J. H. Mellink, *Physica,* **13,** 180, 197, 1947.
[2] C. Grenier, *Phys. Rev.,* **83,** 598, 1951.
[3] K. Mendelssohn and R. Bowers, *Nature,* **167,** 111, 1951.
[4] W. H. Keesom, "Helium," Amsterdam, Elsevier, 1942.

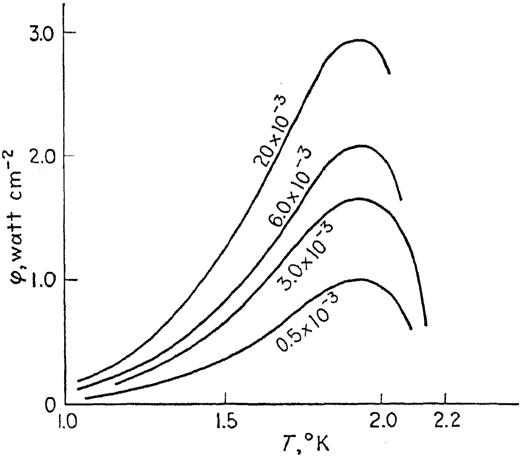

FIG. 5.9. Heat current density vs. temperature. Each curve has a given constant temperature gradient in °K/cm. (*Keesom, Saris, and Meyer, Physica*, **7**, 817, 1940.)

II. The dependence on heat current density was measured by Keesom, Saris, and Meyer[1] and is given in Fig. 5.9. The dependence of the heat conductivity on pressure is shown in the family of curves determined by Allen and Ganz in Fig. 5.10. Ganz[2] made some measurements to determine the speed with which a heat pulse traveled in liquid helium II and concluded that the velocity was about 10^4 cm/sec. A number of years later Peshkov[3] published more exact measurements and found the velocity to be 2×10^3 cm/sec at 1.6°K. Kapitza[4] published some brilliant experiments on heat transfer in helium II which supported his earlier ideas about internal convection currents as the cause of the high heat conduction in capillaries.

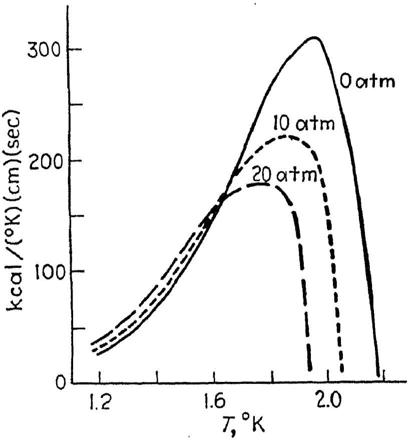

FIG. 5.10. Heat conductivity vs. temperature at different pressures in capillary-tube experiment.

---

[1] W. H. Keesom, B. F. Saris, and L. Meyer, *Physica*, **7**, 817, 1940.

[2] E. Ganz, *Proc. Cambridge Phil. Soc.*, **36**, 127, 1940.

[3] V. Peshkov, *J. Phys. USSR*, **8**, 381, 1944; *ibid.*, **10**, 389, 1946.

[4] P. Kapitza, *J. Phys. USSR*, **4**, 181, 1941.

Velocity and Attenuation of Sound in Liquid Helium

The low-temperature laboratory at Toronto published the first experiments on the velocity of sound (1.3 megacycles/sec) through liquid helium. These studies were made by Findlay, Pitt, Grayson-Smith, and Wilhelm.[1] They used a quartz crystal to set up standing waves between a metal reflector in the helium bath. The reflector distance could be varied, and the resulting nodal positions could be detected by the resonant reaction of the vibrating crystal. The resulting wave-length determination led to the velocity-against-temperature curve shown in Fig. 5.11. At high pressures the velocity of sound showed a discontinuity at the λ point. The authors mentioned considerable difficulty in getting values at the λ point.

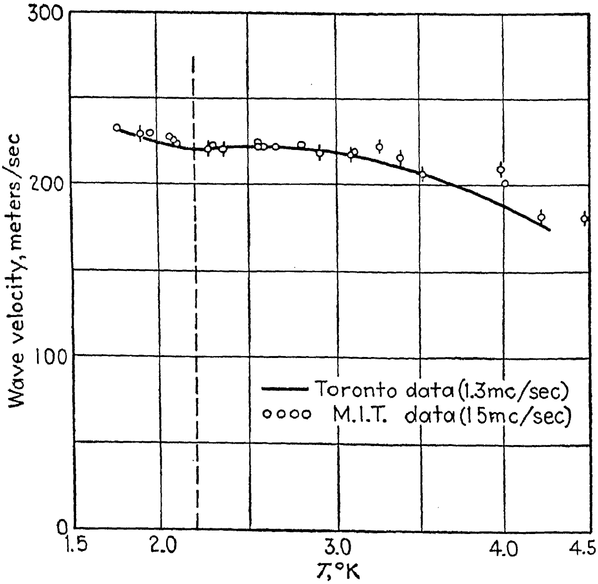

FIG. 5.11. Ultrasonic wave velocity vs. temperature in liquid helium.

Pellam and Squire[2] measured the velocity and attenuation of 15 megacycles/sec sound in liquid helium from 1.57 to 4.5°K. The velocity at 15 megacycles/sec was found to agree with the Toronto results, and hence there is no dispersion in the frequency range. The attenuation measurements exhibit three important features, as shown in Fig. 5.12: (1) in the upper temperature range of He I the measurements agree well with classical theory, (2) at the λ point the attenuation coefficient rises abruptly, presumably to infinity, indicating complete absorption of the ultrasonic energy, (3) just below the λ point the attenuation has its smallest value and with lowering temperature the attenuation increases. One of the interesting features of the attenuation measurements is the manner in which classical theory completely accounts for the energy absorption in helium I at temperatures above 3°K. Values computed on the basis of classical theory are represented by the dotted curve in Fig. 5.12, which above 3°K also represents the best experimental curve. Numerical values of the two classical contributions to absorption are given in Table 5.2, where the attenuation coefficients are

---

[1] J. Findlay *et al.*, *Phys. Rev.*, **54**, 506, 1938; *ibid.*, **56**, 122, 1939.

[2] J. Pellam and C. Squire, *Phys. Rev.*, **72**, 1245, 1947.

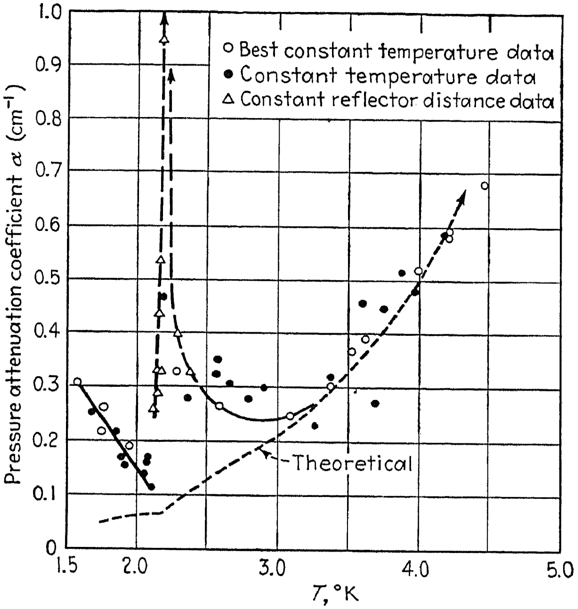

FIG. 5.12. Pressure-attenuation coefficient vs. temperature, by Pellam and Squire. [Atkins and Chase, in *Proc. Phys. Soc. (London)*, **64**, 826, 1951, give $\alpha = 1.0\ \text{cm}^{-1}$ at 1.2°K.]

$$\alpha_{\text{total}} = \alpha_{\text{viscosity}} + \alpha_{\text{thermal conduction}}$$

$$\alpha_{\text{vis.}} = \frac{8\pi^2}{3}\frac{\eta\nu^2}{\rho c^3}$$

$$\alpha_{\text{therm.}} = \frac{2\pi^2(\gamma - 1)}{\rho c^3}\frac{K\nu^2}{C_p}$$

In the above equations, ν is the ultrasonic frequency in cycles per second, c the ultrasonic velocity in centimeters per second, η the coefficient of viscosity in poises, ρ the liquid density in grams per cubic centimeter, K the heat conductivity coefficient in cal/(°K)(cm)(sec), C_p the specific heat at constant pressure in cal/(g)(°K), and γ the ratio of specific heats.

The excellent agreement above the 3°K temperature means that there is a good internal consistency of the many measured quantities which went into the calculation. In the region of the λ point and below in temperature, the classical theory is inadequate and points to some other mechanism. Just at the λ point the energy gap between helium I and helium II must be very small, and the energy in the sound pulse might be sufficient to cause a transition of those atoms of the superfluid type into the normal type of atoms. Below the λ point the classical theory is obviously inadequate because of the new quantum state. Atkins and Chase[1] were stimulated by the ultrasonic results, so much so that they built similar sound equipment and obtained more precise results over a wider temperature range. Some interesting speculations have been advanced for dissipation effects. Among them are those by Gorter and Mellink,[2] by Tisza,[3] and by Pippard.[4] The work by Khaltnikov[5] has had success in explaining quantitatively the absorption of ordinary sound in liquid helium II and in predicting the dispersion of second sound in the region below 1°K and of its attenuation near the λ point.

TABLE 5.2. VALUES OF α, THE ATTENUATION COEFFICIENT

T, °K	$\gamma - 1$	$\alpha_{\text{viscosity}}$	α_{thermal}	Total $\alpha_{\text{theoretical}}$	Total $\alpha_{\text{exptl.}}$
5.10 ± 0.1°K	....	.....	.....	.....	(1.78 cm^{-1})
4.47 ± 0.01	....	.....	.....	.....	0.68
4.22 ± 0.01	1.35	0.244	0.382	0.62	0.58
4.00 ± 0.01	1.14	0.200	0.260	0.46	0.52
3.62	0.80	0.131	0.198	0.33	0.39
3.52	0.72	0.122	0.184	0.30	0.37
3.38	0.58	0.114	0.164	0.28	0.30
3.08	0.38	0.103	0.122	0.22	0.25
2.58	0.14	0.087	0.055	0.14	0.27
2.28	0.03	0.079	0.015	0.09	0.33
λ point (2.19)	0	0.077	0	0.077	(∞)
2.11	....	0.071	0	0.071	0.11
1.94	....	0.061	0	0.061	0.15
1.76	....	0.050	0	0.050	0.24
1.57	....	0.042	0	0.042	0.30

Second Sound or Thermal Waves in Liquid Helium II

The brilliant theoretical prediction by Tisza[6] that there should exist in helium II a propagation of heat energy by a wave moving with velocity

---

[1] K. Atkins and C. Chase, *Proc. Phys. Soc. (London)*, **64**, 826, 1951.

[2] C. Gorter and J. Mellink, *Physica*, **14**, 285, 1949.

[3] L. Tisza, *Phys. Rev.*, **72**, 838, 1947.

[4] A. B. Pippard, *Phil. Mag.*, **42**, 1209, 1951.

[5] I. Khalatnikov, *J. Exptl. Theoret. Phys. USSR*, **20**, 243, 1950.

[6] L. Tisza, *J. phys. radium*, **8**, 164, 350, 1940; *Phys. Rev.*, **72**, 838, 1947.

c_2 different from sound velocity c_1 was experimentally found by Peshkov during the war. The thermal waves called *second sound* were detected by Peshkov by means of a resistance thermometer. Peshkov set up standing waves in the liquid helium II and moved his detector from temperature maximum to temperature minimum. The velocity of second sound c_2 is given in Table 5.3. J. R. Pellam used pulsed heat from which he could measure both the velocity and the attenuation. His results are also shown in Table 5.3. Lane, Fairbank, and Fairbank[1] used the standing-wave technique and a pressure microphone detector placed out in the vapor phase. There is a conversion to first sound at the interface. Pellam's experimental equipment may be represented in block diagram, as shown in Fig. 5.13. Video voltage pulses from the

TABLE 5.3. VELOCITY OF SECOND SOUND AT VARIOUS TEMPERATURES

T, °K	C_2, m/sec	
	(a)	(b)
2.180	4.3	3.0
2.176	5.0	3.12
2.150	7.5	9.0
2.127	10.0	11.6
2.101	12.0	12.6
2.00	16.53	16.77
1.936	17.96	18.0
1.79	20.0	19.7
1.63	20.3	20.2
1.52	20.4	20.0
1.43	19.9	20.0
1.32	19.2	19.8
1.44	18.8	19.4
1.15	18.7	19.1

[a] V. Peshkov, *J. Phys. USSR*, **8**, 381, 1944; *ibid.*, **10**, 389, 1946.
[b] J. R. Pellam, *Phys. Rev.*, **75**, 1183, 1949.

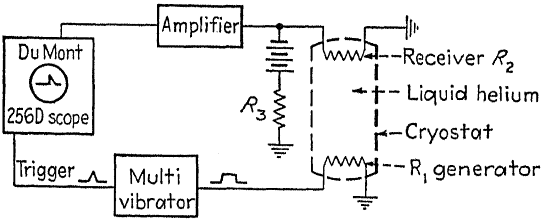

FIG. 5.13. Equipment diagram for pulsed thermal waves.

---

[1] C. Lane, H. Fairbank, and W. Fairbank, *Phys. Rev.*, **71**, 9, 1947.

multivibrator of about 150 μsec duration were imposed across the resistor R_1. These developed thermal pulses in the liquid helium II. The temperature fluctuation was detected on arrival at R_2 because the resistance change resulted in a voltage pulse, and this was amplified and fed to the vertical plates of the scope. Velocity is read directly from the scope time axis and the distance of separation between R_1 and R_2; for example, 61.1 μsec for a distance of 7.57 cm at 1.673°K. There was no observable frequency dispersion. Attenuation was observed by the diminution of received pulses with increased separation of R_1 and R_2. The temperature fluctuation obeys the relationship

$$\Delta T = \Delta T_0 e^{-\alpha x}$$

where x is the distance traveled by the wave and the attenuation coefficient is as given in Fig. 5.14. Osborne[1] has obtained smaller attenuation for signals of greater pulse length. Attenuation was studied by Peshkov[2] by the method of decay time in a resonator, but his techniques did not permit an exact numerical determination. In this same paper, Peshkov reported the production of second sound by first sound and the use of a filter to separate the two. He also reported a critical flow density of heat as 0.4×10^{-2} watt/cm². Pellam[3] has discussed the theory of second-sound conversion to first sound. His experimental observations came in a later paper.[4]

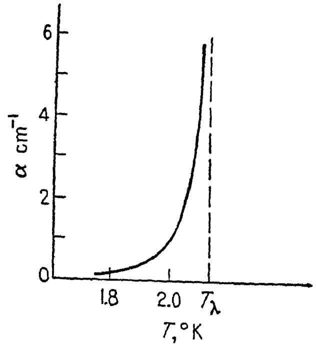

FIG. 5.14. Attenuation coefficient vs. temperature for second sound. (*Pellam, Phys. Rev.*, **75**, 1190, 1949.)

Second-sound Velocity at Very Low Temperatures. V. Peshkov[5] was the first to show the increase of second-sound velocity with lowering of temperature below 1.1°K. These results are in support of the latest variant of theories advanced by Landau.[6] Maurer and Herlin[7] used Pellam's equipment and by vigorous pumping to cool the helium got the results on the velocity of second sound shown in Table 5.4. Pellam and Scott have cooled liquid helium by demagnetization of iron alum salt from near 1.0°K and observed at the lowest temperatures produced (probably about 0.1°K) that the second-sound velocity had risen to 33.9 m/sec. At the lowest temperatures reached, the received d-c pulse widths increased by a factor from 3 to 5, showing no observable decrease in signal strength.[*] We recall that the heat conductivity of liquid helium is very small at these extremely low temperatures. One can only conclude that the capillary-tube measurements introduced attenuation which the open bath does not place on the temperature waves.

---

[1] D. V. Osborne, *Proc. Phys. Soc. (London)*, **64**, 114, 1951.

[2] V. Peshkov, *J. Exptl. Theoret. Phys. USSR*. **18**, 867, 1948.

[3] J. R. Pellam, *Phys. Rev.*, **73**, 608, 1948.

[4] J. R. Pellam, *Phys. Rev.*, **75**, 1190, 1949.

[5] V. Peshkov, *J. Exptl. Theoret. Phys. USSR*, **18**, 951, 1948.

[6] L. Landau, *J. Exptl. Theoret. Phys. USSR*, **11**, 91, 1947.

[7] R. D. Maurer and M. A. Herlin, *Phys. Rev.*, **76**, 948, 1949.

Figure 5.15 gives the velocity of second sound as a function of temperature for a number of constant pressures and for the liquid's own vapor pressure. Maurer and Herlin[1] obtained these interesting results.

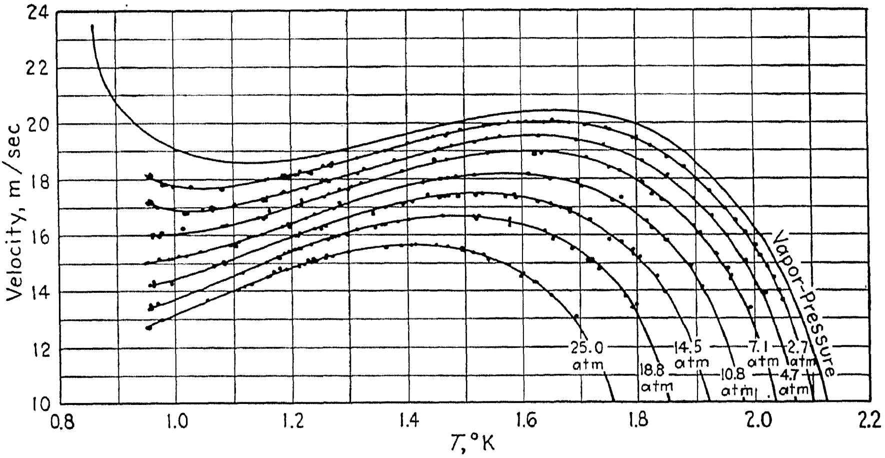

FIG. 5.15. Velocity of second sound vs. temperature at various pressures. (*Maurer and Herlin, Phys. Rev.*, **81**, 444, 1951.)

TABLE 5.4. VELOCITY OF SECOND SOUND AT LOW TEMPERATURES

T, °K	c_2, m/sec
1.45	19.95
1.40	19.78
1.35	19.55
1.30	19.20
1.25	18.95
1.20	18.75
1.15	18.75
1.05	19.00
1.00	19.40
0.95	20.05
0.90	21.20
0.86	23.00

Thermal Rayleigh Disk in Helium II

Pellam and Morse[2] carried out the first experiments on a thermal wave producing a torque on a small circular disk placed in its path. Pellam and Hanson[1] refined the equipment and carried out extensive measurements which not only support the two-fluid hypothesis but reveal the consistency of some of the basic thermal properties discussed in Chap. 4. Figure 5.16 shows the Rayleigh disk supported by a torsion fiber and hanging in the center of a cavity. One end of the cavity is a solid plane glass surface through which a light beam can enter and reflect off the mirror disk to a scale placed outside of the equipment. The other end of the cavity is a flat surface made up of a carbon resistor which serves as a periodic heat source for the production of thermal waves or second sound. The entire assembly of Fig. 5.16 is contained in a bath of liquid helium II, and all of this is surrounded by liquid nitrogen. Clear windows in the surrounding Dewar vessels permit the optical path to be free.

---

[*] See note added in page proof on page 109.

[1] R. D. Maurer and M. A. Herlin, *Phys. Rev.*, **81**, 444, 1951.

[2] J. Pellam and P. Morse, *Phys. Rev.*, **78**, 474, 1950.

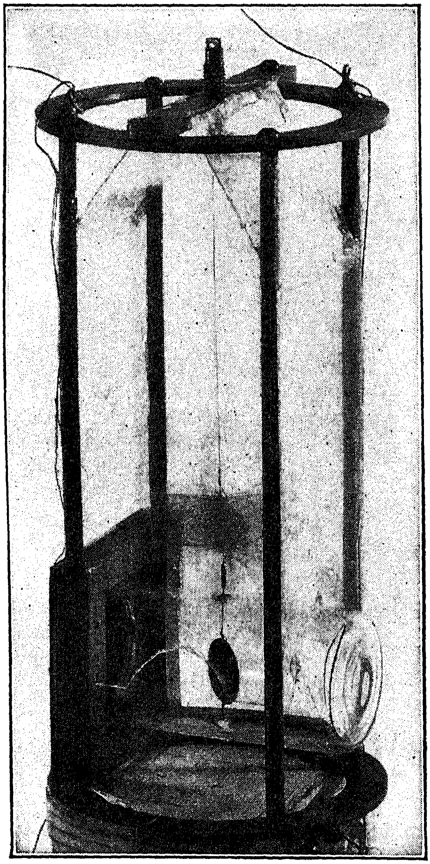

FIG. 5.16. Photograph of thermal Rayleigh disk. (*Pellam, National Bureau of Standards.*)

We recall from the classical theory of sound that such a disk tends to swing crosswise to the propagation axis of an ordinary sound wave regardless of the instantaneous direction (sign) of the particle flow. Both halves of the cycle contribute constructively. The resultant rectifying action enables this device to detect and measure ordinary sound intensity. This same property of responding to a particle flow irrespective of its actual direction enables the Rayleigh disk to detect the internal counterflow associated with heat flow in liquid helium II.

The condition of zero net particle velocity for heat flow in liquid helium II is written

$$\rho_n v_n + \rho_s v_s = 0$$

Here, as elsewhere in the book, the symbols ρ_n and ρ_s are the densities of the normal and superfluid components, respectively, while v_n and v_s

---

[1] J. Pellam and W. Hanson, *Phys. Rev.*, **87**, 216, 1952.

are the corresponding particle velocities. Even when the internal counterflow accompanying thermal current in helium II is periodic, as for second sound, the disk still responds indiscriminately to both halves of the cycle. Pellam showed that the expected torque exerted on the disk by the normal fluid component would be

$$\tau_n = \frac{4a^3}{3}\rho_n(v_n^2)_{\text{av.}}$$

where the radius of the disk is a and the mean square value of particle velocity is $(v_n^2)_{\text{av.}}$, giving an average value of the torque τ_n. If now we express v_n in terms of the heat flow density $\dot{Q}$, which was first given by H. London,

$$\dot{Q} = T\rho S v_n$$

where now we have the net fluid density ρ, the entropy S, and temperature T, then we can express the normal fluid torque as

$$\tau_n = \frac{4a^3}{3}\rho_n\frac{(\dot{Q}^2)_{\text{av.}}}{(\rho ST)^2}$$

Similarly Pellam gives the torque τ_s exerted by superfluid

$$\tau_s = \frac{4a^3}{3}\rho_s v_s^2 = \frac{4a^3}{3}\rho_n\frac{(\rho_n)}{(\rho_s)}\frac{(\dot{Q}^2)_{\text{av.}}}{(\rho ST)^2}$$

The combined torque is the sum of the individual contributions. The result is

$$\tau_n + \tau_s = \frac{4a^3}{3}\rho\frac{\rho_n}{\rho_s}\frac{(\dot{Q}^2)_{\text{av.}}}{(\rho ST)^2}$$

The results by Pellam and Hanson are given in Fig. 5.17. The contribution of each fluid component is shown by the theoretical curves, and their sum is given. The measured torque agrees with the theoretical sum curve. The numerical values for the fluid densities ρ_n and ρ_s were taken from the work of Andronikashvili which we quoted in Chap. 4. The values of TS are taken from the work by Kapitza quoted in Chap. 4.

It will be noticed in Fig. 5.17 that the curve for torque $\tau_s/(\dot{Q}^2)_{\text{av.}}$ caused by the superfluid component rises sharply in the immediate vicinity of the λ point. Thus the superfluid contribution appears to be enhanced most in the temperature range for which the superfluid concentration is least. Pellam has pointed out that this takes place because as superfluid becomes sparse its particle velocity v_s increases to maintain zero net momentum transfer. And since the torque varies as the square of this velocity, the decrease of density of these superfluid particles is more than offset. Likewise, at the low temperatures the normal fluid component in turn increases manyfold, and for similar reasons.

Pellam concludes that the agreement shown by theory and experiment in Fig. 5.17 tends to confirm the generalized Bernoulli relationship given by Pellam and Morse:[1]

$$\frac{1}{2}\rho v^2 + \frac{1}{2}\rho\frac{\rho_n}{\rho_s}\frac{(\dot{Q}^2)}{(\rho ST)^2} + \rho gh + p = \text{constant}$$

Pellam[2] has reported an actual hydrostatic pressure arising from the new term in the Bernoulli equation, a pressure which he measured with the conventional pitot tube technique. Weinstock and Pellam[3] have carried out thermal Rayleigh disk measurements on a 4 per cent mixture of helium 3 in helium 4. Figure 5.18 shows the second-sound velocity for this mixture to be considerably higher at 1°K than for the pure He^4 liquid. At 0.9°K the torque in the 4 per cent mixture has fallen within a few tenths' per cent of that of pure He^4.

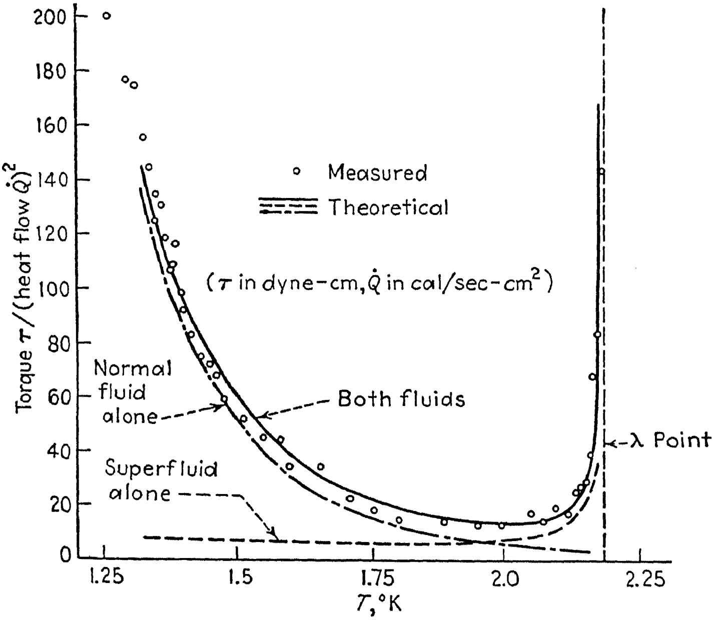

FIG. 5.17. Torque on Rayleigh disk vs. temperature. (*National Bureau of Standards.*)

---

[1] J. Pellam and P. Morse, *Phys. Rev.*, **78**, 474, 1950.

[2] J. R. Pellam, *Phys. Rev.*, **78**, 818, 1950.

[3] B. Weinstock and J. Pellam, *Phys. Rev.*, **88**, 1952; *Bull. Am. Phys. Soc.*, **27**, 11, 1952.

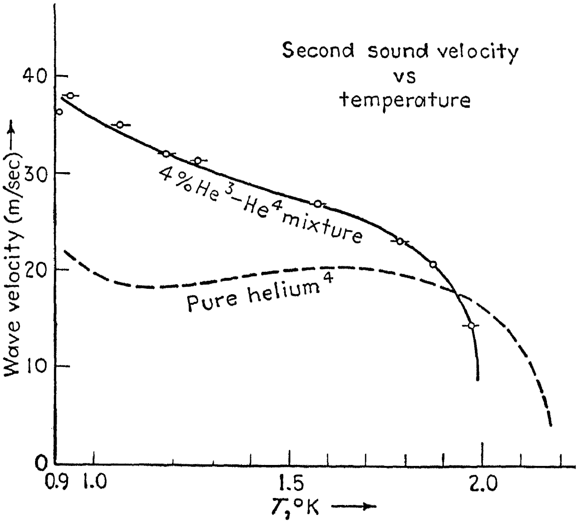

FIG. 5.18. Second-sound velocity vs. temperature.

Mixtures of He^3 and He^4 in Liquid and Vapor Phase

The studies on pure He^4 have revealed amazing physical properties associated with the two-fluid model. Pure He^3 does not show superfluid properties, although it does show characteristic quantum properties at low temperatures. Studies on mixtures of He^3 and He^4 are interesting because of the possible information they might give on the nature of superfluidity. Physical scientists have always been concerned with the effect of a solute on the properties of the solvent. One certainly would not expect an ideal classical theory to be valid for the mixture of He^3 and He^4. Perhaps intuitively we expect that the λ transition of He^4 would be affected by the addition of He^3 atoms to the liquid. Because of the cooperative nature required between the He^4 atoms for such a second-order transition, the addition of He^3 atoms would naturally lower the temperature at which the transition occurs. This effect is analogous to the lowering of the freezing point of a solvent by the addition of a solute. The temperature T_λ^s of a solution of He^3 in liquid He^4 is given in Table 5.5, and this is the temperature for which the superfluid property begins. This work was first done by Abraham, Weinstock, and Osborne,[1] and further work was carried out by Daunt and Heer.[2]

The questions which arise in studies of these mixtures are how we know the concentrations and what they are between the liquid and vapor phases. The use of a mass spectrograph to measure the mass abundance has been most essential. The technique of sampling the mixture from the vapor phase just above the liquid is direct and reliable at temperatures above the λ point. Below the λ point there can be serious complications and wide divergences.[1]

---

[1] B. Abraham, B. Weinstock, and D. Osborne, *Phys. Rev.*, **76**, 864, 1949.

[2] J. Daunt and C. Heer, *Phys. Rev.*, **79**, 46, 1950.

TABLE 5.5. SUPERFLUID TRANSITION TEMPERATURE IN He^3-He^4 MIXTURES

Solution Concentration, C_L, %	T_λ^s, °K
2.4	2.04 ± 0.05^a
10.7	1.92 ± 0.05^a
20.3	1.63 ± 0.05^a
28.2	1.56 ± 0.05^a
42 ± 2	1.15 ± 0.05^b
61 ± 2	0.82 ± 0.03^b
71 ± 2	0.69 ± 0.03^b
78 ± 2	0.64 ± 0.03^b
81 ± 2	0.56 ± 0.03^b
89 ± 2	0.38 ± 0.03^b

[a] B. Abraham, B. Weinstock, and D. Osborne, *Phys. Rev.*, **76**, 864, 1949.
[b] J. D. Daunt and C. Heer, *Phys. Rev.*, **79**, 46, 1950.

The careful results of Sommers[2] at the Los Alamos laboratories have shown how to get around these difficulties. He has measured the vapor pressures of He^3-He^4 mixtures below the λ point. The concentration of He^3 in the He^4 was measured by a mass spectrograph. Thus the initial supply reservoir was analyzed and the gas pumped by a Toepler pump into the sample chamber (see Fig. 5.19). Known amounts of gas are pumped in this way. The pressures P of the mixture gas, P_4^0 of the pure He^4 vapor, and ΔP of their difference are determined, as shown in Fig. 5.19. So long as all of the mixture sample is in the vapor phase, the concentration of He^3 is the same as that of the reservoir from which the

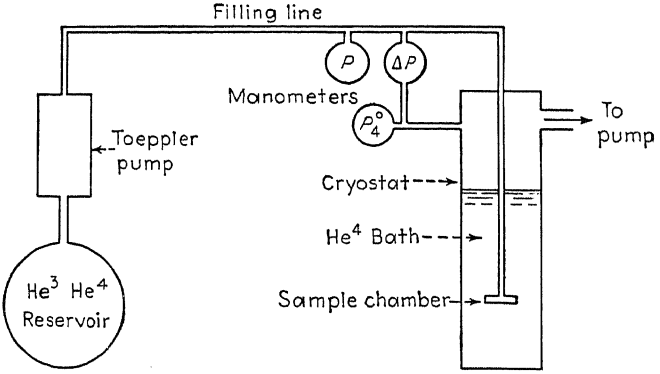

FIG. 5.19. Apparatus (schematic) for vapor-pressure studies on He^3-He^4 mixtures.

---

[1] C. Lane *et al.*, *Phys. Rev.*, **75**, 46, 1949.
[2] H. S. Sommers, *Phys. Rev.*, **88**, 113, 1952.

gas mixture is taken. Just at the dew point this is so. Also just at the dew point the mass of gas added to the sample chamber begins to change the value of ΔP, but very little. Thus Sommers determined the vapor pressure of a series of mixtures whose vapor-phase concentration he knew quite accurately; for a given temperature of the outer bath the dew-point pressure was determined. Tables are given in the Appendix for a series of vapor-phase concentrations.

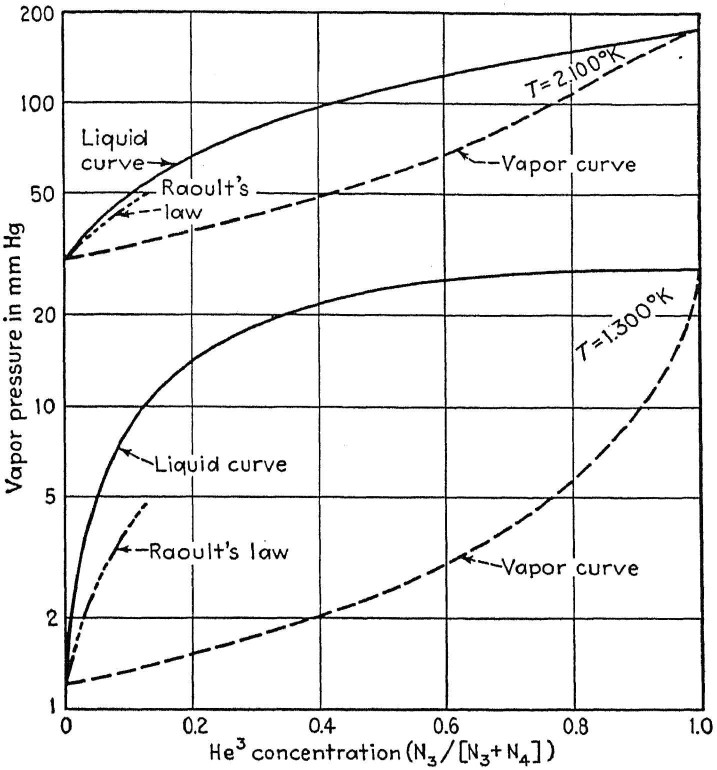

FIG. 5.20. Phase diagram for He^3-He^4 mixtures.

On the other hand, if all the mass of the mixture taken from the reservoir is forced over into the sample chamber and held there in the liquid state, then surely that liquid has the concentration of the reservoir from which it was taken (conservation of mass). The vapor pressure of such liquids was determined. The temperature was taken from the vapor pressure of the pure He^4 bath. Thus Sommers determined the vapor pressure as a function of temperature for various mixtures of He^3 and He^4 whose concentration he knew in the liquid phase. Tables are given in the Appendix.

Figure 5.20 shows Sommers's results for known concentrations in the liquid phase and for known concentrations in the gas phase. These solid curves are for two representative liquid-phase isothermals (2.100 and 1.300°K). Raoult's law, as shown by dot-dashed lines, indicates that the deviation from ideal solution theory is largest at low temperatures. The corresponding isothermals of the vapor phase are shown in Fig. 5.20. The curves are extended to pure He^3 in each case. The extent of fractionation which occurs at low temperatures is most pronounced. Sommers[1] has compared his work with a number of theories and in particular with that of Heer and Daunt[2] and of De Boer and Gorter.[3] A most useful review article on these matters has been written by Daunt.[4]

[1] *Ibid.*

[2] C. Heer and J. Daunt, *Phys. Rev.*, **81**, 447, 1951.

[3] J. De Boer and C. Gorter, *Physica*, **16**, 225, 1950.

[4] J. Daunt, *Advances in Phys.*, **1**, 209, 1952 (*Phil. Mag.* supplement); J. Daunt and C. Heer, *Phys. Rev.*, **86**, 205, 1952.

CHAPTER 6

THEORY OF LIQUID HELIUM

With the experimental evidence before us we can now turn our attention to the theories which have been advanced. Actually the theories were developed along with the experiments and played an important role in the development of the subject. We have already seen that the physical properties of helium gas at low temperatures revealed the onset of quantum effects, and these were equally important to helium isotope 4 as to the isotope 3. The question of the symmetry of the wave function enters at very low temperature. Now, however, we are interested in the liquid where the density is so high that the interaction of pairs of atoms or a cluster of three is no longer quite adequate.

Quantum Theories of F. London

Helium atoms have such a small mass and such weak interactions that they preserve their gaslike character even in the liquid. There is the evidence of the heat conductivity, the viscosity, and the velocity of sound in liquid helium I. It seems proper therefore that one must use the wave nature of the helium atom. Just as for electrons and other fundamental particles, we describe the helium atom with a wave function of time and space. The probability for finding the atom at a certain place, at a certain time, is given by the square of the wave amplitude. The position of the helium atom may be anywhere within the extension of the wave by which it is described, and so we say that there exists an uncertainty in the physical quantities such as space and momentum. Heisenberg's uncertainty relation tells us that the more accurately the position of a particle is defined, the less accurately is its momentum or velocity defined. Thus

$$\Delta p \, \Delta q \geq \frac{h}{2\pi} \tag{6.1}$$

As the temperature of the helium atoms is lowered, the available volume for each atom is decreased, and the wave functions become compressed. Ultimately this means, according to the uncertainty principle, an increase of momentum. Suppose the atom is restricted to move with an uncertainty of position of the order of the distance to the nearest neighbors in liquid helium. Experimentally we know the density, and we know that this distance is two or three times larger than the dimension of the potential field at its minimum. If we denote the mean distance between atoms by R, the wave function must have the form

$$\psi_n = A_n \sin \frac{\pi n x}{R} e^{-i\omega t} \tag{6.2}$$

where n is an integer and A is a constant. Substituting this solution of the wave equation into the Schrödinger equation

$$\frac{d^2\psi}{dx^2} + \frac{2mE}{\hbar^2} \psi = 0 \tag{6.3}$$

we have the allowed energy values

$$E_n = \frac{h^2 n^2}{8mR^2} \tag{6.4}$$

The lowest possible energy may be taken from the uncertainty condition

$$E_0 = \frac{P_0^2}{2m} = \frac{h^2}{8\pi^2 mR^2} \tag{6.5}$$

This lowest energy is the kinetic zero-point energy. If we were to place the atoms so close together as to be in the potential energy minimum, the kinetic zero-point energy would be so large as to overbalance the gain of potential energy. In such a case it will be more favorable to give a preference to minimizing the kinetic energy, even if this entails a spread of the possible location of the atoms over a considerably larger region. This is why liquid helium does not form a solid and has such a "blown-up" volume. These ideas were first discussed by F. London.[1] In Chap. 3 we discussed the free-volume model of high-density gases and liquids. We observed that only the proper use of the potential variables ϵ and σ for helium would permit us to use the free-volume model for a liquid like helium I.

What are we to make of the drop in entropy when the liquid helium II is formed? Since we cannot have an order in ordinary space (q space), we must look for the possibility of an order in momentum space (p space) and accept the consequence. The small value of Δp implies such a large spread of location in ordinary space that actually a dissolution of the system into separated wave packets of different molecules becomes impossible. We must think of wave functions:

$$\psi_n = A_n \sin \frac{\pi n x}{L} e^{-i\omega t} \tag{6.6}$$

where L is the dimension of the vessel holding the liquid helium. From the experimental evidence about the properties of liquid helium II we are already well aware that the particles in this new quantum state behave as though the wave function extended great distances.

---

[1] F. London, *Proc. Roy. Soc.* (*London*), **153**, 576, 1936; *Phys. Rev.*, **54**, 947, 1938.

Several years ago F. London[1] gave some evidence to support the idea that the peculiar phase transition at the λ point might be due to the condensation mechanism characteristic of the ideal Einstein-Bose gas but modified slightly by the presence of molecular forces. Einstein[2] first called attention to the possibility of such a condensation phenomenon. For a system of N particles we may ask how many particles N_i are in the energy state E_i. Suppose though that there are G states very close to E_i; how many ways can we arrange N_iG atoms in G states? The answer is

$$\frac{(N_iG + G - 1)!}{(N_iG)!(G - 1)!} \tag{6.7}$$

As an example, suppose we have two atoms ($N_iG = 2$) and three states ($G = 3$). We may arrange these in the states in the following ways:

States	1	2	3	
	xx	0	0	6 ways
	x	x	0	
	x	0	x	
	0	xx	0	
	0	x	x	
	0	0	xx	

The formula gives $\dfrac{(2 + 3 - 1)!}{2!(3 - 1)!} = 6$ ways.

The number of complexions (using Sterling's theorem) becomes

$$\frac{[(N_i + 1)G/e]^{(N_i+1)G}}{\left[\dfrac{N_iG}{e}\right]^{N_iG}\left[\dfrac{G}{e}\right]^{G}} = \left[\frac{(1 + N_i)^{1+N_i}}{N_i^{N_i}}\right]^{G} \tag{6.8}$$

The fraction f_i of the system in the ith microscopic state is then

$$f_i = \frac{1}{\prod\limits_i [(1 + N_i)^{1+N_i}/N_i^{N_i}]} \tag{6.9}$$

The entropy is

$$S = -k \sum_i f_i \ln f_i \tag{6.10}$$

The energy is

$$U = \sum_i N_iE_i \tag{6.11}$$

---

[1] *Ibid.*

[2] A. Einstein, *Ber. Berlin Akad.*, **261,** 1924; *ibid.*, **3,** 1925.

The Helmholtz potential $A = U - TS$ now becomes the statistical expression

$$A = \sum_i [N_iE_i + kTN_i \ln N_i - kT(1 + N_i) \ln (1 + N_i)] \tag{6.12}$$

If A is to be a minimum

$$dA = 0 = \sum_i \left[E_i + kT \ln \frac{(N_i)}{(1 + N_i)}\right] dN_i \tag{6.13}$$

Since the number of particles must stay constant,

$$\sum_i dN_i = 0 \tag{6.14}$$

Thus we deduce that

$$E_i + kT \ln \frac{(N_i)}{(1 + N_i)} = \text{constant} = -\alpha \tag{6.15}$$

Solving for N_i, we have

$$N_i = \frac{1}{e^{(E_i - \alpha)/kT} - 1} \tag{6.16}$$

Thus, as Einstein[1] first pointed out, when $(E_i - \alpha)/kT$ becomes small, the number of atoms in the lowest state becomes large. This situation represents a sort of condensation into the lowest state at low temperature.

F. London[2] has shown the temperature at which this condensation occurs for helium atoms. Starting from the Einstein-Bose distribution,

$$N_i = \frac{g_i}{e^{\beta(E_i - \alpha)} - 1} \tag{6.17}$$

where $\beta = 1/kT$, g_i is the statistical weight of the state of energy E_i, and α is taken as the chemical potential instead of the Gibbs potential. The statistical weight is the density of states between E and $E + \Delta E$ and is

$$g(E)\,\Delta E = 4\pi V \left(\frac{2m}{h^2}\right)^{\frac{3}{2}} E^{\frac{1}{2}}\,\Delta E \tag{6.18}$$

This relationship is true for completely free particles and should be altered for a true gas with interaction forces. The density of energy states expression [Eq. (6.18)] comes from the volume element in momentum space $4\pi p^2\,dp$ multiplied by the volume V and divided by h^3, which quantity is the density of points in phase space between momentum p and $p + \Delta p$. The energy $E = p^2/2m$, so the increment in momentum space is

---

[1] *Ibid.*

[2] F. London, *Nature,* **141,** 643, 1938.

$$dp = (2m)^{\frac{1}{2}} \frac{dE}{E^{\frac{1}{2}}} \tag{6.19}$$

and thus the volume element is Eq. (6.18). In Eq. (6.17) we now want to substitute for the expression

$$\frac{1}{e^{\beta(E-\alpha)} - 1} = \sum_{n=1} e^{n\beta(\alpha-E)} \tag{6.20}$$

We have the total number of particles

$$N = \sum_i N_i \tag{6.21}$$

We can integrate Eq. (6.17) and have

$$N = \int_0^\infty 4\pi V \left(\frac{2m}{h^2}\right)^{\frac{3}{2}} \sum_{n=1}^{\infty} e^{n\beta\alpha} E^{\frac{1}{2}} e^{-n\beta E}\, dE \tag{6.22}$$

At very low temperatures α approaches zero. For $\alpha = 0$ we may write

$$\begin{aligned} N &= \frac{4\pi V}{h^3} (2m)^{\frac{3}{2}} \sum_{n=1}^{\infty} \int_0^\infty E^{\frac{1}{2}} e^{-n\beta E}\, dE \\ &= \frac{4\pi V}{h^3} (2m)^{\frac{3}{2}} \sum_{n=1}^{\infty} \frac{1}{2n\beta} \left(\frac{\pi}{n\beta}\right)^{\frac{1}{2}} \end{aligned} \tag{6.23}$$

We may factor Eq. (6.23) and evaluate the sum as follows:

$$\begin{aligned} N &= \frac{2V}{h^3} (2\pi mkT)^{\frac{3}{2}} \sum_{n=1}^{\infty} n^{-\frac{3}{2}} \\ &= 2.612 \frac{V}{h^3} (2\pi mkT)^{\frac{3}{2}} \end{aligned} \tag{6.24}$$

We may compute the temperature T_0 which satisfies Eq. (6.24) by using for helium mass $Nm = M = 4$ g/mole and volume $V = 27.6$ cm^3/mole

$$T_0 = 3.14°\text{K}$$

London[1] has pointed out that the statistical weight of the lowest state ($p = 0$) incorrectly acquires the value 0 according to the above method of replacing the summation by integration. The zero-point energy never allows the momentum $p = 0$ in any case. But it could be quite small.

---

[1] F. London, *Proc. Roy. Soc. (London)*, **153**, 576, 1936; *Phys. Rev.*, **54**, 957, 1938.

If the helium atoms are confined to a box of sides L cm, the energy states according to the method of Eqs. (6.2), (6.3), and (6.4) would be

$$E_{k,l,m} = (k^2 + l^2 + m^2) \frac{h^2}{2mL^2} \tag{6.25}$$

These energy states have the huge dimension L^2 in the denominator as compared with the interatomic distance R^2 in Eq. (6.3). With these energy states the total number of particles is the sum

$$N = \sum_{k,l,m} \frac{1}{e^{\sigma(k^2+l^2+m^2)+\alpha'} - 1} \tag{6.26}$$

where $\sigma = h^2/2MkTL^2$ and where $\alpha' = -\alpha/kT$. The right-hand side of Eq. (6.26) is not bounded by a finite limit when $\alpha \rightarrow 0$. London considers a group of lowest energy states with

$$k^2 + l^2 + m^2 \leq \rho^2$$

such that for energy states from ρ to ∞ the summation may be replaced by an integration. The number of lowest states is small and is given by

$$g_0 = \frac{V}{h^3} \frac{4\pi}{3} \rho^3 \tag{6.27}$$

Thus London[1] writes

$$N = \frac{g_0}{e^{\beta E_0+\alpha'} - 1} + \frac{4\pi V}{h^3} \int_{\rho h/L}^{\infty} \frac{p^2\,dp}{e^{\alpha'+p^2/2MkT} - 1} \tag{6.28}$$

where $E_0 = \frac{3}{10}(\rho^2 h^2/ML^2)$. Beyond this point in our discussion of London's work we shall not carry out a complete and rigorous account.[2] For $T < T_0$ the first term of Eq. (6.28) is the only significant contribution to the total number of particles. As the temperature becomes even lower, the second term contributes very little indeed. The number of atoms in the lowest state is

$$N_0 = N\left[1 - \left(\frac{T}{T_0}\right)^{\frac{3}{2}}\right] \tag{6.29}$$

Those atoms not in this lowest state have kinetic energy which gives a free energy ($T < T_0$):

$$G = -0.514RT\left(\frac{T}{T_0}\right)^{\frac{3}{2}} \tag{6.30}$$

There is nothing in the character of a finite energy gap between the lowest state and the first excited states. In both Eqs. (6.29) and (6.30) the size of ρ does not appear. The introduction of nonideal gas conditions might in some way steepen the dependence on temperature. London finds a specific heat for an ideal Einstein-Bose gas, as shown in Fig. 6.1. The entropy for $T < T_0$ is

---

[1] *Ibid.*

[2] See the rigorous account by A. R. Fraser, *Phil. Mag.*, **42,** 156, 165, 1951.

$$S = 1.283R\left(\frac{T}{T_0}\right)^{\frac{3}{2}} \tag{6.31}$$

This entropy is due only to those atoms excited above the lowest state. In a general way these concepts seem to fit the experimental evidence. We may well ask how the property of vanishing viscosity comes about.

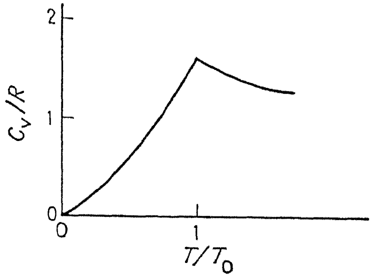

FIG. 6.1. Specific heat of an ideal Einstein-Bose gas.

Thermodynamics of the Two-fluid Model for Liquid Helium II

In the previous paragraphs we have seen the concept of a two-fluid model as a consequence of Einstein-Bose statistics. Those atoms in excited states form the normal fluid, and those in the lowest state may be identified with the superfluid. We turn our attention to the thermodynamics of such a model and follow the remarks by Professor C. J. Gorter.[1] The Gibbs phase rule tells us that for a one-component system (all He atoms) we may have equilibrium between the gas and liquid phase at various temperatures depending on the pressure. This is the vapor-pressure curve with which we are familiar. If now another phase is present, the equilibrium between three phases may exist at only one set of values for temperature and pressure (triple point). Therefore, in helium II we have not two phases in the liquid but a liquid whose Gibbs potential $G(p,T,x)$ is a nonlinear function in the relative concentration x of the normal fluid: $x = \rho_n/\rho$. The equilibrium conditions are

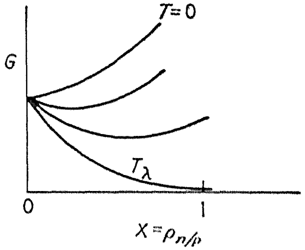

FIG. 6.2. Gibbs potential vs. density ratio for liquid helium II at various temperatures. (*Theory by Gorter.*)

$$G_l(p,T,x) = G_{\text{vap.}}(p,T) \tag{6.32}$$

At the constants p and T there is a minimum in x such that

$$\left(\frac{\partial G}{\partial x}\right)_{p,T} = 0 \tag{6.33}$$

The plot of G against x is given in Fig. 6.2 for several temperatures between $T = T_\lambda$ and $T = 0°\text{K}$. The system is in equilibrium at the minimum for each temperature. The question is what function should be used for $G(p,T,x)$? The entropy $S = -(\partial G/\partial T)$ has been assumed by Tisza to be proportional to x, such that $S = S_\lambda(\rho_n/\rho) = \alpha(x)$. This relationship is in good agreement with Kapitza's classic experiments on entropy values. Such a functional choice is equivalent to taking the Gibbs potential as

---

[1] C. J. Gorter, *Physica*, **15**, 523, 1949.

$$G = -\alpha(p,x)T + h(x,p) \tag{6.34}$$

Tisza's Phenomenological Theory of the Dynamic Properties of He II

L. Tisza[1] has given a two-fluid model for helium II in which he emphasized the complete lack of rigidity in liquid helium and gave the role of the two fluids in dynamic equations. In helium II all of the entropy S belongs to the so-called normal-type atoms. The entropy of thermal vibrations, phonons, belongs to both type atoms and is small in relation to S except below 1°K. The two-fluid model permits the propagation of ordinary compressional waves such that the particle displacement is given by the usual wave equation (constant entropy):

$$\frac{\partial^2 \xi}{\partial t^2} = \left(\frac{\partial P}{\partial \rho}\right)_S \nabla^2 \xi \tag{6.35}$$

The velocity of this normal sound is

$$c_1 = \left(\frac{\partial P}{\partial \rho}\right)_S^{\frac{1}{2}} \tag{6.36}$$

The quantity $(\partial P/\partial \rho)_S$ is the adiabatic force constant for compression. Now consider second sound. A spring whose force constant is K is compressed by a distance x, which gives a potential energy stored in the spring,

$$U = \int_0^x Kx\,dx = \tfrac{1}{2}Kx^2 \tag{6.37}$$

Similarly for a volume compression of the liquid helium we have

$$U = \frac{1}{2}\left(\frac{\partial^2 U}{\partial V^2}\right)_S (\Delta V)^2 = \frac{1}{2}\left(\frac{\partial P}{\partial V}\right)_S (\Delta V)^2 \tag{6.38}$$

We may express this last equation in the form

$$U = \frac{1}{2}\left(\frac{\partial P}{\partial \rho}\right)_S \left(\frac{\Delta \rho}{\rho}\right)^2 \tag{6.39}$$

Equation (6.39) represents the potential energy stored in the compressional part of the sound wave. The two types of particles of helium II move together in such compressional modes. The plot of energy U

---

[1] L. Tisza, *J. phys. radium*, **8**, 1, 165, 350, 1940; *Phys. Rev.*, **72**, 838, 1947.

against volume V is shown in Fig. 6.3*a*. The velocity of normal sound is determined from the shape of this curve.

Now let us use the above technique for a qualitative understanding of second sound or thermal waves in helium II. The two-fluid liquid helium has the possibility of a change of entropy in a volume element by the counterflow of the two kinds of particles, and at the same time there can be no change of density. This possible mode of motion gives rise to the second sound or to a temperature wave. The energy as a function of entropy is shown in Fig. 6.3*b*. The potential energy stored in a volume element in which there has been an entropy displacement is

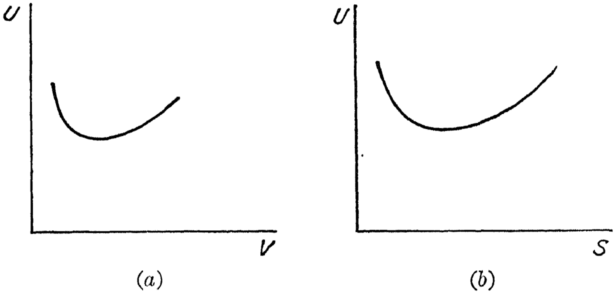

FIG. 6.3. (*a*) Energy vs. volume for liquid helium (schematic). (*b*) Energy vs. entropy for liquid helium (schematic).

$$\frac{1}{2}\left(\frac{\partial^2 U}{\partial S^2}\right)_V (\Delta S)^2 = \frac{1}{2}\left(\frac{\partial T}{\partial S}\right)_V (\Delta S)^2 = -\frac{1}{2}\frac{\partial T}{\partial(1/S)}\left(\frac{\Delta S}{S}\right)^2 \tag{6.40}$$

There is assumed to be no entropy associated with the superfluid particles. The velocity of the temperature waves is

$$c_2 = \left[\frac{-dT}{d(1/S)}\frac{\rho_s}{\rho_n}\right]^{\frac{1}{2}} \tag{6.41}$$

For the empirical relation

$$S = S_\lambda\left(\frac{T}{T_\lambda}\right)^{5.5} = 0.405\left(\frac{T}{T_\lambda}\right)^{5.5} \tag{6.42}$$

Tisza obtained the second-sound velocity as a function of temperature:

$$c_2 = 26\left\{\frac{T}{T_\lambda}\left[1 - \left(\frac{T}{T_\lambda}\right)^{5.5}\right]\right\}^{\frac{1}{2}} \quad \text{cm/sec} \tag{6.43}$$

The velocity c_2 approaches 0 as $T \to 0$, according to the above equation. However, the entropy relation on which it is based is not valid below 1°K.

Second-sound-wave Equation. D. Gogate and P. Pathak[1] have given a simple derivation of the second-sound-wave equation and of the velocity.

---

[1] D. Gogate and P. Pathak, *Proc. Phys. Soc.* (*London*), **59**, 457, 1947.

The total density is made up of the normal part ρ_n and of the superfluid part ρ_s such that

$$\rho = \rho_n + \rho_s$$

The superfluid part has zero entropy so that the entropy S per gram of the fluid of density ρ is related to the entropy of the normal part of the fluid by

$$\rho_n S_n = \rho S$$

In dealing with problems in which no net mass flow takes place, we may write

$$\rho_n v_n + \rho_s v_s = 0$$

where v_n is the particle velocity of the normal component and v_s is that of the superfluid component. The kinetic energy of the fluid may be written

$$U = \frac{1}{2}(\rho_s v_s^2 + \rho_n v_n^2) = \frac{(\rho_n v_n + \rho_s v_s)^2}{2\rho} + \frac{\rho_n \rho_s}{2\rho}(v_n - v_s)^2$$

where on the right-hand side a little algebraic rearrangement has been used. This is done to bring out the two modes of motion, *i.e.*, when the two fluids move together and when they are moving opposite to one another. In our considerations the first mode is zero and only the relative motion exists. Thus, in this case

$$U = \frac{\rho\rho_n}{2\rho_s} v_n^2$$

Now consider the reversible work done in transferring heat across a parallelogram of thickness Δx whose opposite faces have the temperature $T + \Delta T$ and T, respectively. By the second law of thermodynamics this work is QdT/T. Now the heat current across the thickness Δx is $\rho S T v_n$ which, when multiplied by the increment of time dt, is the quantity of heat Q. Thus the work done is

$$\text{Work} = (\rho S T v_n\, dt)\frac{dT}{T}$$

The work brings about a change in kinetic energy within the thickness Δx such that we may equate

$$dU\, dx = -\rho S v_n\, dt\, dT$$

or

$$\frac{\partial U}{\partial t} = -\rho S(v_n \cdot \text{grad } T)$$

But the derivative with respect to time of the kinetic energy of relative motion is

$$\frac{\partial U}{\partial t} = \frac{\rho\rho_n}{\rho_s} v_n \dot{v}_n$$

and we assume that the quantities $\dot{\rho} = 0$ for small thermal oscillations. Equating the last two expressions gives

$$\dot{v}_n + \frac{\rho_s}{\rho_n} S \operatorname{grad} T = 0$$

Now the continuity equation for the entropy in a volume element is

$$\frac{\partial}{\partial t}(\rho S) + \operatorname{div}(\rho S v_n) = 0$$

Eliminating v_n in these last two equations gives

$$\frac{\partial^2 S}{\partial t^2} - \frac{\rho_s}{\rho_n} S^2 \operatorname{div} \operatorname{grad} T = 0$$

Since the specific heat is

$$C = \left(\frac{\partial S}{\partial T}\right)_V \cong \left(\frac{\partial S}{\partial T}\right)_P$$

we may substitute and obtain the wave equation in temperature

$$\frac{C}{T}\frac{\partial^2 T}{\partial t^2} - \frac{\rho_s}{\rho_n} S^2 \operatorname{div} \operatorname{grad} T = 0$$

The velocity squared of the temperature waves described by this equation is

$$c_2^2 = \frac{\rho_s}{\rho_n}\frac{S^2}{C} = -\frac{\rho_s}{\rho_n}\frac{dT}{d(1/S)}$$

Transmission Line Analogy

The propagation of energy by means of waves has been treated as a transmission line problem in acoustics, in electromagnetics, and in vibrating strings. The characteristic impedance of the medium is variously defined according to the physical quantities involved; for the string this is the force divided by the particle velocity, etc. In discussing the results of their experiments, Pellam,[1] Peshkov,[2] and Osborne[3] have used the concept of a characteristic impedance for entropy waves in liquid helium II. The characteristic impedance is given by $Z = \Delta T/W$, which is the ratio of the temperature rise ΔT to the flow of heat per unit area of wave front W. Since $W = \rho C \, \Delta T c_2$, where ρC is the specific heat of helium II per unit volume and c_2 is the velocity of the wave, we may now write

$$Z = \frac{1}{\rho C c_2} \qquad (6.44)$$

---

[1] J. Pellam, *Phys. Rev.*, **73**, 608, 1948.

[2] V. Peshkov, *J. Exptl. Theoret. Phys. USSR*, **18**, 857, 1948.

[3] D. Osborne, *Nature*, **162**, 213, 1948; *Proc. Phys. Soc.* (*London*), **64**, 114, 1951.

There have been a number of theoretical papers concerned with introducing terms into the equation of motion of second sound which will account for dissipation effects and the conversion to ordinary sound. Temperley[1] investigated the wave form to see if shock waves might be formed. His dynamical equations start from the conservation of momentum, energy, and the laws of thermodynamics. Zilsel[2] published similar results.

Theory of L. Landau

L. Landau[3] has published a theory of liquid helium II in which he asserts that the physical properties have nothing to do with an Einstein-Bose condensation. He adopts a two-fluid model having some properties in common with Tisza's model in that the superfluid type has zero entropy and zero viscosity. His brilliant work predicted not only second sound but the experiment of Andronikashvili about the dependence of ρ_n/ρ on temperature. Landau allows two modes of excitation to occur for the superfluid as energy is added in bringing the temperature up from 0°K to some value $T < T_\lambda$. The two modes are: (1) rotation by a group of atoms called rotons and (2) the translational type of motion by a group called phonons. Landau indicates an energy gap Δ between these excitation modes and obtains a second-order phase transition in agreement with the entropy and specific heat curves. Rotons go over into phonons as the λ point is approached. Recently Landau[4] has considered viscosity effects in helium II. Landau has a second-sound velocity formula identical to the Tisza relation:

$$c_2 = \left[- \frac{\rho_s}{\rho_n} \frac{\partial T}{\partial(1/S)} \right]^{\frac{1}{2}}$$

Landau would have $\rho_n \approx T^4$ and the entropy $S \approx T^3$ at temperatures below 1°K. Thus c_2 approaches a constant value as $T \rightarrow 0°\text{K}$. Experiments seem to bear this point out and support this part of Landau's theory.

Ward and Wilks[5] have extended Landau's ideas and shown how phonons play an important role at temperatures below 1°K. Each phonon has an energy $h\nu$ such that the ensemble of phonons has an energy

$$E = \frac{4\pi}{c_1^3} \int_0^\infty \frac{h\nu^3 d\nu}{e^{h\nu/kT} - 1} = \frac{4\pi^5 k^4}{15 h^3 c_1^3} T^4$$

---

[1] H. Temperley, *Proc. Phys. Soc. (London)*, **14**, 105, 1951.

[2] P. Zilsel, *Phys. Rev.*, **79**, 309, 1950.

[3] L. Landau, *J. Phys. USSR*, **5**, 81, 1941.

[4] L. Landau, *J. Exptl. Theoret. Phys. USSR*, **19**, 637, 709, 1949.

[5] J. Ward and J. Wilks, *Phil. Mag.*, **42**, 314, 1951.

where c_1 is the velocity of sound at temperatures below 1°K in the liquid. The specific heat is then

$$C = \frac{16\pi^5 k^4 T^3}{15h^3c_1^3} = 7.52 \times 10^{-4}T^3 \qquad \text{cal/(cm}^3\text{)(°K)}$$

This is in agreement with the measurements below 0.6°K by Gorter *et al.* The entropy per gram is identified with the entropy of the normal component

$$S_n = \frac{16\pi^5 k^4}{45h^3c_1^3}\frac{T^3}{\rho}$$

The density of the phonon gas, *i.e.*, the mass associated with its momentum, is

$$\rho_n = \left(\frac{16\pi^5 k^4}{45h^3c_1^3}\right)\left(\frac{T^4}{c_1^2}\right)$$

Thus the velocity of second sound should approach the value

$$c_2 = \frac{c_1}{\sqrt{3}} = 137 \text{ m/sec} \qquad (T \to 0°\text{K})$$

Landau's theory of liquid helium has been reviewed by Dingle[1] and by De Boer.[2] These matters are still highly controversial and will require more and better experiments[3] and a great deal of careful exchange of ideas.*

---

* Note added in page proof: D. De Klerk, R. Hudson, and J. Pellam (*Phys. Rev.*, **89,** 326, 1953) have measured second sound velocity at 0.1°K and find a value of 192 m/sec. This is in general accord with the large value found earlier by K. Atkins and D. Osborne (*Phil. Mag.*, **41,** 1078, 1950) and also has been confirmed by V. Mayper and M. Herlin (*Phys. Rev.*, **89,** 523, 1953).

[1] R. Dingle, *Advances in Phys.*, **1,** 111, 1952 (*Phil. Mag.* supplement).

[2] J. De Boer, *Nederland. Tijdschr. Natuurk.*, **16,** 89, 1952.

[3] D. De Klerk, R. Hudson, and J. Pellam, Conference at General Electric Co., Schenectady, N.Y., Oct. 6–7, 1952.

CHAPTER 7

SUPERCONDUCTIVITY

Nearly every elementary text on physics mentions that at very low temperatures a number of metals exhibit the striking property of abruptly losing all resistance to the flow of an electric current. This effect was discovered by H. Kamerlingh Onnes in Leiden, Holland, nearly fifty years ago. Since no potential is observable across a superconductor, we may conclude that inside the metal the electric field is zero, $\mathbf{E} = 0$. The superconductor, as we shall presently see from the experiments by Meissner and Ochsenfeld, also exhibits the abrupt new property of having the magnetic induction field equal to zero, $\mathbf{B} = 0$, inside the metal. At the very outset we should think of these metals as showing not only superconducting properties but as showing superdiamagnetic properties equally well. The new behavior of metals at very low temperatures does not require any revision of the basic laws of electricity. Ohm's law for metals, $j = \sigma\mathbf{E}$, is not a basic law of electricity but is a law of a few materials, namely, metals. Thus a superconductor requires a new law to describe, for example, its finite current density j when the metal is placed in a magnetic field. The basic equations of electrodynamics are put here for convenience:

$$\begin{aligned}
\oint \mathbf{H}\,ds &= i + \int \frac{\partial \mathbf{D}}{\partial t}\,dA \\
\oint \mathbf{E}\,ds &= -\int \frac{\partial \mathbf{B}}{\partial t}\,dA \\
\int \mathbf{D}\,dA &= \int \rho\,dV \\
\int \mathbf{B}\,dA &= 0
\end{aligned}$$

To these equations we must add the relations $\mathbf{D} = \epsilon\mathbf{E}$ and the magnetic equation $\mathbf{B} = \mu\mathbf{H}$. In Chaps. 8 and 10 we shall consider more general relationships between these vectors when the quantities ϵ and μ are considered complex. For most purposes in the present chapter we shall regard the electric and magnetic permeabilities as having their values for empty space even though we shall be dealing with superconducting metals. These are

$$\begin{aligned}
\epsilon_0 &= 8.85 \times 10^{-12}\ \text{coulomb}^2/\text{newton-m}^2 \\
\mu_0 &= 12.57 \times 10^{-7}\ \text{weber/amp-m}
\end{aligned}$$

Resistance Studies

In Fig. 7.1 we plot for an arbitrary metal the ratio of the resistance at any temperature T to the resistance at room temperature R_0. There are a few exceptions, but most of the metals behave so. At some very low temperature, usually below 10°K, the resistance abruptly falls away from the experimental curve it had followed and drops to zero. The effect of impurities on the resistance is shown in Fig. 7.1, and for moderate amounts of impurity the superconducting transition temperature T_0 is changed but slightly. We refer here to d-c measurements of resistance and shall take up the matter of high-frequency effects at a later point. We shall, for the most part, confine our discussion to the pure elements which are superconductors and leave the question of alloys,

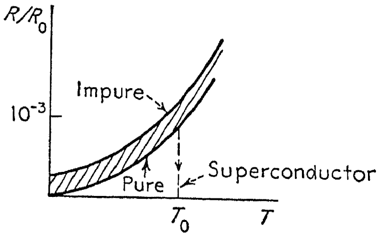

FIG. 7.1. Resistance ratio vs. temperature for a typical metal superconductor.

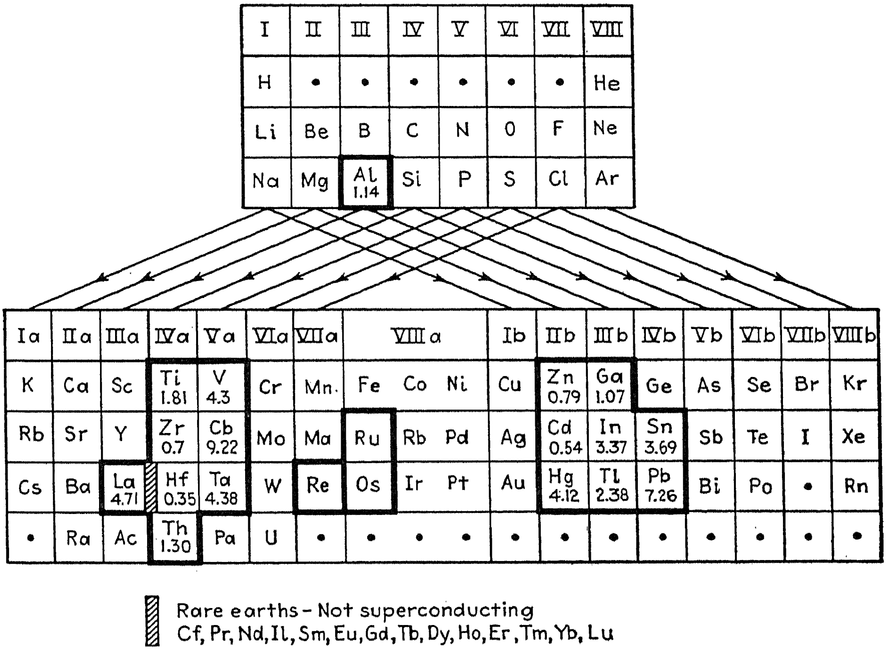

I	II	III	IV	V	VI	VII	VIII
H	•	•	•	•	•	•	He
Li	Be	B	C	N	O	F	Ne
Na	Mg	Al 1.14	Si	P	S	Cl	Ar

Ia	IIa	IIIa	IVa	Va	VIa	VIIa	VIIIa			Ib	IIb	IIIb	IVb	Vb	VIb	VIIb	VIIIb
K	Ca	Sc	Ti 1.81	V 4.3	Cr	Mn	Fe	Co	Ni	Cu	Zn 0.79	Ga 1.07	Ge	As	Se	Br	Kr
Rb	Sr	Y	Zr 0.7	Cb 9.22	Mo	Ma	Ru	Rb	Pd	Ag	Cd 0.54	In 3.37	Sn 3.69	Sb	Te	I	Xe
Cs	Ba	La 4.71 ▨	Hf 0.35	Ta 4.38	W	Re	Os	Ir	Pt	Au	Hg 4.12	Tl 2.38	Pb 7.26	Bi	Po	•	Rn
•	Ra	Ac	Th 1.30	Pa	U	•	•	•	•	•	•	•	•	•	•	•	•

▨ Rare earths - Not superconducting
Cf, Pr, Nd, Il, Sm, Eu, Gd, Tb, Dy, Ho, Er, Tm, Yb, Lu

FIG. 7.2. Position of superconducting elements in the periodic table. The elements [Os, 0.71°], [Ru, 0.47°], [Re, 2.42°] are superconductors and fall outside of the grouping.

mixtures, and compounds to a later paragraph. Kamerlingh Onnes first discovered superconduction in the element Hg at about 4.1°K. Since then, a very great number of elements have been examined at temperatures as low as 0.05°K, and the list with position in the periodic table is given in Fig. 7.2. The superconducting elements fall in the group II*b*, III*a*, IV*b*, V*a*, which is to say in the middle region of the chart. The elements Os, Re, and Ru are superconducting and fall outside of these groups. Pure Ti becomes superconducting at about 0.38°K.

Crystal Structure and Volume

The superconductors exhibit all types of structure, such as body-centered cubic, hexagonal close-packed, etc. The lattice does play some role in that the atomic volume plotted against atomic number (Fig. 7.3) shows a distinct preference for a tight but not too tight packing of atoms. This suggests that the electronic energy states for metals showing superconduction are in some way made unique by lattice distances. A change of volume caused by a stress upsets these conditions, and superconduction occurs at a different temperature. The X-ray patterns[1] taken on superconductors reveal no change of crystal structure nor any change of interatomic distances.

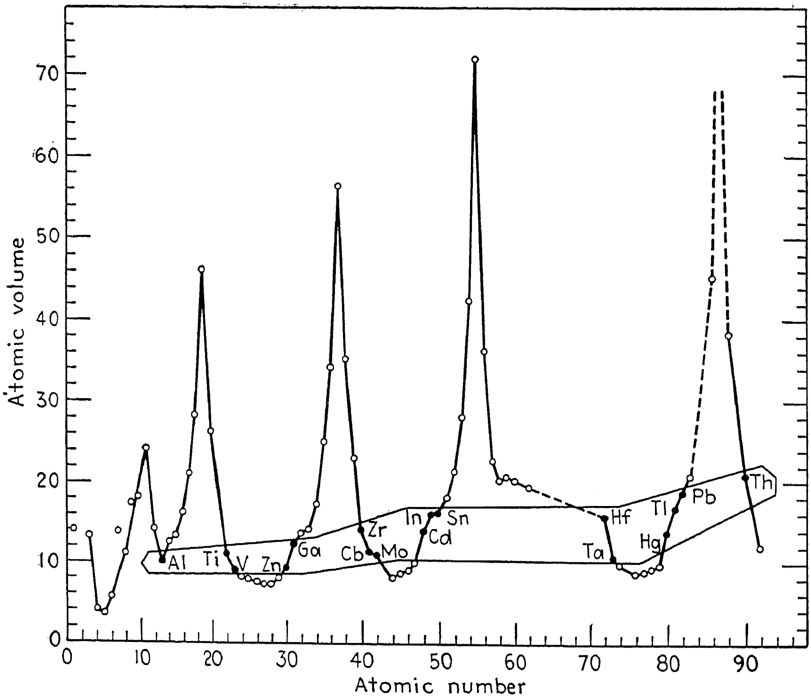

FIG. 7.3. Atomic volumes of the superconducting elements.

---

[1] B. Lasarev and L. Kan, *J. Phys. USSR*, **8**, 361, 1944.

Isotope Effect

At the National Bureau of Standards, E. Maxwell found that the superconductor's transition temperature depends on the isotope mass. At the same time at Rutgers University, B. Serin and coworkers made a similar discovery. The results (Table 7.1) are quoted from their résumé, and we are to note that $M^{\frac{1}{2}}T_0$ is constant. The heavier mass of the nucleus could only cause a shift of the lattice vibrations to slightly lower values. We inject into the discussion at this point the effect on the transition temperature of In when alloyed with various percentages of T_1. Both metals are superconductors, and they are rather similar physically (Table 7.2).

TABLE 7.1. TRANSITION TEMPERATURES

Mercury Isotopes[a]		Tin Isotopes[b]	
Average Mass Number	°K	Average Mass Number	°K
199.7	4.167	118.7	3.742
200.7	4.154	123.1	3.662
202.0	4.147	113.58	3.808
203.4	4.137		

[a] C. Reynolds *et al.*, *Phys. Rev.*, **78**, 487, 1950; *ibid.*, 813, 1950; *ibid.*, **86**, 162, 1952.

[b] E. Maxwell, *Phys. Rev.*, **78**, 477, 1950; *ibid.*, **79**, 173, 1950; *ibid.*, **86**, 235, 1952.

TABLE 7.2. TRANSITION TEMPERATURES, ZERO FIELD

In-Tl Alloys[a]

% Tl	Mag. Ind.	$R/R_n = 0.5$
0	3.408	3.404
5	3.302	3.300
10	3.263	3.279
15	3.238	3.253
20	3.209	3.221

[a] W. F. Love, E. Callen, and F. Nix, *Phys. Rev.*, **87**, 844, 1952.

Consequences of Infinite Conductivity

Consider the following experimental arrangement (Fig. 7.4). A magnetic field is made to thread through a toroid of metal such as lead or tin. The metal is then cooled below its superconducting transition temperature. Next the magnet is switched off and removed, and the ring is left with an induced superconducting current. The current induced in the ring will continue to flow for as long a time as the metal is kept below its transition temperature T_0. There is no damping of this large current. Hundred of amperes may flow in the ring under these conditions. The electron motion is perpetual, just as the electron motion about the nucleus is perpetual. The current can be further demonstrated by breaking the ring at some section (removable plug) and allowing the current to dump through a galvanometer, the leads of which are tied to each side of the break. Let us try to explain this experiment.

The basic equation

$$\oint \mathbf{E}\,ds = -\int \frac{\partial \mathbf{B}}{\partial t}\,dA$$

assures us that, if within the metal of the ring $\mathbf{E} = 0$, then there can be no change of the total magnetic flux linked by the superconducting ring. Thus when one turns off the external field and attempts in this way to change the magnetic flux linked by the toroid, a current is set up by the metal to maintain the magnetic flux.

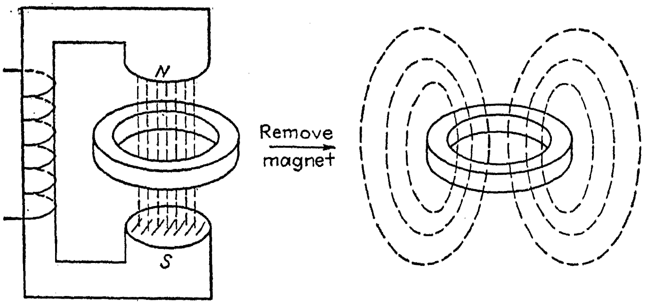

FIG. 7.4. Permanent magnetic moment induced in superconducting ring.

Another interesting version of the same experiment is the following arrangement of multiple connected loops of superconducting wire (Fig. 7.5). A magnetic dip needle serves to detect a magnetic field in the center of the loops. When the wires below the transition are cooled and current I flows, the dip needle stays the same with $I = I_1 + I_2$. If the external battery is removed, the dip needle again stays the same! This is because the system becomes a two-coil loop of current; in each wire the same current flows and in the same direction. In the circuit of Fig. 7.5 the loops might be cooled below the transition without the external battery, *i.e.*, with no initial current. If the battery is now connected, the currents flow in such a way as to produce no magnetic field and hence the dip needle does not deflect. All these combinations are explained on the basis of there being no change of the total flux linked by the superconductor.

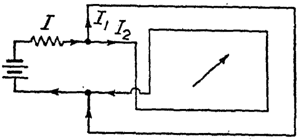

FIG. 7.5. Current loops which maintain the total magnetic flux constant.

Magnetic Critical Field

The resistance of a superconducting wire can be restored by a suitably large external magnetic field. At constant temperature, a plot of R vs. applied field is given for superconducting tin in Fig. 7.6. The value of the critical magnetic field $\mathbf{B}_c$ is a function of the temperature (Fig. 7.7).

How this field is produced does not seem to matter to the superconductor. Silsbee predicted, and it has been verified experimentally,[1] that a current within the wire of magnitude sufficient to produce its own critical magnetic field at the surface of the wire would destroy the superconducting state.

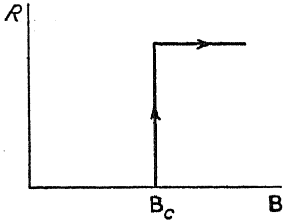

FIG. 7.6. Resistance vs. applied magnetic field along cylinder axis.

Meissner Effect

The experiments of Meissner and Ochsenfeld[2] on pure solid superconducting spheres bring to light a new property not explained by infinite conductivity. The results show that within the solid metal superconductor the magnetic field **B** is everywhere zero. The experimental arrangement is shown in the schematic drawing (Fig. 7.8). The experiment itself is described by the drawings. In the top drawing the

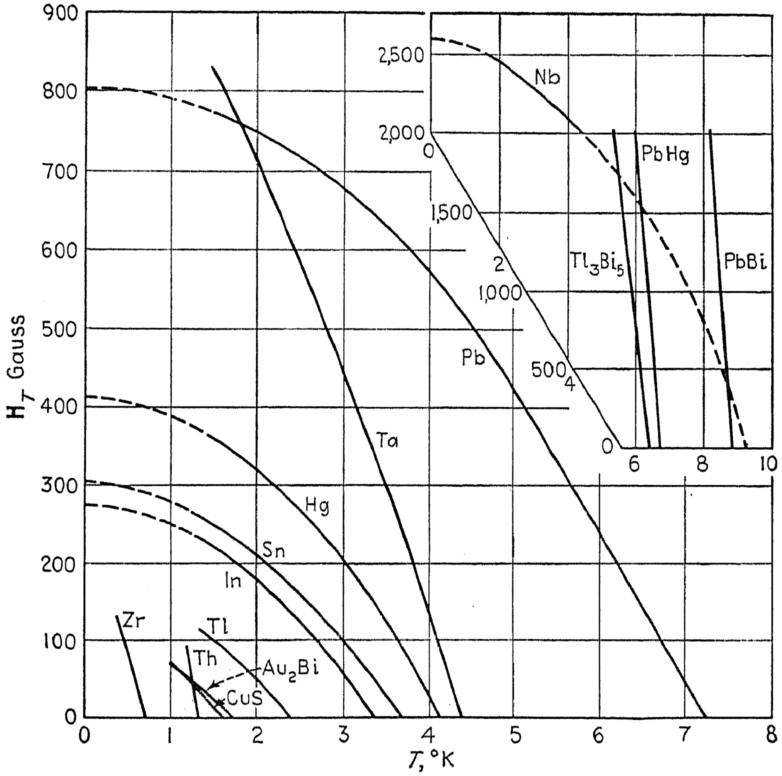

FIG. 7.7. Threshold magnetic field of superconductors.

---

[1] R. Scott, *J. Research Nat. Bur. Standards*, **41,** 581, 1948.

[2] W. Meissner and L. Ochsenfeld, *Naturwissenschaften*, **21,** 787, 1933.

solid sphere of metal is cooled below its transition temperature and then placed in a magnetic field. Infinite conductivity would predict that the sphere would not permit the field to penetrate. The second experiment shows that the field is kicked out of the sphere when the metal is cooled into the superconducting phase. The flux does not stay constant; in fact inside the metal $B = 0$. We must conclude that a current spontaneously sets up about the sphere such that the vector $\mathbf{H}$ at any point within the sphere is exactly equal and opposite to the vector $\mathbf{H}$ of the externally applied field. In this way $\mathbf{B} = \mu\mathbf{H} = 0$. It may well be argued that indeed μ could be zero and that experimentally the situation may be indistinguishable. In strongly diamagnetic materials there is always a physical situation whereby electrons can orbit through large areas when an external magnetic field is applied. Might not then a superconductor be an extreme case in which current loops are formed within the material having an orbit radius of many thousands of angstrom units? Returning to the experiment itself, the complete Meissner effect ($\mathbf{B} = 0$) is difficult to obtain experimentally, and there is a high percentage of the flux "locked in." Tantalum and niobium seem to lock in nearly all of

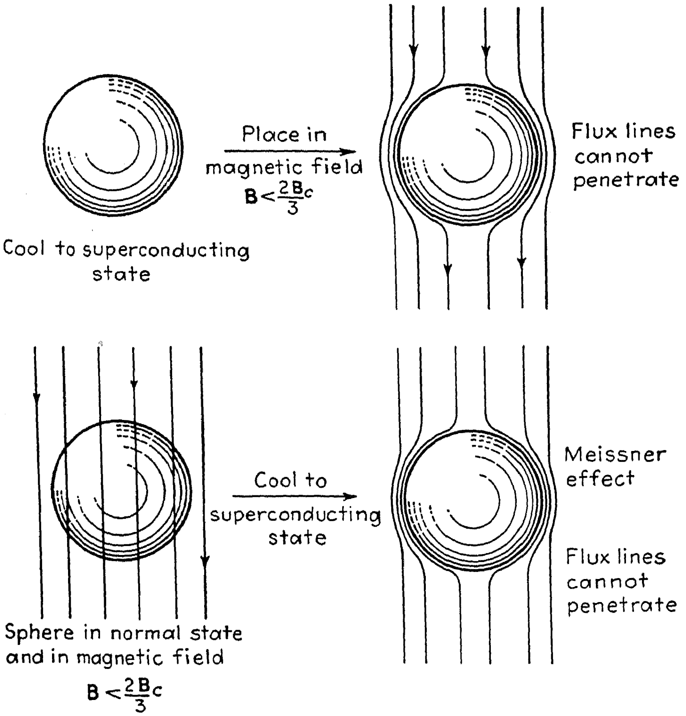
Cool to superconducting state
Place in magnetic field
$B<\frac{2B_c}{3}$
Flux lines cannot penetrate
Sphere in normal state and in magnetic field
$B<\frac{2B_c}{3}$
Cool to superconducting state
Meissner effect
Flux lines cannot penetrate

FIG. 7.8. Experiments on solid spheres showing Meissner effect.

the flux. One further remark concerning Fig. 7.8. The magnetic field used on the spheres must be less than $2\mathbf{B}_c/3$ because with this size field the value at the equator of the sphere is just $\mathbf{B}_c$ owing to the bunching of the flux lines.

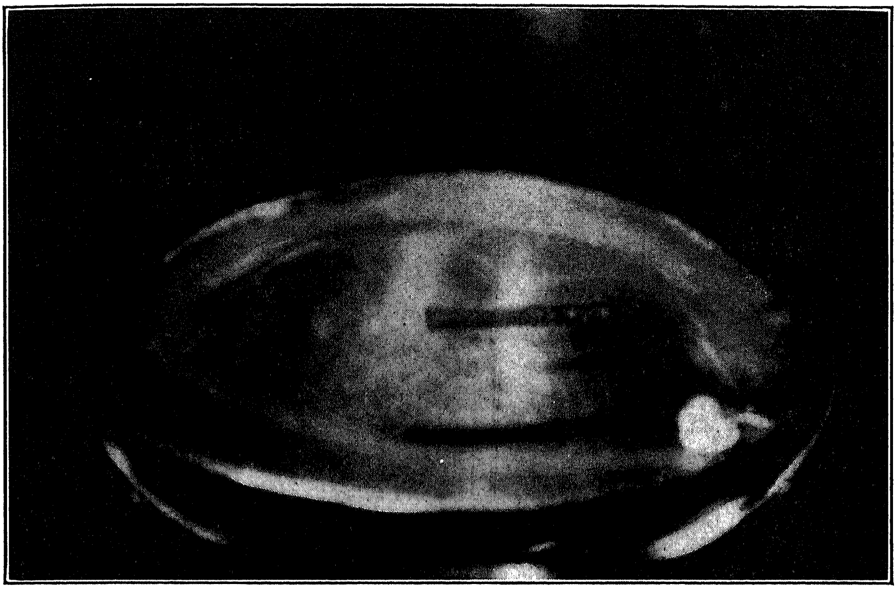

A permanent magnet floats above the superconducting tin dish because of the Meissner effect. The white object in the lower right of the tin dish is some solid air which fell into the inner liquid helium flask. *(Photographed by Dr. E. Maxwell and Dr. R. Scott, National Bureau of Standards.)*

Thermal Properties of Superconductors

Specific Heat and Entropy. We shall next examine the thermal properties of superconductors. The specific heat of a superconductor, in zero magnetic field, is given by Fig. 7.9. The entropy vs. temperature from integration of the heat capacity data is given in Fig. 7.10. We see that the transition to the superconducting state is a second-order phase transition because the entropy curve is continuous. The latent heat which characterizes a first-order transition is now spread out over a temperature interval from T_0 down to some very much lower temperature. If we were to study the specific heat of the metal at temperatures below the transition T_0, but in sufficiently large field $\mathbf{B} > \mathbf{B}_c$, we would find that the experimental values of the specific heat represented a continuation of the high-temperature values. The entropy of the extrapolated normal phase continues down to zero at the absolute zero of temperature. The entropy of the superconducting phase is also zero at the absolute zero of temperature. The difference in entropy of the normal and of the superconducting phase is plotted as a function of temperature in Fig. 7.11. In Chap. 9 we shall discuss the contribution to the entropy of the lattice vibrations and of the electronic motion in the metal. There we shall

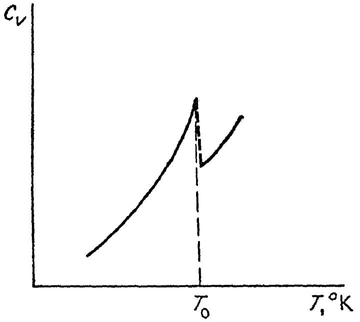

Fig. 7.9. Specific heat of superconductor.

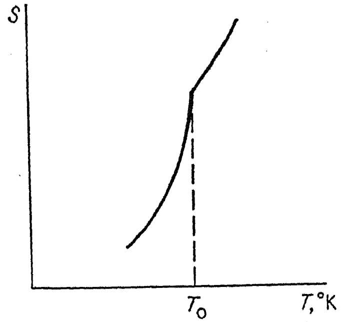

Fig. 7.10. Entropy of superconductor.

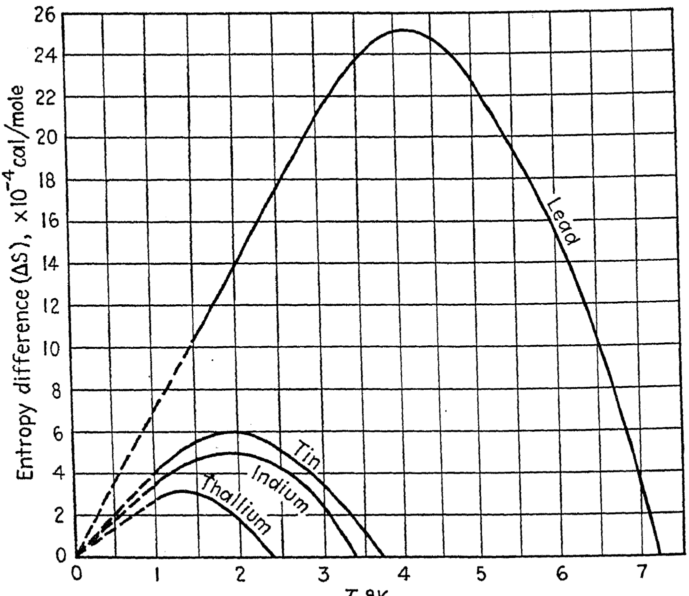

Fig. 7.11. Entropy differences between super and normal state vs. temperature.

attempt to separate the contributions to the total energy of the system and to assign experimental values to the purely superconducting phase transition. Let us bear in mind that Figs. 7.9, 7.10, and 7.11 are schematic and represent the gross thermodynamic values. In Chap. 9 we shall present evidence that the specific heat due to the free electrons in the metal is about equal in magnitude to the lattice specific heat at temperatures of about 2°K. Below this temperature range the lattice specific heat becomes even smaller than the electronic contribution. Since we have experimental evidence that there is no observable lattice change at the superconducting transition, the interpretation of the changes in specific heat and entropy is that the free electrons enter a new set of energy states.

Now the entropy curves are physically significant because we must attach the meaning of creating order from disorder in lowering the entropy. Thus the concept of order in the electronic system demands either an electronic lattice (space order) or a phase space condensation below the transition temperature T_0. Whatever theory is proposed should be capable of describing the experimentally observed entropy and specific heat curves. A thermodynamic treatment of these quantities was given by Gorter and Casimir,[1] and we shall discuss this bit of general theory at this point. It has to do with the Meissner effect and the critical field $\mathbf{B}_c$ of Fig. 7.7.

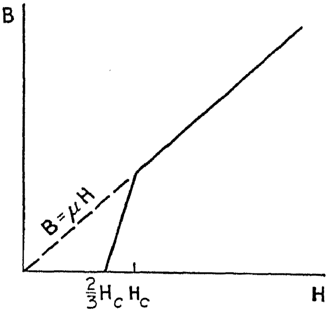

FIG. 7.12. Plot of **B** vs. **H** for a spherical superconductor.

For the present let us take as experimentally established the fact that the complete Meissner effect on very pure solid spheres can be obtained. Now even in this case we have a region in which the transition is, so to speak, intermediate. The curve of Fig. 7.12 indicates how for a sphere the value of **B** is zero for external applied fields until a field $\mathbf{H} = 2\mathbf{H}_c/3$ is reached, and at this point the external field at the equator of the specimen is actually equal to $\mathbf{H}_c$ because of the demagnetization factor. This means that for a region around the equator the superconduction property $\mathbf{B} = 0$ no longer exists and the external field begins to penetrate. The boundary conditions require that the normal component of **B** remain constant across an interface unless there are surface currents. There are surface currents. In any case we must have a complicated pattern of field penetration for this intermediate state. Finally at $\mathbf{H} = \mathbf{H}_c$ the last regions of superconduction are destroyed, and the linear relation $\mathbf{B} = \mu\mathbf{H}$ obtains inside the metal. **H** has its full value and is not partially cancelled out by superconducting currents. However, the plot in Fig. 7.7 of the critical field $\mathbf{B}_c$ against T represents a phase boundary between the two conducting phases, and the two phases differ by a Gibbs potential difference:

$$\Delta G = \frac{\mathbf{B}_c^2 V}{2\mu}$$

---

[1] C. J. Gorter and H. Casimir, *Physica*, **1**, 306, 1934; Z. *tech. Physik.*, **15**, 539, 1934.

This equation asserts that the change of Gibbs potential is the magnetic energy density multiplied by the volume of the superconductor. If we had taken the shape of the superconductor to be a cylinder with the magnetic field applied parallel to the long axis, then the complication of the intermediate state would not confuse us. With a cylinder taken as very long so that end effects may be neglected, the magnetic field does not penetrate until $\mathbf{B} = \mathbf{B}_c$ (see Fig. 7.6).

The entropy difference is

$$\Delta S = -\frac{\partial}{\partial T}(\Delta G) = -\frac{V\mathbf{B}_c}{\mu}\frac{\partial \mathbf{B}_c}{\partial T}$$

Since $\mathbf{B}_c$ vanishes at $T = T_0$ and yet has a finite slope at that point, we may conclude that at $T = T_0$ there is no jump in the entropy ΔS between the two phases. At other temperatures the ΔS is finite, and owing to the shape of Fig. 7.7, we get Fig. 7.11 for the entropy difference in accord with the experimentally determined values.

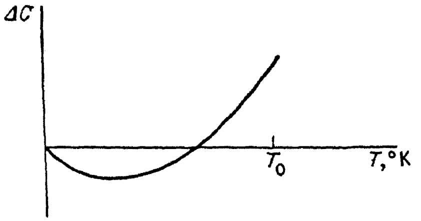

FIG. 7.13. Difference in specific heat between super and normal state plotted against temperature.

The specific heat shows a discontinuity (Fig. 7.13) according to this theory:

$$C_n - C_s = -T\frac{\partial^2}{\partial T^2}\left(\frac{\mathbf{B}_c^2 V}{2\mu}\right)$$

Table 7.3 gives a comparison between the above theoretical expression for the jump in specific heat at the transition temperature T_0 and the value measured by Keesom and Van Laer. At other temperatures the results on tin are given in Table 7.4, and again the agreement is quite good. Mendelssohn and Moore[1] showed that, when a great deal of magnetic flux is frozen in, giving no Meissner effect, then the experimental specific heat follows the normal metal specific heat curve and gives no noticeable discontinuity.

TABLE 7.3. SPECIFIC HEAT JUMP AT TRANSITION TEMPERATURE

Metal	$\Delta C_{\text{exptl.}*}$, cal/°K	ΔC_{theory}
Tl	1.48×10^{-3}	1.44×10^{-3}
Sn	2.4×10^{-3}	2.29×10^{-3}

* W. H. Keesom and P. H. Van Laer, *Physica*, **5**, 193, 1938.

---

[1] K. Mendelssohn and J. R. Moore, *Proc. Roy. Soc. (London)*, **152**, 34, 1935.

TABLE 7.4. SPECIFIC HEAT JUMP OF TIN AND LEAD

T, °K	C*, calorimetric cal/(mole)(°K)	C†, magnetic, cal/(mole)(°K)
	Tin	
1.1	-0.35×10^{-3}	-0.33
1.5	-0.25	-0.22
2.0	-0.04	$+0.05$
2.5	$+0.60$	$+0.60$
3.0	$+1.18$	$+1.17$
3.3	$+1.5$	$+1.58$
	Lead‡	
6.75	0.0104	0.0096
7.00	0.0117	0.0112
7.23	0.0126	0.0126

* W. H. Keesom and P. H. Van Laer.

† J. G. Daunt and K. Mendelssohn.

‡ J. Clement and E. Quinnell, *Phys. Rev.*, **85**, 502, 1952.

Magneto-caloric Effect in Superconductors

Mendelssohn and coworkers[1] obtained evidence for a drop in temperature when a magnetic field was applied adiabatically to a superconductor. This may be understood from the entropy considerations which we have just examined. At any temperature below T_0 the entropy is higher in a magnetic field. So if the field is applied adiabatically, the temperature must drop.

Electrodynamic Studies

Gyro-magnetic Effect. We shall now concern ourselves with an examination of a group of experiments which bring out still further the unique characteristic of superconductors. The experiment by Kikoin and Gubar[2] showed that the magnetic property $\mathbf{B} = 0$ of a solid superconductor is caused by orbital motion of the electrons. The experiment has been repeated by Pry, Lathrop, and Houston.[3] The experiment consisted of suspending from a torsion fiber a solid sphere of superconducting lead. A magnetic field, whose direction could be reversed at a frequency corresponding to the natural frequency of the undamped mechanical system, was placed parallel to the axis of the oscillator. This essentially repeats the Einstein and de Haas experiment on ferromagnetic material, except now one has effectively a very strong diamagnetic substance. The observed gyro-magnetic effect on a metal exhibiting infinite conductivity requires that the momentum exchange arise from the coupling action of the fields rather than from any collision process between the electrons and the lattice. We do not wish to imply that in the case of ferromagnetism there was any such collision process, and the matter of spin-lattice coupling will be taken up in Chap. 8. Let us recall that magnetization implies a current loop or in other words an angular momentum by a charged particle. Thus a change of magnetization ΔM implies a change in angular momentum ΔP, and if this occurs in a time Δt, there will be a torque

---

[1] K. Mendelssohn *et al.*, *Nature*, **133**, 413, 1934; *Proc. Intern. Congr. Refrig. 7th Congr., The Hague-Amsterdam*, 1936.

[2] I. Kikoin and J. Gubar, *J. Phys. USSR*, **3**, 333, 1940.

[3] R. Pry, A. Lathrop, and W. V. Houston, *Phys. Rev.*, **86**, 905, 1952.

$$\tau = \frac{\Delta P}{\Delta t} = \frac{dP}{dt} = \frac{2m}{e}\frac{dM}{dt} \qquad \text{newton-m}$$

The equation is valid if the gyro-magnetic ratio is $2m/e$. This torque may drive the oscillator and twist the suspension fiber. In the experiment a steady-state amplitude of oscillation was observed. Kikoin and Gubar were careful to eliminate all other torques which might influence the motion of the oscillator, and they did this by using a very pure lead made into a most accurate sphere which was suspended on a diameter. The earth's field was cancelled out. In this way there was no frozen-in flux, and the sphere became superconducting in the absence of an external field. Thus when the external field was turned on, supercurrents were set up on the surface layer of the sphere.

We shall presently see that such supercurrents on a sphere of radius R give a magnetic moment according to the London[1] theory

$$M = \frac{2\pi R^3 \mathrm{B}}{\mu}$$

This is valid so long as R is large compared to the depth of penetration of the magnetic field. This is so for $R = 1$ cm. Now the Kikoin-Gubar experimental oscillator may be described during one half period of motion as

$$\theta = \theta_0 e^{-\delta t} \cos \omega t$$

The momentum is

$$I\dot{\theta} = -I\theta_0(\omega e^{-\delta t} \sin \omega t - \delta e^{-\delta t} \cos \omega t)$$

where I is the measured moment of inertia and δ the decay constant due to damping effects of the helium gas on the torsion pendulum. There is no damping due to the steady magnetic field. Thus the momentum lost in one half period occurs in the time interval $-\pi/2\omega$ to $+\pi/2\omega$ and is

$$\Delta|P| = -I\theta_0\delta\pi + \text{small terms}$$

[1] F. London, *Physica*, **3**, 458, 1936; "Superfluids," New York, Wiley, 1950.

The change of momentum due to magnetization in a field which changes from $+\mathbf{B}$ to $-\mathbf{B}$ is

$$\Delta|P| = \frac{2m}{e}\frac{4\pi R^3\mathbf{B}}{\mu}$$

At steady-state angular amplitude the momentum lost per half period is equal to the momentum gained. Thus

$$\theta_0 = \frac{2m}{e}\frac{4\pi R^3\mathbf{B}}{\mu}\frac{1}{I\delta\pi}$$

Theory and experiment are in complete agreement. The gyro-magnetic ratio is $2m/e$ for a superconductor. The direction of the torque acting on the body is in the following way: the magnetic induction change $d\mathbf{B}/dt$ produces an electric field $\mathbf{E}$ which pushes on the positive ion lattice.

Torsion Pendulum Studies—Infinite Conductivity and Superconductivity. The apparatus for torsion pendulum studies on superconductors used by Houston and Muench is shown in Fig. 7.14. The tin sphere was cast in vacuum from spectroscopically pure tin and carefully machined to a diameter of 1.0000 ± 0.0004 in. Consider the tin sphere at 4.2°K where it is a normal conductor but a very good conductor. Now the normal conductor oscillating in a steady magnetic field of the Helmholtz coils can be approximated closely by a constant field and by a small alternating field at right angles to the constant field with the sphere remaining fixed. The eddy current produced by the alternating field can be computed classically, and the force due to its interaction with the constant field gives the desired torque. The alternating field, and hence the torque, can be expressed in terms of the angle of rotation of the sphere. The computed torque is

$$\tau = \frac{-2\pi\mathbf{B}^2R^3}{\mu}\left(1 - \frac{3}{x}\frac{\sinh x - \sin x}{\cosh x - \cos x}\right)\theta$$
$$- \frac{2\pi\mathbf{B}^2R^3}{\mu\omega}\left(\frac{3}{x}\frac{\sinh x + \sin x}{\cosh x - \cos x} - \frac{6}{x^2}\right)\dot{\theta}$$

where R is the radius of the sphere, τ is its specific resistivity, ω is the angular frequency, and the quantity x is

$$x = \left(\frac{2\omega\mu R^2}{\tau}\right)^{\frac{1}{2}}$$

The second term represents a damping torque, and the magnitude of τ necessary to give the observed damping was considered reasonable for tin at 4.2°K. The first term represents a restoring torque which is very small at ordinary temperatures but becomes large at small value of τ.

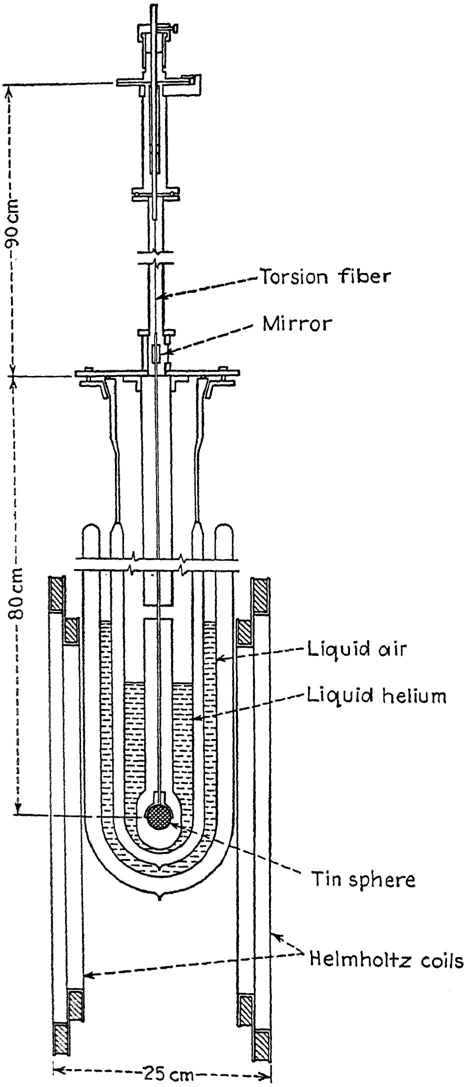

Fig. 7.14. Torsion pendulum apparatus. (*Houston and Muench*, *Phys. Rev.*, **84**, 104, 1951.)

Houston and Muench explain the period dependence on the magnetic field at 4.2°K as being caused by the first term restoring torque. Superconductivity is not a continuation of the above classical theory to smaller values of τ because the experiments showed no field dependence for the period in the superconducting state. The damping torque likewise vanished in the superconducting state.

Love, Blunt, and Alers[1] found that, if a tin sphere at 4.2°K was set into rotation, the eddy current induced by a steady magnetic field was of the same size and distribution as the supercurrents for the complete Meissner effect. Alers, McWhirter, and Squire[2] gave a quantitative theory for the induced eddy currents and compared the magnitude with the London theory.

Skin Depth of Penetration of a Magnetic Field

These remarks about the superconductor in a magnetic field lead us naturally into the studies by Shoenberg and others on the depth of penetration of a magnetic field in a superconductor. The London theory, which we shall examine in more detail, has the parameter $m/ne^2 = \lambda$, where m is the electron mass, n the number per unit volume, and e the electron charge. This parameter determines the skin depth $\delta = 1/\sqrt{\mu/\lambda}$ for penetration of the magnetic field. Thus direct measurements on skin depth δ are of interest in evaluating a theoretically important parameter. D. Shoenberg and E. Laurmann[3] used a method first suggested by Casimir.[4] The mutual inductance of two coils wound on a superconducting core is measured as a function of temperature at low frequencies. At first glance one would think the slight penetration by the magnetic field to be a quantity beyond the error limits of detection in this way. The results were found to be very sensitive to surface conditions, but single crystals with smooth surfaces gave reproducible measurements of the relative skin depth $\delta(T) - \delta(2.17°\mathrm{K})$ as a function of temperature T. These were consistent with the formula

$$\delta(T) = \delta_0 \left[1 - \left(\frac{T}{T_c} \right)^4 \right]^{-\frac{1}{2}}$$

where T_c is the transition temperature and δ_0 was found to be 5.2×10^{-6} cm for tin and 4.3×10^{-6} cm for mercury. There was no evidence for any dependence of δ on a steady magnetic field, though an increase of 10 up to 80 per cent of the critical field is not excluded. These results agree with high-frequency studies by Pippard.[5] Since the skin depth must be translated back to the parameter λ by means of the equation $\delta = 1/\sqrt{\mu/\lambda}$, we realize that we only know a ratio of the electron mass m to the number n per unit volume. If we suppose the electron mass is the same for the normal electron, the Shoenberg and Laurmann result would give only about one electron from every three atoms as a superconducting electron.

---

[1] W. Love, R. Blunt, and P. Alers, *Phys. Rev.*, **76**, 305, 1949.

[2] P. Alers, J. McWhirter, and C. Squire, *Phys. Rev.*, **84**, 104, 1951.

[3] D. Shoenberg and E. Laurmann, *Proc. Roy. Soc.* (*London*), **198**, 560, 1949.

[4] H. Casimir, *Physica*, **7**, 887, 1940.

[5] A. B. Pippard, *Proc. Roy. Soc.* (*London*), **203**, 210, 1950.

Thermal Conductivity of Superconductors

De Haas and Bremmer[1] have measured the thermal conductivity of metals which become superconductors, and they have shown that the conductivity is smaller in the new state. Recent measurements confirm this point of view according to Rademaker.[2] The electrons responsible for superconductivity must be excluded from taking part in thermal phenomena. The number of superconducting electrons increases from the value zero at the transition temperature to a large percentage of available electrons at much lower temperatures; *e.g.*, for tin 0 per cent at 3.72°K to 35 per cent at 2°K. Recently Heer and Daunt[3] have shown that for tin the normal conductivity at 0.65°K is about forty times that of the thermal conductivity in the superconducting state; for tantalum the thermal conductivity drops $\frac{1}{60}$ at 0.55°K. Daunt and Heer proposed to use this property in order to obtain extremely low temperatures with a magnetic cooling technique. In Fig. 7.15 the results of Mendelssohn and Olsen show that for alloys the heat conductivity may increase on going into the superconducting state.

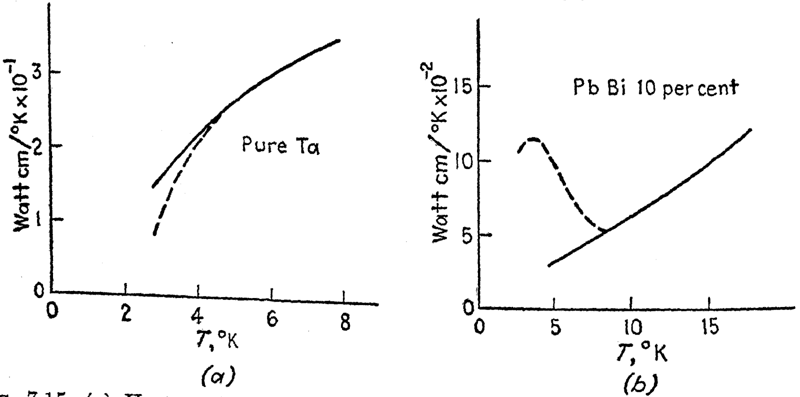

FIG. 7.15. (*a*) Heat conductivity of tantalum. The continuous curve denotes the normal state of the metal (kept so by a magnetic field which everywhere exceeds the threshold value), the broken curve the superconducting state. (*b*) Heat conductivity of Pb-Bi 10 per cent alloy. Continuous curve denotes the normal metal state, broken curve the superconducting state. [*Mendelssohn and Olsen, Proc. Phys. Soc. (London)*, **63**, 2, 1950.]

Thermoelectric Effect in Superconductors

The thermoelectric force between two superconductors has been measured to be zero by Keesom.[4] Daunt and Mendelssohn[5] have shown that the Thomson heat is zero in a superconductor, and this is not surprising since the electric field $E = 0$ inside the metal. They concluded that no heat is given out or taken up by persistent currents in a superconductor. Yet the persistent currents in a superconductor decrease as the temperature is raised so that the threshold current is not exceeded; *i.e.*, the magnetic field produced by the current must not exceed the critical magnetic field. Thus Daunt and Mendelssohn state that the number of superconducting electrons must decrease with rising temperature corresponding to a smaller current density, $j_s = n_s ev$, because the velocity is unaffected. Electrons which leave the superconducting state may take up an excitation energy ΔE so that the specific heat should be

---

[1] W. J. de Haas and H. Bremmer, *Proc. Koninkl. Nederland. Akad. Wetenschap.*, **34**, 325, 1931.

[2] A. Rademaker, *Physica*, **15**, 849, 1949.

[3] C. V. Heer and J. G. Daunt, *Phys. Rev.*, **76**, 854, 1949.

[4] W. H. Keesom, *Proc. Koninkl. Nederland. Akad. Wetenschap.*, **34**, 1365, 1931.

[5] J. Daunt and K. Mendelssohn, *Proc. Roy. Soc. (London)*, **185**, 225, 1946.

$$C_e = \Delta E \frac{dN}{dT}$$

This specific heat is superimposed on the lattice specific heat and the normal electron specific heat. These ideas of Daunt and Mendelssohn are an interesting possibility, but one should take the standpoint that such matters are still controversial.

Effect of Strain on a Superconductor

We have already seen that the atomic volume is a most important parameter in determining whether a metal becomes a superconductor. Lazarev and Galkin[1] put tin wire under large tension and shifted the temperature of transition into the superconducting state from the normal value of 3.72 to 9°K. Similarly the magnetic field required to destroy superconduction at 2°K was raised from 210 gauss to the enormous value of 15,000 gauss. The shift of the transition temperature is so large that one would seem unable to explain the matter as simply as the isotope effect, *i.e.*, this cannot be a matter of the shift of the zero-point vibration.

High-frequency Measurements on Superconductors

It is known that a superconductor is not a perfect reflector of infrared radiation and that the normal conducting electrons at these frequencies present an impedance with a normal resistance term and a mass controlled reactance term. On the other hand the superconducting electrons show zero resistance but present a pure imaginary impedance at quite high radio frequency. H. London[2] investigated super and normal electron behavior at 1,500 megacycles/sec and concluded that there was some resistance below the transition point. The presence of some normal electrons within the superconductor was thus verified. London also observed an anomalous resistance at low temperatures just before the superconducting transition which he attributed to a long mean free path of electrons compared to the skin depth of penetration of the electric field.

---

[1] B. Lazarev and A. Galkin, *J. Exptl. Theoret. Phys. USSR*, **18**, 1948.

[2] H. London, *Proc. Roy. Soc. (London)*, **176**, 522, 1940.

There is a second consideration which makes high-frequency studies interesting. From the point of view of setting $h\nu = kT$, where the energy gap between the super and normal state might be $h\nu$, we may identify this gap between the super and normal state with the energy kT at the transition temperature. The frequency to be expected for a resonance absorption is of the order 100,000 megacycles/sec. Just after the war high-frequency measurements were made by Slater *et al.*[1] on a lead cavity with 3-cm waves, and in the superconducting state Q values of 10^6 were found. Pippard[2] examined the anomalous resistance and the superconducting state at 25 cm by measuring the Q value of a shorted transmission line placed in a well-shielded chamber which was fed by a transmission line. Pippard[3] also carried out studies at a free-space wave length of 3.2 cm. The results on tin and mercury are given in Table 7.5. Maxwell, Marcus, and Slater[4] examined the surface impedance of normal and superconducting lead and tin at 24,000 megacycles/sec between 2 and

TABLE 7.5. RADIO FREQUENCY ($\lambda \approx 25$ cm) RESULTS BY A. B. PIPPARD[a]
Percentage Change of Resistance on Becoming Superconductor

Sn		Hg	
T, °K	$100R/R_n$	T, °K	$100R/R_n$
3.712	100	4.1525	100
3.702	70	4.141	60
3.6835	40	4.108	15
3.598	10	4.010	3
3.455	4	3.09	0.3
3.150	2	2.20[a]	0.05

Anomalous Skin Effect for Normal Metals (Silver at $\lambda \approx 25$ cm)

T, °K	Skin Conductivity[b] Σ ohm^{-1}
290	113.5
77	254
20.4	396
4.2	397

[a] The author concedes that for Hg the last value at 2.20°K may actually be zero.
[b] The skin conductivity is directly proportional to Q.

---

[1] J. C. Slater *et al.*, *Phys. Rev.*, **70**, 97, 1946.
[2] A. B. Pippard, *Proc. Roy. Soc. (London)*, **191**, 370, 1947.
[3] A. B. Pippard, *Proc. Roy. Soc. (London)*, **203**, 78, 1950.
[4] E. Maxwell, P. M. Marcus, and J. C. Slater, *Phys. Rev.*, **76**, 1332, 1949.

300°K. The walls of a resonant cavity were made of the metal under study, and a great deal of attention was given to the condition of the surface so that it was of crystalline structure. Figure 7.16*a* shows the results of experiments by Slater *et al.* The effective resistance to high-frequency fields is larger than in the simple classical theory because the field penetration is small at these high frequencies and high conductivities—so small that the electric field is not constant over the path which the electron makes between collisions. The theory has been adequately worked out by Reuter and Sondheimer.[1] Sondheimer[2] has reviewed the problem of the mean free path L of electrons in metals.

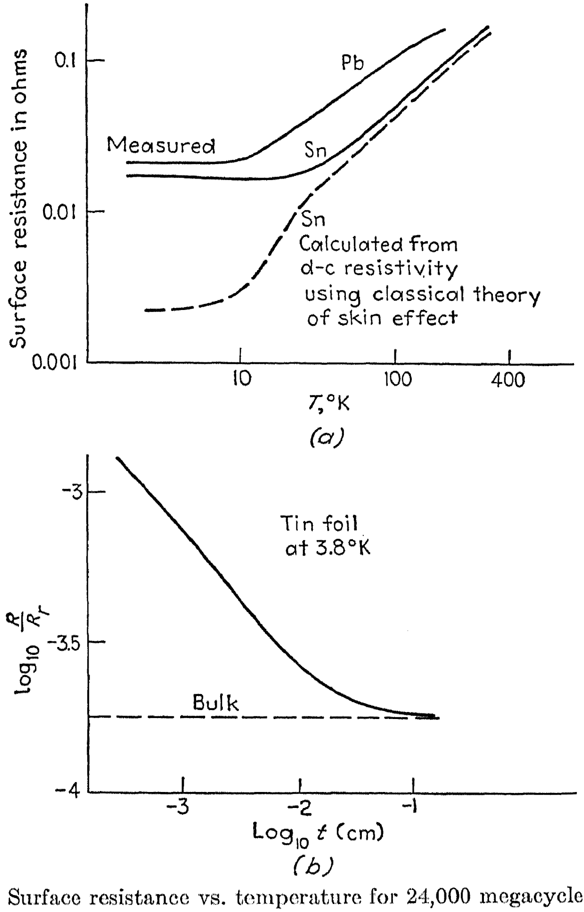

FIG. 7.16. (*a*) Surface resistance vs. temperature for 24,000 megacycles/sec. (*Maxwell, Marcus, and Slater, Phys. Rev.*, **76**, 1332, 1949.) (*b*) Logarithmic plot of the resistance against foil thickness. [*Andrew, Proc. Phys. Soc. (London)*, **62**, 77, 1949.]

---

[1] G. E. Reuter and E. H. Sondheimer, *Proc. Roy. Soc. (London)*, **195**, 336, 1948.

[2] E. H. Sondheimer, *Advances in Phys.*, **1**, 1, 1952 (*Pl.I. Mag.* supplement).

With the number of free electrons per unit volume n and the electric conductivity σ_0, the Sommerfeld theory gives

$$n = \frac{8\pi}{3}\left(\frac{m\bar{v}}{h}\right)^3; \qquad \sigma_0 = \frac{ne^2L}{m\bar{v}}$$

where h is Planck's constant, $-e$ is the charge, m is the mass of an electron, and $\bar{v}$ is the velocity of an electron at the surface of the Fermi distribution. The mean free path L is of the order of several hundred interatomic distances and becomes quite large at very low temperatures. Owing to lattice imperfections and impurities, there is a residual value L_r at these low temperatures.

With simplifying assumptions the following relationship may be derived:

$$\frac{1}{\sigma_0} = \frac{m\bar{v}}{ne^2L_r} + \left(\frac{m}{2}\right)^{\frac{1}{2}} \frac{9\pi h^2C^2}{8n\,\Delta e^2Mk\theta\xi^{\frac{3}{2}}}\left(\frac{T}{\theta}\right)^5 \int_0^{\theta/T} \frac{z^5\,dz}{(e^z-1)(1-e^{-z})}$$

The new symbols in this last equation are

ξ = Fermi energy level, $\frac{1}{2}mv^2$
θ = Debye temperature (see Chap. 9)
M = mass of an atom
Δ = volume of unit cell
C = constant of lattice electron interaction

Thus the residual resistance is simply additive, and the ordinary electrical resistance is proportional to T at high temperatures and to T^5 at very low temperatures. Sondheimer[1] has reviewed the work of Andrew in which foils of pure metal are studied at very low temperatures. The foils were so thin that the mean free path L became large compared to the foil thickness, and the resistance became influenced by scattering of electrons from the surface boundary. Figure 7.16*b* shows Andrew's results. Sondheimer has given a table of results taken by Chambers

TABLE 7.6. SKIN EFFECT AT HIGH FREQUENCY[a]

Metal.	$(\sigma_0/L) \times 10^{-22}$, gaussian units	n/n_a
Cu	13.9	1.0
Ag	8.3	0.68
Au	7.6	0.60
Sn	8.6	1.1
Hg	3.3	0.23
Al	5.5	0.37

[a] R. G. Chambers, Ph.D. Dissertation, Cambridge, 1952, in E. H. Sondheimer, *Advances in Phys.*, 1, 1, 1952 (*Phil. Mag.* supplement).

---

[1] *Ibid.*

from the anomalous skin effect at ultra-high frequencies. Table 7.6 gives these results and shows Chambers' values of σ_0/L together with the ratio n/n_a, the number of conducting electrons per atom.

Grebenkemper and Hagen[1] have shown the high-frequency resistance in the superconducting region to vary with frequency as the three-halves power.

Theories of Superconductivity

Theory of H. London and F. London. An adequate presentation of all the theories which have been advanced about superconductivity would expand this book beyond reason. The theories have in part been given by F. London[2] in his book "Superfluids." Likewise the book "Theory of Superconductivity" by M. von Laue[3] contains interesting material about the phenomenological approach to the problem of superconductivity. We shall briefly consider the theory of H. and F. London[4] and that of F. London.[5] This theory deals with the Meissner effect. In later paragraphs we shall examine the basic ideas behind more current theories about the superconducting state.

The entropy curve plotted against temperature suggests that the normal conducting electrons gradually become fewer in number below the transition temperature, while the number of superstate electrons increases on lowering the temperature. We must assume that the total current density is part normal current $\mathbf{J}_n$ and part supercurrent $\mathbf{J}_s$.

$$\mathbf{J} = \mathbf{J}_s + \mathbf{J}_n \tag{7.1}$$

Actually the $\mathbf{J}_s$ "short-circuits" the metal so that fields do not act on normal electrons. The normal current density is determined by Ohm's well-known law $\mathbf{J}_n = \sigma\mathbf{E}$. What about the supercurrent? The essential idea in the London theory is to account for the Meissner effect by allowing the supercurrent density $\mathbf{J}_s$ to be maintained by the local magnetic field $\mathbf{B}$ by the equation

$$\text{curl}\,\lambda\mathbf{J}_s = -\mathbf{B} \tag{7.2}$$

In this equation $\lambda = m/ne^2$ which is a constant characteristic of the superconductor. The equation may now be used in conjunction with Maxwell's equations to show that the magnetic field is zero inside a superconductor except very near the surface where it builds up exponentially to match the external field value at the boundary. From the equation curl $\mathbf{H} = \mathbf{J} + \dot{\mathbf{D}}$ we solve for the current density:

---

[1] C. Grebenkemper and J. Hagen, *Phys. Rev.*, **86**, 673, 1952.

[2] F. London, "Superfluids," New York, Wiley, 1950.

[3] M. von Laue, "Theory of Superconductivity," New York, Academic, 1952.

[4] F. London and H. London, *Proc. Roy. Soc.* (*London*), **149**, 71, 1935; *Physica*, **2**, 341, 1935; *Nature*, **140**, 793, 834, 1937.

[5] F. London, *Phys. Rev.*, **74**, 562, 1948.

$$\mathbf{J} = \mathbf{J}_s = \operatorname{curl} \frac{\mathbf{B}}{\mu} - \dot{\mathbf{D}} \tag{7.3}$$

Putting in $\mathbf{J}_s$ is perhaps only strictly true at $T = 0°\mathrm{K}$, but it is nearly true at all temperatures below the transition temperature because the superconducting electrons serve to shield or short-circuit the normal electrons. If now we substitute the empirical equation of London, we obtain

$$\operatorname{curl} \lambda \left[\operatorname{curl} \frac{\mathbf{B}}{\mu} - \dot{\mathbf{D}} \right] = -\mathbf{B} \tag{7.4}$$

We may then write

$$\lambda \operatorname{curl} \operatorname{curl} \frac{\mathbf{B}}{\mu} - \lambda \operatorname{curl} \epsilon \dot{\mathbf{E}} = -\mathbf{B} \tag{7.5}$$

where μ and ϵ are the magnetic and electric permeabilities, respectively, of the metal and specifically their values do not change for the metal becoming superconducting.

Since div $\mathbf{B} = 0$ and since curl curl $\mathbf{B}$ = grad div $\mathbf{B} - \nabla^2\mathbf{B}$ and since further we may replace curl $\mathbf{E} = -\dot{\mathbf{B}}$, we obtain

$$-\frac{\lambda}{\mu} \nabla^2\mathbf{B} - \lambda\epsilon\ddot{\mathbf{B}} + \mathbf{B} = 0 \tag{7.6}$$

If the magnetic field does not change with time, the equation reduces to

$$\nabla^2\mathbf{B} - \left(\frac{\mu}{\lambda}\right)\mathbf{B} = 0 \tag{7.7}$$

The solution for the radial field outside of a sphere of superconducting metal is

$$\mathbf{B}_r = \mathbf{B}_0 \left(1 + \frac{M}{r^3}\right) \cos\theta \tag{7.8}$$

In this last equation the distance r is measured from the surface of the sphere, and the polar angle θ has its customary meaning. The sphere acts like a dipole with current orbiting the radius a of the sphere. The strength of the dipole is given by

$$M = -a^3 \left[1 - \frac{3}{\sqrt{\mu/\lambda}\, a} \coth \sqrt{\mu/\lambda}\, a + \frac{3}{(\sqrt{\mu/\lambda}\, a)^2} \right] \tag{7.9}$$

At the surface of the sphere, r equals a, and the field produced by the dipole is a maximum. The terms in the quantity M show the small penetration of the magnetic field. Inside the metal the solution is of the form

$$\mathbf{B} = \mathbf{B}_0 e^{-(\mu/\lambda)^{\frac{1}{2}} r} \tag{7.10}$$

Thus the field falls off very rapidly with distance r inside the metal. The current density approximation $\mathbf{J} = \mathbf{J}_s$ is regarded as valid in steady fields at finite temperatures below the transition temperature. Thus we see that the Meissner effect is accounted for by the introduction of the empirical equation of H. and F. London.

One may try to justify the empirical equation with the following considerations: an electric field $\mathbf{E}$ can only cause an acceleration since there is no resistive action:

$$\lambda \dot{\mathbf{J}}_s = \mathbf{E} \tag{7.11}$$

where $\lambda = m/ne^2$ has its usual meaning. Combining this with the equation

$$\operatorname{curl} \mathbf{E} = -\dot{\mathbf{B}} \tag{7.12}$$

one has

$$\operatorname{curl} \lambda \dot{\mathbf{J}} = -\dot{\mathbf{B}} \tag{7.13}$$

The London equation is then the time integral of the results from an acceleration theory in which the integration constants are identically zero. The justification for setting the integration constants equal to zero represents the problem in this theoretical approach.

We may take still another approach to the London equation with the expression for the density of the electric current in quantum theory

$$\mathbf{J} = \frac{eh}{4\pi i m} (\psi \operatorname{grad} \psi^* - \psi^* \operatorname{grad} \psi) - \frac{e^2}{m} \psi\psi^* A \tag{7.14}$$

where ψ is the wave function of a single electron in the self-consistent field of the others. Summing over all electrons $\Sigma\psi\psi^*$ gives the number n of electrons per unit volume. Thus the last term is

$$-\frac{e^2}{m} nA$$

Now in the absence of a perturbation on the free electrons, they will occupy a spherical volume in momentum space so that the wave functions in the first term are such as to make the first term zero. Thus with unperturbed wave functions

$$\mathbf{J}_s = -\frac{ne^2}{m} A \tag{7.15}$$

and taking the curl of each side of the equation gives

$$\operatorname{curl} \lambda \mathbf{J}_s = -\operatorname{curl} A = -\mathbf{B} \tag{7.16}$$

Actually the wave functions are considerably disturbed by a magnetic field in normal metals. But if a superconductor permits some form of interaction between the electrons, then perhaps the wave functions remain unperturbed so long as the magnetic field is sufficiently weak. We may consider these ideas as part of a program to understand the nature of the superconducting state.

Quantum Theories of Superconductivity. Slater[1] examined the theory of energy bands in metals and considered the possibility of a new low-lying energy state which might arise from perturbation and exist at extremely low temperatures. Efforts along this line have been made more recently by M. Born and K. C. Chang[2] and by W. Heisenberg.[3]

To an electron wave moving through a metal, there is a periodic disturbance caused by the potential field of the atomic centers, and the result is that the lattice acts like a low-pass filter on the electron waves. The system is analogous to an acoustic system which may filter high-frequency waves and to electrical networks which are capable of such action. In addition the lattice points are in vibration so that the potential system is itself disturbed and may scatter the electron waves. Now the electron wave function has the form

$$\psi = e^{i(kx)}u(x)e^{-i2\pi Et/h} \tag{7.17}$$

where $u(x)$ is periodic with period of atomic centers and serves to modulate the plane waves whose wave length is $2\pi/k$. The low-pass filter allows values of k up to a certain cut-off value beyond which solutions do not exist. These cut-off values make the edge of a so-called "Brillouin zone" in the k space.

Now the electrons in a metal can also be treated like a gas which obeys the Fermi-Dirac statistics. The electrons under these statistics occupy a volume in momentum space which is spherical and of such a size that even at quite low temperatures there are a number of electrons which move very fast and which are at the surface of the momentum space configuration. M. Born has asserted that superconductivity is exhibited by those metals whose radius of the momentum sphere is the same size as the distance to the corner of the boundary planes of the Brillouin zone. The k vector is related to the momentum vector by $k = p/h$. Born[4] asserts that some electrons migrate into the second allowed zone because of an exchange force between electrons with parallel spins. These matters are controversial.

Bardeen[5] and Frohlich[6] have independently brought out a theory requiring strong interaction between the electrons and the vibrations of the crystal lattice. These ideas seem to be supported by the effect of atomic isotopes on the transition temperature of the superconductor. Bardeen[1] has summarized the theoretical discussions about electron-vibration interactions and superconductivity. The perturbation calculation is controversial, and one cannot yet say that an adequate theory of superconductivity exists. The interaction which causes scattering, and therefore resistance to electron flow in a metal at ordinary temperatures, contributes at low temperatures a term to the energy of the system of electrons plus normal modes of vibration. Bardeen attempted to show that this interaction lowers the energy of those electrons having energies near the surface of the Fermi surface and at the same time lowers the zero-point motion of the ions. The Hamiltonian of the system of electrons plus lattice vibrations is

---

[1] J. C. Slater, *Phys. Rev.*, **51**, 195, 1937; *ibid.*, **52**, 214, 1937.

[2] M. Born and K. C. Chang, *Nature*, **161**, 968, 1948; *J. phys. radium*, **9**, 249, 1948.

[3] W. Heisenberg, *Z. Naturforsch.*, **2a**, 185, 1947.

[4] M. Born and K. C. Chang, *Nature*, **161**, 968, 1948; *J. phys. radium*, **9**, 249, 1948.

[5] J. Bardeen, *Phys. Rev.*, **79**, 167, 1950; *ibid.*, **80**, 567, 1950; *ibid.*, **81**, 829, 1951; *ibid.*, **82**, 978, 1951.

[6] H. Frohlich, *Phys. Rev.*, **79**, 845, 1950; *Proc. Phys. Soc. (London)*, **64**, 129, 1951.

$$\mathbf{H} = \mathbf{H}_e + \mathbf{H}_1 + \mathbf{H}_i \tag{7.18}$$

The term for the electrons is

$$\mathbf{H}_e = \sum_i \mathbf{H}_{ei} \qquad i = 1, 2, \ldots, n \tag{7.19}$$

and where

$$\mathbf{H}_{ei} = -\frac{\hbar^2}{2m}\nabla_i^2 + V(x_i) \tag{7.20}$$

with x_i the coordinate of the ith electron. The potential $V(x_i)$ is the regular ionic field and does not allow for the perturbation of the potential due to lattice motion. Let $U(x)$ denote the difference in potential due to the ion displacement q. This difference is caused by lattice vibration. The lattice Hamiltonian in normal coordinates of the modes of motion is

$$\mathbf{H}_1 = \sum_r \left(\frac{-\hbar^2}{2\mu} \frac{\partial^2}{\partial q_r^2} + \frac{1}{2} K_r q_r^2 \right) \tag{7.21}$$

such that the force constant $K_r = \mu\omega_r^2$ in terms of the mass μ and of the angular frequency ω_r of the mode of lattice motion. The indices $r = 1, 2, \ldots 3N$. The interaction term is

$$\mathbf{H}_i = \sum_{i,s} U_s(x_i) q_s \tag{7.22}$$

This term contains both the coordinate of the ith electron and the normal coordinate of the sth mode of motion of the lattice. Such an interaction leads to the theory of scattering of electron flow in metals at normal temperature. Developments of this program to show that the interaction leads to superconductivity will be followed with interest.

---

[1] J. Bardeen, *Revs. Mod. Phys.*, **23**, 261, 1951.

Two-electron Fluid Model

Bender and Gorter[1] have examined the two-electron-state model of superconductivity and shown that the experimental results can be easily interpreted with the following assumptions: (1) There exists an energy gap β between the normal electron state and the superelectron state. The energy gap may be expressed on a per unit volume basis just as we denote the number n_s of superelectrons per unit volume. (2) The fraction f of superelectrons at any temperature $T < T_c$ is given by

$$f = \frac{n_s(T)}{n_s(0°\mathrm{K})}$$

and this fraction is 1 at 0°K and is 0 at T_c°K.

The Gibbs potential for the superconducting state is

$$G_s = U_0 - V[\beta f - \gamma \tfrac{1}{2}(1 - f)^{\frac{1}{2}}T^2] + G(T)_{\text{lat.}}$$

The Gibbs potential for the normal state is

$$G_n = U_0 - V\frac{\gamma T^2}{2} + G(T)_{\text{lat.}}$$

Since we shall be interested in the difference $G_n - G_s$, we need not concern ourselves with the lattice energy because these terms cancel. The electron gas contribution to the potential comes through the term with γ, and we must refer the reader to Chap. 9 for evaluation. We can say here that γ depends on the density of energy states at the top of the Fermi distribution of energy states. For this reason Bender and Gorter have introduced for the superconducting state a change from the normal-state value of γ to the value $\gamma(1 - f)^{\frac{1}{2}}$. The justification for this empirical factor is not only that it fits the experimental results but that one understands a need for a change in the density of states at the surface of the Fermi level.

At $T = 0$°K the difference

$$(G_n - G_s)_{0°\mathrm{K}} = V\beta = \frac{\mathrm{B}_0^2 V}{2\mu}$$

which is the magnetic energy density × volume required by the Meissner effect and where B_0 is the critical magnetic induction at 0°K. Thus, β, the energy gap per unit volume, is defined uniquely for each superconductor. It would of course depend upon the isotopic mass just as B_0 does for each superconducting element.

For stable equilibrium at any temperature we require

$$\frac{\partial G_s}{\partial f} = 0 = -\beta V + \frac{\gamma T^2}{4}(1 - f)^{-\frac{1}{2}}V$$

---

[1] P. L. Bender and C. J. Gorter, *Physica*, **18**, 597, 1952.

so that

$$f = 1 - \left(\frac{\gamma T^2}{4\beta}\right)^2$$

We demand that $f \rightarrow 0$ as $T \rightarrow T_c$ so we require that

$$\frac{\gamma}{4\beta} = \frac{1}{T_c^2}$$

or that

$$\gamma = \frac{4\beta}{T_c^2} = \frac{2\mathrm{B}_0^2}{\mu T_c^2}$$

This last relationship was first recognized by Kok in Leiden from a study of the experimental data.

Let $t = T/T_c$; then at any temperature $T < T_c$ the difference in Gibbs potential may be written

$$G_n - G_s = \frac{V\mathbf{B}_0^2}{2\mu}(t^4 - 2t^2 + 1)$$

so that by differentiation and substitution we have the difference in specific heats

$$C_n - C_s = \gamma VT - \frac{3\gamma VT^3}{T_c^2}$$

which relation is experimentally true and was first derived from thermodynamics by Gorter and Casimir.[1]

---

[1] C. J. Gorter and H. Casimir, *Physica*, **1**, 306, 1934; *Z. tech. Physik.*, **15**, 539, 1934.

CHAPTER 8

MAGNETISM AT LOW TEMPERATURES

The study of the magnetic properties of matter at low temperatures has been of as much interest to physicists as have the investigations made on superconductors and on liquid helium. It is at once obvious that the quantity $\beta\mathbf{B}/kT$, which enters into the statistical expression for the magnetization of a substance, becomes quite large at low temperatures and at high field strengths. We shall see that for ideal paramagnetic salts such conditions bring about the phenomena of saturation or maximum alignment of dipoles. Departures from ideal behavior may be attributed to interaction effects such as antiferromagnetism. We shall see that at very low temperatures the thermal vibrations of the atoms contribute a vanishingly small term to the entropy. The entropy of the electronic system and even of the nuclear system then becomes the principal entropy of the entire array. Magnetic cooling is then possible. We shall begin the survey of this field by a brief presentation of the basic ideas and experiments on magnetism.

Some Fundamental Concepts of Magnetization

In a phenomenological approach to the magnetization of a substance we begin by drawing a close analogy with dielectrics. We say that the ratio of a coil's self-inductance with the specimen material filling the coil to that of the empty coil is just the ratio of the permeabilities of the medium to that of empty space.

$$\frac{L}{L_0} = \frac{\mu}{\mu_0} \tag{8.1}$$

The general relationship between **B** and **H** is given by

$$\mathbf{B} = \mu\mathbf{H} \tag{8.2}$$

We attempt to describe the behavior of the material in the induction coil by writing

$$\mathbf{B} = \mu_0(\mathbf{H} + \mathbf{M}) \qquad \text{weber/m}^2 \tag{8.3}$$

Comparing these expressions, we see that the ratio is

$$\frac{\mu}{\mu_0} = 1 + \frac{\mathbf{M}}{\mathbf{H}} = 1 + \chi \tag{8.4}$$

The quantity **M** is the induction magnetization, or more precisely the magnetic moment per unit volume. The quantity χ is the magnetic susceptibility per unit volume: it is generally a complex number. The units of **M** are the same units as **H**, amperes per meter. We may write

$$\mathbf{M} = \frac{\beta}{V} \tag{8.5}$$

where the magnetic moment β is a current times an area and V is a volume.

Electronic Magnetic Moment—Orbital Motion

We may get some impression of the magnitudes by considering an electron orbiting about the nucleus of an atom whose charge is Ze. Then, balancing the centrifugal force against the coulomb force, we obtain

$$m\omega^2 r = \frac{Ze^2}{\epsilon_0 r^2} \tag{8.6}$$

Solving,

$$\omega = \frac{e}{r}\left(\frac{Z}{\epsilon_0 m r}\right)^{\frac{1}{2}} \approx 10^{16} \text{ rad/sec} \tag{8.7}$$

The magnetic moment is

$$\beta = IA = e\nu\pi r^2 \tag{8.8}$$

For the orbiting electron this expression becomes

$$\beta = \frac{e^2 r}{2}\left(\frac{Z}{\epsilon_0 m r}\right)^{\frac{1}{2}} \approx 10^{-23} \text{ amp-m}^2 \tag{8.9}$$

The evidence for the magnetic moment of the atom was inferred from the early classic work of P. Curie, but it was the famous Stern-Gerlach experiment which demonstrated the intrinsic magnetic moment of atoms. A beam of silver atoms from a furnace was caused to deflect by an inhomogeneous magnetic field and the magnetic moment computed from the geometry of the apparatus, the field gradient, the observed deflection, and the temperature of the furnace. The magnitude of the atomic magnetic moment was of the order to be expected for the orbiting electron, and the space quantization of the beam led to an understanding of discrete magnetic states.

Larmor Precession

The ratio of the orbital magnetic moment to the orbital angular momentum is simply

$$\frac{\vec{\beta}}{\vec{p}} = \frac{\pi r^2 e\nu}{mr^2 2\pi\nu} = \frac{e}{2m} \tag{8.10}$$

If one has an orbiting electron in a steady magnetic field, then one has a torque acting between the magnetic moment and the field, which will cause a slow precession of the angular momentum vector about the field. The situation is analogous to a spinning top which precesses about the gravitational field. The situation is demonstrated in Fig. 8.1, and the torque components are identified with the time rate of change of the angular momentum components.

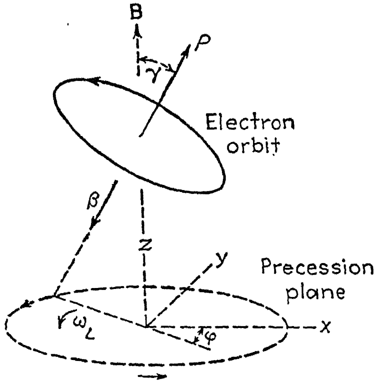

FIG. 8.1. Electron orbit showing precession in magnetic field.

The angular momentum vector p makes an angle γ with the magnetic field **B**, which is directed along the z axis. The magnetic moment β precesses about the z axis with an angular velocity in the precession plane $\omega_L = d\phi/dt$. The motion results from the torque between the magnetic field **B** and the magnetic moment

$$\vec{T} = \beta \times \mathbf{B} = \beta \cdot \mathbf{B} \sin \gamma \tag{8.11}$$

The components of the torque are

$$T_x = -\beta\mathbf{B} \sin \gamma \cos \phi \tag{8.12a}$$
$$T_y = \beta\mathbf{B} \sin \gamma \sin \phi \tag{8.12b}$$
$$T_z = 0 \tag{8.12c}$$

The components of the angular momentum are

$$p_x = p \sin \gamma \cos \phi \tag{8.13a}$$
$$p_y = p \sin \gamma \sin \phi \tag{8.13b}$$
$$p_z = p \cos \gamma \tag{8.13c}$$

The torque cannot change the magnitude of the angular momentum, but it can change its direction (the two vectors are orthogonal). Setting the time rate of change of the angular momentum equal to the torque,

$$T_x = \frac{dp_x}{dt}, \qquad T_y = \frac{dp_y}{dt}, \qquad T_z = \frac{dp_z}{dt} \tag{8.14}$$

we obtain the set of equations

$$-\beta\mathbf{B} \sin \gamma \sin \phi = -p \sin \gamma \sin \phi \cdot \omega_L \tag{8.15a}$$
$$\beta\mathbf{B} \sin \gamma \cos \phi = p \sin \gamma \cos \phi \cdot \omega_L \tag{8.15b}$$
$$p \cos \gamma = \text{constant} \tag{8.15c}$$

These equations require that

$$\omega_L = \frac{\beta \mathbf{B}}{p} = \frac{e}{2m}\mathbf{B} \tag{8.16}$$

The Larmor frequency is given by

$$\begin{aligned} \nu_L &= \frac{e}{4\pi m}\mathbf{B} \qquad \text{for orbital motion} \\ &= 1.41 \times 10^{10}\mathbf{B} \qquad \text{cycles/sec (in mks units)} \\ &= 1.41 \times 10^{6}\mathbf{B} \qquad \text{cycles/sec (in Gaussian units)} \end{aligned} \tag{8.17}$$

Diamagnetism

As a result of the Larmor precession, each atom gets an angular momentum pointing in the field direction, and this does not depend upon the direction of rotation of the orbiting electron. The induced magnetic moment is therefore always opposite to the applied field and is called diamagnetism. The size of the induced moment is

$$\beta_i = e\nu_L\pi(x_i^2 + y_i^2) \tag{8.18}$$

The total diamagnetism induced is

$$\mathbf{M} = -\frac{ne^2\mathbf{B}}{6m}\sum r_i^2 \tag{8.19}$$

where the area of the precession plane is computed from the orbital radius r_i of the ith electron and where the sum is over all the electrons of the atom. There are n atoms per unit volume. Such induced diamagnetism is generally very small.

Electron Spin Magnetic Moment

The classical concepts are useful but must be modified with quantum mechanics. As is well known, the angular momentum is quantized as we write

$$p = l\frac{h}{2\pi} \tag{8.20}$$

$$\beta = \frac{e}{2m}p = l\left(\frac{eh}{4\pi m}\right) = l\beta_0 \tag{8.21}$$

where l is an integer, h is Planck's constant, and β_0 (the Bohr magneton) $= 9.12 \times 10^{-24}$ mks units $= 9.12 \times 10^{-21}$ ergs/gauss.

Atomic spectra and the atomic beam experiments gave ample evidence that the term *electron orbit* could only be thought of as a statistical distribution of the electron's possible position and velocity corresponding to one of its possible energy states. Even more important is the concept of electron spin which comes from experiment and from the quantum theory.

The spin angular momentum has magnitude $\frac{1}{2}$ in units of $h/2\pi$. The spin axis sets itself parallel or antiparallel to the orbital momentum in much the same way as a gyroscopic compass. The total electron angular momentum quantum number is

$$j = l \pm \tfrac{1}{2} \tag{8.22}$$

The magnetic moment of the electron spin is *not* $\frac{1}{2}$ in units of the Bohr magneton but is exactly 1. Thus for spin

$$\beta = s\,\frac{eh}{2\pi m} = 2s\beta_0 \tag{8.23}$$

where the total atomic spin quantum number s has half-integer values. The Larmor precession frequency for electron spin moments is twice the frequency for orbital motion.

Spin-orbit Coupling

We shall need one more atomic quantum number called $\mathbf{M}_j$. If we provide the atom with an axis of reference by the application of an external magnetic field, then $\mathbf{M}_j$ is the component of the total atomic momentum J, in units of $h/2\pi$, in the field direction. In low-temperature magnetism we shall not be dealing with atoms having excited electronic states, and so the principal quantum number n will always refer to the ground state. The vector model most applicable to magnetism discussed here is shown in Fig. 8.2. Total angular momentum J is made up of components from orbit l and from spin s. The projection along the applied field axis is $\mathbf{M}_j$. All vectors are in units of $h/2\pi$. Values of $\mathbf{M}_j$ run between $+J$ and $-J$, and there are $(2J + 1)$ possible values. Thus the electronic state is $(2J + 1)$-fold degenerate in the absence of a magnetic field. Turning on a field $\mathbf{B}$ produces $(2J + 1)$ states. The energy value of each state is described by $\mathbf{M}_j g\beta_0\mathbf{B}$, where the quantum number $\mathbf{M}_j$ takes on all allowed values between $+J$ and $-J$. In Fig. 8.3 the total magnetic moment $\beta = g\sqrt{J(J+1)}\,\beta_0$ is shown. The quantity g is the trigonometric factor in forming the vector sum. The quantity $g\sqrt{J(J+1)}$ is the number of Bohr magnetons. The magnetic moment has a component along the field direction given by $\mathbf{M}_j g\beta_0$ where again

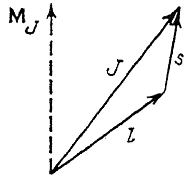

FIG. 8.2. Vector model of spin-orbit combination.

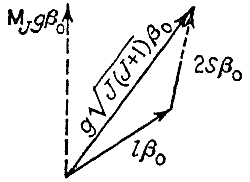

FIG. 8.3. Magnetic moment vector combination.

$\mathbf{M}_j$ runs from $-J$ to $+J$. Table 8.1 gives the number of Bohr magnetons for magnetic ions of the iron group and for the rare-earth group. In this table of a few of the ions showing paramagnetism, the rare-earth group shows good agreement between theory and experiment. The iron group shows that the magnetic moment is caused by the electron spin and that the orbital magnetism is canceled. By this we mean that the orbits are locked into the crystalline electric field and are not affected by any magnetic field which we can produce. The value of $g = 2$ will require closer examination.

In these last paragraphs we have reviewed the fundamentals of electronic motion within the atom. Orbital and spin motion of each electron produces a magnetic moment, and the vector sum of these motions summed over all electrons may produce a net magnetic moment for the atom or ion. We shall now consider an assembly of atoms having a net magnetic moment.

TABLE 8.1. NUMBER OF BOHR MAGNETONS

Ion	Theory $g\sqrt{J(J+1)}$	Theory $2\sqrt{S(S+1)}$	Experimental
Ce . . .	2.54		2.4
Pr . . .	3.58		3.6
Nd . . .	3.62		3.6
Gd . . .	7.94		7.9
Ti . . .	1.55	1.73	1.75
Cr . . .	0.77	3.87	3.8
Mn . . . , Cr . .	0	4.90	4.9
Fe . . . , Mn . .	5.92	5.92	5.9
Fe . .	6.70	4.90	5.5
Co . .	6.54	3.87	4.4–5.3
Ni . .	5.59	2.83	3.2
Cu . .	3.55	1.73	1.9

Statistical Mechanics of Paramagnetism

Consider now an assembly of N atoms in a magnetic field. The well-known distribution function giving the number of atoms in the ith energy state is

$$f(i) = \frac{Ne^{-u(i)/kT}}{\Sigma e^{-u(i)/kT}} \tag{8.24}$$

The presence of a magnetic field requires that the energy be characterized by the quantum number $\mathbf{M}_j$ and is

$$u(\mathbf{M}_j) = -\mathbf{M}_j g \beta_0 \mathbf{B} \tag{8.25}$$

The probability function can be used to compute the average projection $\bar{\beta}$ of the magnetic moment along the field:

$$\bar{\beta} = \frac{\sum\limits_{\mathrm{M}_j=-J}^{\mathrm{M}_j=J} \mathrm{M}_j g\beta_0 e^{M_j g\beta_0 B/kT}}{\sum\limits_{\mathrm{M}_j=-J}^{\mathrm{M}_j=J} e^{M_j g\beta_0 B/kT}} \tag{8.26}$$

If the energy of separation of the lowest and first excited electronic levels in the ion is large compared to both the energy of interaction with the magnetic field and to kT, we may compute the value of $\bar{\beta}$. Let us first take an even simpler situation in which $\mathrm{M}_j g\beta_0 \mathrm{B}/kT$ has small values. Then $\exp(x) = 1 + x + x^2/2 + \cdots$ gives just $(2\mathrm{J} + 1) \cdot 1$ for the denominator as we sum over $(2\mathrm{J} + 1)$ terms and consider terms in x, x^2, etc., too small to count.

The term arising from the unity of the expansion in the numerator is zero, since $\Sigma \mathrm{M}_j$ extended over both positive and negative M_j values from J to $-J$ is zero. The next term does not vanish and is linear in T^{-1}. The numerator is then

$$\sum_{\mathrm{M}_j=-J}^{\mathrm{M}_j=J} \mathrm{M}_j g\beta_0 \frac{\mathrm{M}_j g\beta_0 \mathrm{B}}{kT} = \mathrm{B}\frac{g^2\beta_0^2}{kT} \sum_{\mathrm{M}_j=-J}^{\mathrm{M}_j=J} \mathrm{M}_j^2$$

$$= \mathrm{B}\frac{g^2\beta_0^2}{kT} \frac{(J+1)J(2J+1)}{3} \tag{8.27}$$

Thus we obtain for the average magnetic moment

$$\bar{\beta} = \frac{1}{3}\frac{g^2\beta_0^2 J(J+1)}{kT}\mathrm{B} \tag{8.28}$$

This last expression is a form of Curie's law. The susceptibility is

$$\chi = \frac{N\bar{\beta}}{\mathrm{H}} = \frac{C}{T} \tag{8.29}$$

Low Temperatures and High Magnetic Fields—Saturation

The Curie law for a number of paramagnetic salts is valid at moderate temperatures and magnetic fields. From the experimental values of the susceptibility and their corresponding temperatures we may evaluate the Curie constant and compute the number of Bohr magnetons. At very low temperatures and in large magnetic fields the method of calculation is no longer valid, and we must return to the statistical expression for the average projection $\bar{\beta}$ of the magnetic moment along the field and seek a more complete expression. Writing the expression

$$X = e^{g\beta_0 B/kT} \tag{8.30}$$

the statistical expression is

$$\bar{\beta} = \frac{g\beta_0 \sum\limits_{\mathrm{M}_j=-J}^{\mathrm{M}_j=J} \mathrm{M}_j X^{M_j}}{\sum\limits_{\mathrm{M}_j=-J}^{\mathrm{M}_j=J} X^{M_j}} = g\beta_0 X \frac{d}{dX}\left(\ln \sum_{\mathrm{M}_j=-J}^{\mathrm{M}_j=J} X^{M_j}\right) \tag{8.31}$$

Brillouin Function. The last equation can be shown to be the so-called "Brillouin[1] function"

$$\bar{\beta} = g\beta_0\left[\left(J+\frac{1}{2}\right)\coth\frac{(J+\frac{1}{2})g\beta_0\mathbf{B}}{kT} - \frac{1}{2}\coth\frac{g\beta_0\mathbf{B}}{2kT}\right] \tag{8.32}$$

For paramagnetism of the spin only, *i.e.*, of salts of the type listed in Table 8.1, we have the expression

$$\mathbf{M} = N\bar{\beta} = N\beta_0\left[(2S+1)\coth\frac{(2S+1)\beta_0\mathbf{B}}{kT} - \coth\frac{\beta_0\mathbf{B}}{kT}\right] \tag{8.33}$$

At low temperatures and high magnetic fields one gets the phenomena of saturation, and **M** is not linear in **H**. An example of the saturation has been worked out experimentally by Gorter, de Haas, and van den Handel[2] on potassium chromium alum. Their results have been extended by Henry,[3] whose results are shown in Fig. 8.4. The experiments were done on a solid sphere of the salt, and the solid line in the figure represents the above theoretical function with a value $S = \frac{3}{2}$.

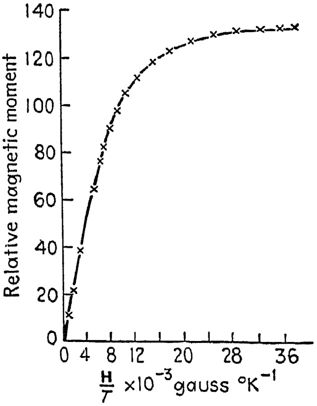

FIG. 8.4. Relative magnetic moment vs. **H**/T for a solid sphere of potassium chromium alum. The Brillouin function (shown by curve) is matched to the experimental moment at the largest value of **H**/T.

Measurement of Magnetic Susceptibility and Moments

Balance Method. The most direct method of measuring the magnetic susceptibility of a paramagnetic or diamagnetic body is to determine the force exerted on a test specimen by an inhomogeneous magnetic field. This experiment is most easily done by a direct weighing method, using a laboratory balance of sufficient sensitivity, *i.e.*, 2 × 10^{-4} gram detection.

[1] L. Brillouin, *J. phys. radium*, **8**, 74, 1927; R. H. Fowler and E. A. Guggenheim, "Statistical Thermodynamics," London, Cambridge, 1939.

[2] C. J. Gorter, W. J. de Haas, and J. van den Handel, *Proc. Koninkl. Nederland. Akad. Wetenschap.*, **36**, 158, 1933.

[3] W. Henry, *Phys. Rev.*, **85**, 487, 1952.

In Fig. 8.5 we show a sphere of material whose permeability is μ, volume V, placed in a field which is slightly inhomogeneous and having a value $\mathbf{B}$ over the small volume of the specimen. The energy density is changed in this region of space by the insertion of the specimen and may be written

$$\Delta U = \frac{V(\mu - \mu_0)\mathbf{B}^2}{2\mu_0^2} = \frac{V}{2}(\mu - \mu_0)\mathbf{H}^2 \tag{8.34}$$

If we consider a small displacement of the body to a point where the magnetic field is slightly different and set this change of energy density equal to the work done by a mechanical force F moving through the displacement dx, we may write the following in terms of susceptibility per unit volume:

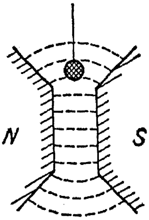

FIG. 8.5. Paramagnetic salt in spherical form in an inhomogeneous field.

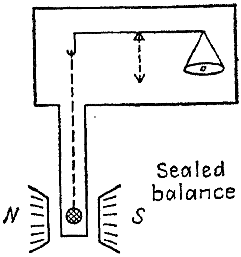

FIG. 8.6. Balance method for magnetic measurements.

$$F = \frac{V}{2}\chi\mu_0 \operatorname{grad} \mathbf{H}^2 \qquad \text{newtons} \tag{8.35}$$

The measurement of susceptibility by this method has been used at liquid helium temperatures by Gorter, de Haas, and van den Handel.[1] The specimen hangs freely in a glass tube filled with helium gas, and the liquid helium or other bath temperature liquid is contained in a Dewar flask. The name of L. G. Gouy[2] is associated with this technique when a cylindrical length L of the specimen is employed. A force acts with magnitude:

$$F = \frac{1}{2}\frac{\chi m}{L}(\mathbf{H}_1^2 - \mathbf{H}_2^2) \qquad \text{dynes} \tag{8.36}$$

In this last equation the mass in grams of the substance is m, the susceptibility per gram is χ, $\mathbf{H}_1$ is the magnetic field at the end of the specimen near the pole pieces, and $\mathbf{H}_2$ the field at the other end of the specimen in gaussian units.

The Gouy method is very straightforward, and calibration can be done against salts whose value of χ is already well established. For example, the salt manganous ammonium sulfate has a susceptibility per mole such that

---

[1] C. J. Gorter, W. J. de Haas, and J. van den Handel, *Proc. Koninkl. Nederland. Akad. Wetenschap.*, **36**, 158, 1933.

[2] L. G. Gouy, *Compt. rend.*, **109**, 935, 1889.

$$\chi_m T = 4.37$$

The special precautions to be taken when the balance is used to measure the susceptibility are simple. Care should be taken to avoid the condensation of water vapor or of any other gas on the specimen when quite low temperatures are used. For this reason the entire balance may be enclosed in a gastight box with a tube leading down to the magnetic field (Fig. 8.6).

Induction Coils for Magnetic Susceptibility at Low Temperatures. The principle used by a great many low-temperature laboratories in determining paramagnetic susceptibilities is that of the ballistic throw given to a galvanometer by the flux change in a secondary coil, as shown in Fig. 8.7. The two secondaries are wound on the primary with equal numbers of turns but of opposite direction. Usually some extra turns are put on the ends of the primary to ensure a uniform field inside around the specimen. As an example, the glass tube on which the primary is wound may be 2.5 cm in diameter and 40 cm long. One may put about 2,500 turns of No. 36 copper wire as a primary. Over a segment 3.81 cm long a secondary having 1,900 turns of No. 38 wire forms one of the secondary coils. The ballistic deflections are proportional to the susceptibility of the specimen and to the current sent through the primary coil. Many laboratories use a 60-cycle current through the primary coil and continuously obtain an a-c output signal. The entire coil assembly and specimens are immersed in liquid helium. The coils produce emf's which just balance in magnitude and phase when the specimen is removed completely.

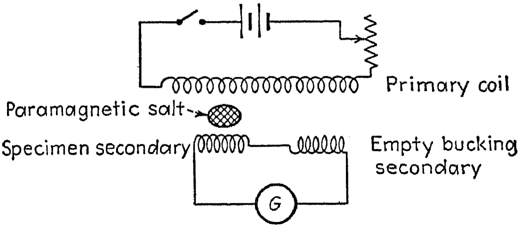

FIG. 8.7. Induction coil method for magnetic measurements.

Giauque, Fritz, and Lyon[1] published details of the coil assembly used to measure susceptibilities in the presence of large steady magnetic fields. The coil forms were of bakelite-impregnated molded paper (Dilecto) because its average coefficient of expansion over the temperatures 4 to 290°K is the same as that of the copper wire wound on it.

---

[1] W. F. Giauque, J. Fritz, and D. Lyon, *J. Am. Chem. Soc.*, **71**, 1657, 1949.

Demagnetization Factor. Demagnetization corrections have been worked out in charts and in formulas by Osborn[1] for an ellipsoid of any shape. Also Stoner[2] has computed tables for the ellipsoid. These are useful quantities for the experimental research worker in the field of low-temperature magnetism because the correction factor becomes important. The field $\mathbf{B}_0$ outside the salt at great distance is considered unaltered by the magnetization $\mathbf{M}$ of the salt. However the field in the salt is not $\mathbf{B}_0$ but is altered by the magnetization per unit volume. For an ellipsoid

$$\mathbf{B} = \mathbf{B}_0 - \mu_0\alpha\mathbf{M}$$

where α is the demagnetization coefficient. For a sphere $\alpha = 4\pi/3$ and for a very long cylindrical specimen with the field along the length direction, the value of $\alpha = 0$. For a disk the value of $\alpha = 4\pi$, and this is important in resonance cavity studies. The general ellipsoid value of α depends upon the field direction as well as upon the shape. The demagnetization factor is uncertain where the specimen is a loosely packed powder of the substance, and for this reason most experimenters use either a true solid specimen or very highly compressed powders (Bleaney and Hull[3]). If $\mathbf{M}$ is not large under experimental conditions, we make only a small error in neglecting the demagnetization factor.

Some Typical Experimental Results

Ideal Salts—Curie Law. For the next few paragraphs we shall be discussing paramagnetic salts whose magnetic moment per unit volume is a linear function of $\mathbf{H}$ for the temperatures and fields used. We shall be speaking of low-frequency measurements, and we shall be referring to the so-called "initial susceptibility":

$$\chi = \left(\frac{d\mathbf{M}}{d\mathbf{H}}\right)_{H=0}$$

The plot of $1/\chi$ against T exhibits a linear relationship and establishes the Weiss modification of Curie's law:

$$\chi(T - \theta) = \text{constant}$$

The value of θ is quite small for most paramagnetic salts whose magnetic ions are well separated, and it vanishes toward 0°K the more ideal a salt becomes. The quantity θ reflects the perturbing influence of the crystalline electric field and other interaction forces. The ideal magnetic salts are those whose magnetic ions are diluted by many molecules of water within the crystal, and they show deviations from the Curie-Weiss law at temperatures of 1°K and below. We shall begin by discussing this type of salt.

---

[1] J. A. Osborn, *Phys. Rev.*, **67**, 351, 1945.

[2] E. C. Stoner, *Phil. Mag.*, **36**, 803, 1945.

[3] B. Bleaney and R. Hull, *Proc. Roy. Soc.* (*London*), **178**, 86, 1941.

Ferrous ammonium sulfate has 24 molecules of water and may be considered as an example of a paramagnetic salt showing ideal behavior above 1°K. Kamerlingh Onnes and Oosterhuis obtained the values shown in Table 8.2 for this salt. Perrier and Onnes[1] studied the magnetic susceptibility of ferrous sulfate heptahydrate down to 14°K. The effect of concentrating the ferrous ion slightly in changing to only seven waters of crystallization is to cause deviations from Curie's law below about 60°K. Between 20 and 14°K the susceptibility is strikingly different than the Curie law would predict. Recently Lyon and Giauque have examined ferrous sulfate heptahydrate as to its initial magnetic susceptibility between 0.9 and 20°K (Fig. 8.8 and Table 8.3). These last

TABLE 8.2. PARAMAGNETISM OF FERROUS AMMONIUM SULFATE, $Fe_2(SO_4)_3(NH_4)_2SO_4 \cdot 24H_2O$[a]

T, °K	$\chi \cdot 10^6$	$\chi T \cdot 10^5$
290.0	30.4	882.0
169.6	51.8	879.0
77.3	114.7	887.0
20.4	432.0	881.0
14.7	598.0	879.0

[a] H. Kamerlingh Onnes and E. Oosterhuis, *Commun. Kamerlingh Onnes Lab. Univ. Leiden*, **129b**, 1914.

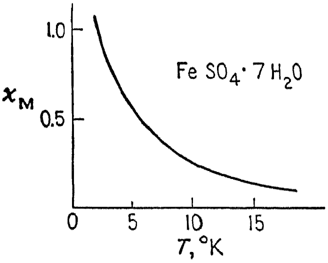

FIG. 8.8. Magnetic susceptibility per mole vs. temperature for $FeSO_4 \cdot 7H_2O$.

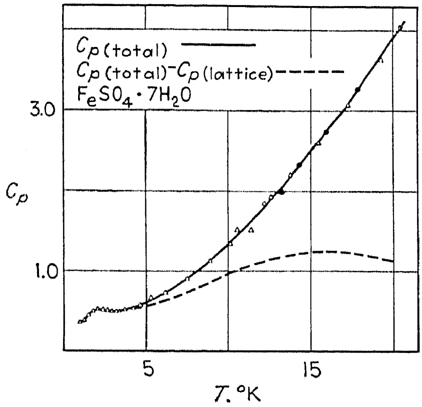

FIG. 8.9. Heat capacity vs. temperature for $FeSO_4 \cdot 7H_2O$. (*Lyon and Giauque, J. Am. Chem. Soc.*, **71**, 1647, 1949.)

---

[1] H. Kamerlingh Onnes and A. Perrier, *Commun. Kamerlingh Onnes Lab. Univ. Leiden*, **122a**, 1911.

TABLE 8.3. PARAMAGNETISM OF FERROUS SULFATE HEPTAHYDRATE[a]

T	χ_M	$\chi_M \cdot T$
0.84	1.504	1.26
1.160	1.285	1.49
2.182	0.890	1.94
3.303	0.665	2.19
4.204	0.552	2.32
10.77	0.291	3.14
20.31	0.156	3.16

[a] W. F. Giauque and D. Lyon, *J. Am. Chem. Soc.*, **71**, 1647, 1949.

authors have measured the heat capacity of this salt, $FeSO_4 \cdot 7H_2O$, and the data are plotted in Fig. 8.9. There is a decided hump in the measured values between 1 and 4°K. Further, the heat capacity remains larger than one would expect from pure lattice vibrations on up above 20°K. Similar studies on $CoSO_4 \cdot 7H_2O$ have been made by Fritz and Giauque.[1]

Antiferromagnetism. Paramagnetic salts whose magnetic ions are close together, such as the anhydrous salts, show marked deviation from Curie's law at much higher temperatures. This deviation may be antiferromagnetism, an effect demonstrated by Bizette, Squire, and Tsai[2] and by Squire[3] in the salts MnO, MnS, MnSe, and MnTe. At a temperature, characteristic for each salt, the susceptibility breaks away from the Weiss-Curie law and decreases with lowering of temperature. Figure 8.10 shows the results on MnO and MnS. The transition temperatures are 247°K for MnSe and 307°K for MnTe. The temperature of the transition becomes higher the greater the mass of the combining atom. Below the transition temperature, which is now called the Néel temperature, the susceptibility is field-dependent. There is a large hump in the heat capacity curve according to Kelley.[4] B. Ruhemann[5] found by X-ray studies a rapid expansion at the transition on warming. C. G. Shull and J. S. Smart[6] have examined antiferromagnetism by neutron diffraction. The neutron diffraction pattern on MnO at 80°K,

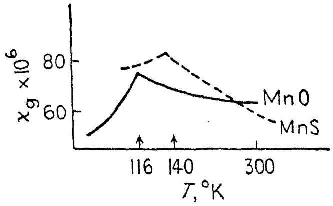

FIG. 8.10. Antiferromagnetism in manganous salts. Magnetic susceptibility per gram vs. temperature for MnO and MnS.

---

[1] W. F. Giauque and J. Fritz, *J. Am. Chem. Soc.*, **71**, 2168, 1949.
[2] H. Bizette, C. Squire, and B. Tsai, *Compt. rend.*, **207**, 449, 1938.
[3] C. Squire, *Phys. Rev.*, **56**, 922, 1939.
[4] K. Kelley, *J. Am. Chem. Soc.*, **61**, 203, 1939.
[5] B. Ruhemann, *Physik. Z. Sowjetunion*, **7**, 590, 1935.
[6] C. G. Shull and J. S. Smart, *Phys. Rev.*, **76**, 1256, 1949.

i.e., below the transition, shows the appearance of a magnetic unit cell twice as large as the chemical unit cell (Fig. 8.11). By this we mean that the Mn ions have their magnetic moments antiparallel in such a way that a beam of monochromatic neutrons is differently scattered by each type of ion.

We should mention that Klemm and Haraldsen[1] studied some of these types of salts without clearly recognizing their antiferromagnetic nature. Many salts are not recognized as antiferromagnetic. The theory has been discussed by L. Néel[2] and by J. H. Van Vleck,[3] who assumed special conditions would permit a negative exchange integral to orient the spins antiparallel. We shall not develop the theory here. Instead, we return now to studies on paramagnetic salts which obey the Curie law and which are used for cooling.

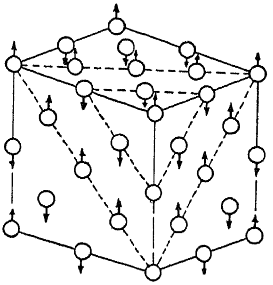

FIG. 8.11. Magnetic moment orientation in unit cell of antiferromagnetic structure existing in MnO below its Curie temperature of 120°K. The magnetic unit cell has twice the linear dimensions of the chemical unit cell. Only Mn ions are shown in the diagram.

Magnetic Cooling

Thermodynamics and Statistical Mechanics of the Method. W. F. Giauque[4] and, independently, P. Debye[5] suggested in 1926 that by use of a large magnetic field one could cool certain paramagnetic salts below the temperature available with liquid helium. Giauque and MacDougall[6] at Berkeley, Calif., were the first to overcome the experimental difficulties and realize temperatures well below 1°K. Shortly thereafter, similar results were reported at Leiden by de Haas and Wiersma[7] and at Oxford by Kurti and Simon.[8] Temperatures as low as 0.0004°K are now reliably obtained according to De Klerk, Steenland, and Gorter.[9] Research using the method of cooling is being conducted in many laboratories, so that properties of matter may be studied in the new region of very low temperatures. Let us examine the experimental and theoretical problem of cooling below 1°K.

---

[1] W. Klemm and H. Haraldsen, *Z. anorg. Chem.*, **220**, 183, 1934.

[2] L. Néel, *Ann. phys.*, **17**, 64, 1933.

[3] J. H. Van Vleck, *J. Chem. Phys.*, **9**, 85, 1941.

[4] W. F. Giauque, *Ind. Eng. Chem.*, **28**, 743, 1936; *J. Am. Chem. Soc.*, **49**, 1864, 1926.

[5] P. Debye, *Ann. Physik*, **81**, 1154, 1936; *ibid.*, **32**, 85, 1938.

[6] W. F. Giauque and D. P. MacDougall, *Phys. Rev.*, **43**, 768, 1933.

[7] W. J. de Haas and E. C. Wiersma, *Compt. rend.*, **196**, 1975, 1933.

[8] N. Kurti and F. Simon, *Proc. Roy. Soc. (London)*, **149**, 152, 1935.

[9] D. De Klerk, M. Steenland, and C. J. Gorter, *Physica*, **15**, 649, 1949; *ibid.*, **15**, 711, 1949.

If we are to produce temperatures below those which are available with vigorously pumped liquid helium, we must look for a system which still contains disorder at 1°K and on which we may operate in such a way as to bring about order. Such a system is to be found in those paramagnetic salts whose internal magnetic dipoles show a random space orientation even at 1°K. This arbitrariness of orientation on the part of the dipoles (or more properly the electron spin moment) constitutes a degree of disorder, and it may be brought into a degree of order by means of a magnetic field. Thus a magnetic field is the parameter which brings the entropy to a lower value, and during this process heat is given off from the salt to the surrounding liquid helium bath. The amount of heat given off can be readily measured from the extra amount of helium which is vaporized in order to keep the temperature at 1°K. Thus from the relation $\Delta S = \Delta Q/T$ the drop in entropy for the applied field can be experimentally determined.

After the heat of magnetization has been removed, the salt is then suspended in a vacuum chamber whose outer walls are still in thermal contact with the liquid helium bath. This maneuver allows us to perform an adiabatic demagnetization when the external field is switched off. It is then discovered that the temperature has dropped. How did this happen, and how low does the temperature drop?

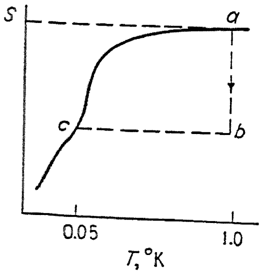

FIG. 8.12. Entropy vs. temperature diagram for magnetic cooling process.

In Fig. 8.12 we show on the entropy-temperature diagram the value at 1°K for the entropy of a salt which arises from the disorder in the dipoles. The contribution to the entropy arising from the lattice vibrational energy is negligible at these temperatures. We may now make use of the third law of thermodynamics and say that at the absolute zero of temperature the entropy of the system is zero. Thus on lowering the temperature, we may expect that the salt will of itself lower the entropy, and so we may draw some seemingly arbitrary connecting curve, as in Fig. 8.12. This comes about in part from mutual interaction forces between the magnetic moments and has an analogy, as we have seen, in gases whose interaction forces become important and cause an entropy drop when they are cooled to the point of actual liquefaction. Thus we can understand that the magnitude of the interaction forces on and between the electron spin moments is the determining factor on just how low the temperature may drop when the field is removed. The process is shown in Fig. 8.12 for the magnetization *a* to the point *b* during which heat is evolved and the entropy drops. The path *b* to the point *c* is a constant-entropy process which represents a change of parameters from the applied field to the lower temperatures. We have just seen such a change of parameters with the Claude expansion engine for the cooling of a gas (Chap. 1). In the expansion engine the energy was removed by the piston rod, and in the magnetic case before us the magnetic energy density is dissipated by eddy currents and by ohmic heating in the external magnet circuit. We must emphasize again that the process of demagnetization is done at constant entropy and that therefore the degree of order which was achieved among the elementary dipoles when the magnet was on is now nearly all preserved by the salt itself. Therefore the dipoles either stay aligned as they were or become mutually antiparallel which is equivalent entropywise. The entropy in the lattice vibrations is so small at 1°K that the further cooling off of the lattice vibrations represents an almost indetectable influence on the order of the dipoles.

We have therefore an understanding of magnetic cooling from the thermodynamic viewpoint. We should seek more detailed information from statistical mechanics, and for this reason we have to return to the ideas of magnetism of matter as it is related to our problem. As we have shown, at temperatures of 1°K there are a group of paramagnetic salts, such as Fe-alum and the hydrate of gadolinium sulfate, whose magnetic ions are sufficiently far apart that Curie's law is valid. At these temperatures and in strong magnetic fields the magnetization shows experimentally the saturation effects predicted by the Brillouin function. The change in entropy brought about by the applied field at constant temperature is given by

$$\Delta S = \int_0^{\mathrm{B}} \left(\frac{\partial \mathrm{M}}{\partial T}\right)_B d\mathrm{B} \tag{8.37}$$

The value of the magnetization $\mathbf{M} = N\bar{\beta}$ is obtained from the Brillouin function and from this the slope required with respect to temperature for the above equation. We may restate with statistical mechanics the dependence of the entropy upon the magnetic field at a constant temperature (1°K) for an assembly of free dipoles. The Helmholtz potential is

$$A = -kT \ln \sum_i g_i e^{-E_i/kT} \tag{8.38}$$

The energy levels for the salt Fe-alum are

$$E_i = \pm 5\beta\mathrm{B}, \qquad \pm 3\beta\mathrm{B}, \qquad \pm\beta\mathrm{B} \tag{8.39}$$

The Helmholtz potential for N atoms is

$$A = -NkT \ln 2(\cosh 5x + \cosh 3x + \cosh x) \tag{8.40}$$

where $x = \beta\mathrm{B}/kT$. Now since

$$S = -\left(\frac{\partial A}{\partial T}\right)_B \tag{8.41}$$

we therefore obtain by differentiation

$$S = Nk \ln \left(\frac{\sinh 6x}{\sinh x} \right) - Nkx(6 \coth 6x - \coth x) \tag{8.42}$$

As we have indicated earlier in our discussion, this entropy change may be directly measured from $\Delta S = \Delta Q/T$, where the ΔQ is taken from the heat of vaporization and the quantity of the extra helium boiled away by the magnetization of the salt. The possibility of understanding the interaction forces which influence the entropy at low temperatures and in the absence of the magnetic field is now before us. The degeneracy of the electronic energy state of Fe-alum is such as to give a value of $R \ln 6$ to the entropy, and owing to the existence of the crystalline electric field, there is the possibility that, at sufficiently low temperatures, the degeneracy may appear to be removed. The electric field splits the energy states not just at low temperatures but at all temperatures. The splitting is such a small amount that only at these low temperatures does the system occupy the lower states in great density. Even so, there is left for the lowest state a twofold degeneracy corresponding to the parallel or antiparallel orientation of the dipoles to a possible external magnetic field. Thus the entropy is lowered to $R \ln 2$ when the kT energy is comparable to the energy splitting by the electric field. The effect of the magnetic coupling between the dipoles is to lower the entropy even further. This means that the energy states are split by internal magnetic fields, and again we may get a greater density in the lowest state with quite low temperatures. Before this action sets in, one may consider the salt as composed of N nearly independent paramagnetic ions. After the lowest state begins to contain the entire system, the crystal behaves like a giant molecule which has a single lowest energy state.

Experimental Methods in Magnetic Cooling. The experimental techniques for cooling below 1°K and for measuring the temperatures are best illustrated by means of Fig. 8.13. The salt, such as $Gd_2(SO_4)\cdot 8H_2O$ or $FeNH_4(SO_4)\cdot 12H_2O$, is pressed into a sphere or ellipsoid. Often the specimen is then coated with a thin layer of stopcock grease to prevent oxidation or dehydration. It is then hung on fine threads of silk in the exchange gas chamber so that its position is centered with respect to one of the secondary coils used to measure the magnetic susceptibility. We have discussed this measuring technique in an earlier part of this chapter. The entire calorimeter is placed in a liquid helium bath which is in turn surrounded by a liquid nitrogen bath. The liquid helium bath is vigorously pumped to about 1°K, and during the pumping down from the normal boiling point the salt is cooled via the exchange gas (helium whose pressure is about 0.1 mm Hg). During the pump down the vapor pressure is from time to time steadied to a constant value by throttling the pump so that a constant bath temperature is obtained. This is done for at least five different temperature values, such as 4.201, 2.086, 1.476, 1.206, and 1.037°K. At these known temperatures the magnetic susceptibility (proportional to the ballistic galvanometer deflection) is carefully measured so that the Curie-Weiss law is determined. For these ideal salts the Weiss field is just the demagnetization factor due to the specimen shape. A plot of the reciprocal of the galvanometer deflection per unit of current in the primary coil against $(T - \theta)$ determines a straight line whose extrapolation into the temperature region of 0.001°K is boldly carried out. The galvanometer deflections in this new low-temperature range are kept on the measuring scale by reducing the current in the primary coils by factors of 10 and 100.

The temperature thus determined from the galvanometer deflection is called T^*, and this is identical to T only for temperatures at and above 1°K. For temperatures which are below 1°K one knows that T^* must not be taken as the absolute temperature, since the interaction forces on the magnetic dipoles become important in just this new region and invalidate the Curie-Weiss law.

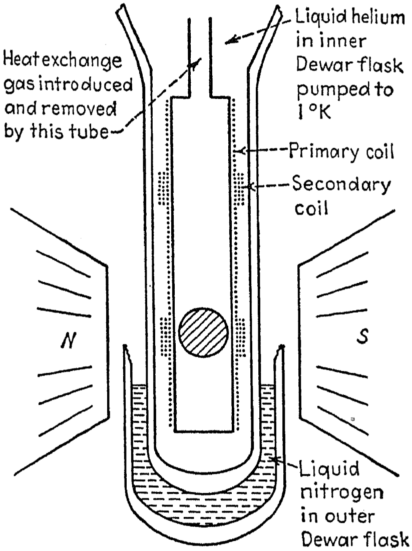
Heat exchange gas introduced and removed by this tube
Liquid helium in inner Dewar flask pumped to 1 °K
Primary coil
Secondary coil
N
S
Liquid nitrogen in outer Dewar flask

FIG. 8.13. Schematic drawing of magnetic cooling apparatus.

At the lowest temperature obtained with the helium bath, the exchange gas pressure is checked and more added if surface absorption has severely depleted it. The cryostat is then placed in between the pole pieces of an electromagnet. The magnetic field is then turned on to full value in a continuous manner over several minutes. Heat is given out by the salt to the exchange gas and hence to the helium bath.

Remarks on the Magnetization Process. We must be clear about what goes on inside the specimen when one does such a simple thing as turning on a magnetic field. The $(2J + 1)$-degenerate states split up in the presence of a magnetic field. If the set of electrons were adiabatically isolated, then when the field is turned on, exactly half of the electrons would be found in the upper states and half in the lower states. There would be no net magnetization. A net magnetization arises only if the population of the lower-lying levels (moments parallel to the field) increases because of the Boltzmann distribution at the temperature T.

In other words, we require that the set of electrons be in thermal equilibrium with the ensemble of atoms so that they may tumble down from the upper states by giving off energy to the lattice vibrations. Such spin-lattice interaction is almost instantaneous for the electron system at 1°K, but we shall see that for nuclear spin systems the interaction with lattice motion is extremely feeble in some circumstances. The finite time required to magnetize the paramagnetic salt at 1°K and 30,000 gauss is taken up mostly by the slow heat conduction from the center of the crystal to its surface.

Demagnetization. The heat of magnetization having been absorbed by the bath, the exchange gas is then pumped out vigorously. The pumping out requires as much as $\frac{1}{2}$ hr in some experimental arrangements. During this time the magnetic field is held steady on its predetermined value. The end vacuum having been reached, the magnetic field is then turned off and the magnet completely removed from the neighborhood of the cryostat. A set of Helmholtz coils is frequently employed to remove the ambient earth's field in the laboratory. The salt is found to be at a temperature characterized by its own entropy curve and by the magnetic field strength employed during the entropy-lowering process.

Determination of Temperature. The new very low temperature is immediately evident from the huge deflections obtained on the galvanometer. But this is the T^* temperature, and we wish to know the thermodynamic absolute temperature. The absolute temperature of a system is

$$T = \frac{\Delta Q}{\Delta S} = \frac{(\partial Q/\partial T^*)_{B=0}}{(\partial S/\partial T^*)_{B=0}} \tag{8.43}$$

The procedure is to determine two plots: one is the plot of entropy against T^*, and the other is the plot of heat content against T^*. The entropy vs. T^* is obtained from the initial conditions where a known magnetic field strength has changed the entropy by a known amount. A series of demagnetizations from different field values, each of which gives a definite final low temperature T^*, allows us to plot S vs. T^* in zero field. We shall presently examine such plots.

The next step requires the measurement of Q against T^*. Having made a demagnetization to quite low temperatures, the procedure calls for pouring in a known amount of heat ΔQ and measuring continuously the T^*. Giauque, Stout, Egan, and Clark[1] used a carbon heater on the glass capsule containing the specimen, and at higher temperatures this carbon resistor served also as a thermometer. Earlier Giauque and MacDougall[2] had used an induction heater of a gold alloy. Kurti,

---

[1] W. F. Giauque *et al.*, *J. Am. Chem. Soc.*, **63**, 405, 1941.

[2] W. F. Giauque and D. P. MacDougall, *J. Am. Chem. Soc.*, **60**, 376, 1938.

Laine, and Simon[1] heated with γ rays from a radium salt in order to be sure to obtain thermal equilibrium throughout the salt. The unknown constant in the heating rate with γ rays is determined by permitting the absolute temperature to be identified with the T^* temperature at and near 1°K. De Klerk, Steenland, and Gorter[2] heated by an alternating magnetic field because at very low temperatures there is a hysteresis phenomenon, and even somewhat above these temperatures there are relaxation effects which contribute to the imaginary part of the magnetic susceptibility. The heating supplied to the sample per unit time is

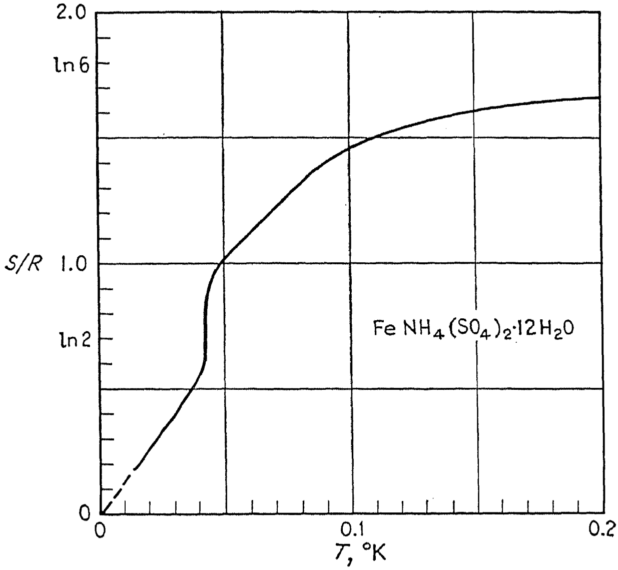

FIG. 8.14. Entropy vs. temperature for iron ammonium alum. (*Reported by Kurti and Simon, Proc. Intern. Conf. Low Temperatures, MIT*, 1949.)

$$\frac{dQ}{dT} = \frac{1}{2}\,\mathbf{H}_0^2\omega\chi'' \tag{8.44}$$

where $\mathbf{H}_0$ is the magnitude of the alternating field whose frequency is $\omega/2\pi$. Bridge measurements gave both the real and imaginary components of the susceptibility:

$$\chi = \chi' - i\chi'' \tag{8.45}$$

Experimental Results

Iron Ammonium Alum. The results of the entropy-vs.-temperature plots have shown the interaction effects which lower the entropy (Fig. 8.14). A rise in entropy with temperature means a high specific heat.

---

[1] N. Kurti, P. Laine, and F. Simon, *Compt. rend.*, **204**, 675, 754, 1937.

[2] D. De Klerk, M. Steenland, and C. J. Gorter, *Physica*, **15**, 649, 711, 1949.

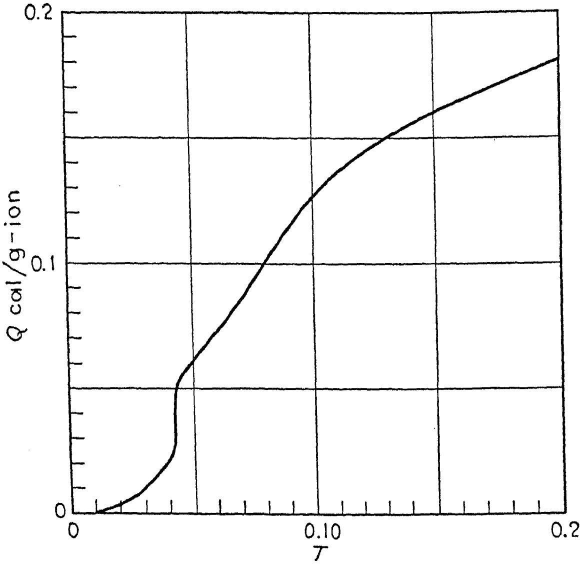

FIG. 8.15. Heat content vs. temperature for iron ammonium alum. (*Kurti and Simon.*)

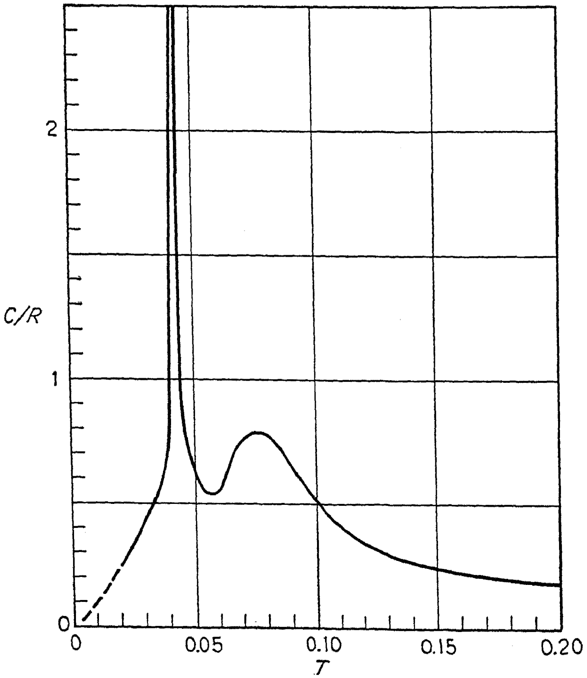

FIG. 8.16. Specific heat vs. temperature for iron ammonium alum. (*Kurti and Simon.*)

TABLE 8.4

Heat Capacity of 1 Gram-ion of Gadolinium Sulfate[a]

T, °K	1.6	1.8	2.0	2.5	3.0	3.5	4.0	6.0	8.0	10.0	14.0	20.0
C_p, cal/°K	0.25	0.20	0.17	0.11	0.08	0.06	0.05	0.05	0.11	0.23	0.80	2.30

Giauque's Results on Gadolinium Phosphomolybdate, $GdPMo_{12}O_{40} \cdot 30H_2O$

T, °K	0.187	0.272	0.391	0.545	0.704	0.862	1.027	1.325
C_p, cal/(°K)(mole)	1.01	1.93	0.72	0.471	0.336	0.280	0.212	0.164

[a] N. Kurti, *Z. physik. Chem.*, **B20**, 316, 1933.

The steep rise in entropy comes at the Curie point. The plot of Q against T is shown in Fig. 8.15. The specific heat plotted against T is given in Fig. 8.16. The first evidence for the specific heat hump which accompanies these processes was obtained by N. Kurti. Kurti's results on gadolinium sulfate and similar results by Giauque are shown in Table 8.4.

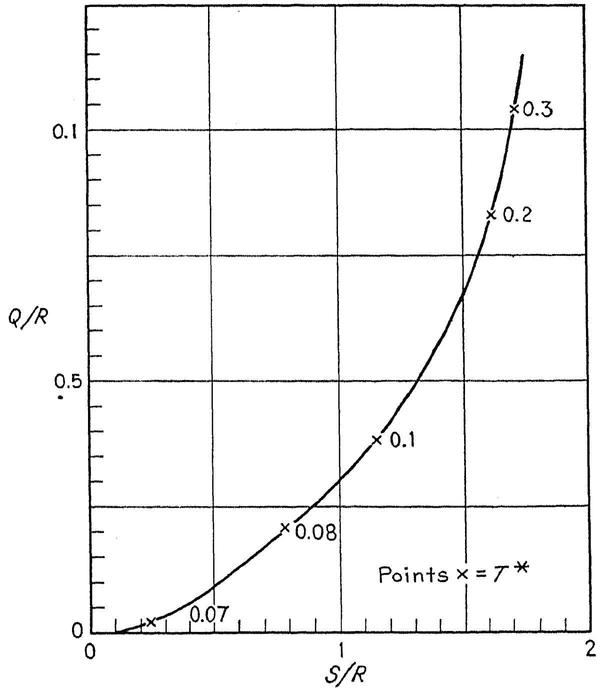

FIG. 8.17. Heat content vs. entropy (in reduced coordinates) for iron ammonium alum. Values of T^* are indicated. (*Kurti and Simon.*)

The research done by Kurti and Simon[1] on the salt $FeNH_4(SO_4)_2 \cdot 12H_2O$ was the first to show hysteresis effects in the magnetization at the Curie

---

[1] N. Kurti and F. Simon, *Compt. rend.*, **204**, 675, 754, 1937.

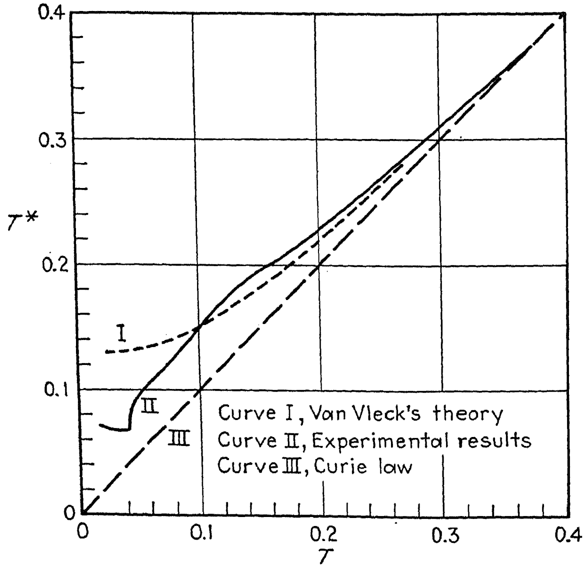

FIG. 8.18. Magnetic temperature vs. absolute temperature for iron ammonium alum. (*Work done by Kurti, Laine, and Simon.*)

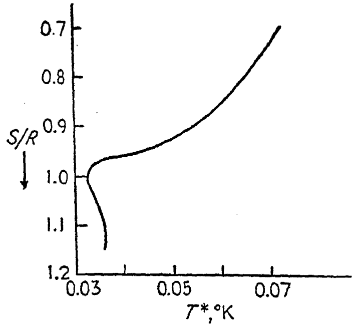

FIG. 8.19. Entropy vs. magnetic temperature for chromium potassium alum. (*Work of De Klerk, Physica,* **15**, 649, 711, 1949.)

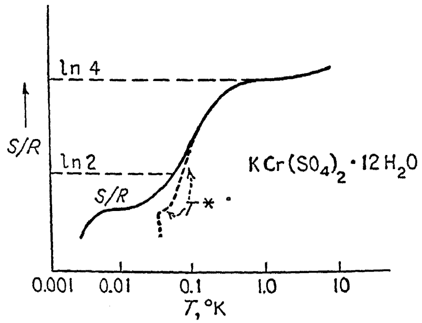

FIG. 8.20. Entropy vs. temperature for chromium potassium alum. (*Work of De Klerk, Physica,* **15**, 649, 711, 1949.)

point. The war interrupted their work, and the details have only begun to appear in the literature.[1,2] Kurti and Simon[3] showed that below the Curie point, 0.04°K, for iron ammonium alum an adiabatic magnetization

---

[1] N. Kurti and F. Simon, *Proc. Intern. Conf. Low Temperatures MIT*, September, 1949.

[2] A. H. Cooke, *Proc. Phys. Soc.* (*London*), **A62**, 269, 1949.

[3] N. Kurti and F. Simon, *Proc. Intern. Conf. Low Temperatures MIT*, September, 1949.

produces cooling. Above the Curie point such adiabatic magnetization produces heating.

Figure 8.17 shows Q plotted against S. The way in which T and T^* deviate is shown in Fig. 8.18. All T^* values refer to a spherical specimen. Before we try to understand these results from application of statistical expressions, let us examine another salt, chromium potassium alum, and then we may put theoretical ideas together.

Chromium Potassium Alum. D. De Klerk[1] has studied chromium potassium alum in the temperature region below 1°K, and in Fig. 8.19 his results are shown for entropy vs. the magnetic temperature T^*. Having also found the plot of Q vs. T^*, De Klerk was able to plot the entropy vs. the absolute temperature, as shown in Fig. 8.20. It is surprising not to find the Curie point at the entropy value $R \ln 2$. The hysteresis loop at 0.004°K is shown in Fig. 8.21.

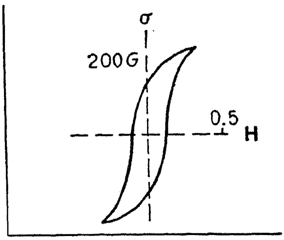

FIG. 8.21. Adiabatic magnetization. The hysteresis loop at 0.004°K.

Theoretical Analysis

The results on Fe-alum have been compared with the theory which was developed by Van Vleck[2] and by Hebb and Purcell.[3] Assuming that the electric field of the crystal lattice possesses cubic symmetry, the sixfold degenerate levels are split into two groups, one of twofold degeneracy and one of fourfold degeneracy. The energy of separation is denoted as δ, and the partition function becomes

$$Z = 2(1 + 2e^{-\delta/kT}) \tag{8.46}$$

From this expression the entropy and specific heat may be computed. Comparison with experimental results gives $\delta/k = 0.20$°K for iron ammonium alum. The above partition function is valid only for the region where the electric field splitting causes an effect, and at lower temperatures we would expect magnetic coupling to give an additional term to the partition function.

P. Debye[4] considered the effect of the splitting of states by the crystalline electric field by using the theory of Van Vleck and Penney[5] and in zero magnetic field obtained a partition function identical to that of Hebb and Purcell. Debye considered the dipole-dipole coupling as a

---

[1] D. De Klerk, *Physica*, **15**, 649, 711, 1949.

[2] J. H. Van Vleck, *J. Chem. Phys.*, **5**, 320, 1937.

[3] M. Hebb and E. Purcell, *J. Chem. Phys.*, **5**, 338, 1937.

[4] P. Debye, *Ann. phys.*, **32**, 85, 1938.

[5] J. H. Van Vleck and W. Penney, *Phil. Mag.*, **17**, 961, 1934.

Weiss field. Luttinger and Tisza[1] have examined the question of the field at a dipole due to an array of dipoles having perfect order or zero entropy. The hysteresis and seemingly ferromagnetic properties of these salts at very low temperatures cannot be understood from a simple near-neighbor dipole interaction.

The splitting by the electric field to decompose the ^6S level of the Fe-ion in iron ammonium alum is often expressed in reciprocal wave lengths, cm^{-1}. The adiabatic demagnetization studies have given values from 0.155 cm^{-1} (Kurti and Simon) to 0.120 cm^{-1} (Casimir, de Haas, and De Klerk). Dispersion studies by DuPre at 4°K have given a value of the splitting to be 0.125 cm^{-1}. At higher temperatures, 77°K, Broer has given a value of 0.135 cm^{-1}.

A theoretical discussion of the very low-temperature behavior of chromium potassium alum has been given by Hebb and Purcell,[2] Broer,[3] and Weiss.[4] The chromium ion is in a ^4F state; the three d electrons with spins parallel form the saturated magnetic moment, and the susceptibility is for three free spins. This means that the F state is split by the electric field such that the fourfold degeneracy is split into two twofold degenerate states. The symmetry of the electric field is trigonal. The two states with angular momentum $\frac{3}{2}$ and $-\frac{3}{2}$ in the direction of the trigonal axis will be separated from the two states with angular momentum $\frac{1}{2}$ and $-\frac{1}{2}$. The parameter δ will be the energy distance between the two groups of levels, which De Klerk gives as $\delta/k = 0.251$°K. The partition function in zero field is then

$$Z = 2(1 + e^{-\delta/kT}) \tag{8.47}$$

The entropy of the system is

$$S = Nk\left[\ln 2(1 + e^{-\delta/kT}) + \frac{\delta}{kT}\frac{e^{-\delta/kT}}{1 + e^{-\delta/kT}}\right] \tag{8.48}$$

The specific heat of the chrom-alum is then

$$C = \frac{\delta^2}{4k^2T^2}(Nk)\frac{4e^{-\delta/kT}}{(1 + e^{-\delta/kT})^2} \tag{8.49}$$

The splitting factor δ for various chromic alums is different at any given temperature. For any given chromic alum, such as the potassium chrom-alum, the splitting factor is a function of the temperature and of the crystalline direction. For example, the potassium chrom-alum at 290°K has a splitting factor $\delta = 0.12\ \text{cm}^{-1}$, and at 193°K the value is 0.055 cm^{-1}.

---

[1] J. M. Luttinger and L. Tisza, *Phys. Rev.*, **70**, 954, 1946; *ibid.*, **72**, 257, 1947.

[2] M. Hebb and E. Purcell, *J. Chem. Phys.*, **5**, 338, 1937.

[3] L. Broer, *Physica*, **9**, 547, 1942.

[4] P. R. Weiss, *Phys. Rev.*, **73**, 470, 1948.

At temperatures below 20°K the value is 0.27 cm^{-1} along one axis and 0.15 along another. These remarks serve to show that the crystalline electric field depends upon many factors within the solid. The specific heat of the chrom-alum is shown in Fig. 8.22, and the values are given for zero magnetic field, 5 and 10 kilogauss. Such large magnetic fields produce a Zeeman splitting of the energy states which completely dominate the small Stark splitting due to the crystal. In the above discussion of the theory for the specific heat of chrom-alum we have confined our remarks to the effect of the electric field and have not entered into the controversial problem of magnetic interaction.

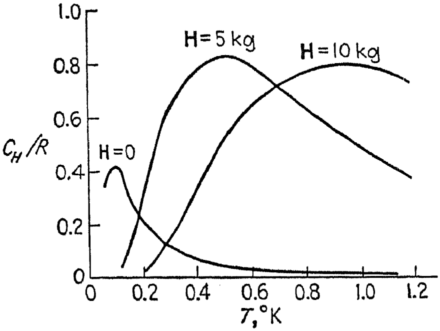

FIG. 8.22. Specific heat at constant magnetic field in chrom-alum. (*Mendoza, "Les Phenom. cryomag.," Collège de France,* 1948.)

Nuclear Alignment

There has been a great deal of interest over the problem of nuclear magnetic moment alignment and the possibility which this presents of cooling to temperatures of 10^{-4} °K. Our ideas concerning the process follow those which we have discussed with the electronic system. Suppose that we have a set of nuclear energy levels whose energy difference represents the various orientations of the nuclear spin in an external magnetic field. By cooling to low enough temperatures, the lower levels will be preferentially populated, and this corresponds to a spatial alignment. Lazarev and Schubinkov[1] obtained nuclear alignment when they first detected the nuclear contribution to the magnetic susceptibility of solid hydrogen at very low temperatures. A great deal of experimental and theoretical effort has gone into the problems of cooling of a nuclear spin system by means of a paramagnetic salt and then of carrying out a second demagnetization on the nuclear system after the thermal bridge to the paramagnetic salt has been destroyed. As a matter of fact, Rollin and Hatton[2] produced a cooling of the nuclear spin system for about 60 sec but not by the above method. We shall discuss their work in a later paragraph.

Gorter[3] proposed a method of producing nuclear alignment by making use of the interaction between the electron magnetic moment with the nuclear moment. The field at the nucleus is 10^5 to 10^6 gauss, so that, if a small field is applied to align the electronic moment, the nuclei will also be aligned. Temperatures of the order 0.01°K are required for the nuclear levels to be populated in this way. Rose[1] made similar suggestions for the purpose of nuclear alignment. Gorter[2] and coworkers reported inconclusive results on the first experiments which they made.

---

[1] B. Lasarev and L. Schubinkov, *Physik. Z. Sowjetunion,* **11,** 445, 1937.

[2] B. Rollin and J. Hatton, *Proc. Roy. Soc. (London),* **199,** 222, 1949.

[3] C. J. Gorter, *Physica,* **14,** 504, 1948; *ibid.,* **15,** 679, 1949.

Bleaney[3] pointed out that in certain cases for single crystals the electronic moments need not be held aligned by an external magnetic field because the crystalline electric field can cause an anisotropy in the hyperfine structure. Thus if the single crystal were sufficiently dilute with magnetic ions so that the field produced by one on another is very weak, there would be a possibility of nuclear alignment in zero external field at 0.01°K. Daniels, Grace, and Robinson[4] produced just such nuclear alignment in a salt containing 1 per cent cobalt which was radioactive with respect to γ-ray emmision. The γ-ray radiation was not isotropic because the Co nuclei were partially aligned.[5]

Magnetic Resonance

As one stands at the threshold of this important field of physics and surveys the many research papers in experiment and theory, one is impressed with the impetus given this subject by Professor C. J. Gorter, director of the Leiden laboratories. Starting with his first experiments[6] on the heat developed in paramagnetic substances under the influence of a high-frequency alternating magnetic field, one can see Gorter's influence on the growth and development of magnetic resonance in electronic and nuclear systems.[7] The early work described the absorption of energy from the r-f field by means of a classical analogy to a damped oscillator driven not too far from resonance. The actual oscillator was a magnetic oscillator whose amplitude gave the magnetization **M** from which the complex susceptibility could be described. Identification with the Lamor precession frequency came out of theory by Landau and Lifshitz[8] and experiment by Frenkel and Zavoisky.[9] Cummerow and Halliday[10] also reported electronic magnetic resonance. Nuclear resonance absorption was first reported by Purcell, Torrey, and Pound,[11] and nuclear induction by Bloch, Hansen, and Packard.[1] Historically the subject of resonance absorption goes back in optics to the work of R. W. Wood,[2] in electric dipoles to that of P. Debye,[3] and in molecular beam magnetic dipoles to that of I. Rabi.[4] Indeed one can find even earlier evidence for magnetic resonance in the work of Faraday on the rotation of the plane of polarization of light by substances when placed in a magnetic field.

---

[1] M. E. Rose, *Phys. Rev.*, **75**, 213, 1949.

[2] C. J. Gorter, *Physica*, **14**, 504, 1948; *ibid.*, **15**, 679, 1949.

[3] B. Bleaney, *Proc. Phys. Soc. (London)*, **64**, 315, 1951.

[4] J. M. Daniels, M. Grace, and F. Robinson, *Nature*, **168**, 780, 1951.

[5] J. Spiers, *Nature*, **161**, 807, 1948.

[6] C. J. Gorter, *Physica*, **3**, 503, 1936.

[7] C. J. Gorter, "Paramagnetic Relaxation," Amsterdam, Elsevier, 1947.

[8] L. Landau and E. Lifshitz, *Physik. Z. Sowjetunion*, **8**, 153–169, 1935.

[9] J. Frenkel and E. Zavoisky, *J. Phys. Chem. USSR*, **9**, 211, 1945.

[10] R. Cummerow and D. Halliday, *Phys. Rev.*, **70**, 433, 1946.

[11] E. Purcell, H. Torrey, and R. Pound, *Phys. Rev.*, **69**, 37, 1946.

Let us return to our fundamental concepts of magnetism with which we started this present chapter. We had indicated that the ratio of the self-inductance of a coil when filled with matter to that when empty was

$$\frac{L}{L_0} = \frac{\mu}{\mu_0} \tag{8.50}$$

Now let the field strength produced by current in a coil be given by

$$\mathbf{H} = \mathbf{H}_0 e^{j\omega t} \tag{8.51}$$

The expression for the magnetic induction **B** will in general show a shift in phase with respect to **H** so that

$$\mathbf{B} = \mathbf{B}_0 e^{j(\omega t - \delta)} \tag{8.52}$$

Thus the permeability μ which equals the quotient $\mathbf{B}/\mathbf{H}$ is complex,

$$\mu = \frac{\mathbf{B}}{\mathbf{H}} = \frac{\mathbf{B}_0 e^{-j\delta}}{\mathbf{H}_0} = \frac{\mathbf{B}_0}{\mathbf{H}_0}(\cos\delta - j\sin\delta) \tag{8.53}$$

How does this phase shift arise from the magnetic moment of the electron spin? This phenomenon is a consequence of the existence of gyro-magnetic resonance. We shall approach the problem in the classical way of Beljers and Snoek[5] and of Hogan.[6] The electron spin may be regarded as a charged sphere rotating about an axis so that it has a magnetic moment and mechanical angular momentum. There is a close analogy between the behavior of the spin system in an external magnetic field and that of the spin system in a gravitational field. The electron spin system behaves like a gyroscopic pendulum (Fig. 8.23). The angular momentum of the spin is

$$P = I\omega_s \tag{8.54}$$

where I is the moment of inertia about the spin axis and ω_s is the angular velocity of that rotation. The pendulum is out at an angle γ so that there is a torque driving the pendulum toward the position of equilibrium:

$$\tau = FL\sin\gamma \tag{8.55}$$

---

[1] F. Bloch, W. Hansen, and M. Packard, *Phys. Rev.*, **69**, 680, 1946.

[2] R. W. Wood, "Physical Optics," New York, Wiley, 1936.

[3] P. Debye, "Polar Molecules," Chap. V, Leipzig, Chemical Catalog, 1929.

[4] I. I. Rabi, *Phys. Rev.*, **53**, 318, 1939; *ibid.*, **55**, 526, 1939.

[5] H. Beljers and J. Snoek, *Philips' tech. Rundschau*, **11**, 313, 1950.

[6] C. Hogan, *Bell System Tech.*, **31**, 1, 1952.

where F is the weight of the pendulum and L the distance from the center of mass to the point of suspension. The precession velocity is

$$\omega_L = \frac{FL}{P} \tag{8.56}$$

which is independent of the angle γ.

Let us suppose that the gyro is rotating with its axis vertical so that there is no torque and no precession to start with (position A, Fig. 8.24). Now let us suddenly turn the direction of the force of gravity over a small angle γ in the plane of the drawing. Precession will start with γ as half-apex angle, as in Fig. 8.23. When, after half a cycle has been completed (position B), we suddenly cause the force of gravity to make an angle $-\gamma$ with the vertical, the half-apex angle becomes 3γ. If the gravitational field is again reversed after the gyroscope completes another half cycle in its precession (position C), the gyroscope will precess in a larger circle. If this process is continued indefinitely the gyroscope will precess in larger and larger circles around the vertical until damping action may become large enough to contain the gyroscope in some equilibrium circle. If the alternating action is discontinued so that one has a steady gravitational field, the damping action would gradually decrease the amplitude of the precession circle.

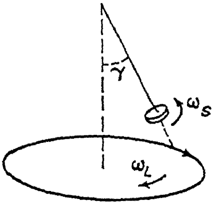

FIG. 8.23. Gyroscopic pendulum.

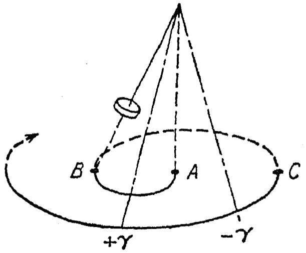

FIG. 8.24. Increase of precession orbit of gyroscopic pendulum.

It is not easy to switch the gravitational field in this way, but one may demonstrate the behavior by causing an air jet to impinge on the gyroscope each time it comes around the precession circle. It will then widen out the circle. But the magnetic analogy is easy to perform so far as the field switching is concerned. We must compare the precession discussed above with the Larmor precession for electron spin discussed in the beginning of the present chapter. The Larmor precession is

$$\omega_L = \frac{e}{m}\mathbf{B}$$

We may supply an alternating magnetic field b so that the resultant field $\mathbf{B}$ appears to shift the small angle γ in the way described above for the gravitational field. Under these conditions the precession circle widens out to some steady magnitude. Like any resonant system it will respond with a smaller amplitude if it is not driven at just the resonant frequency. We may understand that with an alternating magnetic field applied along the x axis (steady field along the z axis) there will appear an alternating magnetic moment directed along the x axis and in phase with the external alternating field. Also there will be an alternating magnetic moment directed along the y axis, and this lags 90 deg in phase behind the applied alternating field. If we include the damping action, the equations for the magnitude of these magnetic moments may become complicated but not obscure. We shall examine the magnetic gyrator and the phenomenon of resonance by following the work by F. Bloch.[1] Let us begin then with Bloch's experiment.

Nuclear Magnetic Induction. The experimental arrangement for studying nuclear magnetic resonance is shown in Fig. 8.25. The specimen containing the magnetic gyrator may be several cubic centimeters of water whose proton moment is the gyrator. It is placed in the center coil (x direction) of the equipment shown between the pole pieces of a magnet. In a field of, say, 1,826 gauss, z direction, the protons have a Larmor precession frequency of 7.765×10^6 cycles/sec. The transmitter coil is driven at this frequency (y direction). The steady field (z direction) is modulated $\pm \Delta B$ by a small 60-cycle current so that resonance conditions are passed through repeatedly but momentarily. At resonance the transmitter coil is able to feed energy into the proton spin system and cause a change of magnetization, dM_y/dt, along the direction of the center pick-up coil of the detector. The induced emf is amplified and displayed on the scope. The shape of the signal on the scope depends upon a number of conditions but chiefly upon the speed with which the large field is pushed through the resonance field value.

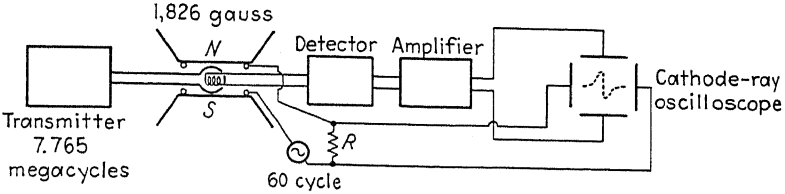

FIG. 8.25. Schematic diagram of nuclear resonance experiments.

Theoretical Analysis of Magnetic Induction. We are not totally unprepared for the acceptance of the magnetic induction because of our understanding of the classical behavior. Let us recall the quantum theory of the magnetization for the nuclear energy states in a steady field. The energy of separation of the split degenerate states is quite small compared to kT. Hence, the statistical expression for the average magnetic moment is

---

[1] F. Bloch, *Phys. Rev.*, **70**, 460, 1946.

$$\bar{\beta} = \frac{1}{3}\left[\frac{g^2\beta_0^2 I(I+1)}{kT}\right]\mathbf{B} \tag{8.57}$$

where I is the spin quantum number for the nucleus and the Bohr magneton for the nucleus is denoted by β_0. Owing to the weak spin-lattice interaction, this degree of magnetization is not reached instantly when the external field is applied but is reached in perhaps several seconds to several hours. This is shown in Fig. 8.26. We may write the following equation for the magnetization along the z axis:

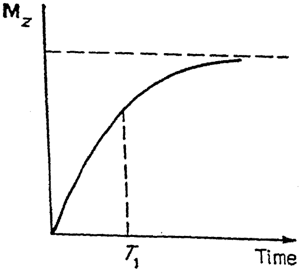

FIG. 8.26. Magnetization vs. time for a group of magnetic moments.

$$\dot{\mathbf{M}}_z = \frac{1}{T_1}(\mathbf{M}_0 - \mathbf{M}_z) \tag{8.58}$$

where T_1 is called the *longitudinal relaxation time* or sometimes the *spin-lattice relaxation time.*

What about the expected time rate of change of magnetization in the x and y directions? So far we have not considered the alternating field, but there are internal fields which now alternate. Consider two protons of magnetic moment β separated a distance r in a field of, say, 10^3 gauss. Then the field at one proton due to the second is β/r^3, or about 1 gauss for water. This field oscillates so as to induce transitions in the split energy states.[1] Such a field oscillation will give

$$\dot{\mathbf{M}}_x = -\frac{1}{T_2}\mathbf{M}_x \tag{8.59}$$

and

$$\dot{\mathbf{M}}_y = -\frac{1}{T_2}\mathbf{M}_y \tag{8.60}$$

Besides these changes of the magnetization with time, we have direction changes with which we are more familiar and which arise from the torque

$$\tau = [\mathbf{M} \times \mathbf{B}] = \dot{P} \tag{8.61}$$

We may multiply the time rate of change of angular momentum $\dot{P}$ by the gyro-magnetic ratio γ and obtain the time rate of change of magnetization:

$$\dot{\mathbf{M}} = \gamma\dot{P} = \gamma[\mathbf{M} \times \mathbf{B}] \tag{8.62}$$

---

[1] N. Bloembergen, E. Purcell, and R. Pound, *Phys. Rev.*, **73**, 679, 1948.

Putting the time rate of changes of magnetization into one equation gives the following components:

$$\dot{\mathbf{M}}_z = \gamma[\mathbf{M} \times \mathbf{B}]_z + \frac{1}{T_1}(\mathbf{M}_0 - \mathbf{M}_z) \tag{8.63a}$$

$$\dot{\mathbf{M}}_x = \gamma[\mathbf{M} \times \mathbf{B}]_x - \frac{1}{T_2}(\mathbf{M}_x) \tag{8.63b}$$

$$\dot{\mathbf{M}}_y = \gamma[\mathbf{M} \times \mathbf{B}]_y - \frac{1}{T_2}(\mathbf{M}_y) \tag{8.63c}$$

In the above equations we refer to the z component of the vector product by the symbol $[\mathbf{M} \times \mathbf{B}]_z$, etc.

The components of the magnetic field are

$$\mathbf{B}_z = \mathbf{B}_0 + \Delta\mathbf{B} \cos 377t \tag{8.64a}$$

$$\mathbf{B}_x = \mathbf{B}_1 \cos \omega t \tag{8.64b}$$

$$\mathbf{B}_y = \mathbf{B}_1 \sin \omega t \tag{8.64c}$$

where $2\mathbf{B}_1$ is the amplitude of the magnetic field in the r-f coil and the $-$ sign is taken if γ is positive, the $+$ sign if γ is negative. The r-f coil magnetic field has thus been described by two oppositely rotating fields. For convenience we shall now define

$$\mathbf{M}_x = u \cos \omega t - v \sin \omega t \tag{8.65a}$$

$$\mathbf{M}_y = \mp (u \sin \omega t + v \cos \omega t) \tag{8.65b}$$

$$\mathbf{M}_z = \mathbf{M}_z \tag{8.65c}$$

And in addition we define the group of symbols

$$\tau = |\gamma|\mathbf{B}_1 t \qquad \beta = \frac{1}{|\gamma|\mathbf{B}_1 T_2}$$

$$\alpha = \frac{1}{|\gamma|\mathbf{B}_1 T_1} \qquad \delta = \frac{|\gamma|\mathbf{B}_0 - \omega}{|\gamma|\mathbf{B}_1}$$

With these new symbols we may now write the z-component equation of magnetization

$$\dot{\mathbf{M}}_z - \gamma(\mathbf{M}_x\mathbf{B}_y - \mathbf{M}_y\mathbf{B}_x) + \frac{\mathbf{M}_z}{T_1} = \frac{\mathbf{M}_0}{T_1} \tag{8.66}$$

as the equation

$$\frac{d\mathbf{M}_z}{dt} + \gamma\mathbf{B}_1 \sin \omega t(u \cos \omega t - v \sin \omega t) + \gamma\mathbf{B}_1 \cos \omega t(-u \sin \omega t - v \cos \omega t) + \frac{\mathbf{M}_z}{T_1} = \frac{\mathbf{M}_0}{T_1} \tag{8.67}$$

Further substitution into this equation gives

$$\frac{d\mathbf{M}_z}{d\tau} + \alpha\mathbf{M}_z - v = \alpha\mathbf{M}_0 \tag{8.68a}$$

The equations for magnetization of the x and y components become

$$\frac{du}{dt}\cos\omega t - \omega u\sin\omega t - \frac{dv}{dt}\sin\omega t - \omega v\cos\omega t - \gamma(-u\sin\omega t - v\cos\omega t)\mathbf{B}_0$$
$$+ \gamma(\mathbf{M}_z)(-\mathbf{B}_1\sin\omega t) + \frac{u\cos\omega t}{T_2} - \frac{v\sin\omega t}{T_2} = 0 \qquad (8.68b)$$

$$-\frac{du}{dt}\sin\omega t - \omega u\cos\omega t - \frac{dv}{dt}\cos\omega t + \omega v\sin\omega t - \gamma(\mathbf{M}_z\mathbf{B}_1\cos\omega t)$$
$$+ \gamma(u\mathbf{B}_0\cos\omega t - v\mathbf{B}_0\sin\omega t) - \frac{1}{T_2}u\sin\omega t - \frac{1}{T_2}v\cos\omega t = 0 \qquad (8.68c)$$

Multiply the top equation by $\cos\omega t$ and the bottom one by $\sin\omega t$. Subtracting one from the other gives

$$\frac{du}{dt} - \omega v + \gamma\mathbf{B}_0 v + \frac{u}{T_2} = 0 \qquad (8.69)$$

Dividing by $1/\gamma\mathbf{B}_1$ and collecting terms gives

$$\frac{du}{d\tau} + \frac{(\gamma\mathbf{B}_0 - \omega)v}{\gamma\mathbf{B}_1} + \frac{u}{T_2\gamma\mathbf{B}_1} = 0 \qquad (8.70)$$

Substituting from our defined set of symbols, we obtain

$$\frac{du}{d\tau} + \delta v + \beta u = 0 \qquad (8.71)$$

Likewise we may obtain an equation for magnetization of the out-of-phase component:

$$\frac{dv}{d\tau} + \beta v - \delta u + \mathbf{M}_z = 0 \qquad (8.72)$$

Repeating our former equation of magnetization for the z component, we obtain

$$\frac{d\mathbf{M}_z}{d\tau} + \alpha\mathbf{M}_z - v = \alpha\mathbf{M}_0 \qquad (8.73)$$

These three equations form a system of linear differential equations with almost constant coefficients.

Particular Solution. We shall now consider a particular solution of the above equations of magnetization, namely, the one in which δ and $\mathbf{M}_0$ are so slowly varying as to be considered constant. Assume then that u, v, and $\mathbf{M}_z$ are practically constant so that

$$\frac{du}{d\tau} = \frac{dv}{d\tau} = \frac{d\mathbf{M}_z}{d\tau} = 0 \qquad (8.74)$$

This does not mean that $\mathbf{B}_0$ is a constant but only that the time of variation of $\mathbf{B}_0$ is long compared with the relaxation time. Under these conditions the equations of magnetization become

$$v = \alpha \mathbf{M}_z - \alpha \mathbf{M}_0 \tag{8.75a}$$

$$\beta\alpha \mathbf{M}_z - \beta\alpha \mathbf{M}_0 - \delta u + \mathbf{M}_z = 0 \tag{8.75b}$$

$$\beta\alpha \mathbf{M}_z - \beta\alpha \mathbf{M}_0 + \frac{\delta^2}{\beta}(\alpha \mathbf{M}_z - \alpha \mathbf{M}_0) + \mathbf{M}_z = 0 \tag{8.75c}$$

Solving, we obtain the relations

$$\mathbf{M}_z = \frac{\alpha(\beta^2 + \delta^2)\mathbf{M}_0}{\alpha(\beta^2 + \delta^2) + \beta} \tag{8.76a}$$

$$v = \frac{-\alpha\beta \mathbf{M}_0}{\alpha(\delta^2 + \beta^2) + \beta} \tag{8.76b}$$

$$u = \frac{\delta \mathbf{M}_0}{\delta^2 + \beta^2 + \beta/\alpha} \tag{8.76c}$$

Now we may unscramble our notation and return to a set of symbols which show clearly the customary resonance conditions. For this let us denote the difference between the Larmor precession velocity and the r-f coil angular velocity by

$$\gamma \mathbf{B}_0 - \omega = \Delta\omega \tag{8.77}$$

We now have the three equations

$$u = \frac{\gamma \mathbf{B}_1(\Delta\omega) T_2^2 \mathbf{M}_0}{1 + (T_2\,\Delta\omega)^2 + (\gamma \mathbf{B}_1)^2\, T_1 T_2} \tag{8.78a}$$

$$v = \frac{-(\gamma \mathbf{B}_1 T_2)\mathbf{M}_0}{[1 + (T_2\,\Delta\omega)^2] + (\gamma \mathbf{B}_1)^2 T_1 T_2} \tag{8.78b}$$

$$\mathbf{M}_z = \left[\frac{1 + (T_2\,\Delta\omega)^2}{1 + (T_2\,\Delta\omega)^2 + (\gamma \mathbf{B}_1)^2 T_1 T_2}\right]\mathbf{M}_0 \tag{8.78c}$$

These last three equations are Bloch's equations (57*a*), (57*b*), (57*c*).[1] In the magnetic induction experiment by Bloch, Hansen, and Packard, the detection coil reacts to changes in $\mathbf{M}_y$:

$$\mathbf{M}_y = \mp(u \sin \omega t + v \cos \omega t) \tag{8.79}$$

The out-of-phase component v is small compared with u. The equation for u in our special solution shows that, at resonance, u equals 0, so the signal in the detection coil is 0 at resonance. Off resonance the maximum value of u is obtained whenever

$$(T_2\,\Delta\omega)^2 = 1 + (\gamma \mathbf{B}_1)^2 T_1 T_2 \tag{8.80}$$

so that

$$u_{\max} = \left[\frac{\gamma \mathbf{B}_1 T_2}{\sqrt{1 + (\gamma \mathbf{B}_1)^2 T_1 T_2}}\right]\mathbf{M}_0 \tag{8.81}$$

---

[1] F. Bloch, *Phys. Rev.*, **70**, 460, 1946.

If in addition we make the quantity

$$(\gamma \mathbf{B}_1)^2 T_1 T_2 \gg 1$$

then (compare with H. Torrey[1])

$$u_{\max} = \sqrt{\frac{T_2}{T_1}}\,\mathbf{M}_0 \tag{8.82}$$

One gets absorption from the v term. Absorption applies to the experiments of Purcell, Torrey, and Pound.[2] The absorption of energy is due to the magnetization component out of phase with the r-f field. We can describe this component as the imaginary part of the magnetic susceptibility $\chi''_{\text{r.f.}}$. This part of the dynamic susceptibility can be obtained by taking the ratio of v to $\mathbf{H}_1$.

$$\chi''_{\text{r.f.}} = \frac{|\gamma| T_2 \mathbf{M}_0}{1 + (T_2\,\Delta\omega)^2 + (\gamma \mathbf{B}_1)^2 T_1 T_2} \tag{8.83}$$

As shown in Fig. 8.27, the expression has a maximum for resonance, $\Delta\omega = 0$. The greatest effect is obtained for

$$(\gamma \mathbf{B}_1)^2 T_1 T_2 = 1$$

The maximum value of v is then

$$v_{\max} = \sqrt{\frac{T_2}{T_1}}\,\mathbf{M}_0 \tag{8.84}$$

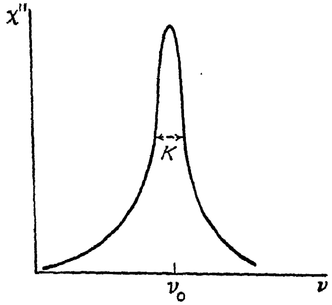

FIG. 8.27. Paramagnetic resonance absorption. Pure imaginary component of magnetic susceptibility vs. frequency.

Some General Remarks about Magnetic Induction and Absorption. The classical theory of Bloch[3] which we have just sketched is identical to a quantum-mechanical description of the phenomenon. We must realize that any system possessing a magnetic moment has a degeneracy in energy levels which is removed by a magnetic field. The separation of the energy levels is by an amount $h\nu$, and an oscillating magnetic field will be able to induce transitions between these levels if it has the frequency ν and if the transition is allowed. For nuclear systems in a field of several thousand gauss the frequency lies in the radio range, but for paramagnetic ions the same magnetic field requires microwave equipment.

We have already recognized that for a spin system to show a net magnetization the density of population of the lower energy states must be greater than the upper ones. The energy lost in establishing the Boltzmann distribution was quite apparent in paramagnetic salts which were magnetized at 1°K for the magnetic cooling process. The alternating magnetic field applied in these resonance experiments causes energy to be absorbed and causes an upset of the equilibrium distribution over the states. If the spin system can transfer or radiate the absorbed energy to the heat reservoir comprising all other degrees of freedom, then the absorbed energy will not cause the spin system to get too hot. The balance established depends on the spin-lattice interaction and is characterized by the time T_1 in Bloch's theory. We shall be interested in how the time T_1 is affected by lowering the temperature. Work on a theory for the relaxation time has been done by Waller,[1] Kronig,[2] Van Vleck,[3] and by Teller and Heitler.[4]

---

[1] H. Torrey, *Phys. Rev.*, **76**, 1059, 1949.

[2] E. Purcell, H. Torrey, and R. Pound, *Phys. Rev.*, **69**, 37, 1946.

[3] F. Bloch, *Phys. Rev.*, **70**, 460, 1946.

Experimental Results

Solid Hydrogen. The experimental method for detecting nuclear magnetic resonance has given accurate values of the nuclear magnetic moment of many nuclei and has given the sign and magnitude of the gyro-magnetic ratio. The techniques have advanced so rapidly that one finds many laboratories using the detector signal to measure the magnitude of the external magnetic field and to monitor such fields during precise measurements. The relaxation times are from 10^{-5} seconds to many seconds depending on conditions. We shall be interested in measurements carried out at very low temperatures in so far as they may throw light on the properties of matter at low temperatures. Let us begin with the studies by Rollin and Hatton[5] on solid hydrogen.

The resonance absorption due to the proton in liquid and solid hydrogen showed no appreciable change at the phase transition. At lower temperatures the absorption line showed a considerable broadening (below 4°K). Two subsidiary absorption peaks appeared at 1.3°K. Figure 8.28 shows the block diagram for the equipment used by Rollin and Hatton for measuring the absorption of energy and for the spin-lattice relaxation time.

Absorption of energy changes the circuit impedance, and the resonance is observed as a change of r-f voltage across the circuit. The magnetic field is modulated at audio frequency so that the change of nuclear absorption gives rise to an a-f modulation of the r-f voltage across the circuit. This audio signal is observed on the scope or measured by the output meter. Measurements were made at 2 to 5 megacycles/sec.

---

[1] I. Waller, *Z. Physik,* **79,** 37, 1932.

[2] R. Kronig, *Physica,* **6,** 33, 1939.

[3] J. H. Van Vleck, *Phys. Rev.,* **75,** 426, 1940.

[4] E. Teller and W. Heitler, *Proc. Roy. Soc.* (*London*), **155,** 629, 1936.

[5] B. V. Rollin and J. Hatton, *Nature,* **159,** 201, 1947; *Phys. Rev.,* **74,** 346, 1948; *Proc. Roy. Soc.* (*London*), **199,** 222, 1949.

The sample coil was wrapped around a glass cylinder, and the specimen placed inside was cooled by helium exchange gas which made contact with a liquid helium bath or with a paramagnetic salt where that was used as a refrigerant below 1°K. As was noted in the theory by Bloch concerning the absorption experiments, a large field $\mathbf{B}_1$ by the r-f coil can put so much energy into the spin system as to fill the empty energy levels so that no more energy can be received. Hatton and Rollin applied such a strong r-f field that the nuclear-spin temperature was raised above the lattice temperature, and then they quickly reduced to a very small r-f field and timed the exponential growth of the output signal as the temperature of spin and lattice became equal. The results on liquid and solid hydrogen whose ortho-para ratio was presumed to be 3:1 are given in Table 8.5, in which T is the temperature, T_1 the relaxation time, and $\Delta\mathbf{H}$ the line width.

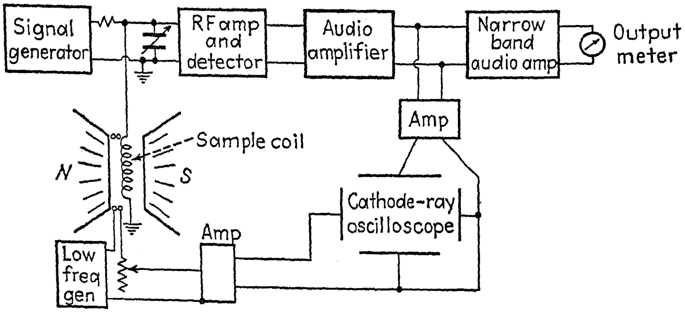

FIG. 8.28. Diagram of apparatus (schematic) for resonance studies.

TABLE 8.5. NUCLEAR ABSORPTION IN SOLID AND LIQUID HYDROGEN SHOWING RELAXATION TIME AND LINE WIDTH[a]

T, °K	20	14.0	11	4.2	1.85	1.3	1.1
T_1, sec	0.02	0.1	0.2	0.3	0.5	2	2
ΔH, gauss	0.1	0.1	1.0	8	10	50	50

[a] B. V. Rollin and J. Hatton, *Nature*, **159**, 201, 1947; *Phys. Rev.*, **74**, 346, 1948; *Proc. Roy. Soc. (London)*, **199**, 222, 1949.

At the lowest temperature (1.0°K) there is a very broad resonance with two peaks separated by 50 gauss (Fig. 8.29). It is interesting to compare this field separation with the much smaller separation caused by one proton on another in a solid dichloroethane crystal, as reported by Gutowsky, Kistiakowsky, Pake, and Purcell.[1] From an analysis of the factors which influence the line width the conclusion is that for hydrogen even below the solid point (14°K) the molecules have considerable relative motion. At about 2°K all rotation of the molecule has ceased, and at 1°K the twin peaks of absorption are attributed to the mutual interaction of the protons. These ideas about the motion of the solid hydrogen molecule will be examined again in Chap. 9.

---

[1] H. Gutowsky *et al.*, *J. Chem. Phys.*, **17**, 972, 1949.

Studies on Solids at Low Temperature. N. Bloembergen[1] has pointed out that, owing to the large signal output at low temperatures, one can measure gyro-magnetic ratios of the rarer isotopes with some ease.

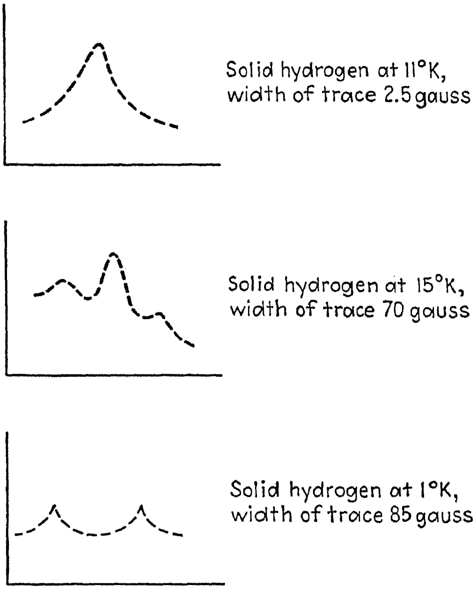

FIG. 8.29. Cathode-ray scope pattern of nuclear resonance absorption in solid hydrogen. [*Work done by Hatton and Rollin, Proc. Roy. Soc. (London),* **199**, 222, 1949.]

Both Bloembergen and Rollin[2] have reported that the spin-lattice relaxation time T_1 for metals is inversely proportional to the temperature at 1°K with values of 0.1 sec for copper and aluminum. For metals there is a field dependence of the relaxation time, which is longer in higher fields. Both Bloembergen and Rollin report that insulating crystals have relaxation times from 1 to 10^3 sec at 1°K and that slight paramagnetic impurities play a most important role in such relaxation times. This method of cutting down on the relaxation time was first noted by Bloch, Hansen, and Packard.[3]

---

[1] N. Bloembergen, Thesis, University of Leiden, 1948, published by Nishoff, The Hague, 1948.

[2] B. V. Rollin and J. Hatton, *Nature,* **159**, 201, 1947; *Phys. Rev.,* **74**, 346, 1948; *Proc. Roy. Soc. (London),* **199**, 222, 1949.

[3] F. Bloch, W. Hansen, and M. Packard, *Phys. Rev.,* **69**, 680, 1946.

Bitter and coworkers[1] found narrow lines in liquids and broad lines in solids, which agrees with the theory of rotational states in the liquid. The proton resonance of solid methane at liquid helium temperature was broad (12 gauss at 30 megacycles/sec). When the solid methane warmed up through its λ transition in the solid state at 20°K, the broad line changed to a narrow line of 1 gauss or less. This result indicated that the solid-state second-order transition was caused by rotation of the hydrogen atom around the carbon and that this degree of freedom allows the internuclear field to average out, thus giving a narrow line. Similar results were found in deuterated methane. Transitions of the λ type in hydrogen chloride at 98.4°K do not show a line-width change and are therefore considered as order-disorder changes. The λ transition in ammonium chloride at −30°C is also considered to be order-disorder from line-width constancy.

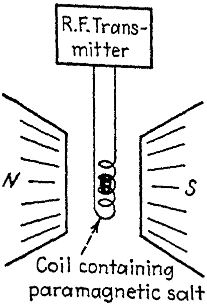

FIG. 8.30. Simple schematic diagram for apparatus in electronic resonance absorption studies.

Paramagnetic Resonance Absorption by Electron Systems. The research by Gorter[2] and coworkers pioneered the subject of absorption of r-f energy by paramagnetic salts. From a most general point of view we can understand the absorption in the experimental arrangement of Fig. 8.30. The paramagnetic salt, such as copper sulfate, is placed in a steady magnetic field $\mathbf{B}_c$, and a r-f coil is used to induce transitions among the energy levels of the electron system. We have seen in the nuclear magnetization that increasing the magnitude of the r-f field $\mathbf{B}_1$ could increase the energy absorbed until the spin system could absorb no more energy. In electron paramagnetism the interaction with the lattice is so strong that relaxation times are very short, for example 10^{-9} sec, and the energy absorbed by the electron spin can be quite large because it feeds over into the lattice at once. Gorter enclosed the salt in a glass bulb which in turn was part of a sensitive constant-volume helium gas thermometer so that small temperature rises of the entire salt could be detected. In the absence of any interactions the external field will act on the electrons to give a set of equally spaced energy levels. There will be just one absorption line. Actually there are many lines, and there is a great deal of interaction. At first this was thought to be the electric field of the lattice on the spin system as we indicated in the discussion of magnetic cooling. Now we must consider each salt as a problem of its own and ask about the symmetry of the electric field, about electron spin interaction, and about nuclear spin interaction. Let us

---

[1] F. Bitter *et al.*, *Phys. Rev.*, **71**, 738, 1947; N. Alpert, *Phys. Rev.*, **72**, 637, 1947.
[2] C. J. Gorter, "Paramagnetic Relaxation," Amsterdam, Elsevier, 1947.

examine the block diagram of the experimental equipment which leads to such information.

Figure 8.31 shows the schematic diagram of the equipment used by Whitmer, Weidner, Hsiang, and Weiss[1] at Rutgers University. The frequency used in the resonance cavity is in the microwave region. A similar apparatus for use at low temperatures was described by Bagguley *et al.*[2] The decrease in the Q of a resonant cavity containing the salt was measured through the reflected power of the magic-T bridge as the steady magnetic field moved through the resonance field value. Figure 8.32 shows the results by Whitmer *et al.*[3] on an ammonium chrom alum single crystal. The principal absorption peak comes at the expected value 3,340 gauss, but we see that the lines are several hundred gauss wide and that there is a multiple structure. We are in an excellent position to grasp the reason for this, because of our careful analysis

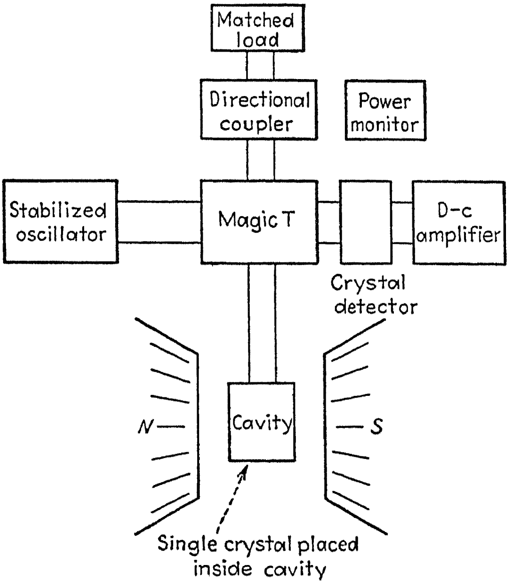

FIG. 8.31. Microwave equipment diagram for electronic resonance absorption.

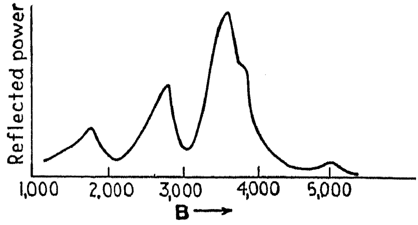

D-c field in gauss applied perpendicular to a (111) face

FIG. 8.32. Output signal vs. magnetic field showing resonance absorption.

---

[1] C. Whitmer *et al.*, *Phys. Rev.*, **74**, 1478, 1948.

[2] D. Bagguley *et al.*, *Proc. Phys. Soc.* (*London*), **61**, 542–551, 1948.

[3] C. Whitmer *et al.*, *Phys. Rev.*, **74**, 1478, 1948.

of the extreme low-temperature behavior of the susceptibility and specific heat of these salts. The electric field of the crystal ions causes a fine splitting of the degenerate states of the order of 0.1 cm^{-1}, and so we understand that with a steady magnetic field applied in the above manner different pairs of levels are brought into the resonance condition. We are thus able independently to obtain the magnitude of the electric field splitting for the zero magnetic field condition. We need to check these observations against the extreme low-temperature results.

TABLE 8.6. Observed and Calculated Magnetic Field Values[a] of the Absorption Maxima for $\nu = 9{,}375$ Mc/sec

The values of δ and of g used for the calculated values are those listed in the table. Spaces marked with an asterisk indicate unresolved peaks.

	$NH_4Cr(SO_4)_2 \cdot 12H_2O$				$KCr(SO_4)_2 \cdot H_2O$			
	Undiluted		Diluted		Undiluted		Diluted	
δ......	0.143 cm^{-1}		0.100 cm^{-1}		0.130 cm^{-1}		0.91 cm^{-1}	
g......	1.99		1.97		1.99		1.98	
H, oersteds	Calc.	Exptl.	Calc.	Exptl.	Calc.	Exptl.	Calc.	Exptl.
(111) axis	1,830	1,830	2,310	2,270	1,990	1,990	2,390	2,450
	2,780	2,720	2,970	2,980	2,840	2,800	3,020	3,020
	3,370	3,370	3,400	3,400	3,370	3,340	3,390	3,380
	3,770	*	3,720	2,710	3,750		3,670	3,670
	4,910	4,920	4,490	4,480	4,760	4,760	4,380	3,450
(110) axis	2,390	2,380	2,740	2,740	2,500	2,530	2,790 }	2,850
	2,630	*	2,860	2,880	2,730	*	2,890 }	
	3,240	3,220	3,330	3,330	3,280	3,240	3,330	3,340
	3,580	3,600	3,500	3,500	3,550	3,600	3,480	3,460
	3,910	*	3,830	3,820	3,850	*	3,790 }	3,850
	4,310	4,190	3,910	3,920	4,070	4,130	3,880 }	
(100) axis	3,120		3,280	3,300	3,170		3,280	3,300
		3,250				3,260		
	3,540		3,480	3,480	3,520		3,450	*

[a] C. Whitmer *et al.*, *Phys. Rev.*, **74**, 1482, 1948.

The work of Bleaney and Penrose[1] indicates that it is necessary to measure the absorption peaks at low temperatures (20°K) in order to obtain the correct zero-field splitting to be used below 0.1°K in the demagnetization experiments. They showed that the splitting value δ in ammonium chrom alum decreases in magnitude from room temperature down to 80°K when an abrupt increase occurs. The experiments of Whitmer, Weidner, Hsiang, and Weiss were carried out at room temperature on single crystals in which three orientations of the d-c field along different crystal axes were used. Their data are summarized in Table 8.6.

---

[1] B. Bleaney and R. Penrose, *Proc. Phys. Soc. (London)*, **60**, 395, 1948.

Penrose and Stevens[1] studied the paramagnetic resonance of a single crystal of nickel fluosilicate. The values of the spectroscopic splitting factor g, together with the energy of separation δ and the temperature T, are given in Table 8.7. The splitting does not agree with the value deduced from specific heat studies by Benzie and Cooke.[2] The lack of agreement is attributed by these last authors to an exchange coupling.

Using centimeter wave length, Bleaney and Ingram[3] have studied the paramagnetic resonance spectra of manganese fluosilicate and manganese ammonium sulfate. The spectra show that the splitting is consistent with a mechanism suggested by Abragam and Pryce.[4] In the absence of an external field the ^6S state is split by the magnetic interaction between the five electrons—a sort of "fine structure." Thus when an external field is applied, the levels are perturbed so that their spacings are not identical. Furthermore each level is split into six levels by the nuclear magnetic interaction—a hyperfine structure. Thus the contribution to the specific heat at temperatures below 1°K does not come purely from a cubic electric field splitting, as formerly supposed. Bleaney and Ingram[5] have studied the resonance and hyperfine structure in a series of cobalt salts. These salts exhibit anisotropy both in the g values and in the hyperfine structure. A tetragonal electric crystal field is used to analyze the results. It turns out that the magnetic entropy of cobalt sulfate must be taken as $R \ln 2$ at 1°K, and the results of Fritz and Giauque[6] are given a new interpretation.

Table 8.7. Paramagnetic Resonance from Nickel Fluosilicate[a]

T, °K	195	90	60	20	14
$g_{\text{parallel}} - g_{\text{perpendicular}}$	2.29	2.26	....	2.29	
δ, cm^{-1}	0.32	0.17	0.14	0.12	0.12

[a] R. P. Penrose and K. W. H. Stevens, *Proc. Phys. Soc. (London)*, **63**, 29, 1950.

With so many interesting experimental results on paramagnetic resonance it is difficult to keep this portion of our discussion of low-temperature physics within bounds. The theory of paramagnetic relaxation and of the resonance line widths in crystals has been studied by Broer,[1] Van Vleck,[2] Wright,[3] and by Pryce and Stevens.[4] We have referred to the work by Abragam and Pryce.[5]

---

[1] R. P. Penrose and K. W. Stevens, *Proc. Phys. Soc. (London)*, **63**, 29, 1950.

[2] R. J. Benzie and A. H. Cooke, *Proc. Phys. Soc. (London)*, **63**, 213, 1950.

[3] B. Bleaney and D. Ingram, *Proc. Roy. Soc. (London)*, **205**, 336, 1951.

[4] A. Abragam and M. Pryce, *Proc. Roy. Soc. (London)*, **205**, 135, 1951.

[5] B. Bleaney and D. Ingram, *Proc. Roy. Soc. (London)*, **208**, 143, 1951.

[6] W. F. Giaque and J. Fritz, *J. Am. Chem. Soc.*, **71**, 2168, 1949.

Diamagnetism of Free Electrons

De Haas-van Alphen Effect. Magnetic studies on metals at low temperatures have brought out some interesting diamagnetic properties. Superconductors are in a special class, and we have discussed the complete diamagnetism which they exhibit. Pure copper has been studied, and the diamagnetism is temperature-independent.[6] Small traces of impurity of a paramagnetic substance can become so important at low temperatures as to cause the diamagnetism of copper to diminish. The most interesting studies have been carried out by de Haas and van Alphen[7] on pure single crystals of bismuth. The diamagnetism shows a peculiar periodiclike dependence on the magnetic field when the temperature is below 20°K (Figs. 8.33*a* and 8.33*b*).

The de Haas-van Alphen effect now appears to be more general and has been found in other diamagnetic metals. Shoenberg[8] and Marcus[9] have studied bismuth crystals. Sydoriak and Robinson[10] reported the effect in zinc at 4.2°K and found that the variation with field is so large as to sometimes swing to paramagnetism. Shoenberg[11] reported that the effect exists in gallium and graphite, while negative results have been obtained with antimony, indium, lead, and mercury in fields up to 9.5 kilogauss and at temperatures down to 1.4°K. The effect in tin fades out between 2 and 4.2°K. Shoenberg[12] has reported that from his work and that by Lazarev the following metals show the de Haas-van Alphen effect: Bi, Zn, Ga, C (graphite), Sb, Al, Hg, Tl, Sn, In, Cd, Be, and Mg. Metals which do not show the effect in fields up to 15,000 gauss and temperatures down to 1.2°K are Pb, Cu, Au, Ge, and Te. All the metals in which the effect has been observed have a complicated electronic structure, and the effect is always highly anisotropic and only occurs along certain crystallographic directions in single crystals (Figs. 8.33*a* and 8.33*b*).

---

[1] L. Broer, *Physica*, **10**, 801, 1943; Thesis, University of Amsterdam, 1945.
[2] J. H. Van Vleck, *Phys. Rev.*, **74**, 1168, 1948.
[3] A. Wright, *Phys. Rev.*, **76**, 1826, 1949; Thesis, Harvard, 1949.
[4] M. Pryce and K. Stevens, *Proc. Phys. Soc. (London)*, **A63**, 36, 1950.
[5] A. Abragam and M. Pryce, *Proc. Roy. Soc. (London)*, **205**, 135, 1951.
[6] F. Bitter and A. Kaufmann, *Phys. Rev.*, **56**, 1044, 1939.
[7] W. de Haas and P. van Alphen, *Commun. Kamerlingh Onnes Lab. Univ. Leiden*, **208d**, **212a**, 1930.
[8] D. Shoenberg, *Proc. Roy. Soc. (London)*, **170**, 341, 1939.
[9] J. Marcus, *Phys. Rev.*, **76**, 413, 1949.
[10] S. Sydoriak and J. Robinson, *Phys. Rev.*, **75**, 118, 1949.
[11] D. Shoenberg, *Nature*, **164**, 225, 1949.
[12] D. Shoenberg, *Trans. Roy. Soc. (London)*, **245**, 1, 1952.

Theory of Diamagnetism of Free Electrons. The magnetic field energy density is $\mathbf{B}^2/2\mu$, and this is divided in two parts by the relationship

$$\mathbf{B} = \mu_0(\mathbf{H} + \mathbf{M}) \tag{8.85}$$

The first part is the magnetic energy density of the space without the system of electrons, $\mu_0\mathbf{H}^2/2$, and the second part is the energy of the system per unit volume:

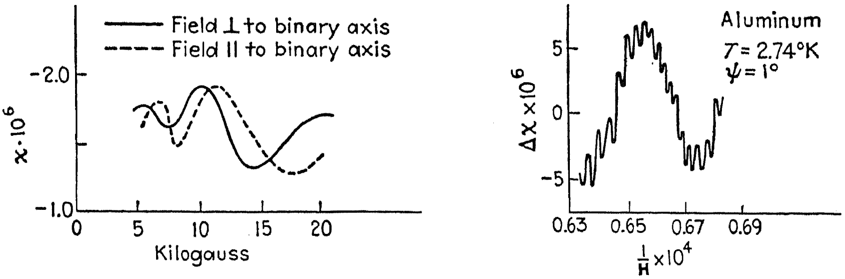

(*a*) (*b*)

FIG. 8.33. (*a*) Diamagnetic susceptibility vs. magnetic field for bismuth. Temperature, 14.8°K. (*b*) Diamagnetic anisotropy in aluminum.

$$\int \mathbf{H}\, d\mathbf{M}$$

In other words, we may use thermodynamics in which we write the energy conservation as

$$dQ = dU - \mathbf{H}\, d\mathbf{M} \tag{8.86}$$

The familiar laws of thermodynamics for a gaseous system can be taken over by replacing equations containing P by the field $\mathbf{H}$ and by replacing V by $\mathbf{M}$. The vacuum energy density $\mu_0\mathbf{H}^2/2$ does not belong to the system of electrons. The magnetization may be computed from the Helmholtz potential

$$\mathbf{M} = -\left(\frac{\partial A}{\partial \mathbf{H}}\right)_{T,V} \tag{8.87}$$

In order to calculate the Helmholtz potential we must form the partition function. The partition function may be formed by direct summation over the energy levels where we must calculate the energy levels from the Schrödinger equation for the system of electrons in a magnetic field. One therefore considers a system of large but finite volume, and one is forced to consider the influence of the boundary of the system.

Following the method of Van Vleck,[1] the Schrödinger equation is written in cylindrical coordinates r, z, θ and separated as

$$\Psi = \Omega(z)\psi(r,\theta) \tag{8.88}$$

The component z with energy E_1 can be neglected because with the magnetic field applied in this direction there is no force on the electron in this dimension. The energy $E_2 = (E - E_1)$ remaining for the motion in r, θ gives (in gaussian units)

$$-\frac{\hbar^2}{2m}\left(\frac{\partial^2\psi}{\partial r^2} + \frac{1}{r}\frac{\partial\psi}{\partial r} + \frac{1}{r^2}\frac{\partial^2\psi}{\partial\theta^2}\right) + \frac{\hbar e\mathbf{H}}{2mic}\frac{\partial\psi}{\partial\theta} + \left(\frac{\mathbf{H}^2e^2r^2}{8mc^2} - E_2\right)\psi = 0 \tag{8.89}$$

We assume a solution

$$\psi(r,\theta) = e^{in\theta}f(r) \tag{8.90}$$

Then $f(r)$ satisfies the equation

$$\frac{d^2f}{dr^2} + \frac{1}{r}\frac{df}{dr} + \frac{2m}{\hbar^2}\left(E_2 - \frac{e\hbar n\mathbf{H}}{2mc} - \frac{e^2\mathbf{H}^2r^2}{8mc^2} - \frac{\hbar^2 n}{2mr^2}\right)f = 0 \tag{8.91}$$

In this last equation the values of $n = 0, \pm 1, \pm 2$, etc., because the function in θ is periodic. This last equation is that of a two-dimensional oscillator of frequency:

$$\nu = \frac{e\mathbf{H}}{2\pi mc} \tag{8.92}$$

Now the quantum theory allows the linear oscillator to have the energy values

$$E_n = \left(n + \frac{1}{2}\right)h\nu = \left(n + \frac{1}{2}\right)h\frac{e\mathbf{H}}{2\pi mc} \tag{8.93}$$

We may regard the two-dimensional oscillator to be made up of two linear oscillators at right angles to one another. The total energy is the sum of the two oscillators, and we may add to this the kinetic energy in the z direction:

$$E = 2\beta_0\mathbf{H}\left(n + \frac{1}{2}\right) + \frac{p_z^2}{2m} \tag{8.94}$$

The last expression is to be summed over all states. β_0 is the Bohr magneton in cgs. units, 0.912×10^{-20}.

The degenerate electron gas has the Fermi-Dirac distribution so that the Helmholtz potential is given by

$$A = NE_0 - 2kT\sum_n \ln\left(1 + e^{-(E_n - E_0)/kT}\right) \tag{8.95}$$

---

[1] J. H. Van Vleck, "Electric and Magnetic Susceptibility," p. 353, London, Oxford, 1932.

In this equation N is the total number of electrons, n one of the possible states of motion, and E_n the energy for state n. The energy E_0 is the Fermi energy level and is determined by the condition

$$N = 2 \sum_n \frac{1}{e^{(E_n - E_0)/kT} + 1} \tag{8.96}$$

The factor 2 accounts for the spin of the electron, *i.e.*, the two possible orientations of spin in an applied magnetic field.

Attempts have been made to compute the Helmholtz potential by integrating. Such a method requires the number of states of motion per unit volume $g(E,\mathbf{H})$ which have energy below E_n. For a piece of metal whose volume is V, length L, and cross-sectional area D, there are $2L(2mE_n)^{\frac{1}{2}}/h$ translational states, and there are $eD\mathbf{H}/2\pi\hbar c$ states of the orbital motion. Blackman[1] has obtained

$$g(E,\mathbf{H}) = \frac{e\mathbf{H}(2m)^{\frac{1}{2}}V}{\pi^2\hbar^2 c} \sum_n [E - (2n + 1)\beta_0\mathbf{H}]^{\frac{1}{2}} \tag{8.97}$$

The Helmholtz potential is then

$$A = NE_0 - kTV \int_{-\infty}^{\infty} \frac{dg}{dE} \ln\left(1 + e^{-(E_n - E_0)/kT}\right) dE \tag{8.98}$$

This last equation has been expressed by Mott and Jones[2] as

$$A = NE_0 - \frac{8\pi m}{h^3}\beta_0\mathbf{H}kT \sum_{n=0}^{\infty} \int_{-\infty}^{\infty} \ln\left(1 \pm e^{\frac{[E_0 - 2\beta_0\mathbf{H}(n+\frac{1}{2}) - (pz^2/2m)]}{kt}}\right) dp_z \tag{8.99}$$

The first terms are

$$A = NE_0 - \frac{16\pi(2m)^{\frac{3}{2}}E_0^{\frac{5}{2}}}{15h^3} + \frac{2\pi(2m)^{\frac{3}{2}}E_0^{\frac{1}{2}}(\beta_0\mathbf{H})^2}{3h^3} \tag{8.100}$$

The magnetization is then to this approximation:

$$\mathbf{M} = -\frac{4\pi}{3h^3}(2m)^{\frac{3}{2}}E_0^{\frac{1}{2}}\beta_0^2\mathbf{H} \tag{8.101}$$

The value of E_0 is put equal to its value in zero field, and at very low temperatures

$$E_0 = \frac{h^2}{2m}\left(\frac{3N}{8\pi}\right)^{\frac{2}{3}} \tag{8.102}$$

The magnetic susceptibility is then

$$\chi = \left(\frac{d\mathbf{M}}{d\mathbf{H}}\right)_{H=0} = -\frac{4\pi m}{3h^2}\left(\frac{3N}{\pi}\right)^{\frac{1}{3}}\beta_0^2 \tag{8.103}$$

---

[1] M. Blackman, *Proc. Roy. Soc. (London)*, **166**, 1, 1938.

[2] N. Mott and H. Jones, "Properties of Metals and Alloys," p. 205, London, Oxford, 1936.

The last expression was first given by L. Landau and in numerical form becomes

$$\chi = -0.623 n_0^{\frac{1}{3}} \rho^{-\frac{1}{3}} A^{-\frac{1}{3}} \times 10^{-6} \text{ cgs units} \tag{8.104}$$

where n_0 is the number of free electrons per atom in the metal, ρ is the density, and A the atomic weight. Thus the total contribution to magnetic susceptibility by free electrons is very small with such a theory. The extension of the above theory to account for the de Haas-van Alphen effect has been made by L. Landau,[1] and it appears in the appendix of a paper by D. Shoenberg.

Recently Sondheimer and Wilson[2] have given a new formulation of the Landau result, and we shall briefly examine their derivation. In Chap. 3 we used Slater's result that the sum over states may be replaced by an integration over configuration space.

$$Z = \sum_n e^{-E_n/kT} \tag{8.105}$$

$$Z = \int \left[\sum_n |\psi_n(q_1 \cdots q_N)|^2 e^{-E_n/kT} \right] dq_1\, dq_N \tag{8.106}$$

We saw in Chap. 3 that repeated operation of the Hamiltonian operator on the Schrödinger wave function allowed us to write

$$Z = \sum_n e^{-E_n/kT} = \sum_n \int \psi_n^*(r) e^{-H/kT} \psi_n(r)\, d\tau \tag{8.107}$$

We now have the partition function represented with the density matrix:

$$Z = \int \Psi(r,r,\gamma)\, d\tau \tag{8.108}$$

where by writing $\gamma = 1/kT$ we have defined the function

$$\Psi(r',r,\gamma) = \sum_n \psi_n(r')^* e^{-\gamma H} \psi_n(r) \tag{8.109}$$

Sondheimer and Wilson show that, if we differentiate the density matrix, we have

$$-\frac{\partial \Psi}{\partial \gamma} = H\Psi \tag{8.110}$$

We must seek a solution of this differential equation. Introducing cylindrical polar coordinates (ρ,ϕ,z) and the vector potential of the magnetic field $(0,\mathbf{H}\rho/2,0)$, we write the equation

$$\frac{\partial \Psi}{\partial \gamma} = \left[\frac{h^2}{8\pi^2 m} \left(\frac{\partial}{\partial \rho^2} + \frac{1}{\rho}\frac{\partial}{\partial \rho} + \frac{1}{\rho^2}\frac{\partial^2}{\partial \phi^2} + \frac{\partial^2}{\partial z^2} \right) - \frac{eh\mathbf{H}}{4\pi i m c}\frac{\partial}{\partial \phi} - \frac{e^2\mathbf{H}^2}{8mc^2}\rho^2 \right] \Psi \tag{8.111}$$

---

[1] L. Landau, *Proc. Roy. Soc. (London)*, **170**, 341, 1939.

[2] E. Sondheimer and A. H. Wilson, *Proc. Roy. Soc. (London)*, **210**, 173, 1951.

Standard procedures are followed on solving the equation. This leads to a partition function per unit volume which is

$$Z = \Psi(r,r,\gamma) = \left(\frac{2\pi m}{h^2\gamma}\right)^{\frac{3}{2}} \frac{\beta_0\mathbf{H}\gamma}{\sinh \beta_0\mathbf{H}\gamma} \tag{8.112}$$

where β_0 is the Bohr magneton $eh/4\pi mc$. Sondheimer and Wilson use the above Z function in the Fermi-Dirac statistics and obtain Landau's result for the magnetic moment per unit volume:

$$\mathbf{M} = \frac{8\pi m^{\frac{3}{2}}\beta_0^2(2E_0)^{\frac{1}{2}}\mathbf{H}}{3h^3}\left\{1 + \frac{3\pi kT}{\beta_0\mathbf{H}}\left(\frac{E_0}{\beta_0\mathbf{H}}\right)^{\frac{1}{2}}\sum_{r=1}^{\infty} \cdot \frac{(-1)^r \sin\left[(r\pi E_0/\beta_0\mathbf{H}) - (\pi/4)\right]}{r^{\frac{1}{2}} \sinh\,(r\pi^2kT/\beta_0\mathbf{H})}\right\} \tag{8.113}$$

The periodic field dependence of the susceptibility at low temperatures seems to be contained in the result. It is remarkable that no knowledge of the energy levels is required and that no complicated arguments involving boundary electrons are necessary.

CHAPTER 9

THERMAL ENERGY IN THE SOLID STATE AT LOW TEMPERATURES

In this chapter we shall consider the thermal energy in the solid state with particular emphasis on the low-temperature region. The specific heat C_p plotted against temperature T is the measured quantity, and this is processed to obtain entropy and free energy. These values are then compared with theoretical calculations concerning the motion within the solid. We have already considered some of these. In the last chapter we saw how electronic spin systems could contribute to most of the thermal energy at temperatures below 1°K. In the discussion of nuclear resonance in solids, particularly solid hydrogen, we saw the evidence for molecular rotation. We shall discuss the specific heat evidence for this in later paragraphs. In metallic conductors the free electrons contribute an observable thermal energy at low temperatures. We saw how this was particularly true for superconductors. We shall begin this chapter with a brief review of the physical ideas behind the theory of lattice vibration and of electronic thermal energy in the solid state. Then we shall examine some typical experimental results.

Lattice Vibration

Consider a solid which is made up of identical atoms regularly spaced to form a single crystal. Suppose now that we have this crystal very close to the absolute zero of temperature. The three-dimensional array of atoms may be thought of as being linked together through bonds to nearest neighbors and through weaker bonds to next-nearest neighbors. As a simple mechanical model we may consider each atom as a mass point joined by a spring to its nearest neighbors. Figure 9.1 is a one-dimensional model of such a crystal. A simple Hooke law of force would be an oversimplification, since we know that with rise in temperature the crystal expands. For this reason the potential energy of binding must have a steeper slope when the atoms approach than when they separate from their equilibrium position.

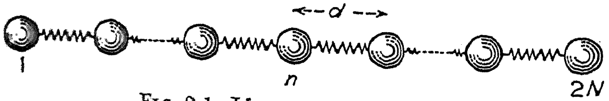

FIG. 9.1. Linear array of atoms.

Now consider what happens to this system as energy is fed into the possible modes of motion. The simple atomic model suggests treating the array of $2N$ atoms like a string of length L held clamped at each end. The elastic waves traverse the length and reflect at the boundary, and they may be described with modes determined by the standing waves (see Fig. 9.2). If the wave velocity is c and the frequency of a normal mode is $\nu_n = nc/2L$, then the amplitude is given by the series sum

$$y = \sum_{n=1}^{\infty} A_n \sin \frac{n\pi x}{L} \cos \left(\frac{n\pi ct}{L} - \phi_n \right) \tag{9.1}$$

The energy is the sum of the energy in each mode:

$$E = \sum_{n=1}^{\infty} \left(\frac{\pi nc}{L} \right)^2 A_n^2 \tag{9.2}$$

But our mechanical model is not a continuum, and the ends are not clamped down. The oversimplification turns out to be not too bad, and the well-known theory of Debye[1] follows from this physical concept of the solid state. We shall not reproduce Debye's theory in detail, as this is to be found in many texts. The equations from the Debye theory are sometimes used by experimenters to extrapolate their results to the absolute zero of temperature. More often they are used for assignment of some portion of the observed specific heat to lattice vibration, and the remainder is then assigned to other causes or is denoted as an anomaly.

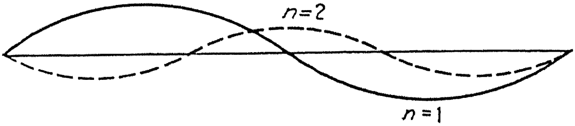

FIG. 9.2. Characteristic modes of a flexible string.

The energy stored in the mode of motion whose frequency is ν appears as a function of the temperature according to quantum statistics:

$$E(\nu) = \frac{1}{2} h\nu + \frac{h\nu}{e^{h\nu/kT} - 1} \tag{9.3}$$

The number of normal modes of the crystal between ν and $\nu + d\nu$ is described by $f(\nu)\, d\nu$ such that the total number adds up to the number of degrees of freedom. If there are $3N$ degrees of freedom, we must have an upper limit to the integral

$$\int f(\nu)\, d\nu = 3N \tag{9.4}$$

---

[1] P. Debye, *Ann. Physik*, **39**, 789, 1912.

The bounded three-dimensional continuum of volume V gives

$$f(\nu)\,d\nu = BV\nu^2\,d\nu \tag{9.5}$$

where

$$B = 4\pi\left(\frac{1}{c_L^3} + \frac{2}{c_t^3}\right) \tag{9.6}$$

and where the symbols c_L, c_t are the wave velocities of longitudinal and transverse waves. The elastic waves are part longitudinal and part transverse. The transverse wave has a plane of polarization, and this may be determined by resolving the amplitude along two mutually perpendicular directions; hence the factor 2 in the above equation.

The total internal energy in the crystal is then

$$U = \int f(\nu)E(\nu)\,d\nu = BV\int_0^{\nu_D} \nu^2 E(\nu)\,d\nu \tag{9.7}$$

where $\nu_D^3 = 9N/BV$ and where ν_D represents the upper limit of integration. Introducing a characteristic temperature θ_D such that $k\theta_D = h\nu_D$, one has the following useful formulas for the specific heat at constant volume for the low-temperature region:

$$C_v = \left(\frac{dU}{dT}\right)_v = 233.82Nk\left(\frac{T}{\theta_D}\right)^3 \quad \text{ergs/(°K)(g-atom)} \tag{9.8}$$

or

$$C_v = 464.5\left(\frac{T}{\theta_D}\right)^3 \quad \text{cal/(°K)(g-atom)} \tag{9.9}$$

The velocity of the waves through the solid depends upon the interatomic binding and at very low temperatures becomes nearly constant. Thus the value of B may be expected to remain constant, and likewise θ_D should remain constant in the very low-temperature region. Ultrasonic pulse methods have given these velocities as a direct function of temperature, and they do not change at low temperatures.[1] Before these electronic methods the sound velocities were computed from the density ρ, the adiabatic compressibility K, and the sheer modulus μ:

$$c_L^2 = \frac{K + (\frac{4}{3})\mu}{\rho} \tag{9.10a}$$

and

$$c_t^2 = \frac{\mu}{\rho} \tag{9.10b}$$

These relations are for an isotropic medium, which is of course the model of the Debye theory in any case. These parameters tend to remain constant as $T \to 0$°K.

---

[1] J. Galt, *Phys. Rev.*, **73**, 1460, 1948; W. Overton and R. Swim, *Phys. Rev.*, **84**, 758, 1951.

We return now to the one-dimensional array of atoms shown in Fig. 9.1 and examine the mechanics of these coupled oscillators. For the one-dimensional array, the equation of motion of the nth atom is

$$m\ddot{\xi}_n + \alpha[(\xi_{n+1} - \xi_n) - (\xi_n - \xi_{n-1})] = 0 \tag{9.11a}$$

or

$$m\ddot{\xi}_n + \alpha(2\xi_n - \xi_{n+1} - \xi_{n-1}) = 0 \tag{9.11b}$$

where ξ is the particle displacement, m the mass, α the force constant of the interatomic "spring" or bond. If we restrict ourselves to low temperatures, the force constant may be considered independent of temperature. The solution of the above equation is a wave which is periodic:

$$\xi_n = Ae^{i\omega(t+nd/v)} = Ae^{i(\omega t+2\pi nd/\lambda)} \tag{9.12a}$$

or

$$\xi_n = Ae^{i(\omega t+np/N)} \tag{9.12b}$$

where the integer

$$-N < p \leq N$$

Substitution into the equation of motion gives the necessary conditions on the frequency:

$$\nu^2 = \frac{\alpha}{\pi^2 m}\left(1 - \cos\frac{\pi p}{N}\right) = \frac{\alpha}{\pi^2 m}\sin^2\frac{\pi p}{2N} \tag{9.13}$$

Putting the quantity

$$\nu_0^2 = \frac{\alpha}{\pi^2 m} \tag{9.14}$$

we may write

$$\nu^2 = \nu_0^2 \sin^2\frac{\pi p}{2N} \tag{9.15}$$

Solving for the integer p gives

$$p = \frac{2N}{\pi}\sin^{-1}\frac{\nu}{\nu_0} \tag{9.16}$$

which is plotted in Fig. 9.3. This theory means that the allowed frequencies are equal in pairs for equal positive and negative values of p. The system acts as a mechanical low-pass filter with a sharp cutoff of all frequencies above ν_0. The system is formally identical to acoustic and electrical filter networks (see L. Brillouin[1]).

M. Blackman[2] examined the meaning of the maximum allowed frequency ν_0 as compared with the continuum theory ν_D. The number of frequencies between ν and $\nu + d\nu$ is

$$f(\nu)\,d\nu = \frac{4N}{\pi}\,d\left(\sin^{-1}\frac{\nu}{\nu_0}\right) = \frac{4N}{\pi\nu_0}\,\frac{d\nu}{(1 - \nu^2/\nu_0^2)^{\frac{1}{2}}} \tag{9.17}$$

---

[1] L. Brillouin, "Wave Propagation in Periodic Structures," New York, McGraw-Hill, 1946.

[2] M. Blackman, *Proc. Roy. Soc.* (*London*), **148**, 384, 1935.

For small values of ν/ν_0 this reduces to $4N\,d\nu/\pi\nu_0$ corresponding to the linear continuum. We must choose an upper limit to the integral of ν_D in order to get the number of degrees of freedom:

$$2N = \int_0^{\nu_D} 4N \frac{d\nu}{\pi\nu_0} \tag{9.18}$$

The upper limit is

$$\nu_D = \frac{\pi\nu_0}{2} \tag{9.19}$$

The distribution for the frequencies of the real one-dimensional lattice shows a heaping up of vibrations near the maximum frequency ν_0.

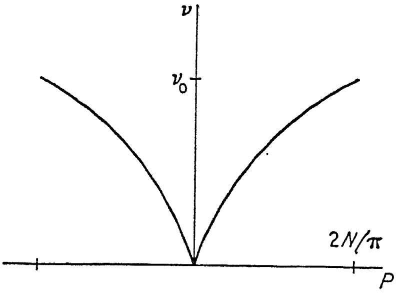

FIG. 9.3. Allowed frequencies of linear array of atoms.

J. Slater[1] considered the one-dimensional system made up of diatomic molecules, as shown in Fig. 9.4. The atoms have masses m and m' with distances d and d'. The force constants are α for interaction between atoms in different molecules and α' for atoms in the same molecule. The equations of motion are

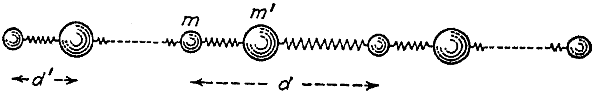

FIG. 9.4. Linear array of molecules.

$$m\ddot{\xi}_n = -\alpha(\xi_n - \xi'_{n-1}) - \alpha'(\xi_n - \xi'_n) \tag{9.20a}$$
$$m'\ddot{\xi}'_n = -\alpha(\xi'_n - \xi_{n+1}) - \alpha'(\xi'_n - \xi_n) \tag{9.20b}$$

We consider periodic solutions:

$$\xi_n = Ae^{i(\omega t+\pi pn/N)} \tag{9.21a}$$
$$\xi'_n = A'e^{i(\omega t+\pi pn/N)} \tag{9.21b}$$

Substitution gives the pair of equations

$$(\alpha + \alpha' - m\omega^2)A - (\alpha' + \alpha e^{-i\pi p/N})A' = 0 \tag{9.22a}$$
$$-(\alpha e^{i\pi p/N} + \alpha')A + (\alpha + \alpha' - m'\omega^2)A' = 0 \tag{9.22b}$$

The secular equation is

$$\begin{vmatrix} \alpha + \alpha' - m\omega^2 & -\alpha' - \alpha e^{i\pi p/N} \\ -\alpha e^{i\pi p/N} - \alpha' & \alpha + \alpha' - m'\omega^2 \end{vmatrix} = 0 \tag{9.23}$$

and the expansion of this equation allows the frequencies to be computed:

---

[1] J. Slater, "Introduction to Chemical Physics," Chap. XV, New York, McGraw-Hill, 1939.

$$\omega^2 = \frac{m + m'}{mm'}\left(\frac{\alpha + \alpha'}{2}\right) \pm \sqrt{\left[\left(\frac{m + m'}{mm'}\right)\left(\frac{\alpha + \alpha'}{2}\right)\right]^2 - \frac{4\alpha\alpha'}{mm'}\sin^2\frac{\pi p}{2N}} \qquad (9.24)$$

where $\omega = 2\pi\nu$ relates frequency to angular velocity. This last equation shows that for the one-dimensional model there is an upper and lower branch of allowed frequencies. The filter action of this mechanical array is like a band-stop filter for electrical networks. The continuum theory for $f(\nu)\,d\nu$ would be quite inadequate for such an array of molecules.

Blackman[1] has examined the two-dimensional array, using force constants α and β along the rows and across the diagonal, respectively. The frequency spectrum has two branches, and the density function is quite complicated. These interesting studies grew out of the classic work by Max Born and Th. von Kármán.[2]

There have been some recent attempts at handling the formidable problem of the three-dimensional array and at establishing a distribution function which could be evaluated. W. V. Houston and his students[3] have devised methods of approximation which permit numerical evaluation. In these works the equations of motion are transformed to normal coordinates resulting in a set of $3N$ equations, where N is the number of different types of atoms included in the basic crystal cell. The secular determinant can be solved for the allowed frequencies in terms of the wave propagation vectors of the first Brillouin zone of reciprocal lattice space. The results indicate a serious deviation from the continuum theory because of the piling up of oscillators about certain characteristic frequencies. In concluding these remarks about crystals, we call attention to the theoretical analysis by E. Montroll[4] on this subject of normal vibrations in crystal lattices.

The Difference $C_p - C_v$ for Solids

Experiment on the specific heat of a solid gives the value of C_p, and at very low temperatures this may be taken equal to C_v. As the temperature increases, the expansion of the crystal no longer permits the difference $C_p - C_v$ to be neglected. From thermodynamics we may show that, so long as the equation of state of the solid may be expressed as $P = P(V,T)$, then

$$C_p - C_v = \frac{-T(\partial V/\partial T)_p^2}{(\partial V/\partial p)_T} \qquad (9.25)$$

---

[1] M. Blackman, *Proc. Roy. Soc. (London)*, **159**, 416, 1937.

[2] M. Born and Th. von Kármán, *Physik, Z.*, **13**, 297, 1912; *ibid.*, **14**, 15, 1913.

[3] W. V. Houston, *Revs. Mod. Phys.*, **20**, 161, 1948; *Z. Naturforsch*, **36**, 607, 1948; P. C. Fine, *Phys. Rev.*, **56**, 355, 1939; R. Leighton, *Revs. Mod. Phys.*, **20**, 167, 1945.

[4] E. Montroll, *J. Chem. Phys.*, **10**, 218, 1942; *ibid.*, **11**, 481, 1943; *ibid.*, **12**, 98, 1944.

We define the following coefficients for a solid:

$$\alpha = \frac{1}{V}\left(\frac{\partial V}{\partial T}\right)_P \qquad \text{expansion at constant pressure} \qquad (9.26)$$

$$\chi = -\frac{1}{V}\left(\frac{\partial V}{\partial P}\right)_T \qquad \text{compression at constant temperature} \qquad (9.27)$$

Thus we may compute $C_p - C_v$ from the measured values of these coefficients. We obtain

$$C_p - C_v = TV\frac{\alpha^2}{\chi} \qquad (9.28)$$

The values of the coefficients are themselves functions of the temperature. At room temperature the following values illustrate the difference:

Substance	χ, cm^2/dyne	α, °K^{-1}	ρ, g/cc	at wt, g	$C_p - C_v$, cal/°K
Cu	0.72×10^{-12}	0.516×10^{-4}	8.9	63.57	.17
Pb	2.30×10^{-12}	0.864×10^{-4}	11	207.2	.40
W	0.30×10^{-12}	0.13×10^{-4}	18.8	184.0	.036

Electronic Specific Heat at Low Temperature in Metals

The introduction to electron theory of metals is usually made through an analysis of the very small specific heat of the free electrons. It is pointed out that the classical theory for an electron gas would contribute an energy of $3kT/2$ for each electron and hence a specific heat $3R/2$ per mole. In reality such a large contribution to the specific heat is not observed at ordinary temperatures. A plot of energy of the electron U against $3kT/2$, as shown in Fig. 9.5, might then be expected because in this manner the increase of energy with temperature would be slight and the specific heat extremely small. This seems to be the case. Only at quite high temperatures does the assembly of electrons behave like a classical gas. A. Sommerfeld[1] used the quantum statistics of Fermi and Dirac to show that the specific heat of the electron gas in a metal was indeed very small because the energy U_0 at the absolute zero of temperature was so very large. The specific heat for a metal at very low temperatures was given by Professor Sommerfeld as

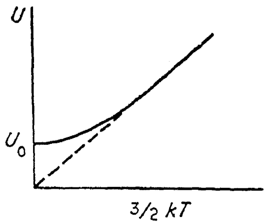

FIG. 9.5. Energy of an electron gas vs. $\frac{3}{2}kT$.

$$C_v = bT^3 + \gamma T \qquad (9.29)$$

---

[1] A. Sommerfeld, P. *Physik*, 47, 1, 1928.

where the first term is the lattice specific heat treated by the continuum approximation and where the linear term is the electronic specific heat. The coefficient is

$$\gamma = \frac{\pi^2 nmk}{h^2}\left(\frac{8\pi V}{3nN}\right)^{\frac{2}{3}} R = 3.26 \times 10^{-5} V^{\frac{2}{3}} n^{\frac{1}{3}} \qquad \text{cal}/{}^\circ\text{K}^2 \tag{9.30}$$

where m is the mass of the electron, V the atomic volume at the temperature considered, n the number of free electrons per atom, N Avogadro's number, and k, h, R the usual constants of physics used in this book. To give an idea of the magnitude of these quantities we quote for silver at 2°K: the lattice specific heat amounts to about 3.7×10^{-4} cal/(°K)(g-atom), and the electronic term at 2°K is about 3.1×10^{-4} cal/(°K)(g-atom). Thus at these very low temperatures the electronic specific heat becomes important. Of course where the metal becomes a superconductor, the electronic contribution has still more terms.

The physical ideas behind the electronic specific heat theory may be briefly stated in the following way. The quantum statistics for electrons require that not more than two electrons occupy the same energy state. Even at the absolute zero of temperature the theory demands that the electrons be distributed over their energy states such that some of the electrons have quite high kinetic energy. The number of electrons dN in a given volume of phase space $d\tau$ is, according to the well-known distribution function,

$$dN = \frac{d\tau}{h^3(e^{(E-A)/kT} + 1)} = \frac{V4\pi p^2/dp}{h^3(e^{(E-A)/kT} + 1)} \tag{9.31}$$

where the momentum ($p = mv$) and the volume (V) of the metal form the space volume. At $T = 0$°K the value of E is still less than A so that $\exp((E - A)/kT) \rightarrow 0$. In this limit

$$dN = \frac{V4\pi p^2\,dp}{h^3} \tag{9.32}$$

We may integrate this last expression to $N = 4\pi p_0^3/3h^3$, where p_0 is the upper limit and where we identify the maximum kinetic energy with the expression

$$A_0 = \frac{p_0^2}{2m} = \left(\frac{3N}{4\pi V}\right)^{\frac{2}{3}} \frac{h^2}{2m} = 148 \text{ kg-cal/g-atom} \tag{9.33}$$

This is not the zero-point energy U_0 of Fig. 9.5. To compute the zero-point energy we consider the energy of an electron $\epsilon = p^2/2m$ and define the momentum space in terms of ϵ to get

$$4\pi p^2\,dp = 4\pi(2m\epsilon)(2m\epsilon)^{-\frac{1}{2}} m\,d\epsilon \tag{9.34}$$

The number of states between ϵ and $\epsilon + d\epsilon$ with the temperature still kept at $T = 0°\text{K}$ is

$$f(\epsilon)\, d\epsilon = \frac{V2\pi(2m)^{\frac{3}{2}}\epsilon^{\frac{1}{2}}\, d\epsilon}{h^3} \tag{9.35}$$

The zero-point energy is then

$$U_0 = \int_0^{A_0} \frac{\epsilon[2\pi V(2m)^{\frac{3}{2}}\epsilon^{\frac{1}{2}}]\, d\epsilon}{h^3} = \frac{3A_0}{5} \tag{9.36}$$

Suppose that in Fig. 9.5 we were to connect the value U_0 with the energy value of classical electron gas by a curve as shown. The curve at the low temperature may fit some power series whose first terms can be shown to be

$$U = U_0 + \left(\frac{df}{d\epsilon}\right)_0 \frac{\pi^2}{6} (kT)^2 + \cdots \tag{9.37}$$

from which the linear specific heat term for an electron gas is determined. By differentiation with respect to temperature the first term is a linear function of temperature as indicated by Eq. (9.29). For an ideal electronic gas, the result is

$$C_e = \frac{N\pi^2 k^2 T}{2A_0} \tag{9.38}$$

A more complete discussion may be found in Mott and Jones.[1]

Some Characteristic Experimental Results on Metals

We shall not attempt to be all-inclusive in a survey of the experimental results on metals. Before we take too seriously any measurement, particularly those showing anomalies, we must ask about the purity and homogeneity of the specimen. No matter how reliable a laboratory from which results are published, it is considered of great value to have an independent check by another laboratory. Unfortunately, this is very difficult to obtain on any physical measurement.

Copper. The specific heat of copper is shown in Fig. 9.6. The specimen had a stated purity of 99.9 per cent, and it was a solid block of electrolytic copper. At low temperature the experimental results fall exactly on a curve consisting of the linear electronic specific heat and on the Debye lattice specific heat with $\theta = 335°\text{K}$. The result at higher temperatures agree with earlier studies by Keesom and Kamerlingh Onnes.[2] From the electrical conductivity the value of θ is 333°K.[3]

---

[1] N. Mott and H. Jones, "Properties of Metals and Alloys," p. 178, London, Oxford, 1936.

[2] W. Keesom and H. Kamerlingh Onnes, *Commun. Kamerlingh Onnes Lab. Univ. Leiden*, **147a**.

[3] *Hand. exp. Physik*, **11**, (2), 51, 1935.

This also agrees with a calculation for θ according to Mott and Jones.[1] The electronic term is only 1.5 times the value computed for a single free 4*s* electron per atom, *i.e.*, for the equation

$$C_e = 1.2 \times 10^{-5}T$$

There are other experiments on the specific heat of copper, and we shall quote those of Dockerty. The following table gives Dockerty's results. In Dockerty's work the copper was a bar of commercially pure cold-rolled material. The thermometers were carefully calibrated against standards, and there is no obvious reason why the value of θ should be different from the value 335°K reported by the Leiden laboratories. One must examine more carefully to determine whether purity alone is enough. The use of a large single crystal might be necessary for complete agreement on specific heats by different laboratories.

SPECIFIC HEAT OF COPPER,[a] cal/(°K)(mole)

T, °K	28.64	59.24	74.64	97.41	131.29	164.71
C_p	0.3475	2.035	2.840	3.743	4.597	5.083
$C_p - C_v$	0.0002	0.004	0.009	0.022	0.044	0.068
θ	314	310.7	312.9	314.9	313.9	312.0

[a] S. Dockerty, *Can. J. Research*, **15A**, 59, 1937.

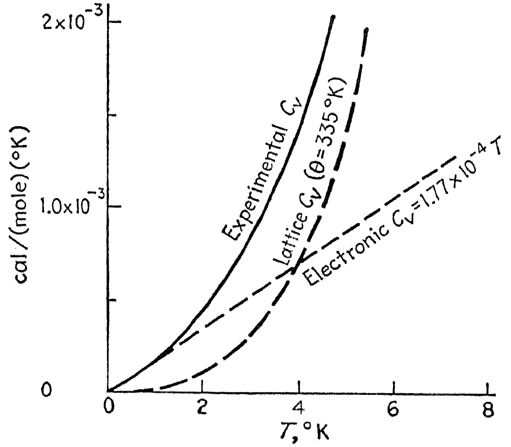

FIG. 9.6. Atomic heat of copper vs. temperature. (*Kok and Keesom, Physica,* 3, 1035, 1936.)

---

[1] N. Mott and H. Jones, "Properties of Metals and Alloys," p. 6, London, Oxford, 1936.

Silver and Gold. For silver and gold Keesom[1] and coworkers obtained the following results. For Ag, $\theta = 215°\text{K}$, and for Au, $\theta = 170°\text{K}$. The electronic terms are decidedly pronounced at temperatures below 3°K and agree with the linear term. For Ag the electronic specific heat is $1.6 \times 10^{-4}T$ cal/(°K)(mole), and for gold it is roughly the same.

Iron, Cobalt, and Nickel. The specific heat of the transition elements Fe, Co, Ni, are most interesting at very low temperatures because they show the effects of the $3d$ energy levels. Both Slater[2] and Mott[3] have explained the very high electronic specific heat found in Ni by Keesom and Clark,[4] in Fe by Keesom and Kurrelmeyer,[5] and in Co by Duyckaerts.[6] The linear term was determined by subtracting from the measured value of C_v the Debye T^3 term caused by lattice vibrations. The results as summarized by Keesom and Kurrelmeyer are given in Table 9.1.

TABLE 9.1. SPECIFIC HEAT COEFFICIENTS AND DEBYE θ[a]

$$C_v = \gamma T + bT^3$$

Metal	γ, cal/(mole) (°K)^2	b, cal/(mole)(°K)^4	θ, °K
Nickel	1.74×10^{-3}	6.60×10^{-6}	413
Copper	0.178	12.90	330
Iron	1.2	4.70	462
Cobalt	1.2	5.36	443
Magnesium	0.325[b]		
Titanium	0.83[b]		
Vanadium	1.4[b]		
Zirconium	0.692[b]		
Chromium	0.374[b]		

[a] W. Keesom and B. Kurrelmeyer, *Physica*, 7, 1003, 1940.

[b] Friedberg, Estermann, and Goldman, *Phys. Rev.*, **85**, 375, 1952.

The very large coefficient in the linear term for the transition elements is interesting. We have seen that the general theoretical expression for the electronic specific heat is

$$C_e = \left(\frac{df}{d\epsilon}\right)\frac{\pi^2}{3}kT = 17.9 \times 10^{-16}\left[\frac{N(E_0)}{n_a}\right]T \qquad \text{cal/(°K)(mole)}$$

where $df/d\epsilon$ is the number of energy levels per unit range, $N(E_0)$ is the number of energy levels per cubic centimeter, and n_a is the number of atoms per cubic centimeter. Now the *d* band in the transition elements is narrow but contains up to ten electrons. Thus the number of energy levels per unit range is very great, and the simple free electron formula is no longer valid.

---

[1] W. Keesom, *Physica*, **1**, 77, 1934; *Commun. Kamerlingh Onnes Lab. Univ. Leiden*, **203d, 219b.**

[2] J. C. Slater, *Phys. Rev.*, **49**, 537, 931, 1936.

[3] N. Mott, *Proc. Roy. Soc. (London)*, **153**, 699, 1936; *ibid.*, **156**, 368, 1936.

[4] W. Keesom and C. Clark, *Physica*, **2**, 513, 1935.

[5] W. Keesom and B. Kurrelmeyer, *Physica*, **6**, 663, 1939.

[6] F. Duyckaerts, *Physica*, **6**, 401, 817, 1939.

Keesom and Kurrelmeyer[1] expected that the value of γ in Table 9.1 would decrease in going from pure nickel through the nickel copper alloy series, until the *s* electrons in copper had filled the "holes" in the *d* band at about 60 per cent copper. Beyond this concentration the value of γ might be expected to be essentially a free electron value. They studied these alloys and also those of iron nickel. The results are given in Table 9.2, and it is evident that experimental agreement with the prediction is not found, *i.e.*, the value of γ does not decrease uniformly with the addition of copper to the nickel.

TABLE 9.2. SPECIFIC HEAT COEFFICIENTS AND DEBYE θ

Alloy with %	γ, cal/(mole) (°K)^2	b, cal/(mole) (°K)^3	θ, °K
$Cu_{20}Ni_{80}$	1.58×10^{-3}	8.11×10^{-6}	386
$Cu_{40}Ni_{60}$	1.52	9.74	363
$Cu_{60}Ni_{40}$	1.66	8.23	384
$Cu_{80}Ni_{20}$	0.457	12.28	335
$Fe_{15}Ni_{85}$	1.16	6.80	409
$Fe_{20}Ni_{80}$	1.08	6.88	407
$Fe_{50}Ni_{50}$	1.21	10.16	358

Palladium and Platinum. The transition elements Pd and Pt have been studied at low temperatures. Pickard and Simon[2] found for Pd the value $\theta = 275°K$ with an electronic term $C_e = 31 \times 10^{-4}\ T$ cal/(°K)(mole). Keesom and Kok[3] give the electronic term for Pt metal at low temperatures as $C_e = 16.1 \times 10^{-4}\ T$. These metals are strongly paramagnetic, and this evidence seems to point to an unfilled *d* band for these metals. Palladium absorbs up to 0.55 hydrogen atoms per atom of palladium, and it has been concluded from the loss of paramagnetism that the hydrogen puts an electron in the empty *d* band.[4]

Specific Heat of Superconductors

Tin. In Chap. 7 we discussed the hump in the specific heat curve for superconductors and indicated the excellent agreement with the thermodynamic prediction by Gorter and Casimir.[5] The results on tin by

---

[1] W. Keesom and B. Kurrelmeyer, *Physica*, **7**, 1003, 1940.

[2] G. Pickard and F. Simon, *Proc. Phys. Soc. (London)*, **61**, 1, 1948.

[3] J. Kok and W. Keesom, *Physica*, **3**, 1035, 1936.

[4] A. Svenson, *Ann. Physik*, **18**, 294, 1933.

[5] C. J. Gorter and H. Casimir, *Physica*, **1**, 306, 1933.

Keesom and Van Laer[1] are typical of many of the other well-behaved superconductors, that is, Pb, Hg, etc. These authors measured the specific heat C_n of tin between 1.1 and 4.0°K while in a magnetic field large enough to destroy superconduction. These values were compared with measurements C_s without a magnetic field and in the superconducting state. The results are shown in Fig. 9.7 and Table 9.3.

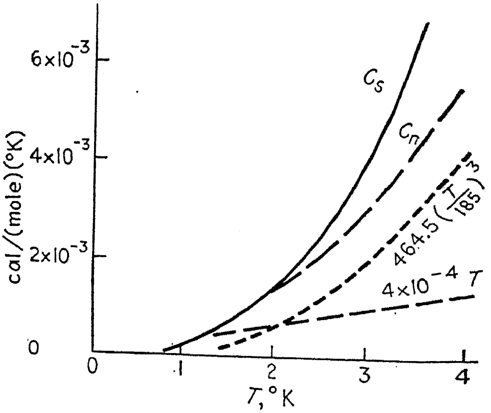

FIG. 9.7. Atomic heat of tin in super and normal state vs. temperature.

TABLE 9.3. SMOOTHED EXPERIMENTAL VALUES OF THE ATOMIC HEAT OF TIN[a]

T, °K	C_s, cal/°K	C_n, cal/°K	$C_s - C_n$, cal/°K
1.0	0.000175	0.000456	−0.000281
1.5	0.000607	0.000848	−0.000241
2.0	0.0146	0.00140	+0.00006
2.5	0.00264	0.00214	+0.00050
3.0	0.00426	0.00319	+0.00107
3.5	0.00680	0.00471	+0.00209
3.72	0.00852	0.00562	+0.00290

[a] W. H. Keesom and P. H. Van Laer, *Physica*, **5**, 193, 1938.

Tantalum. The studies on tantalum by Keesom and Desirant[2] are interesting because they bring out all of the peculiar electronic contributions, *i.e.*, that the metal is a superconductor and is a transition-type element in that the physical properties are influenced by the five electronic states in the d band. The normal state is represented by

$$C_v = 464.5\left(\frac{T}{264.5}\right)^3 + 0.00141T$$

---

[1] W. Keesom and P. Van Laer, *Physica*, **5**, 193, 1938.

[2] W. Keesom and M. Desirant, *Physica*, **8**, 273, 1941.

The superconducting state shows the general thermodynamic features of most superconducting metals, but the specimen in a magnetic field showed some peculiarities in accord with the studies of Mendelssohn and Moore.[1] The purity of the Ta was 99.9 per cent, but the metal is sintered together, and the bad magnetic performance of the specimen, *i.e.*, the absence of the Meissner effect, is probably due to this lack of homogeneity.

Experimental Results on Metals with Anomalous Specific Heats

Tungsten. There are a number of metals whose specific heat has been studied and for which no explanation concerning their anomalous values has been commonly accepted. Tungsten has been studied by Silvidi and Daunt[2] in the liquid helium range of temperature. The specific heat in this range is made up of a T^3 term with $\theta = 169°\text{K}$ and an electronic term, $C_e = 51.1 \times 10^{-4}T$ cal/(°K) (mole). The authors speculate on the very low value of θ and on the high electronic term. The value given for W by Meissner[3] from electrical conductivity studies is $\theta = 333°\text{K}$. P. Fine[4] has made calculations based on $\theta = 367°\text{K}$ in the low-temperature region.

Sodium. The specific heat of sodium has been studied by Pickard and Simon,[5] and earlier studies were made by Simon and Zeidler.[6] The results showing a decided hump at 7°K are given in Table 9.4, with the

TABLE 9.4. ATOMIC HEAT OF SODIUM

T, °K	C_v, cal/(°K) (mole)	θ, °K
2	0.0055	88
3	0.0080	116
4	0.0135	130
5	0.027	129
6	0.059	120
7	0.124	109
8	0.093	137
9	0.100	150
10	0.140	149
12	0.250	147
14	0.385	148
16	0.54	150
18	0.71	152
20	0.90	154
25	1.45	156

---

[1] K. Mendelssohn and J. Moore, *Phil. Mag.*, **21**, 532, 1936.

[2] A. Silvidi and J. Daunt, *Phys. Rev.*, **77**, 125, 1950.

[3] W. Meissner, *Hand. exp. Physik*, **11**, (2), 1935.

[4] P. C. Fine, *Phys. Rev.*, **56**, 355, 1939.

[5] G. Pickard and F. Simon, *Proc. Phys. Soc. (London)*, **61**, 1, 1948.

[6] F. Simon and K. Zeidler, *Z. physik. Chem.*, **A123**, 383, 1926.

θ value required to make theory fit the experiment. The authors believe that the anomaly is too large to be explained by the refinement of the lattice specific heat theory by Blackman and that there is probably some internal transition. Recently MacDonald and Mendelssohn[1] have studied the electrical resistance of pure sodium, as well as of Li, K, Rb, and Cs, and have found no indication of an anomaly in the conductivity of sodium. It is interesting to note that the electrical conductivity yields a value of $\theta = 202°\mathrm{K}$, which is much higher than the caloric value by Simon. Sodium metal is an excellent example of the quasi-free electron model throughout the entire temperature range. Blackman[2] has suggested that electron scattering is caused by longitudinal waves and not by transverse waves; thus the apparent θ from resistance studies should be higher than the true Debye θ.

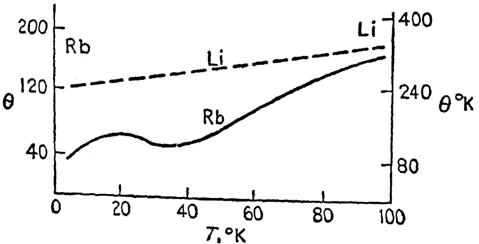

FIG. 9.8. Characteristic Debye θ vs. temperature for Li and Rb.

Lithium. The specific heat of Li has been studied by Simon and Swain[3] from 15 to 300°K, and they found it necessary to allow θ to vary from 420°K at room temperature to a value of $\theta = 340°\mathrm{K}$ at liquid hydrogen temperatures. K. Fuchs[4] has computed the expected variation of θ for Li as the temperature is lowered from the elastic constant theory. Direct measurements would be highly desirable. The electrical resistance studies by MacDonald and Mendelssohn[5] indicate a decided change of θ with temperature for Li, K, Rb, and Cs. Figure 9.8 shows the deviation of θ with temperature for Li and Rb. C. S. Barrett[6] has reported a phase change in Li, showing that it goes from body-centered cubic to hexagonal close-packed on being cooled below 71°K. There is a considerable hysteresis effect in the transition because reversion to the body-centered cubic begins only when the temperature is raised to about 100°K, and an additional 30 or 40 deg is required to complete the reversion. These interesting results by Barrett were made by x-ray diffraction studies, and careful measurements were made on the intensities of the lines.

---

[1] D. MacDonald and K. Mendelssohn, *Proc. Roy. Soc.* (*London*), **202**, 103, 1950

[2] M. Blackman, *Proc. Phys. Soc.* (*London*), **64**, 681, 1951.

[3] F. Simon and Swain, *Z. physik. Chem.* **B28**, 189, 1935.

[4] K. Fuchs, *Proc. Roy. Soc.* (*London*), **153**, 622, 1936; *ibid.*, **157**, 444, 1936.

[5] D. MacDonald and K. Mendelssohn, *Proc. Roy. Soc.* (*London*), **202**, 103, 1950.

[6] C. S. Barrett, "Phase Transitions in Solids," Chap. 13, New York, Wiley, 1951.

Beryllium. The anomalous specific heat in Be at 11°K[1] is interesting because there is no anomaly in the electrical conductivity. W. C. Overton[2] examined the elastic moduli of beryllium by measuring the velocity of longitudinal and transverse ultrasonic waves between 300 and 3°K. Overton observed no change in attenuation or velocity in the region of the specific heat hump and concluded that the mechanism for the anomaly must leave these parameters unaffected within the limits of error.

Rare-earth Elements: Lanthanum, Cerium, Neodymium, and Praseodymium. The atomic heats of the rare-earth elements have been measured from 2 to 180°K by Parkinson, Simon, and Spedding.[3] Figure 9.9 shows the results over a considerable range of temperature. Lanthanum shows an anomaly corresponding to superconductivity at 4.37°K, and the atomic heat shows a $\theta = 140°\text{K}$ which, however, is temperature-dependent. Just before La becomes superconducting, *i.e.*, above 4.4°K, the specific heat obeys the relationship $C_p = 2 \times 10^{-3}T^3 + 1.6 \times 10^{-3}T$.

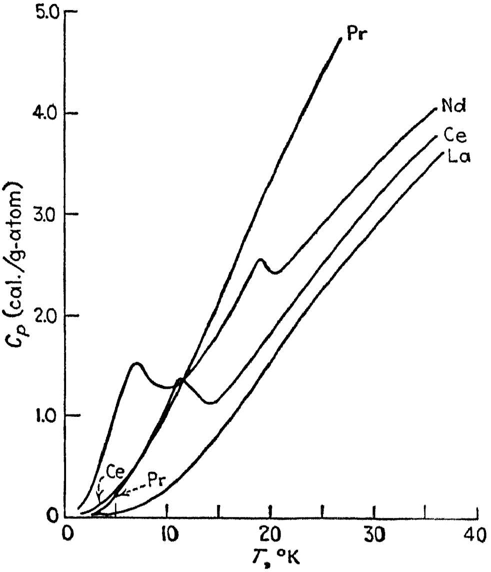

FIG. 9.9. Specific heat C_p vs. temperature for rare-earth elements.

The anomalies in praseodymium and neodymium, together with the low-temperature anomaly in cerium, can be explained qualitatively by the view that the electronic states attributable to the 4*f* electrons are split by the electric fields existing within the metallic crystals. The theory thus far only gives qualitative agreement with experiment.

---

[1] F. Simon *et al.*, *Z. Physik. Chem.*, **B25**, 273, 1934.

[2] W. C. Overton, *J. Chem. Phys.*, **18**, 113, 1950.

[3] D. Parkinson, F. Simon, and F. Spedding, *Proc. Roy. Soc. (London)*, **207**, 137, 1951.

Chromium and Manganese. These two metals are thought to be antiferromagnetic at about 420°K for Cr and at about 100°K for Mn. Evidence came from neutron diffraction studies by C. G. Shull and M. K. Wilkinson.[1] Studies on the specific heat of Cr showed no trace of any anomaly in the work of Weertman, Burk, and Goldman.[2]

Germanium and Hafnium. These two metals are grouped together here for the reason that they once were thought to show anomalies in C_v.[3] Work on Hf by Burk and Darnell[4] showed no anomaly. Work on pure Ge by Estermann and Weertman[5] showed no anomaly. Pure Ge has $\theta = 400°\text{K}$ at $T = 90°\text{K}$ and $\theta = 372$ at $T = 20°\text{K}$ according to these authors.

Specific Heat of Solids with Several Types of Atoms

The simple one-dimensional theory has been discussed with equations where two types of atoms of masses m and m' gave the interesting result that there were two branches to the frequency spectrum. The complete three-dimensional theory would in all likelihood demonstrate the inadequacy of the continuum theory. The theories by Born and his students have been cited, and the calculations on NaCl by Kellerman,[6] as well as those on KCl by Iona,[7] have all demonstrated this inadequacy. The experimental results on solid single crystals of NaCl, KCl, KBr, RbBr, RbI, and LiF by Clusius, Goldmann, and Perlick[8] were carried out in 1934 at Göttingen. Complete tables can be found in their article, and we show in Fig. 9.10 the composite representation of their results on the variation of θ with temperature.

The results on NaCl show a distinct rise in θ at low temperatures in accord with Kellermann's calculation. Clusius *et al.* have compared for NaCl the computed value of θ from elastic constants, $\theta = 292°\text{K}$, from reststrahlen, $\theta = 276°\text{K}$ (Forsterling[9]), and from infrared absorption, $\theta = 235°\text{K}$ (Barnes and Czerny[10]). The frequency distribution computed by Kellermann for NaCl is shown in Fig. 9.11.

---

[1] C. G. Shull and M. K. Wilkinson, *Bull. Am. Phys. Soc.*, **27**, 24, 1952.

[2] J. Weertman, N. Burk, and J. Goldman, *Bull. Am. Phys. Soc.*, **27**, 53, 1952.

[3] F. Simon *et al.*, *Z. Physik. Chem.*, **B25**, 273, 1934.

[4] N. Burk and A. Darnell, *Bull. Am. Phys. Soc.*, **27**, 53, 1952.

[5] I. Estermann and J. Weertman, *Phys. Rev.*, **83**, 228, 1951.

[6] E. Kellerman, *Trans. Roy. Soc. (London)*, **238**, 513, 1940; *Proc. Roy. Soc. (London)*, **178**, 17, 1941.

[7] M. Iona, *Phys. Rev.*, **60**, 822, 1941.

[8] K. Clusius, J. Goldmann, and A. Perlick, *Z. Naturforsch.*, **A4**, 424, 1949.

[9] K. Forsterling, *Ann. Physik*, **61**, 577, 1920.

[10] R. Barnes and M. Czerny, *Z. Physik*, **72**, 447, 1931.

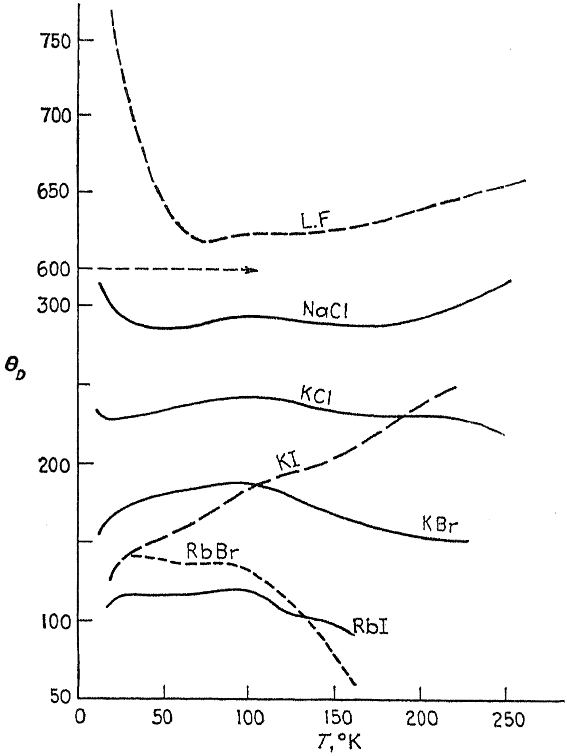

Fig. 9.10. Characteristic Debye θ vs. temperature for alkali halides.

The velocities of propagation of 10 megacycles/sec longitudinal and transverse waves in single crystals of NaCl have been measured over the temperature range from 60 to 300°K by W. C. Overton and R. T. Swim.[1] From these velocities the adiabatic constants have been calculated and are plotted as a function of temperature in Fig. 9.12. The values of these elastic constants extrapolated to absolute zero temperature are in units of dynes/cm^2 $\times 10^{11}$: $c_{11} = 5.750, c_{44} = 1.327$, and $c_{12} = 0.986$. The adiabatic compressibility has been calculated from c_{11} and c_{12} and is 4.07×10^{-12} cm^2/dyne at 300°K. The Debye characteristic temperature is computed to be 292.6°K at $T = 0$°K.

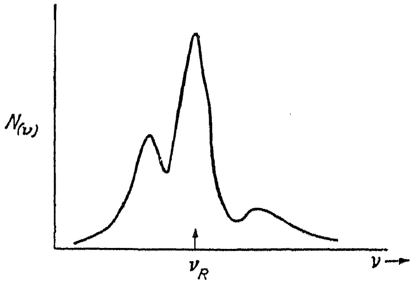

Fig. 9.11. Frequency distribution of NaCl showing residual ray frequency ν_r.

---

[1] W. C. Overton and R. T. Swim, *Phys. Rev.*, **84**, 758, 1951.

J. Galt[1] has measured the elastic constants of NaCl, KBr, and KCl at room temperature. Galt measured KBr down to low temperatures, and his results on c_{11} are shown in Fig. 9.13. The modulus c_{12} was nearly temperature-independent. C. Kittel[2] deduced from Galt's work the values of the compressibility modulus $K = (c_{11} + 2c_{12})/3$ over the temperature range 0 to 300°K where the values join the experimental measurements of Slater.[3] Kittel's results are shown in Fig. 9.14. Kittel was able to compute this curve from other data, namely, the expansion coefficient as a function of temperature and $\theta = 177°K$, which he took from the reststrahlen value.

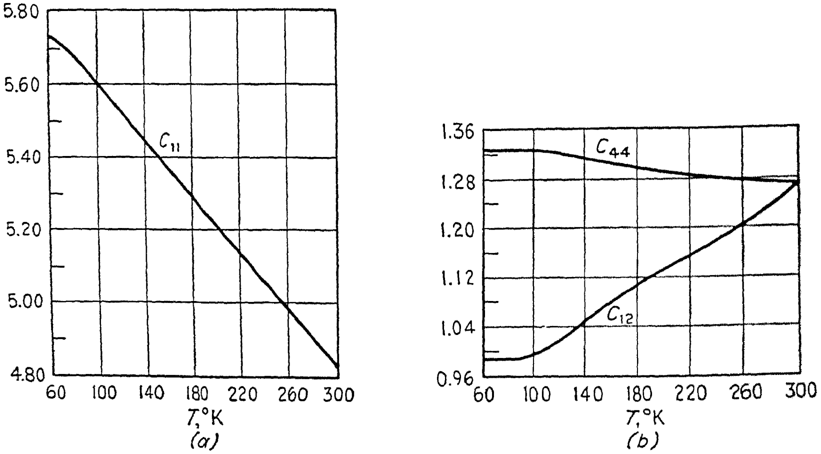

FIG. 9.12. (a) Elastic constant c_{11} of rock salt in units of dynes/cm² × 10^{11}. (b) Elastic constants c_{44} and c_{12} of rock salt in units of dynes/cm² × 10^{11}.

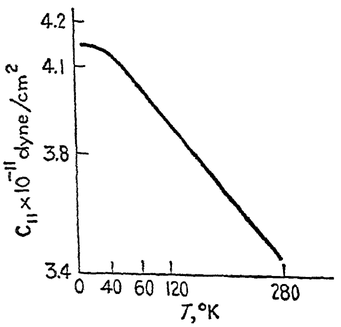

FIG. 9.13. Elastic constant c_{11} of KBr as function of temperature.

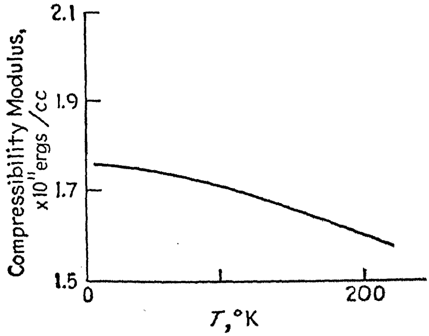

FIG. 9.14. Compressibility modulus of KBr as function of temperature.

---

[1] J. Galt, *Phys. Rev.*, **73**, 1460, 1948.

[2] C. Kittel, *J. Chem. Phys.*, **16**, 850, 1948.

[3] J. Slater, *Phys. Rev.*, **23**, 488, 1924.

The results of Clusius on LiH, KI, etc., are interesting and clearly indicate the need for more experimental information, such as expansion coefficients and elastic moduli.

Rotation of Atoms and Molecules in the Solid State

Hydrogen and Deuterium. L. Pauling[1] was the first to realize the possibility that molecules in the solid state had a transition from libration motions to almost free rotations, *i.e.*, a kind of rotational melting could take place within the solid. This forms the beginning of the general *cooperative phenomena* which will occupy our attention for the remainder of this chapter. At first we shall consider solid hydrogen, and this is because we have seen in Chap. 8 that the nuclear magnetic resonance line width in solid ortho hydrogen (B. Rollin and J. Hatton)[2] clearly demonstrated molecular rotation.

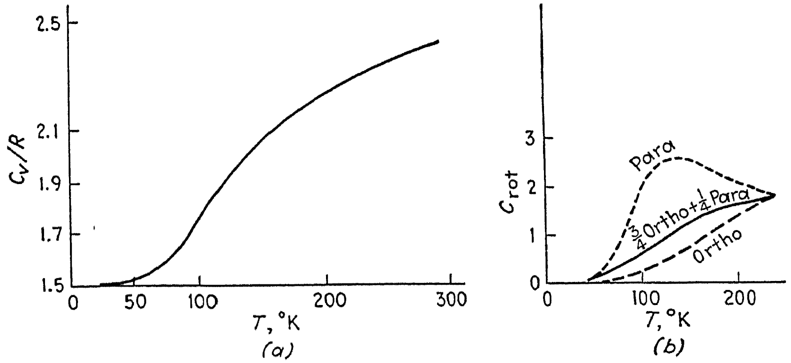

(a) (b)

FIG. 9.15. (*a*) Total specific heat of hydrogen vs. temperature. (*b*) Rotational specific heat of hydrogen vs. temperature.

The hydrogen molecule is an interesting story in the gas phase, and we must start by reviewing the experiment and theory of the gas specific heat. In this way we can understand why there should be rotation in the solid phase. From the work by Eucken and later by Eucken and Hiller[3] and from the research of Clusius, Bartholome, and Hiller[4] the rotational specific heat of ortho and of para hydrogen has been determined. A more detailed account may be found in a book by A. Farkas.[5] We shall be concerned with an explanation of the experimental results given in Figs. 9.15*a* and 9.15*b*.

The quantum theory of the rotational energy states of a diatomic molecule gives

---

[1] L. Pauling, *Phys. Rev.*, **36**, 430, 1930.

[2] B. Rollin and J. Hatton, *Phys. Rev.*, **74**, 346, 1948.

[3] A. Eucken and K. Hiller, *Z. physik. Chem.*, **4**, 142, 1929.

[4] K. Clusius, E. Bartholome, and K. Hiller, *Z. physik. Chem.*, **B30**, 237, 258, 1935.

[5] A. Farkas, "Ortho, Para, and Heavy Hydrogen," London, Cambridge, 1935.

$$E_k = \frac{k(k+1)h^2}{8\pi^2 I} \tag{9.39}$$

where k are quantum numbers 0,1,2, · · · and I is the moment of inertia about the axis of rotation. The partition function is slightly complicated by the $(2k + 1)$-fold degeneracy and is written

$$Z_{\text{rot}} = \sum_k (2k + 1)e^{-k(k+1)h^2/8\pi^2 IkT} \tag{9.40}$$

For hydrogen we must take account of the symmetry properties of the wave functions (Hund[1]), and these are governed by the nuclear spin momentum of each atom. If the two are parallel, the molecule is ortho hydrogen, and if antiparallel, it is para hydrogen. Ordinary hydrogen at room temperature consists of a mixture of ortho and of para in the ratio 3:1. It is experimentally established that the interchange between symmetrical and antisymmetrical states occurs so rarely (in the absence of a catalyst) that the ratio 3:1 remains constant for reasonable times of experimentation. The specific heat then comes from two independent partition functions (Dennison[2]):

$$Z_s = \sum_{k=0,2,4,\cdots} (2k + 1)e^{-E_k/kT} \tag{9.41a}$$

$$Z_a = \sum_{k=1,3,5,\cdots} (2k + 1)e^{-E_k/kT} \tag{9.41b}$$

The specific heat is computed by differentiation of ln Z in the usual way. Theory and experiment are in complete accord, as shown in Figs. 9.15*a* and 9.15*b*. The results on HD and D_2 have been measured by Clusius and Bartholome.[3]

All of this makes it appear that the contribution of the rotational specific heat is negligible below 40°K for ordinary hydrogen. In Fig. 9.16 we show the experimental specific heat of solid hydrogen consisting (*a*) of 100 per cent para and (*b*) of 75 per cent ortho hydrogen measured by Simon, Mendelssohn, and Ruhemann.[4] The solid ortho hydrogen has a very definite hump in the specific heat, reaching a maximum somewhere below 3°K, and from the work of Rollin and Hatton[5] this is around 2°K. The experimental point at 3°K on the para hydrogen (100 per cent) was considered to be above the T^3 curve on the basis of $\theta = 91°\text{K}$ and was attributed to a small ortho-hydrogen impurity. Johnston, Gonzales, and White[1] have reported similar specific heat results for solid deuterium.

---

[1] F. Hund, *Z. Physik*, **42**, 93, 1927.

[2] D. Dennison, *Proc. Roy. Soc. (London)*, **115**, 483, 1927.

[3] K. Clusius and E. Bartholome, *Z. Elektrochem.*, **40**, 524, 1934; *Z. physik. Chem.*, **B29**, 162, 1935; *ibid.*, **B30**, 237, 258, 1935.

[4] F. Simon, K. Mendelssohn, and B. Ruhemann, *Z. physik. Chem.*, **B15**, 121, 1931.

[5] B. Rollin and J. Hatton, *Phys. Rev.*, **74**, 346, 1948.

Giauque and Johnston[2] have calculated the difference in entropy of gaseous hydrogen and crystalline hydrogen from their measurements and find the solid has 4.3 ± 0.1 entropy units more than the lattice motion with characteristic $\theta = 91°\text{K}$ would permit. They attributed this extra entropy to the entropy of mixing of the symmetrical and antisymmetrical hydrogen and to the retention of the statistical degeneracy 9 for the antisymmetrical hydrogen. Pauling[3] assigns the weight 9 to antisymmetrical hydrogen because for $K = 1$ the three rotational characteristic functions can be associated with any one of three spin characteristic functions:

$$S = -\tfrac{1}{4}R \ln \tfrac{1}{4} - \tfrac{3}{4}R \ln \tfrac{3}{4} + \tfrac{3}{4}R \ln 9 + S_{\text{trans.}} = 4.3 \pm 0.1 + S_{\text{trans.}} \qquad (9.42)$$

Thus Pauling[4] obtains agreement with the work of Giauque and Johnston. Similar calculations on deuterium were made by Clusius.[5] According to Pauling at still lower temperatures a separation of the three rotational levels with $K = 1$ will take place. By a cooperative process the hydrogen molecule begins to line up with a preferred axis. Viewed from the location of any one rotating hydrogen molecule, there is a potential field inhibiting the rotation caused by the neighboring molecules. If the neighbors are rotating, the field is symmetric and small; but if they are not rotating or if very few of them are rotating, the potential is larger and not symmetric. Under these latter conditions, the rotation of the molecule in question will indeed be inhibited.

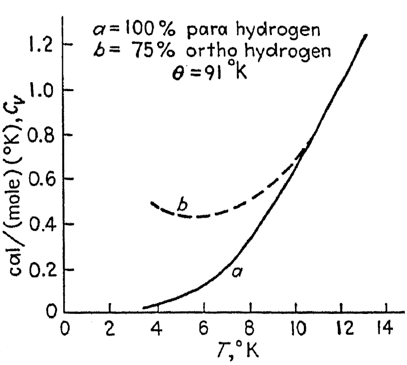

FIG. 9.16. Specific heat of hydrogen at low temperatures. (*Simon, Mendelssohn, and Ruhemann, Z. physik. Chem.*, **B15**, 121, 1931.)

Theory of Cooperative Phenomena. Since Pauling's work, there have appeared some further theoretical considerations which bear on the problem. Frenkel, Todes, and Ismailow[6] have treated the transition of rotation to nonrotation as a sharp process. The work of R. H. Fowler[7] is concerned with the gradual nature of the transition, and we shall now discuss his theory. Fowler has reviewed his own work in his book "Statistical Mechanics."[1] The model assumed by Fowler is the symmetrical rigid rotator without spin about its axis of figure and rotating about its center of mass in a field of potential energy $-W\cos\theta$. The potential field is due to the surrounding molecules, and θ is the angular displacement of the axis of figure from a single preferred direction of equilibrium. The Hamiltonian is

---

[1] H. Johnston, M. Gonzales, and D. White, *Intern. Conf. Phys.*, Oxford, 1951.

[2] W. Giauque and H. Johnston, *J. Am. Chem. Soc.*, **50**, 3221, 1928.

[3] L. Pauling, *Phys. Rev.*, **36**, 430, 1930.

[4] *Ibid.*

[5] K. Clusius, E. Bartholome, and K. Hiller, *Z. physik. Chem.*, **B30**, 237, 258, 1935.

[6] J. Frenkel, I. Todes, and P. Ismailow, *Acta Physicochim. USSR*, **1**, 97, 1934.

[7] R. H. Fowler, *Proc. Roy. Soc. (London)*, **149**, 1, 1935.

$$H = \frac{1}{2I}\left(p_\theta^2 + \frac{p_\phi^2}{\sin^2\theta}\right) - W\cos\theta \tag{9.43}$$

and the partition function for this motion is

$$f(T) = \frac{1}{h^2}\iiiint e^{-H/kT}\,dp_\theta\,dp_\phi\,d\theta\,d\phi \tag{9.44}$$

But now W is not a constant because it depends on the degree of rotation already present among the molecules at the temperature T. To handle this (in approximation) Fowler regards as not rotating all those molecules for which the kinetic energy is

$$\frac{1}{2I}\left(p_\theta^2 + \frac{p_\phi^2}{\sin^2\theta}\right) < \beta W(1+\cos\theta) \tag{9.45}$$

where β is some numerical constant. The fraction of such nonrotating molecules is the ratio of partition functions $f_0(T)/f(T)$ where now

$$f_0(T) = \frac{2\pi}{h^2}\int_0^\pi e^{W\cos\theta/kT}\,d\theta\int_a^\infty e^{\frac{-[p_\theta^2+(p_\phi^2/\sin^2\theta)]}{2IkT}}\,dp_\theta\,dp_\phi \tag{9.46}$$

where the lower limit of integration a is given by

$$a = \left(p_\theta^2 + \frac{p_\phi^2}{\sin^2\theta}\right) < 2I\beta W(1+\cos\theta) \tag{9.47}$$

But before this, the lower limit in momentum was zero in

$$f(T) = \frac{4\pi^2 IkT}{h^2}\int_0^\pi e^{W\cos\theta/kT}\sin\theta\,d\theta = \frac{8\pi^2 IkT}{h^2}\,\frac{kT}{W}\sinh\frac{W}{kT} \tag{9.48}$$

Fowler shows the ratio to be

$$S = \frac{f_0(T)}{f(T)} = 1 - \frac{e^{-\beta W/kT}\sinh[W(1-\beta)/kT]}{(1-\beta)\sinh(W/kT)} \tag{9.49}$$

The assumption is made that the potential $W = SW_0$, which allows the potential to vanish if all the molecules are rotating. With this assumption the fraction of nonrotating molecules is

---

[1] R. H. Fowler, "Statistical Mechanics," 2d ed., London, Cambridge, 1936.

$$S = 1 - \frac{e^{-[\beta S W_0/kT]} \sinh [SW_0(1 - \beta)/kT]}{(1 - \beta) \sinh [SW_0/kT]} \tag{9.50}$$

For any value of the numerical constant β there exists a critical temperature T_c which makes $S \equiv 0$. In the special case $\beta = \frac{1}{2}$, the expression is very simple but does not carry special physical meaning:

$$S = \tanh \frac{SW_0}{2kT} \tag{9.51}$$

Let the roots of the equation for the general ratio S be denoted by S_0 and call the quantity $x = (S_0 W_0/kT)$. The logarithm of the partition function for the N systems of molecules is then written

$$\ln Z = N \ln \frac{8\pi^2 IkT}{h^2} + \int_0^1 g(S) \ln \left(\frac{kT}{SW_0} \sinh \frac{SW_0}{kT} \right) dS \tag{9.52}$$

where $g(S)\,dS$ is the number of systems which are effectively subject to the field, $SW_0 \cos \theta$, and

$$\int_0^1 g(S)\,dS = N \tag{9.53}$$

Taking this number to be simply NS_0 as an approximation, Fowler then obtains the energy and specific heat of hindered rotation:

$$\bar{E}_{rot} = NkT(2 - x \coth x) \tag{9.54}$$

$$C_{rot} = Nk\left(2 - \frac{x^2}{\sinh^2 x}\right) - \frac{NW_0^2}{2kT} \frac{dS_0^2}{dT} \left(\frac{\cosh x \sinh x - x}{x \sinh^2 x} \right) \tag{9.55}$$

Such an expression is full of approximations and still leaves the numerical constant β to be chosen. But it does contain the possible theory of a specific heat shaped like a λ transition, and it does contain the outline of a program for further investigation. Indeed, Fowler did generalize his conceptions beyond what is presented here.

These theoretical concepts were started with the idea of explaining the properties of hydrogen, and we shall presently take up some other examples to which the theory may well be applicable. To complete the account of the solid hydrogen we give a few more details from experiment. Megaw[1] determined the density of solid hydrogen and deuterium at 4.2°K and at pressures up to 100 atm. Clusius and Bartholome obtained values at the triple point for H_2 and D_2. Table 9.5 gives their results. Megaw considered the specific heat results in terms of the continuum theory of Debye and of Gruneisen's relationship. She concluded that such theories do not apply to solid hydrogen and pointed to the large zero-point energy. It would indeed be hard to understand how the lattice specific heat theory with $\theta = 91°K$ for H_2 and $\theta = 89°K$ for D_2 could be taken seriously. Bartholome and Eucken[1] have directly measured the specific heat at constant volume of H_2 and D_2 and found the characteristic temperature $\theta = 105°K$ and $\theta = 97°K$, respectively. At 11°K the experimental points are above the theoretical curve.

---

[1] H. D. Megaw, *Phil. Mag.*, **28**, 129, 1939.

Table 9.5. Molar Volume, Expansion Coefficients, and Compressibility of H_2 and D_2[a]

	Hydrogen	Deuterium
Molar volume (cm^3) at 4.2°K	22.65	19.56
Molar volume (cm^3) at triple point	23.31	20.48
Molar volume (cm^3) at 0°K (calculated)	22.57	19.49
Compressibility (cm^2/kg) at 4.2°K and at 0 kg/cm^2 "pressure"	$(6.8 \pm 1.5) \times 10^{-4}$	$(4.5 \pm 2) \times 10^{-4}$
Volume expansion coefficient at 11°K, calculated from experimental $C_p - C_v$	5.1×10^{-3}	3.7×10^{-3}
Volume expansion coefficient at 4.2°K, calculated by Megaw	2.4×10^{-3}	1.7×10^{-3}

[a] K. Clusius and E. Bartholome, *Z. physik. Chem.*, **B30**, 237, 1935.

Specific Heats Showing λ Transitions. The specific heat of solid methane (Fig. 9.17) has been studied by Clusius and Perlick,[2] and at 20.4°K there is a second-order transition which is probably caused by rotation of the atoms of hydrogen about the carbon, *i.e.*, rotation of the molecule. Evidence for this has been given by Bitter *et al.*[3] and by Frank and Clusius.[4] Likewise in methyl alcohol the heat capacity shows

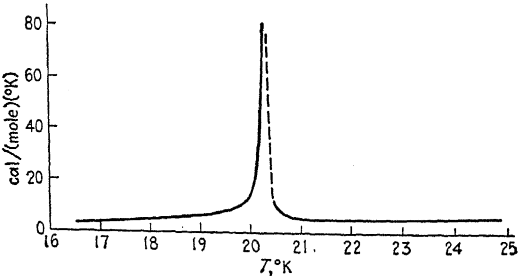

Fig. 9.17. Specific heat of methane vs. temperature. (*Clusius and Perlick, Z. physik. Chem.*, **B24**, 313, 1934.)

---

[1] E. Bartholome and A. Eucken, *Z. Elektrochem.*, **42**, 547, 1936; *Z. physik. Chem.*, **B33**, 387, 1936.

[2] K. Clusius and A. Perlick, *Z. physik. Chem.*, **B24**, 313, 1934.

[3] F. Bitter *et al.*, *Phys. Rev.*, **71**, 738, 1947.

[4] A. Frank and K. Clusius, *Z. physik. Chem.*, **B36**, 291, 1936.

a λ transition at 160°K according to Kelley.[1] Kelley's work on the specific heat of MnO, MnS, MnSe, MnTe has already been cited as showing a λ transition caused by antiferromagnetism. Such an effect has nothing to do with rotation in the solid state. However, the λ transition in SiH_4 at 63.5°K may belong to the rotation class of second-order transitions. Whether the λ transition in HF, HCl, HBr, and HI belongs to this class is not clear, as their behavior is complicated. Giauque and Wiebe[2] have discussed these molecular solids.

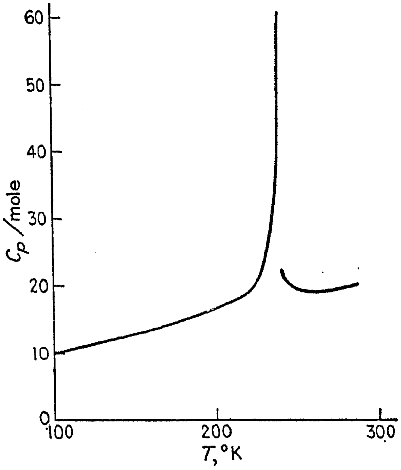

FIG. 9.18. Specific heat of NH_4Cl vs. temperature. (*Simon, Ann. phys.*, **68,** 241, 1922.)

There are a number of λ transitions in solids which have attracted interest because of the work done.[3] The hump in the specific heat of NH_4F at 230.7°K and the one for NH_4Cl at 242.8°K (see Fig. 9.18) are of this type.

The evidence on the nuclear resonance line width for NH_4Cl indicates that there is not a hindered rotation taking place (Bitter *et al.*[4]). The explanation seems to have been given by R. Hettich,[5] who showed that NH_4Cl became piezoelectric below its transition point. Above the transition point the hydrogen atoms take a random distribution about the nitrogen atom. Electron diffraction studies by Lashkarew and Usyskin[6] seem to support this view. It is perhaps interesting that the crystal $NaNO_3$ falls into this general class of order-disorder transition. In the ordered crystal all the NO_3 groups point the same way (Hendricks *et al.*[7]).

Experimental Methods

In Chap. 2, we discussed some of the general principles of cryostats for low-temperature research and in particular we discussed temperature measurements. The determination of low-temperature specific heats is simple in concept and except for some clever instrumentation is the same as the early vacuum calorimeter of Nernst and Eucken.[1] The techniques by Giauque at Berkeley, Calif., those of the Kamerlingh Onnes laboratory in Leiden, and those in England at Oxford and at Cambridge are amply discussed in research reports.

---

[1] K. K. Kelley, *J. Am. Chem. Soc.*, **51,** 180, 1929.

[2] W. F. Giauque and R. Wiebe, *J. Am. Chem. Soc.*, **70,** 101, 1928; *ibid.*, **71,** 1441, 1929.

[3] F. Simon, *Ann. phys.*, **68,** 241, 1922.

[4] F. Bitter *et al.*, *Phys. Rev.*, **71,** 738, 1947.

[5] R. Hettich, *Z. physik. Chem.*, **168,** 353, 1934.

[6] W. Lashkarew and I. Usyskin, *Z. Physik,* **85,** 618, 1933.

[7] S. Hendricks *et al.*, *J. Am. Chem. Soc.*, **53,** 3339, 1931.

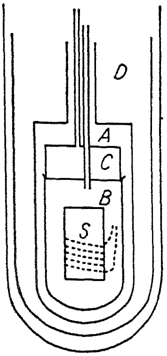

FIG. 9.19. Vacuum calorimeter for specific heat studies.

Figure 9.19 shows a sketch of the vacuum calorimeter by Clusius and Harteck,[2] in which the specimen S is hung by a thread and the vacuum space A contains an inner region B and a condensation cup C. Liquid nitrogen or liquid hydrogen was kept in the outer Dewar flask D. The condensation cup C contained pumped liquid or solid hydrogen, and contact with the specimen was made by an exchange gas of helium. This allowed temperatures as low as 10°K. Obviously, this equipment could be used in a liquid helium bath, and temperatures down to 1°K could be obtained. The exchange gas in B is pumped out to establish thermal isolation.

The heater wire wrapped around the solid specimen is shown schematically in Fig. 9.19. The Leiden laboratories, under the direction of Professor Keesom, sometimes used a heater core which was screwed into the specimen, and this gave contact and no radiation losses. The measurement of energy input means determination of voltage, current, and time. The higher degree of accuracy desired calls for greater care in all three divisions. The temperature drift of the specimen is taken before and after the heating period so that the rise in temperature may be determined. The temperature of the shield forming the vacuum space B is kept very close to the temperature of the specimen, *i.e.*, it is allowed to warm up with the specimen by the aid of separate heaters and by throttling down the pumping action on the condensation cup.

W. F. Giauque and R. Wiebe[3] describe a vacuum calorimeter made of thin gold sheet 0.75 mm thick for holding the specimen of hydrogen chloride, etc. The container was 12 cm in height and 3.75 cm in diameter. It had radial vanes to assist in attaining temperature equilibrium. The combined thermometer-heater was made of gold wire with 0.175 per cent Ag impurity and 0.008 cm in diameter, which was silk-covered and wrapped on the calorimeter with a bakelite lacquer binder. Further, the whole thing was gold-leafed to minimize radiation. Glass tubes led to the calorimeter where glass-to-metal seals were used. Just above the gold calorimeter can was a massive lead block which acted as a heat reservoir, not unlike the condensation cup C of Fig. 9.19.

---

[1] W. Nernst and A. Eucken, "Energie und Warmheit," *Hand. exp. Physik.*, Leipzig, 1929.

[2] K. Clusius and P. Harteck, *Z. physik. Chem.*, **134**, 243, 1928.

[3] W. F. Giauque and R. Wiebe, *J. Am. Chem. Soc.*, **50**, 101, 1928.

In Fig. 9.20 the simplified diagram of the Simon-type expansion liquefier adapted for calorimetry is shown. The vacuum case is surrounded by a Dewar flask of liquid hydrogen, which is not shown. The leads from the heater and thermometers passed out through the bottom via platinum wires passing through a copper-glass vacuum seal. In normal use the calorimeter bottom and thermometer drum were soldered together permanently. The total weight of a calorimeter was about 14 g. Simon and coworkers used platinum and constantan thermometers in these calorimeters, as well as leaded-brass thermometers in others. The range between 4°K and hydrogen temperatures (20°K) was covered, using the calorimeter itself as the bulb of a constant-volume gas thermometer. All thermometer leads were built as nearly as possible to the same geometry and were finally balanced electrically. All leads were of constantan and passed through, and in intimate thermal contact with, a copper block C soldered to the underside of the expansion chamber. The junctions with the copper wires of the external circuit were made outside the apparatus. Each junction was bound to a thin-walled copper drum immersed in a massive oil bath made of brass; thermoelectric effects were reduced to a minimum in this way.

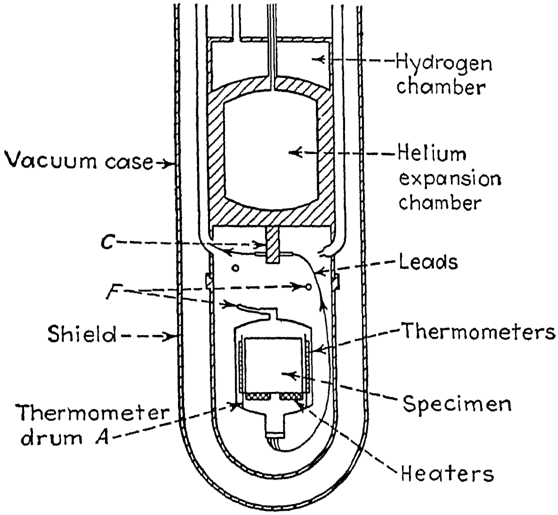

FIG. 9.20. Simplified diagram of expansion liquefier adapted for calorimetry. [*Parkinson, Simon, and Spedding, Proc. Roy. Soc. (London)*, **207**, 137, 1951.]

These details give an impression of the care one must use in precision calorimetry. The heating current is customarily supplied by lead storage batteries whose temperature is kept constant. A dummy load is used so that the current is continuously drawn and the voltage is thereby stabilized. Switches are always of the caliber used on the better-grade potentiometer bridges so that no spurious emfs can develop. Standard cells and standard resistors must be calibrated and held at constant temperature. Stop watches and other timer devices[1] must be calibrated. Considerable attention must be paid to the comfort and ease of operation for the observers during the rather lengthy time required for such calorimetry.

Heat Conductivity in Solids

The heat conduction in a solid at low temperatures is another interesting problem in which tests of theoretical concepts may be made at very low temperatures. In general we think of the solids in the classification of metals, semimetals, and insulators when we discuss electrical conduction. Eucken[2] measured the thermal conductivity of a large number of dielectric crystals and amorphous substances at room and liquid air temperatures. A few results were taken with liquid hydrogen temperatures. Eucken found that the conductivity of single crystals increases with decreasing temperature, while the conductivity of amorphous solids decreases. At about the time of Eucken's work the quantum theories of specific heat were being developed, and Debye[3] was able to explain the behavior in terms of traveling elastic waves and the scattering process involved. We shall discuss these matters more completely after we have examined some experimental evidence. Metallic heat conductivity has been the subject of numerous investigations by Gruneisen and his coworkers.[4] At room temperatures and above, the thermal conductivity of most metals shows little change with temperature. As the temperature is lowered, the thermal conductivity of pure and well-annealed metal specimens first rises in magnitude, passes through a maximum, and then declines more or less linearly toward zero at 0°K. The Wiedemann-Franz law connecting the electrical resistance ρ, the thermal conductivity K, and the temperature T states that

$$\frac{K\rho}{T} = L_0 = \frac{1}{3}\left(\frac{\pi k}{e}\right)^2 = 2.45 \times 10^{-8} \text{ watt-ohm/}^\circ\text{K}^2 \qquad (9.56)$$

This well-known relationship is based on the classical concept of an electron gas carrying the thermal energy. As in electrical conduction, there is a mean free path involved in the theory. Taking the product of heat conductivity with the electrical resistivity removes the mean free path as an unknown, and the above equation is considered valid. Let us examine some experimental results for metals.

---

[1] Precision Timers, Standard Electric Time Co., Springfield, Mass.

[2] A. Eucken, *Ann. Physik*, **34**, 185, 1911; *Physik. Z.*, **12**, 1005, 1911.

[3] P. Debye, "Vortrage uber Theorie etc.," Berlin, Teubner, 1914.

[4] E. Gruneisen, *Ann. Physik*, Sec. **5**, V–XII, 1949.

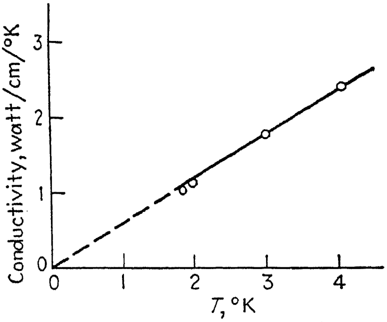

FIG. 9.21. Thermal conductivity of copper vs. temperature. (*Allen and Mendoza, Proc. Cambridge Phil. Soc.,* **44**, 280, 1948.)

Figure 9.21 shows the extremely low-temperature results of studies made by Allen and Mendoza on copper. Figure 9.22 shows the studies by Andrews, Webber, and Spohr on aluminum. Figure 9.23 shows the work on cadmium by Rosenberg and Mendelssohn, and Fig. 9.24 gives the results on iron by Johnston, Powers, and Ziegler. Now the Wiedemann-Franz law is not so bad at these very low temperatures if the resistivity ρ becomes independent of temperature and takes on the residual electrical resistivity ρ_r. Then we may write

$$K = \frac{L_0 T}{\rho_r} \qquad (9.57)$$

which is linear in temperature. The curves for the various metals at low temperatures are not straight lines, and so we may take the next empirical relationship for the thermal resistivity as

$$\frac{1}{K} = \left(\frac{\rho_r}{L_0}\right)\frac{1}{T} + BT^2 \qquad (9.58)$$

The first term on the right is the thermal resistivity due to impurity scattering of the electrons. The second term is due to scattering of the electrons by the lattice vibrations. Such an expression has been theoretically justified by Makinson[1] and by Sondheimer.[2] The value of the constant B is about 2.7×10^{-3} cm/(watt) (°K) for the metal aluminum, according to Andrews, Webber, and Spohr.[3]

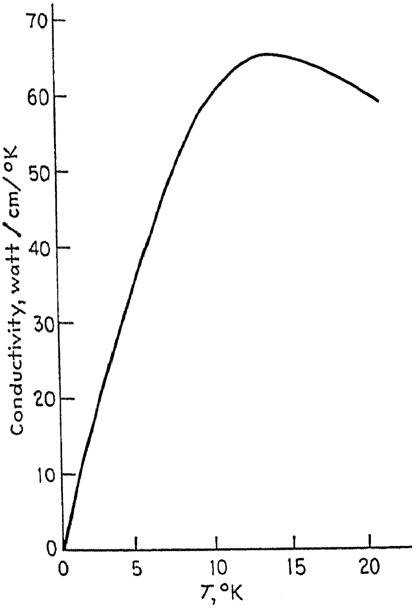

FIG. 9.22. Thermal conductivity of aluminum vs. temperature. (*Andrews, Webber, and Spohr, Phys. Rev.,* **84**, 994, 1951.)

---

[1] R. Makinson, *Proc. Cambridge Phil. Soc.*, **34**, 474, 1938.

[2] E. Sondheimer, *Proc. Roy. Soc. (London)*, **203**, 75, 1950.

[3] F. Andrews, R. Webber, and D. Spohr, *Phys. Rev.*, **84**, 994, 1951.

The thermal conductivity of some alloys at low temperature is shown in Fig. 9.25 and is taken from the studies by Berman. The conductivities are so small that the lattice phonons are considered responsible for a part of the observed result.

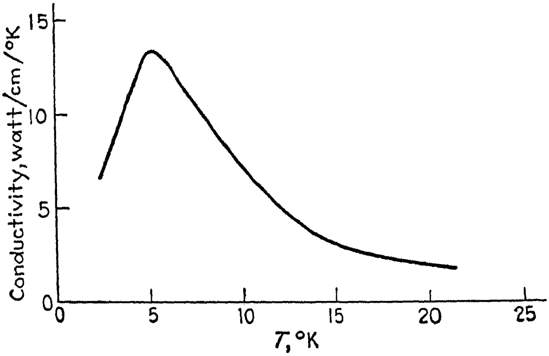

Fig. 9.23. Thermal conductivity of cadmium vs. temperature. (*Rosenberg and Mendelssohn, Proc. Intern. Conf. Oxford*, 1951.)

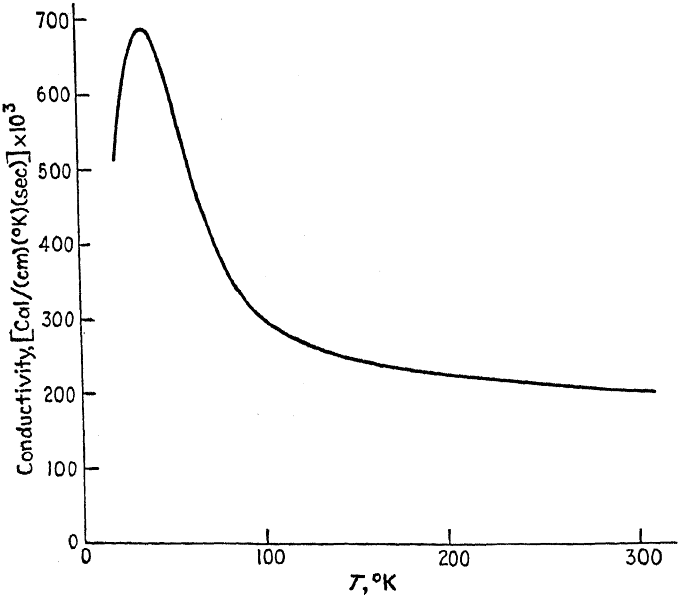

Fig. 9.24. Thermal conductivity of iron vs. temperature. (*Johnston, Powers, and Ziegler, Proc. Intern. Conf. Oxford*, 1951.)

We shall discuss next the experimental results for the thermal conductivity of dielectric crystals. Figure 9.26 shows the studies by Wilks and Wilkinson on solid helium at a density of 0.194 g/cc. The solid is easily compressed to higher densities, and this increases the thermal conduc-

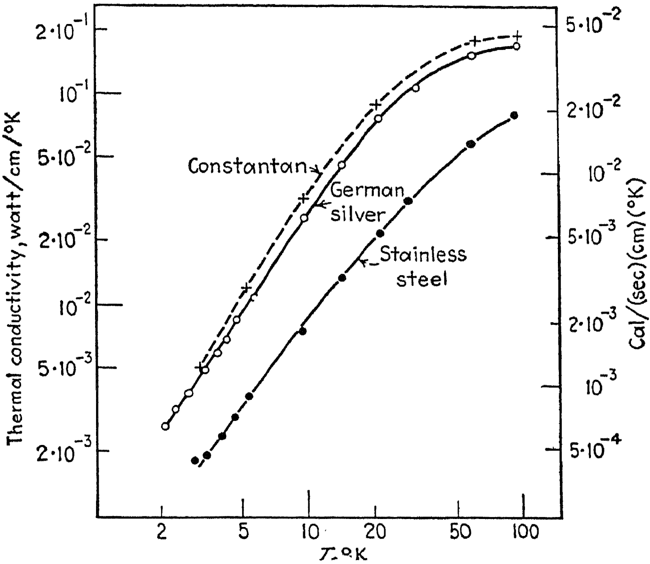

FIG. 9.25. Thermal conductivities of german silver, stainless steel, and constantan. (*Studies by Berman, Phil. Mag.*, **42**, 642, 1951.)

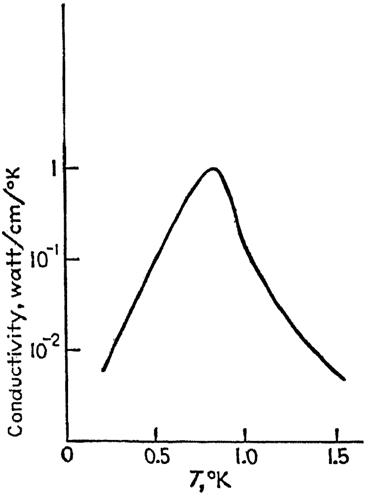

FIG. 9.26. Thermal conductivity of solid helium at density 0.194 g/cc. [*Wilks and Wilkinson, Proc. Phys. Soc. (London)*, **64**, 89, 1951.]

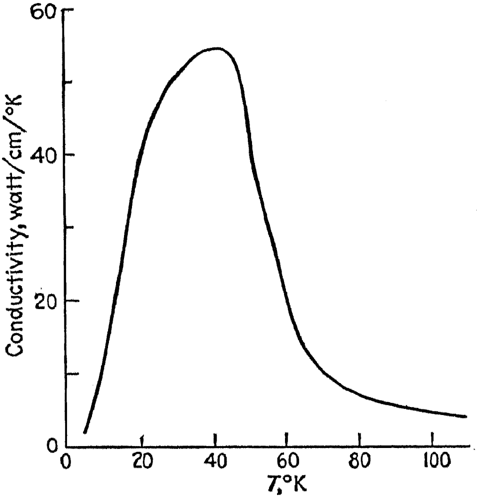

FIG. 9.27. Thermal conductivity of corundum (artificial sapphire); diameter of 3 mm. [*Berman, Proc. Roy. Soc. (London)*, **208**, 90, 1951.]

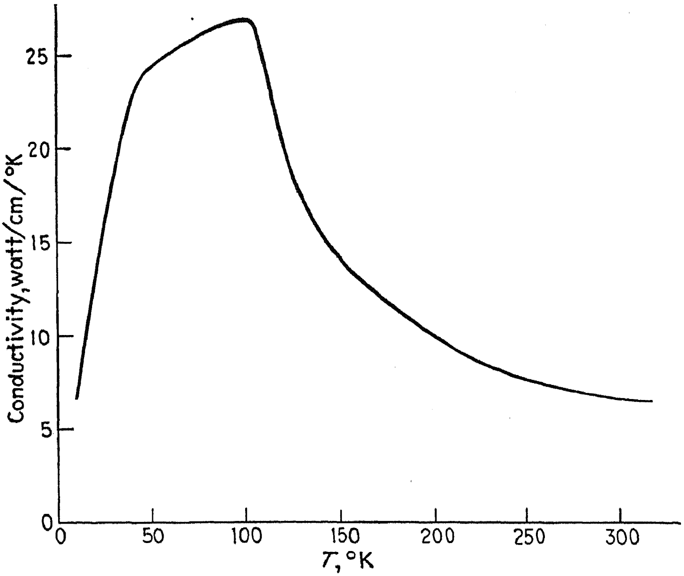

FIG. 9.28. Thermal conductivity of diamond. (*De Haas and Biermasz, Physica*, **5**, 320 and 619, 1938.)

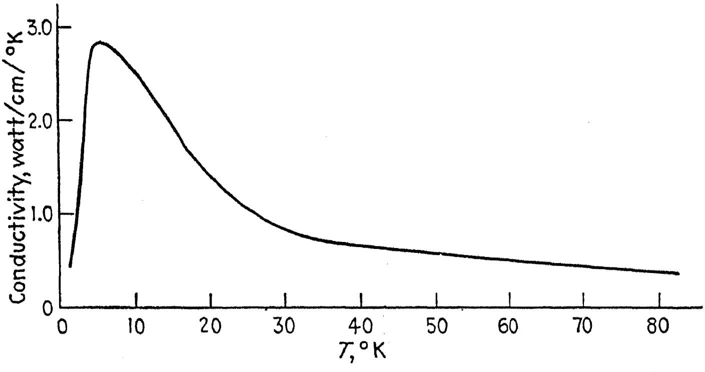

FIG. 9.29. Thermal conductivity of KCl; diameter of rod 0.252 cm. (*De Haas and Biermasz, Physica*, **5**, 47, 1938.)

tivity. The studies by Berman on artificial sapphire at low temperatures show a very large conductivity (Fig. 9.27). These large values are similar to those found by de Haas and Biermasz for diamond (Fig. 9.28). These last authors also studied KCl, as shown in Fig. 9.29, and at the lowest temperature found a dependence upon the diameter of the rod. This size effect had been predicted by Casimir.[1]

Debye[2] considered the heat conductivity in dielectric solids as arising

---

[1] H. Casimir, *Physica*, **5**, 495, 1938.

[2] P. Debye, "Vortrage uber Theorie etc.," Berlin, Teubner, 1914.

mainly through elastic vibrations of the lattice. These thermal vibrations can be resolved into normal modes, as we indicated in the early paragraphs of this chapter. For a perfect crystal these normal modes are traveling waves, but owing to the anharmonicity of the atomic binding, there is a coupling between the modes which is important to the problem of heat transport. Peierls[1] has shown that two waves or oscillations can give rise to a third wave by means of the anharmonicity. The third wave need not have the same direction, and so we regard such a collision as an impedance to energy flow. Peierls calls such a process *Umklapprozesse.* Klemens[2] has extended Peierls' theory, and Berman, Simon, and Wilks[3] have discussed the meaning with respect to experimental results. These last authors consider the Umklapp process to mean that, because the lattice is perturbed by the mode $\overline{K}_2$ (the wave number associated with the phonon), conditions are favorable for the phonon $\overline{K}_1$ to suffer reflection into the phonon $\overline{K}_3$. Peierls showed that the probability of U collisions leads to a heat conductivity of the form

$$K = AT^{a}e^{\theta/2T} \tag{9 59}$$

where A is a constant, a is of the order unity, and θ is the Debye specific heat parameter. Such a term may well explain the large increase in heat conductivity at low temperatures for solid dielectrics. Scattering can arise from geometrical boundaries (size effect) and from lattice defects; presumably these limit the conductivity at very low temperatures.

---

[1] R. Peierls, *Ann. Physik,* **3,** 1055, 1929; *Ann.* inst. Poincaré, **5,** 177, 1935.

[2] P. Klemens, *Proc. Roy. Soc.* (*London*), **208,** 108, 1951.

[3] R. Berman, F. Simon, and J. Wilks, *Nature,* **168,** 277, 1951; A. Herpin, *Ann. phys.,* **7,** 91, 1952.

CHAPTER 10

DIELECTRIC PROPERTIES AT LOW TEMPERATURES

Dielectrics at low temperatures is a subject of growing interest, and the current literature contains many new measurements and theories. The nature of the electric dipole is so different from that of the magnetic dipole that analogies are often misleading. Even so we find ourselves using terms such as *ferro-electric* which are meant to bridge the gap to the familiar and imply permanent polarization. In fact our major interest in the chapter shall be on ferro-electric substances and the temperature dependence of their dielectric constant. For the most part the electronic polarizability of atoms in the solid state is independent of temperature. By this we mean that the pulling of the electron cloud to one side of the nucleus of an atom by an external electric field is independent of temperature. The ionic polarization is temperature-dependent. By ionic polarization we mean pulling the entire ion from its equilibrium position by an electric field.[1]

Some Fundamental Concepts

The dielectric property of matter is related to the ratio of the size of a condenser when filled with the matter to its size when empty. The influence of the material on the electric field is $\mathbf{D} = \epsilon\mathbf{E}$. The displacement vector $\mathbf{D}$ arises from the real charges on the plates, and the electric field $\mathbf{E}$ exists within the region of space whose permittivity is ϵ. The vectors $\mathbf{D}$ and $\mathbf{E}$ need not be parallel, and for anisotropic matter we regard ϵ as a tensor which generally is a linear transform operator. We shall consider ϵ to be a single-valued continuous function of $\mathbf{E}$. In vacuum, $\mathbf{D}$ equals $\epsilon_0\mathbf{E}$, where $\epsilon_0 = 8.854 \times 10^{12}$ farad/m. The ratio $\epsilon/\epsilon_0 = K$, where K is the dielectric constant.

It is customary to introduce the polarization vector $\mathbf{P}$ for the substance between the condenser plates. It is defined

$$\mathbf{P} = \mathbf{D} - \epsilon_0\mathbf{E} \tag{10.1}$$

The ratio $\mathbf{P}/\epsilon_0\mathbf{E} = \chi$, where χ is the electric susceptibility. Now let us inquire about the physical meaning of these symbols. If the charge on the condenser plates alternates rapidly and periodically, we must consider the complex permittivity to allow for a phase lag between **D** and **E**. Since this will depend on the frequency employed, we must seek more information concerning the complex polarization of the matter between the condenser plates:

---

[1] We refer the reader for background information to such excellent monographs and books as H. Frohlich, "Theory of Dielectrics," Oxford, New York, 1951; J. H. Van Vleck, "Electric and Magnetic Susceptibilities," Oxford, New York, 1934; and W. G. Cady, "Piezoelectricity," New York, McGraw-Hill, 1946.

$$\mathbf{P}e^{-iwt} = (\chi' - i\chi'')\epsilon_0\mathbf{E}_0e^{-iwt} \tag{10.2}$$

If the polarization arises from the forced motion of the electron cloud about each atomic nucleus, then the classical theory of a linear oscillator may be used, and we have

$$\mathbf{P} = \alpha\mathbf{E} = \mathbf{E}\sum_k N_k\frac{e^2}{m}\left(\frac{1}{w_k^2 - w^2 - iwg_k}\right) \tag{10.3}$$

The system considered has N_k electrons per unit volume, and the electrons have a characteristic angular velocity w_k and damping constant g_k. Resonance lies in the optical frequency range. The polarization is clearly complex, and the polarizability α, defined above, is also complex. From optical measurements on the index of refraction n we can obtain the dielectric constant (real part) $n = \sqrt{K}$. In this way we can evaluate the electronic polarizability in a way which we shall presently explain.

If the substance contains permanent electric dipoles whose moment is μ, then polarization can arise from their alignment in an applied field. The dipole we have in mind is a positively charged atom linked to a negative charged atom in a gas or liquid. Such orientation is temperature-dependent for these dipoles. In a solid we would expect the atomic dipoles to be locked in place so that no ordinary field which we might apply would produce appreciable realignment. The total polarizability γ is the sum of the electronic term α and of the permanent dipole term $\mu^2/3kT$. The last term is identical in theoretical terms to the magnetic permanent dipole at temperature T and in an applied field. If in the solid the ion is moved by the electric field and if in addition this motion is temperature-dependent, then the value of the total polarizability for such a system is the sum of the electronic term α and the induced dipole term $\beta(T)$. We shall be concerned with this latter type of polarization. The polarization **P** per unit volume is

$$\mathbf{P} = N\gamma\mathbf{E}_L \tag{10.4}$$

where N is the number of atoms per unit volume, γ is the total atomic polarizability, and $\mathbf{E}_L$ is the electric field at the atom.

This local field is assisted by the polarization of the surrounding medium. This field is not easy to compute for a fixed array of atoms. In the simple case of an atom at the center of a sphere on the surface of which there is a density of charge $\mathbf{P}\cos\theta$, due to other polarized atoms, we have a simple expression due to Lorentz. The field at the center of the sphere of radius R is

$$\mathbf{E}_0 = \frac{\mathbf{P}}{2\epsilon_0} \int_0^{\pi} \cos^2 \theta \sin \theta \, d\theta = \frac{\mathbf{P}}{3\epsilon_0} \tag{10.5}$$

This field at the center must be added to the external applied field to give a local field:

$$\mathbf{E}_L = \mathbf{E} + \frac{\mathbf{P}}{3\epsilon_0} \tag{10.6}$$

Then

$$\mathbf{P} = N\gamma \left(\mathbf{E} + \frac{\mathbf{P}}{3\epsilon_0} \right) \tag{10.7}$$

so that where we have considered the dielectric constant as being represented by

$$K = 1 + \frac{\mathbf{P}}{\epsilon_0 \mathbf{E}} \tag{10.8}$$

we may now substitute the polarization and get

$$K = 1 + \frac{N\gamma/\epsilon_0}{1 - N\gamma/3\epsilon_0} \tag{10.9}$$

Thus the dielectric constant can become infinite when $N\gamma/3\epsilon_0$ becomes unity, and this would be possible for a finite value of the polarizability γ. There are several cases of this happening, and each one leads to a ferro-electric substance. These are in Rochelle salt (J. Valasck[1]), in potassium dihydrogen phosphate, and in a number of more recently investigated compounds; such as barium titanate, potassium tartrate, etc. Each of these solid substances at high temperatures exhibits an electric susceptibility which depends on temperature, according to a Curie-Weiss law. Let us examine the experimental facts and then seek an understanding.

Barium Titanate

The huge dielectric constant of barium titanate and its ferro-electric properties below the transition temperature 391°K have led to extensive investigations (Figs. 10.1*a* and 10.1*b*). The early experimental work was done by von Hipple, Breckenridge, Chesley, and Tisza[2] in the United States and by Wul[3] in the USSR. In England the X-ray powder diffraction studies by Megaw[4] and the theories by Devonshire[5] were important contributions. We shall refer to the work of many others in developing the subject.

---

[1] J. Valasck, *Phys. Rev.*, **17**, 475, 1921.

[2] A. von Hipple *et al.*, *Ind. Eng. Chem.*, **38**, 1097, 1946.

[3] B. Wul, *J. Phys. USSR*, **10**, 95, 1946.

[4] H. Megaw, *Proc. Roy. Soc. (London)*, **A189**, 261, 1947.

[5] A. F. Devonshire, *Phil. Mag.*, **40**, 1040, 1949.

Above 391°K the dielectric constant is[1]

$$K = \frac{15 \times 10^4}{T - T_c} \qquad \text{for BaTiO}_3$$

Close to the Curie point T_c the dielectric constant is very large for single crystals, and below the transition there is permanent polarization.[2,3,4,5] At 278°K there is a phase change, and again at 203°K there is another phase change, but permanent polarization persists in both phases. The dielectric constant in single crystals is different for different crystal axes but remains large in these temperature regions. Where there is permanent polarization, there is domain structure. Above the transition at 391°K the crystal is cubic with Ba ions at each corner, 0 ions at the center face, and a Ti ion at the center of the cube. At the 391°K transition there is a slight mechanical deformation as the crystal becomes polarized along the 100 direction. Along this axis the crystal expands, and the two axes at right angles to it contract. The amount of deformation is proportional to the square of the polarization. Both Wul[6] and Blunt and Love[7] measured the dielectric constant of BaTiO$_3$ on ceramic specimens down to liquid helium temperatures (Fig. 10.2) and found a

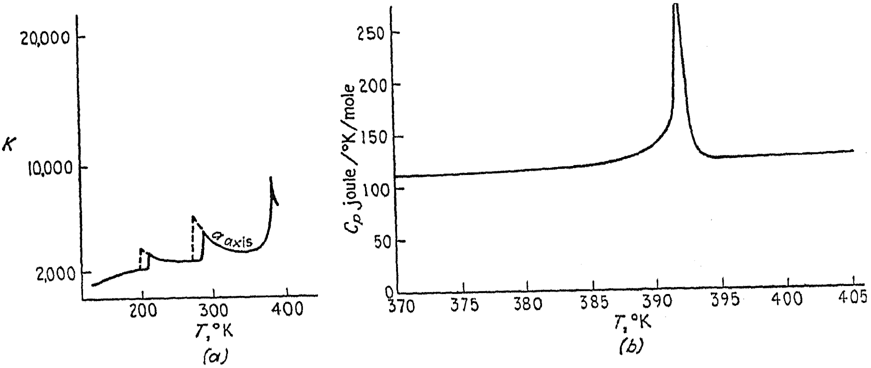

FIG. 10.1. (*a*) Dielectric constant of BaTiO$_3$; single domain crystal. (*b*) Specific heat of barium titanate. (*Volger, Philips Research Repts.*, **7**, 21, 1952.)

---

[1] S. Roberts, *Phys. Rev.*, **75**, 989, 1949; *ibid.*, **76**, 1215, 1949.

[2] B. Mathias and A. von Hipple, *Phys. Rev.*, **73**, 268, 1948.

[3] P. Forsbergh, Jr., *Phys. Rev.*, **76**, 1187, 1949.

[4] W. Merz, *Phys. Rev.*, **76**, 1221, 1949; *ibid.*, **75**, 687, 1949.

[5] G. H. Jonker and J. H. van Santen, *Science*, **109**, 632, 1949.

[6] B. Wul, *J. Phys. USSR*, **10**, 95, 1946.

[7] R. F. Blunt and W. F. Love, *Phys. Rev.*, **76**, 1202, 1949.

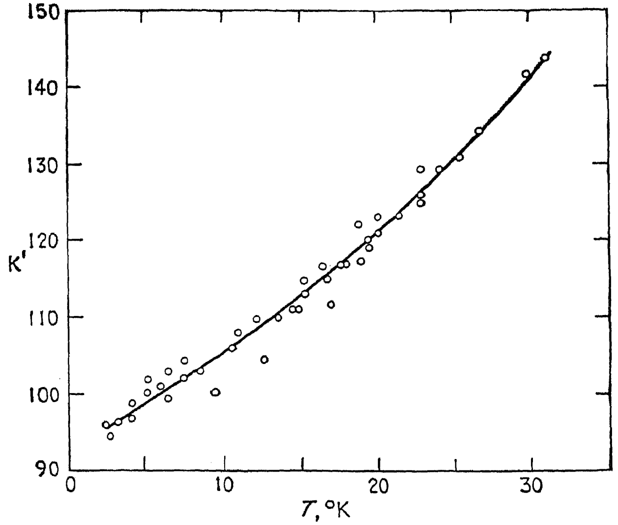

FIG. 10.2. Dielectric constant of barium titanate vs. temperature below 30°K. (*Blunt and Love, Phys. Rev.*, **76**, 1202, 1949.)

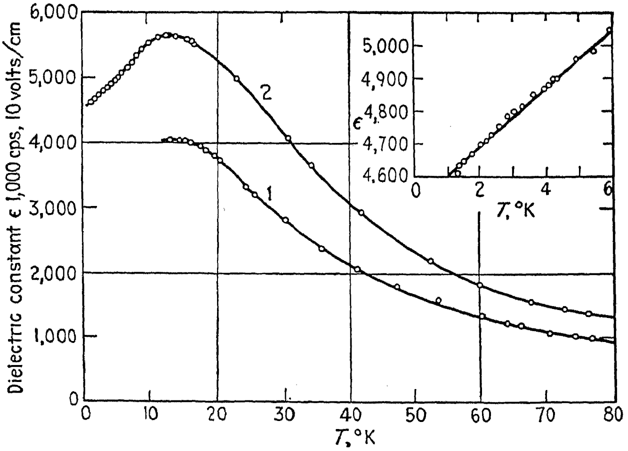

FIG. 10.3. Dielectric constant of $KTaO_3$ at low temperatures. (*Hulm, Mathias, and Long, Phys. Rev.*, **79**, 885, 1950.)

drop with temperature of the dielectric constant K. Merz[1] has shown that on single crystals at low temperatures the coercivity of the material increases with decreasing temperature while the spontaneous polarization remains constant. Schmitt[2] has explained the large temperature variation of the dielectric constant for ceramics as follows: the increase in

[1] W. Merz, *Phys. Rev.*, **81**, 1064, 1951.

[2] R. W. Schmitt, *Phys. Rev.*, **85**, 1, 1952.

coercivity makes it more difficult to change the domain structure, and thus as one lowers the temperature, it becomes more difficult to polarize the specimen. The polarization process has been shown by Schmitt to be thermodynamically irreversible so that there is heating of the specimen with the adiabatic application and removal of an external electric field. This may also explain the very low temperature behavior (Fig. 10.3) of the ferro-electric substance $KTaO_3$ discovered by Hulm, Mathias, and Long.[1]

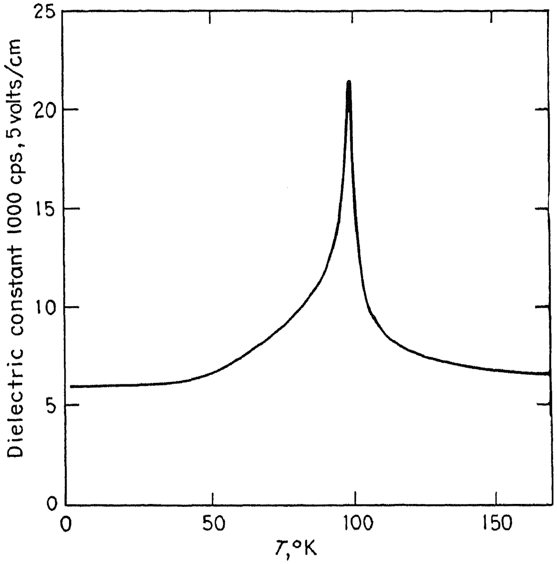

FIG. 10.4. Dielectric constant of lithium tartrate, $LiNH_4C_4H_4O_6 \cdot H_2O$. (*Mathias and Hulm, Phys. Rev.*, **82**, 108, 1951.)

Strontium Titanate

The dielectric properties of $SrTiO_3$ studied by Hulm[2] appear to follow a Curie-Weiss type of law from room temperature down to 50°K:

$$K = \frac{8.3 \times 10^4}{T - T_c} \qquad \text{for } SrTiO_3 \text{ with } T_c - 35°K$$

Below 50°K the dielectric constant K leveled off gently to a constant value of 1,300 at the absolute zero approach. There was no ferro-electric phase for strontium titanate. The effect of diluting barium titanate with strontium titanate has been observed by Jackson and Reddish[3] to shift

[1] J. Hulm, B. Mathias, and E. Long, *Phys. Rev.*, **79**, 885, 1950.

[2] J. Hulm, *Proc. Phys. Soc. (London)*, **63**, 1184, 1950.

[3] W. Jackson and W. Reddish, *Nature*, **156**, 717, 1949.

the transition of the ferro-electric point to lower and lower temperatures as the dilution increases.[1]

Ferro-electric Tartrates

Mathias and Hulm[2] have discovered ferro-electricity in two new tartrates: in $LiNH_4C_4H_4O_6 \cdot H_2O$ at 98.5°K and in $LiTlC_4H_4O_6 \cdot H_2O$ at about 10°K. Figures 10.4 and 10.5 show the temperature dependence of the dielectric constant for these tartrates.

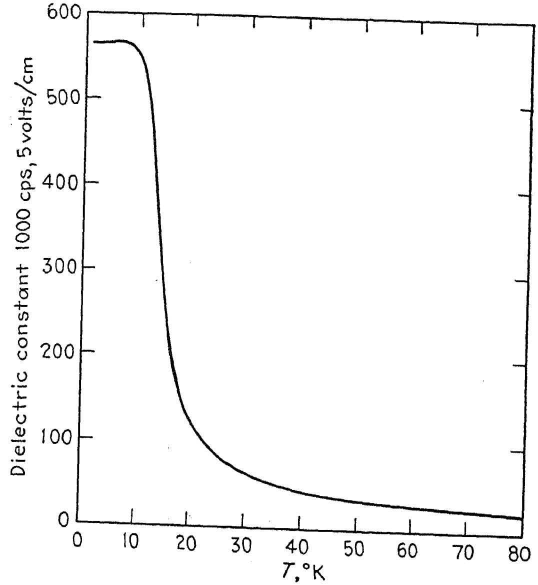

FIG. 10.5. Dielectric constant of lithium tartrate, $LiTlC_4H_4O_6 \cdot H_2O$. (*Mathias and Hulm, Phys. Rev.*, **82**, 108, 1951.)

Solid Hydrogen Bromide

The dielectric behavior of solid hydrogen halides is of considerable interest as one aspect of the cooperative phenomena and solid phase transitions in these molecular crystals. Brown and Cole[3] have examined the complex dielectric constant of solid HBr at the second-order phase transition in the temperature region 70 to 100°K. The static dielectric constant has a value 200 at 89°K.

---

[1] Anti-ferro-electricity in ceramic $PbZrO_3$ has been reported by G. Shirane (*Phys. Rev.*, **86**, 219, 1952) and has received theoretical treatment by C. Kittel (*Phys. Rev.*, **82**, 729, 1951) and by M. Takagi (*Phys. Rev.*, **85**, 315, 1952). The pure $PbZrO_3$ has a dielectric constant which rises to a maximum at about 500°K and then falls abruptly to a low value as the temperature is lowered. There are no hysteresis effects, indicating that there is no spontaneous polarization of the low-temperature phase. The study of anti-ferro-electric substances will be an interesting subject of future development.

[2] B. Mathias and J. Hulm, *Phys. Rev.*, **82**, 108, 1951.

[3] N. Brown and R. Cole, *J. Chem. Phys.*, **20**, 196, 1952; J. Powles, *J. phys. radium*, **13**, 121, 1952.

Theory of Barium Titanate

The principal problem is to show why the dielectric constant has the temperature dependence according to a Curie-Weiss type of law and why it has a Curie point giving permanent polarization. J. C. Slater[1] has given the simplest explanation of these effects, and we shall briefly indicate his theory. According to Slater, the property can be explained by a Lorentz correction to the polarization. The dielectric constants are

$$K = 1 + \frac{N\gamma/\epsilon_0}{1 - N\gamma/3\epsilon_0} \tag{10.10}$$

If the quantity $N\gamma/3\epsilon_0$ shows a slow decrease with temperature, being slightly greater than unity at the absolute zero, and going through the valve unity at a certain temperature T_c, then

$$N\gamma/3\epsilon_0 = 1 - C(T - T_c) \tag{10.11}$$

or

$$K = -2 + \frac{3}{C(T - T_c)} \tag{10.12}$$

If C is of the order 2×10^{-5}, then we may neglect -2 and have a simple Curie law. A. F. Devonshire[2] wrote a report in which he simply accepted these things as so and developed a phenomenological theory for the dielectric constant, heat of polarization, and crystal form. In many respects Slater's theory is similar except for the introduction of the electronic polarizability of all the ions. The optical value of the dielectric constant shows that the value $N\gamma/3\epsilon_0$ arising from the electronic polarization is about 0.61. Thus a further contribution of only about 0.39 must be made to this quantity by the ionic polarizability of the Ti ion, in order to produce ferro-electricity. And this is on the assumption that the local field at the Ti ion is the Lorentz value $\mathbf{E} + \mathbf{P}/3\epsilon_0$.

The field at the Ti ion is actually much greater than this, owing to the position of the neighboring oxygen ions. Slater calculated that the quantity $N\gamma/3\epsilon_0$ need only be 0.06 in order to produce ferro-electricity. The Ti ion is considered to move in a potential well with second- and fourth-power terms in the distance. The elastic forces holding the Ti ion in place are $kx + k^1x^3$. In addition the applied field exerts a force on the Ti ion. Slater considered the potential field of the Ti ion in a cubic lattice and in an electric field as

---

[1] J. C. Slater, *Phys. Rev.*, **78**, 748, 1950.

[2] A. F. Devonshire, *Phil. Mag.*, **40**, 1040, 1949.

$$\varphi = a(x^2 + y^2 + z^2) + b_1(x^4 + y^4 + z^4) + 2b_2(x^2y^2 + x^2y^2 + y^2z^2) - q(x\mathbf{E}_x + y\mathbf{E}_y + z\mathbf{E}_z) \qquad (10.13)$$

Thus the Ti ion is not a simple harmonic oscillator, and we must compute the partition function Z, Helmholtz potential $A_E = -kT \ln Z$, and polarization $-(\partial A_E/\partial \mathrm{E})_T$ for a perturbed harmonic oscillator. The energy levels can be worked out and the Boltzmann statistics used as in Chap. 3. Slater finds the polarizability for the Ti ion to be

$$\alpha^1_{\mathrm{Ti}} = \frac{\mathbf{P}_x}{N\mathbf{E}_x} = \frac{q^2}{2a}\left[1 - \frac{kT(3b_1 + 2b_2)}{a^2}\right] + \text{small terms for small fields} \qquad (10.14)$$

The temperature enters because of the statistical expression $Z = \Sigma e^{\epsilon_i/kT}$. The unperturbed energy is

$$\epsilon_i = \left(l + m + n + \frac{3}{2}\right) h\nu - \frac{q^2\mathbf{E}^2}{4a} \qquad (10.15)$$

The small temperature dependence then comes from a small value $(3b_1 + 2b_2)$, determining the nonlinear behavior of the law of force. In an electric field the Ti ion moves into a region where the restoring forces are greater so that with the same energy the oscillator increases the vibration frequency and decreases its amplitude. Occupation of a smaller volume in real space corresponds to a net drop in entropy of the system, just as the isothermal compression of a gas gives a drop in entropy.

Recently John Barrett[1] has obtained a more complete evaluation of the partition function such that, when the oscillator gets to low temperature and occupies the lowest possible energy state, the dielectric constant becomes independent of temperature. Barrett obtains

$$\alpha^1_{\mathrm{Ti}} = \frac{1}{N}\frac{\mathbf{P}_x}{\mathbf{E}_x} = \frac{q^2}{2a}\left[1 - \frac{(3b_1 + 2b_2)h\nu}{2a^2} \coth \frac{h\nu}{2kT}\right] \qquad (10.16)$$

so that

$$K = \frac{C}{\dfrac{T_1}{2} \coth \dfrac{T_1}{2T} - T_c} \qquad (10.17)$$

where C is a constant, T_1 depends on the force constants and on the Lorentz-type correction but not on temperature, and T_c is a constant. At high temperatures this formula approaches a Curie-Weiss law.

---

[1] J. Barrett, *Phys. Rev.*, **86**, 118, 1952.

APPENDIX

TABLE A.1. VAPOR PRESSURE OF LIQUID HELIUM, AGREED TEMPERATURE SCALE

p, mm	0	1	2	3	4	5	6	7	8	9
0.0010	0.657	662	667	671	674	678	681	684	687	690
0.0020	0.693	696	698	701	703	706	708	710	712	714
0.0030	0.716	717	719	721	723	724	726	728	729	731
0.0040	0.732	734	735	737	738	740	741	742	744	745
0.0050	0.746	747	749	750	751	752	753	754	755	756
0.0060	0.757	758	759	760	761	762	763	764	765	766
0.0070	0.767	768	769	770	771	772	773	773	774	775
0.0080	0.776	777	778	778	779	780	781	781	782	783
0.0090	0.784	785	785	786	787	787	788	789	790	790
0.010	0.791	797	803	809	815	819	824	829	833	837
0.020	0.841	845	848	852	855	858	862	865	867	870
0.030	0.873	875	878	881	883	886	888	890	893	895
0.040	0.897	899	901	903	905	907	909	911	913	915
0.050	0.916	918	920	922	923	925	927	928	930	931
0.060	0.933	934	936	937	939	940	941	943	944	946
0.070	0.947	948	950	951	952	953	955	956	957	958
0.080	0.960	961	962	963	964	965	967	968	969	970
0.090	0.971	972	973	974	975	976	977	979	980	981
0.10	0.982	991	000	009	016	024	030	036	042	048
0.20	1.054	060	065	070	076	080	085	090	094	099
0.30	1.103	107	111	115	118	122	125	129	132	136
0.40	1.139	142	145	149	152	155	158	161	164	166
0.50	1.169	172	175	177	180	182	185	187	189	192
0.60	1.194	196	199	201	203	205	208	210	212	214
0.70	1.216	218	220	222	224	226	228	230	232	234
0.80	1.236	238	239	241	243	245	247	248	250	252
0.90	1.253	255	257	258	260	261	263	265	266	268
1.0	1.269	284	298	312	324	336	347	358	368	377
2.0	1.387	396	404	412	420	428	435	443	450	457
3.0	1.463	470	476	482	489	495	500	506	512	517
4.0	1.523	528	534	539	544	549	554	559	563	568
5.0	1.572	577	581	586	590	594	598	603	607	611
6.0	1.615	618	622	626	630	634	637	641	644	648
7.0	1.651	655	658	662	665	668	672	675	678	682
8.0	1.685	688	691	694	697	700	703	706	709	712
9.0	1.715	718	721	724	726	729	732	735	737	740

Table A.1. Vapor Pressure of Liquid Helium, Agreed Temperature Scale (*Continued*)

p, mm	0	1	2	3	4	5	6	7	8	9
10.0	1.743	745	748	750	753	755	758	761	763	766
11.0	1.768	771	773	775	778	780	783	785	787	790
12.0	1.792	794	797	799	801	804	806	808	810	812
13.0	1.815	817	819	821	824	826	828	830	832	834
14.0	1.836	839	841	843	845	847	849	851	853	855
15.0	1.857	859	861	863	865	867	869	871	873	875
16.0	1.877	879	881	883	884	886	888	890	892	894
17.0	1.895	897	899	901	903	904	906	908	910	912
18.0	1.913	915	917	918	920	922	924	925	927	929
19.0	1.930	932	934	935	937	939	940	942	944	945
20.0	1.947	948	950	952	953	955	956	958	960	961
21.0	1.963	964	966	967	969	970	972	974	975	977
22.0	1.978	980	981	983	984	986	987	989	990	992
23.0	1.993	995	996	998	999	001	002	004	005	007
24.0	2.008	010	011	012	014	015	017	018	020	021
25.0	2.023	024	025	027	028	030	031	033	034	035
26.0	2.037	038	039	041	042	044	045	046	048	049
27.0	2.050	052	053	054	056	057	058	060	061	062
28.0	2.064	065	066	068	069	070	072	073	074	076
29.0	2.077	078	079	081	082	083	085	086	087	088
30.0	2.090	091	092	093	095	096	097	098	100	101
31.0	2.102	103	105	106	107	108	109	111	112	113
32.0	2.114	115	117	118	119	120	121	123	124	125
33.0	2.126	127	128	130	131	132	133	134	135	137
34.0	2.138	139	140	141	142	144	145	146	147	148
35.0	2.149	150	151	153	154	155	156	157	158	159
36.0	2.160	162	163	164	165	166	167	168	169	170
37.0	2.171	172	174	175	176	177	178	179	180	181
38.0	2.182	183	184	185	186	187	188	190	191	192
39.0	2.193	194	195	196	197	198	199	200	201	202
40	2.203	213	223	233	243	253	262	271	280	289
50	2.298	307	315	324	332	340	348	356	364	372
60	2.380	388	395	403	410	418	425	432	439	446
70	2.453	460	467	474	481	487	494	501	507	513
80	2.520	526	533	539	545	551	557	563	569	575
90	2.581	587	593	599	604	610	616	621	627	633
100	2.638	644	649	655	660	665	671	676	681	686
110	2.692	697	701	706	711	717	722	726	731	736
120	2.741	746	750	755	760	765	770	774	779	783
130	2.788	792	797	801	806	810	815	820	824	829
140	2.833	837	842	846	850	855	859	863	868	872
150	2.877	881	885	889	893	897	902	906	910	914

Table A.1. Vapor Pressure of Liquid Helium, Agreed Temperature Scale (*Continued*)

p, mm	0	1	2	3	4	5	6	7	8	9
160	2.918	922	926	930	934	938	942	946	950	954
170	2.958	962	965	969	973	977	981	984	988	992
180	2.996	999	003	007	010	014	018	021	025	028
190	3.032	035	039	042	046	050	053	057	060	063
200	3.067	070	074	077	081	084	087	091	094	098
210	3.101	104	108	111	114	118	121	124	128	131
220	3.134	138	141	144	147	151	154	157	160	164
230	3.167	170	173	176	180	183	186	189	192	195
240	3.198	202	205	208	211	214	217	220	223	226
250	3.229	232	235	238	241	244	247	250	253	255
260	3.258	261	264	267	270	273	275	278	281	284
270	3.287	289	292	295	298	301	303	306	309	312
280	3.314	317	320	322	325	328	331	333	336	339
290	3.341	344	347	349	352	355	357	360	363	365
300	3.368	371	373	376	378	381	384	386	389	391
310	3.394	396	399	402	404	407	409	412	414	417
320	3.419	422	424	427	429	432	434	437	439	442
330	3.444	447	449	452	454	456	459	461	464	466
340	3.468	471	473	475	478	480	483	485	487	490
350	3.492	494	497	499	501	504	506	508	511	513
360	3.515	518	520	522	525	527	529	531	534	536
370	3.538	540	543	545	547	550	552	554	556	558
380	3.561	563	565	567	570	572	574	576	578	581
390	3.583	585	587	589	592	594	596	598	600	602
400	3.605	607	609	611	613	615	617	620	622	624
410	3.626	628	630	632	634	637	639	641	643	645
420	3.647	649	651	653	655	658	660	662	664	666
430	3.668	670	672	674	676	678	680	682	684	686
440	3.688	690	692	694	696	698	700	702	704	706
450	3.708	710	712	714	716	718	720	722	724	726
460	3.727	729	731	733	735	737	739	741	743	745
470	3.747	749	751	752	754	756	758	760	762	764
480	3.766	768	769	771	773	775	777	779	781	783
490	3.784	786	788	790	792	794	796	797	799	801
500	3.803	805	807	809	810	812	814	816	818	819
510	3.821	823	825	827	829	830	832	834	836	838
520	3.839	841	843	845	846	848	850	852	853	855
530	3.857	859	861	862	864	866	868	869	871	873
540	3.875	876	878	880	882	883	885	887	888	890
550	3.892	894	895	897	899	900	902	904	906	907
560	3.909	911	912	914	916	917	919	921	922	924
570	3.926	927	929	931	932	934	936	937	939	941

TABLE A.1. VAPOR PRESSURE OF LIQUID HELIUM, AGREED TEMPERATURE SCALE (*Continued*)

p, mm	0	1	2	3	4	5	6	7	8	9
580	3.942	944	946	947	949	951	952	954	956	957
590	3.959	961	962	964	965	967	969	970	972	974
600	3.975	977	978	980	982	983	985	986	988	990
610	3.991	993	994	996	997	999	001	002	004	005
620	4.007	008	010	012	013	015	016	018	019	021
630	4.022	024	026	027	029	030	032	033	035	036
640	4.038	039	041	042	044	045	047	048	050	051
650	4.053	055	056	058	059	061	062	064	065	067
660	4.068	070	071	073	074	076	077	079	080	082
670	4.083	084	086	087	089	090	092	093	095	096
680	4.098	099	101	102	104	105	107	108	110	111
690	4.112	114	115	117	118	120	121	123	124	126
700	4.127	128	130	131	133	134	136	137	138	140
710	4.141	143	144	146	147	148	150	151	153	154
720	4.156	157	158	160	161	163	164	165	167	168
730	4.170	171	173	174	175	177	178	180	181	182
740	4.184	185	187	188	189	191	192	193	195	196
750	4.198	199	200	202	203	205	206	207	209	210
760	4.211	213	214	216	217	218	220	221	222	224
770	4.225	226	228	229	231	232	233	235	236	237
780	4.239	240	241	243	244	245	247	248	250	251
790	4.252	254	255	256	258	259	260	262	263	264
800	4.266	267	268	270	271	272	274	275	276	278

p, mm	0	10	20	30	40	50	60	70	80	90
800	4.27	28	29	31	32	33	34	36	37	38
900	4.40	41	42	43	45	46	47	48	50	51
1000	4.52	53	54	56	57	58	59	60	61	63
1100	4.64	65	66	67	68	69	70	71	72	74
1200	4.75	76	77	78	79	80	81	82	83	84
1300	4.85	86	87	88	89	90	91	92	93	93
1400	4.94	95	96	97	98	99	00	01	02	02
1500	5.03	04	05	06	07	07	08	09	10	11
1600	5.11	12	13	14	14	15	16	17	17	18
1700	5.19	20	20							

TABLE A.1. VAPOR PRESSURE OF LIQUID HELIUM, AGREED TEMPERATURE SCALE (*Continued*)

T, °K	.00	.01	.02	.03	.04	.05	.06	.07	.08	.09
0.9	0.041	0.047	0.052	0.058	0.064	0.071	0.079	0.088	0.098	0.109
1.0	0.121	0.133	0.146	0.160	0.176	0.193	0.210	0.229	0.249	0.270
1.1	0.293	0.318	0.345	0.373	0.403	0.435	0.468	0.503	0.541	0.583
1.2	0.626	0.671	0.718	0.769	0.823	0.880	0.941	1.005	1.071	1.140
1.3	1.212	1.287	1.365	1.447	1.533	1.624	1.720	1.821	1.927	2.037
1.4	2.152	2.272	2.397	2.527	2.662	2.803	2.950	3.103	3.261	3.424
1.5	3.593	3.767	3.947	4.133	4.325	4.524	4.731	4.946	5.169	5.400
1.6	5.639	5.886	6.141	6.404	6.678	6.960	7.250	7.548	7.854	8.168
1.7	8.49	8.82	9.17	9.53	9.90	10.29	10.68	11.08	11.49	11.91
1.8	12.34	12.79	13.24	13.70	14.17	14.65	15.14	15.65	16.17	16.70
1.9	17.25	17.81	18.39	18.98	19.58	20.20	20.83	21.47	22.12	22.78
2.0	23.45	24.13	24.82	25.52	26.24	26.97	27.71	28.47	29.24	30.03
2.1	30.83	31.65	32.48	33.33	34.19	35.07	35.96	36.87	37.80	38.74
2.2	39.70	40.67	41.66	42.66	43.68	44.72	45.78	46.86	47.96	49.08
2.3	50.22	51.38	52.56	53.75	54.96	56.19	57.44	58.71	60.00	61.30
2.4	62.62	63.96	65.32	66.70	68.10	69.52	70.96	72.42	73.90	75.40
2.5	76.92	78.46	80.02	81.60	83.20	84.82	86.46	88.12	89.80	91.50
2.6	93.22	94.97	96.74	98.53	100.3	102.1	104.0	105.9	107.8	109.7
2.7	111.7	113.7	115.7	117.7	119.8	121.9	124.0	126.1	128.3	130.5
2.8	132.7	134.9	137.1	139.3	141.6	143.9	146.2	148.5	150.8	153.2
2.9	155.6	158.0	160.5	163.0	165.5	168.0	170.6	173.2	175.8	178.5
3.0	181.2	183.9	186.7	189.5	192.3	195.1	198.0	200.9	203.8	206.7
3.1	209.7	212.7	215.7	218.7	221.7	224.8	227.9	231.0	234.1	237.3
3.2	240.5	243.7	247.0	250.3	253.7	257.1	260.6	264.1	267.6	271.2
3.3	274.8	278.4	282.1	285.8	289.5	293.2	297.0	300.8	304.6	308.5
3.4	312.4	316.3	320.3	324.3	328.3	332.4	336.5	340.7	344.9	349.1
3.5	353.4	357.7	362.0	366.4	370.8	375.2	379.7	384.2	388.7	393.3
3.6	397.9	402.5	407.2	411.9	416.6	421.4	426.2	431.1	436.0	441.0
3.7	446.0	451.1	456.2	461.3	466.5	471.7	477.0	482.3	487.6	493.0
3.8	498.4	503.8	509.3	514.8	520.4	526.0	531.7	537.4	543.1	548.9
3.9	554.7	560.6	566.5	572.5	578.5	584.6	590.7	596.8	603.0	609.3
4.0	615.6	622.0	628.4	634.9	641.4	648.0	654.6	661.3	668.0	674.7
4.1	681.5	688.3	695.2	702.1	709.1	716.1	723.1	730.2	737.3	744.5
4.2	751.7	759.0	766.3	773.6	781.0	788.4	795.8	803.3	810.8	818.3

T, °K	p, mm	T, °K	p, mm	T, °K	p, mm	T, °K	p, mm
0.10	$3.4.10^{-32}$	0.30	$3.2.10^{-10}$	0.50	$1.8.10^{-5}$	0.70	$2.3.10^{-3}$
0.20	$7.3.10^{-16}$	0.40	$2.5.10^{-7}$	0.60	$2.8.10^{-4}$	0.80	$1.1.10^{-2}$
4.20	752	4.50	980	4.80	1250	5.10	1580
4.30	825	4.60	1070	4.90	1350	5.20	1720
4.40	900	4.70	1160	5.00	1460		

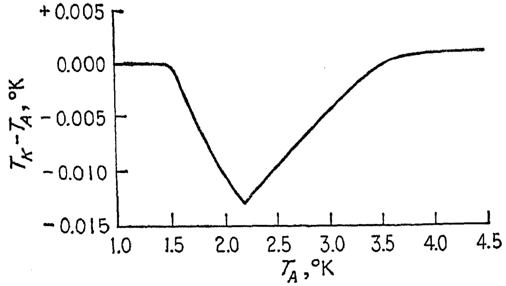

FIG. A.1. Deviations of the temperature T_K, according to Kistemaker, from the "agreed" scale T_A, according to Shoenberg. Curve from Abraham, Osborne, and Weinstock (*Phys. Rev.*, **80**, 366, 1950).

TABLE A.2. VAPOR PRESSURE OF LIQUID HYDROGEN
(0.25 PARA HYDROGEN AND 0.75 ORTHO HYDROGEN)

T, °K	P, mm Hg	T, °K	P, mm Hg	T, °K	P, mm Hg
20.4	762.2	14.4	69.3	9.0	0.472
20.2	718.0	14.2	62.0	8.8	0.353
20.0	675.7	14.1	58.6	8.6	0.260
19.8	635.3	14.05	57.0	8.4	0.189
19.6	596.6	14.04	57.0	8.2	0.135
19.4	559.7	14.0	55.5	8.0	0.095
19.2	524.4	13.8	48.7	7.8	0.066
19.0	490.8	13.6	42.6	7.6	0.045
18.8	458.8	13.4	37.1	7.4	0.030
18.6	428.4	13.2	32.3	7.2	0.020
18.4	399.4	13.0	27.9	7.0	0.013
18.2	371.9	12.8	24.1	6.8	0.008
18.0	345.9	12.6	20.6	6.6	0.005
17.8	321.2	12.4	17.6		
17.6	297.8	12.2	15.0		
17.4	275.7	12.0	12.7		
17.2	254.9	11.8	10.7		
17.0	235.2	11.6	8.96		
16.8	216.7	11.4	7.47		
16.6	199.3	11.2	6.18		
16.4	183.0	11.0	5.09		
16.2	167.7	10.8	4.16		
16.0	153.3	10.6	3.38		
15.8	140.0	10.4	2.73		
15.6	127.5	10.2	2.18		
15.4	115.8	10.0	1.73		
15.2	105.0	9.8	1.36		
15.0	95.0	9.6	1.06		
14.8	85.7	9.4	0.819		
14.6	77.2	9.2	0.625		

TABLE A.3. VAPOR PRESSURE OF LIQUID OXYGEN[a]

T, °K	P, mm Hg	T, °K	$\log_{10} P$, mm Hg
51.296	0.47	54.054	0.014
54.363	1.12	55.556	.211
56.788	2.28	57.143	.408
60.070	5.53	58.824	.605
62.119	9.1	60.606	.802
64.048	13.9	62.500	.999
66.025	21.8	64.516	1.196
67.956	31.9	66.667	1.392
68.989	38.9	68.966	1.587
69.988	46.9	71.429	1.781
70.974	55.7	73.529	1.9342
73.491	85.4	75.188	2.0488
76.534	137.9	76.923	2.1631
78.524	183.8	78.740	2.2772
79.918	222.8	80.000	2.3527
82.522	313.6	82.645	2.5031
84.148	383.8	84.746	2.6156
85.913	473.3	86.207	2.6904
88.045	603.2	88.496	2.80210
89.558	710.9	90.090	2.87626
89.914	720.0	91.743	2.95013
90.068	750.1		
90.231	763.2		
90.604	793.0		

---

[a] H. J. Hoge, *J. Research Nat. Bur. Standards*, **44**, 321, 1950.

TABLE A.4. VAPOR PRESSURE OF MIXTURE OF He^3 AND He^4
FOR A GIVEN FIXED VAPOR CONCENTRATION

X_V, %	T, °K	Vapor pressure, mm Hg	$\Delta P/P$, %	Error	
				Instrumental, %	Deviation from eq., %
Low Concentrations					
5.21	2.153	37.5	4.73	± 2	−1.1
	1.996	24.7	4.95	3	+1.0
	1.868	16.5	4.88	4	−2.0
	1.556	5.0	4.88	13	−4.8
9.49	2.102	34.0	8.84	2	+0.5
	1.804	13.8	9.20	4	+0.8
	1.801	13.6	9.10	4	−0.4
	1.545	4.9	9.43	11	+0.9
13.0	2.159	41.2	11.9	1	−0.2
	2.052	31.3	12.2	1	+0.7
	1.918	21.2	12.4	2	+1.1
	1.702	9.9	12.6	4	−0.3
	1.593	6.3	12.4	8	−2.7
	1.555	5.4	12.9	8	+0.9
	1.536	4.9	12.9	8	+0.7
High Concentrations					
40.5	2.155	56.4	37.0	± 1.2	+0.1
	1.697	14.21	40.9	1.6	+4.3
	1.695	14.13	41.0	1.6	+3.0
	1.285	1.91	41.9	4.3	+3.8
	1.269	1.78	43.8	4.7	+8.5
58.0	1.978	48.5	54.7	1.2	+1.5
	1.662	17.02	57.0	1.4	+1.8
	1.546	10.94	59.4	1.5	+5.1
	1.486	8.20	58.8	1.7	+3.5
	1.448	6.64	58.0	1.7	+1.2
	1.260	2.33	59.6	3.0	+3.5
78.1	2.142	110.0	68.8	1.1	−1.1
	2.138	110.2	69.1	1.1	−0.7
	1.703	35.4	75.7	1.2	+2.7
	1.702	34.2	74.8	1.2	+1.3
	1.688	32.8	75.3	1.2	+1.3
	1.287	4.38	79.6	1.7	+1.9
	1.285	4.94	77.5	1.7	+3.9
	1.268	4.58	78.4	1.9	+2.1
100.0	1.000	8.68	98.6	......	+0.6
	1.100	13.51	97.8	......	+0.7
	1.200	19.93	96.2	......	+0.6
	1.300	28.13	95.1	......	+0.6
	1.400	38.33	93.9	......	+0.3
	1.500	50.72	92.6	......	+0.4
	1.600	65.0	91.2	......	+0.3
	1.700	82.0	89.7	......	−0.1
	1.800	101.5	88.1	......	−0.2
	1.900	123.7	86.4	......	−0.5
	2.000	149.	84.7	......	−0.6
	2.100	178.	83.0	......	−0.5
	2.200	209.	81.2	......	−0.5

TABLE A.4. VAPOR PRESSURE OF MIXTURE OF He^3 AND He^4 (*Continued*)

FOR A GIVEN FIXED LIQUID CONCENTRATION

X_L, %	T, °K	Sample pressure, mm Hg	Instrumental error, %
0.58	2.172	38.41	0.4
	2.066	29.47	0.4
	1.957	21.88	0.4
	1.847	15.61	0.4
	1.749	11.28	0.5
	1.658	8.13	0.5
	1.612	6.74	0.6
	1.517	4.61	0.8
	1.405	2.75	1.5
	1.395	2.60	1.5
	1.295	1.47	3.0
	1.272	1.35	3.5
1.98	2.177	41.97	0.3
	2.176	41.95	0.3
	2.146	39.31	0.4
	2.114	36.66	0.4
	2.082	34.00	0.4
	2.044	31.03	0.4
	1.960	25.12	0.4
	1.855	18.91	0.4
	1.767	14.67	0.4
	1.698	11.89	0.5
	1.667	10.79	0.5
	1.631	9.57	0.5
	1.609	8.96	0.5
	1.500	6.18	0.6
	1.384	3.99	1.1
	1.351	3.49	1.3
5.21	2.176	48.10	0.3
	2.112	42.59	0.3
	1.978	32.43	0.4
	1.788	20.82	0.4
	1.723	17.60	0.4
	1.621	13.55	0.4
	1.453	8.52	0.6
	1.441	8.18	0.7
	1.212	3.89	1.5
	1.194	3.66	1.6
9.49	2.183	58.18	0.3
	2.098	49.44	0.3
	2.044	41.61	0.3
	1.953	37.85	0.4
	1.902	34.25	0.4
	1.866	31.85	0.4
	1.799	27.77	0.4
	1.752	25.15	0.4
	1.704	22.62	0.4
	1.683	21.55	0.4
	1.632	19.21	0.4
	1.586	17.29	0.4
	1.554	15.98	0.4
	1.504	14.17	0.4
	1.402	10.83	0.6
	1.230	6.52	1.0
13.0	2.175	64.23	0.3
	2.070	52.16	0.3
	1.961	43.09	0.3
	1.850	35.35	0.4
	1.748	29.03	0.4
	1.655	23.94	0.4
	1.476	16.16	0.4
	1.394	13.11	0.5
	1.328	11.04	0.7
	1.287	9.89	0.7
	1.255	9.98	0.7

TABLE A.5. PHYSICAL CONSTANTS

Electronic charge, e	1.602×10^{-19} coulomb
Mass of an electron	9.106×10^{-31} kg
Ratio of charge to mass of an electron	1.759×10^{11} coulomb/kg
Mass of a proton	1.673×10^{-27} kg
Ratio of charge to mass of a proton	9.564×10^{7} coulomb/kg
Ratio of mass of a proton to that of an electron	1,837
Planck's constant, h	6.623×10^{-34} joule-sec
Boltzmann's constant, k	1.380×10^{-23} joule/°K
Avogadro's number	6.024×10^{23} per mole
Permittivity of free space, ϵ_0	8.854×10^{-12} farad/meter
Permeability of free space, μ_0	$4\pi \times 10^{-7}$ h/meter
Velocity of light, c	2.998×10^{8} m/sec
Bohr magneton	9.12×10^{-24} mks units; 9.12×10^{-21} erg/gauss
Energy units	1 joule = 10^{7} ergs 1 calorie = 4.19×10^{7} ergs

INDEX

A

Abragam, A., 179, 180
Abraham, B., 70, 71, 93
Adiabatic demagnetization, 151
  experimental method, 154
  experimental results, 157
Alers, P., 125
Allen, J., 74, 79, 80, 83, 215
Alpert, N., 176
Andrew, E., 129
Andrews, F., 215
Andronikashvili, E., 69
Antiferromagnetism, 150
Atkins, K., 85, 109*n.*

B

Bagguley, D., 177
Bardeen, J., 134
Barns, R., 202
Barrett, C., 200
Barrett, J., 228
Beljers, H., 165
Bender, P., 136
Benzie, R., 179
Berman, R., 30, 216, 218
Beth, E., 38, 40, 42, 56
Biermasz, T., 218
Bird, R., 40
Bitter, F., 176, 180, 210, 211
Blackman, M., 183, 189, 191, 200
Bleaney, B., 25, 148, 164, 178, 179
Bloch, F., 165, 167
Bloembergen, N., 168, 175
Blunt, R., 125, 223
Bohr magneton, 141, 182
Boorse, H., 30
Born, M., 134, 191
Bowers, R., 69, 80
Breckenridge, R., 222
Brickwedde, F., 27
Brillouin, L., 145, 189
Broer, L., 162, 180
Brown, N., 30, 226
Burk, N., 202

C

Cady, W., 220
Casimir, H., 119, 125, 137, 162, 197, 218
Cavileer, R., 20, 23
Chambers, R., 130
Chandrasekhar, B., 80
Chase, C., 85
Clark, C., 196
Claude process, 5
Clausius, R., 2
Clement, J., 30, 121
Clusius, K., 202, 205, 206, 207, 210, 212
Cole, R., 226
Collins, S., 1, 16
Compressors, 12
Constants, of gases, 11
  of physics, 238
Cooke, A., 15, 160, 179
Corresponding states, 4, 36
Creep of helium II, 24
Critical temperature and pressure, 3
  tables, 4
Cryostats, 21, 23
Cummerow, R., 164

D

Daniels, J., 164
Daunt, J., 75, 77, 93, 126, 199
De Boer, J., 36, 41, 54, 56, 96, 109
Debye, P., 151, 161, 165, 187, 214, 218
de Haas, W., 126, 145, 151, 162, 180, 218
de Haas-van Alphen effect, 180
De Klerk, D., 109*n.*, 151, 157, 161
Dennison, D., 27, 206
Desirant, M., 198
Devonshire, A., 58, 222, 227
Diamagnetism, in atoms, 141
  in metals, 180, 184
  theory of, 181

Dielectrics, 220
  of anti-ferro-electric substances, 226
  of barium titanate, 222, 227
  of Curie-Weiss type, 225
  of ferro-electric substances, 226
Dingle, R., 109
Dockerty, S., 195
Duerig, W., 23
DuPré, F., 162
Duyckaerts, F., 196

E

Einstein, A., 99, 121
Elastic constants, 203
Enthalpy, 5
Entropy, 4, 162
Equation of state, 1, 2
  of compressed gases, 58
  of De Boer, 41
Estermann, I., 202
Eucken, A., 205, 210, 212, 214
Eyring, H., 58

F

Fairbank, H., 87
Fairbank, W., 87
Faraday, M., 165
Farkas, A., 205
Ferro-electrics, 222
Findlay, J., 84
Fine, P., 199
Forsbergh, P., 223
Forsterling, K., 202
Fountain effect, 80
Fowler, R. H., 35, 145, 207
Free-volume theory, 58
Frenkel, J., 164, 207
Fritz, J., 147, 150, 179
Frohlich, H., 134, 220

G

Galkin, A., 127
Galt, J., 188, 204
Ganz, E., 83
Gas holder, 13
Giauque, W., 20, 22, 74, 147, 149, 151, 156, 179, 207, 211, 212
Gibbs potential, 5, 119
Gogate, D., 105
Goldman, J., 202
Gonzales, M., 207
Gorter, C., 64, 86, 96, 103, 119, 136, 145, 151, 163, 164, 176, 197
Grace, M., 164
Grayson-Smith, H., 84
Grebenkemper, C., 131
Grenier, C., 82
Grilly, E., 27, 41, 71
Gropper, L., 52
Gruneisen, E., 214
Gubar, J., 121
Gutowsky, H., 174

H

Hagen, J., 131
Halliday, D., 164
Hammel, E., 41, 71, 73
Hansen, W., 165
Hanson, W., 90
Harteck, P., 212
Hatton, J., 163, 173, 206
Heat conduction in metals, 30, 214
  in dielectrics, 217
  down open tubes, 23
  Makinson law, 215
  Umklapprozesse, 219
  Wiedemann-Franz law, 214
Hebb, M., 161, 162
Heer, C., 93, 96, 126
Heisenberg, W., 134
Heitler, W., 173
Helium, liquefiers for, 15, 16
  liquid, density, 66
    diagram of state, 60
    dielectric constant, 66
    fountain effect, 80
    heat conductivity, 82
    He^3, isotope, 70
      mixtures with He^4, 93
      theory of entropy, 73
      (*See also* Spin in He^3 isotope)
    latent heat of vaporization, 65, 67
    Rollin film, 75
    specific heat and entropy, 62, 64, 78
    vapor pressure, 229–234
    viscosity of, 68
    zero-point energy, 65

Helium theory, 97
  characteristic impedance, 107
  condensation to He II, 101
  of first sound, 104
  of photons and rotons, 108
  of second sound, 105
  two-fluid, 102, 103
  of zero-point energy, 98
Helmholtz potential, 5, 32, 34
  for an assembly of dipoles, 153
  for dielectrics, 228
  electrons in metal, 182
  in quantum statistics, 100
Hendricks, S., 211
Henry, W., 145
Herlin, M., 88, 89, 109*n*.
Hettich, R., 211
Hiller, K., 205
Hirschfelder, J., 36, 39, 40, 58
Hogan, C., 165
Hoge, H., 27
Hollis-Hallett, A., 70
Houston, W. V., 121, 123, 191
Hudson, R., 109*n*.
Hull, R., 64, 148
Hulm, J., 225, 226
Hund, F., 206
Hydrogen, nuclear resonance, 173
  physical constants, 11, 210
  specific heat, 207
  vapor pressure, 27, 234

I

Ingram, D., 179
Iona, M., 202

J

Jackson, L. C., 77
Jackson, W., 225
Johnston, H., 39, 207, 215
Jones, H., 80, 183, 194
Joule-Thomson expansion, 8

K

Kahn, B., 52, 56
Kan, L., 112
Kapitza, P., 1, 15, 74, 78, 83
Kaufmann, A., 180
Keesom, W., 26, 30, 41, 57, 61, 67, 68, 79, 82, 120, 126, 194, 197, 212
Kellerman, E., 202
Kelley, K., 150, 211
Keyes, F., 39
Khalatinov, I., 70, 75, 86
Kihara, T., 40
Kikoin, I., 121
Kilpatrick, J., 57
Kirkwood, J., 39, 55, 58
Kistemaker, J., 26, 27, 67
Kistiakowsky, G., 174
Kittel, C., 204, 226
Klemens, P., 219
Klemm, W., 151
Kok, J., 137, 195, 197
Kramers, H. A., 24
Kramers, H. C., 64
Kronig, R., 173
Kurrelmeyer, B., 196, 197
Kurti, N., 151, 157, 159

L

Lainé, P., 157
Landau, L., 70, 75, 88, 108, 164, 184
Lane, C., 87, 94
Larmor frequency, 141, 142
  and gyrator, 166
  and resonance, 164
Lasarev, B., 112, 127, 163, 180
Lashkarew, W., 211
Lathrop, A., 121
Laurmann, E., 125
Lennard-Jones, J., 35, 38, 58
Lennard-Jones calculation of molecular constants, 46
Lennard-Jones potential, 34
Level indicators, 22
Lifshitz, E., 73, 164
Linde process, 1, 8
Liquefiers for helium, 15
  Collins, 16
  Kapitza, 16
  Simon type, 15
Little, A. D., Co., 20
London, F., 97, 100, 101, 122, 131
London, H., 79, 127, 131
Long, E., 225

Love, W., 113, 125, 223
Luttinger, J., 162
Lyon, D., 147, 149

M

McCloskey, K., 39
MacDonald, D., 200
MacDougall, D., 151
McGee, W., 73
McWhirter, J., 125
MacWood, R., 68
Magnetism, 138
  antiferromagnetism, 150
  Brillouin function, 145
  Curie's law, 144
  magnetic cooling, 151
  methods of measurement, 145
  nuclear resonance, 163, 164
  and statistical mechanics, 143
Makinson, R., 215
Marcus, J., 180
Marcus, P., 128
Mathias, B., 223, 225, 226
Maurer, R., 88, 89
Maxwell, E., 113, 128
Mayper, V., 109*n.*
Mechano-caloric effect, 77
Megaw, H., 209, 222
Meissner, W., 115, 199
Meissner effect, 115
Mellink, J., 82, 86
Mendelssohn, K., 69, 75, 77, 80, 120, 121, 126, 199, 200, 206, 215
Mendoza, E., 163, 215
Merz, W., 223, 224
Meyer, L., 83
Misener, A., 74, 79
Montroll, E., 191
Moore, J., 120, 199
Morse, P., 89
Mott, N., 183, 194, 196
Muench, N., 123

N

Néel, L., 150
Nernst, W., 212
Nix, F., 113
Nuclear alignment, 163

O

Ochsenfeld, L., 115
Olsen, J., 126
Onnes, H. Kamerlingh, 1, 2, 15, 26, 65, 75, 111, 149, 194
Onnes effect, 75
Osborn, J., 148
Osborne, D., 70, 71, 88, 93, 107, 109*n.*
Overton, W., 188, 201, 203

P

Packard, M., 165
Pake, G., 174
Paramagnetism, 143
Parkinson, D., 201, 213
Partition function, 33, 37
  dense gas and liquid, 58
  and density matrix, 184
  electron-spin system, 161
  gas, in quantum statistics, 34, 48
    in reduced parameters, 45
  of oscillator, 228
  of rotating molecules, 206
Pathak, P., 105
Pauling, L., 205, 207
Peierls, R., 219
Pellam, J., 84, 87, 89, 92, 107, 109*n.*
Penny, W., 161
Penrose, R., 178, 179
Perlick, A., 210
Perrier, A., 149
Peshkov, V., 87, 88, 107
Pickard, G., 197, 199
Pippard, A., 86, 125, 128
Polarization, 220
  and Lorentz correction, 222
Pomeranchuk, I., 73
Pound, R., 164, 168, 172
Powers, E., 215
Pry, R., 121
Pryce, M., 179, 180
Purcell, E., 161, 162, 164, 168, 172, 174

Q

Quinnell, E., 30, 121

R

Rabi, I., 165
Rademaker, A., 126
Rayleigh disk, 89

Reddish, W., 225
Reekie, J., 80
Refrigeration, 9
  and air conditioning, 10
Reuter, G., 129
Roberts, S., 223
Robinson, F., 164
Robinson, J., 180
Rollin, B., 15, 75, 163, 173, 175, 206
Rollin film, 75
Rose, M., 164
Rosenberg, H., 215
Ruhemann, B., 150, 206

S

Saris, B., 83
Schmidt, G., 26
Schmitt, R., 224
Schrödinger equation, for an electron gas, 182
  for a gas, 34, 46
  for a single particle, 98
Schubinkov, L., 163
Scott, R., 27, 115
Second sound or thermal waves, 86
  attenuation, 88
  in He^3 mixtures, 93
  velocity of, 87, 109*n*.
Serin, B., 113
Shirane, G., 226
Shoenberg, D., 25, 125, 180
Shull, C., 150, 202
Silsbee effect, 115
Silvidi, A., 199
Simon, F., 1, 15, 25, 63, 64, 151, 157, 159, 197, 199–201, 206, 211, 213
Slater, J., 5, 37, 39, 48, 128, 134, 190, 196, 204, 227
Slater sum, 49
  in quantum statistics, 52
  in some examples, 50
Smart, J., 150
Snoek, J., 165
Sommerfeld, A., 192
Sommers, H., 94
Sondheimer, E., 129, 184, 215
Sound velocity in liquid helium, attenuation, 84
Specific heat, 186
  apparatus, 211
Specific heat, $C_p - C_v$, 191
  and Debye theory, 188
  electronic, 192, 196
  of hindered rotation, 209
  of metals, 194–202
  of salts, 202
Spedding, F., 201
Spiers, J., 164
Spin in He^3 isotope, 54, 72
  electron, 142
  nuclear, 163
Spohr, D., 215
Spotz, E., 40
Steenland, M., 151
Stevens, K., 179, 180
Stoner, E. C., 148
Storage containers, 20
Stout, J., 74, 156
Superconductivity, 110
  floating magnet, 117
  gyro-magnetic effect, 121
  at high frequency, 127
  isotope effect, 113
  magneto-caloric effect, 121
  Meissner effect, 115
  rotating superconductors, 125
  Silsbee effect, 115
  skin depth of penetration, 125
  table of metals, 111
  tension effect, 127
  and theory, 131
    two-fluid, 136
  thermal conduction, 126
  thermal properties, 117
  thermoelectric effect, 126
  Thomson heat effect, 127
  volume and crystal structure, 112
Svenson, A., 197
Swenson, C., 63
Swim, R., 188, 203
Sydoriak, S., 41, 71, 73, 180

T

Taconis, K., 24
Takagi, M., 226
Teller, E., 173
Temperature and fixed points, 11
  definition, 28
  measurements, 25
Temperley, H., 108

Thermometer, gas, 28
  resistance, 29
  thermocouple, 30
Tisza, L., 75, 77, 86, 104, 162, 222
Torrey, H., 164, 172
Transfer tube, 19

U

Uhlenbeck, G., 38, 40, 42, 52, 56
Ultrasonics, 188
U.S. Bureau of Mines, 13
Usyskin, I., 211

V

Valasck, J., 222
van Alphen, P., 180
van den Berg, G., 68
van den Handel, J., 145
van der Waals, J. D., 2
van Dijk, H., 25, 30
van Itterbeek, A., 68
van Laer, P., 120, 198
Van Vleck, J., 151, 161, 173, 180, 182, 220
Vapor pressure, of liquid helium, 25, 229
    control of, 25
    of He^3, 41
    tables, 229–233
  of liquid hydrogen, 27, 234
    equipment for, 27
    tables, 234
  of liquid oxygen, 27, 235
    tables, 235
Virial coefficients, 2, 32
  in classical statistics, 36, 39
Virial coefficients, ideal quantum gas, 53
  table for helium gas, 41, 57
von Hipple, A., 222
von Laue, M., 131

W

Waller, I., 173
Ward, J. 108
Wasscher, J., 64
Webber, R., 215
Weertman, J., 202
Weinstock, B., 70, 71, 92, 93
Weiss, P. R., 162, 177
Wexler, A., 21
White, D., 207
White, G., 76, 80
Whitmer, C., 177
Wiebe, R., 211, 212
Wiersma, E., 151
Wilhelm, J., 84
Wilkinson, K., 64, 216
Wilkinson, M., 202
Wilks, J., 64, 108, 216
Wilson, A., 184
Wolley, R., 27
Wood, R., 165
Wul, B., 222

Z

Zavoisky, E., 164
Zemansky, M., 2, 30
Ziegler, W., 215
Zilsel, P., 108